Powerful Low-Valent Photocatalysts and Luminophores Based on Earth-Abundant Metals

---

Inauguraldissertation

zur Erlangung der Würde eines Doktors der Philosophie

vorgelegt der
Philosophisch-Naturwissenschaftlichen Fakultät
der Universität Basel

von

Laura Allegra Büldt

aus Bielefeld, Deutschland

Basel, 2016

Genehmigt von der Philosophisch-Naturwissenschaftlichen Fakultät auf Antrag von

Fakultätsverantwortlicher/Dissertationsleiter: Prof. Dr. Oliver S. Wenger
Korreferent: Prof. Dr. Roger Alberto

Basel, den 15.11.2016

Prof. Dr. Jörg Schibler

I love crystals, the beauty of their forms and formation; liquid, dormant, distilling, sloshing! The fumes, the odors good or bad, the rainbow of colors; the gleaming vessels of every size, shape and purpose.

R. B. Woodward

Acknowledgement

First of all, I would like to thank **Prof. Dr. Oliver S. Wenger** for his constant trust in me as, well as taking the time to find the perfect balance between freedom and guidance to help me succeed. You have been the best Doktorvater I could have wished for.
I also thank **Prof. Dr. Roger Alberto** for co-examining this thesis, as well as the possibility to cooperate with his group.
Prof. Dr. Konrad Tiefenbacher is thanked for chairing my examination.
Sylvie Mittelheisser and **Dr. Heinz Nadig** are thanked for measuring elemental analysis and high resolution mass spectra, respectively.
I thank **Marcus Neuburger** and **Alessandro Prescimone** for measuring and solving crystal structures and answering all kinds of related questions.
Special thank is given to **Marcus Hauri** and the whole **Werkstatt-Team** as well as **Brigitte Hohwald** and **Beatrice Erismann** for keeping this department together and making this place such a friendly and welcoming place to work at.
I also thank **Daniel Häusinger** and **Thomas Müntener** for measuring my challenging samples on the 600 MHz NMR machine.
I would also like to acknowledge the **Housecroft/Constable group** for their warm and welcoming attitude. Special thanks go to **Sarah** for helping me with measurement on their instruments, as well as the support in all copper related questions, to **Angelo** for brightening my day on a regular basis, to **Fabian** for the passionate discussions about science (while drinking beer) and to **Max** for measuring "LDI" spectra for me.
Dr. Xingwei Guo is thanked for the helpful discussions, the sealing of NMR tubes and of course for the help with the photocatalysis experiments. It was a pleasure to work with you and I learned so much from you.
I thank **Martin** for the great time we had in our "two people lab community". I am also very thankful for the scientific (and not so scientific) discussions we had and of course for proof-reading this thesis.
Although I did not work with **Chris** for a long time, I really enjoyed it and I am very thankful that he took the time to correct my thesis, especially in respect to language.
Of course I also thank the **AK Wenger** for the nice work atmosphere, as well as my former students who were a real pleasure to tutor.
I also have to thank **Catherine Bronner** for making my first months in Basel bearable. Without you I would probably have quit within the first three month.
I am very grateful for the very positive and relaxed work atmosphere the **Crew of Lab 304**

established in combination with the excellent choice of music.
Claudia Brunner is thanked for her extreme patience with me and her professional handling of my musical anti-talent, as well as helping me to keep in touch with my double bass.
I thank my friends from Bochum with all my heart for the great time we had. They made my undergraduate studies one of the best times I had. Special thanks go to **Ramona** for being my lab buddy. You were the best partner in crime I could possibly find! My ex-flatmate **Thomas** is thanked for making me comfortable in a shared flat, as well as his fine sense of humour and for being my Bochum-family. **Elisabeth** and **Patricia** are thanked for their friendship no matter were we live and the great time we had in Bochum.
I thank my best friend **Rike** for sharing her life with me, although it is completely different to mine. Additionally, I am extremely thankful that she always has my back not matter how long I did not call. I want to thank my oldest friend **Dirk** for always speaking his mind when asked and for challenging me to intellectual contentions.
Furthermore, I would like to thank my precious family who always supported me, worried with me when things did not work my way and celebrated when they did. I thank my **Papa** for warning me about a chemists life and for encouraging me when I started it. My **Mama** is thanked for her never ending love and unlimited support as well as for her honest feedback, although I might not always agree with it. My aunt **Cläuschen** has always been a very important part of my family and I am very thankful for her love and support, especially when I started my life as a chemist in Bochum. I would like to thank my **Oma** for being the strong-minded and independent woman she was. She made it very clear to me that I could do whatever I set my mind on.
Last, I would like to thank **Hauke** for the amazing time we had in Basel. You made me feel at home and gave me a place to rest. Also, I would probably have starved, if it was not for you to cook. I am very grateful that you endured my sudden mood swings in the last year, I know, I was challenging.

Abstract

Facing a growing world population and the concomitant increase in resource and energy consumption, researchers are challenged to make use of sustainable energy sources such as sunlight. Consequent efforts to utilize light as an energy source in chemical reactions established photocatalysis as a major research area. Most of the catalysts used are based on d^6 metal complexes which usually consist of precious metals such as ruthenium(II), rhenium(I) or iridium(III). Although these complexes are generally robust and easily tunable to one's needs, they are limited in their reduction power. This limitation hampers their efficient use in demanding organic reactions or the efficient design of solar fuel production systems.
In **Chapters I** and **II**, a short general introduction followed by a short overview over the relevant theoretical background are given.
Chapter III begins with a discussion of an introductory project which was concerned with the design of a strongly reducing, acid-stable ruthenium tris(2,2′-bipyridne) derivative. The presented complex is robust enough to be employed as a photosensitizer in proton coupled electron transfer (PCET) reactions in presence of strong organic acids.
Subsequently, this thesis presents a new approach to the challenge of designing photocatalysts with low excited state oxidation potentials. The use of chelating aryl isocyanide ligands with a fully aromatic ligand scaffold gives access to robust, earth-abundant molybdenum(0) photocatalysts. These catalyst are some of the strongest ever reported, and catalyse very demanding reduction reactions that have not been accessible with other photocatalysts before. Additional studies exploring the scope of these ligands yielded the first homoleptic chromium(0) complex to be luminescent in solution at room temperature. Also, two homoleptic nickel(0) complexes described in this thesis showed ^{3}MLCT emission at low temperature and related copper(I) complexes (**Appendix A**) were found to be blue emitters in solution as well as the solid state. **Chapter IV** summarizes the results of this thesis and gives a perspective for future developments. The detailed description of the synthesis and experiments are found in **Chapter V**.

Contents

List of Abbreviations

σ	chemical shift
A	electron acceptor
acac	acetic acid anhydride
AcOH	acetic acid
Ar	aryl
ATRA	atom transfer radical addition
BET	back electron transfer
BHAS	base-promoted homolytic aromatic substitution
bpy	2,2′-bipyridine
^{t}Bu	*tert*-butyl
cat	catalyst
COD	1,5-cyclooctadiene
D	electron donor
DCM	dichloromethane
D*i*PA	di(*iso*propyl)amine
DSSC	dye sensitized solar cell
ESI	electron spray ionization
ET	electron transfer
EtOAc	ethyl acetate
Fc	ferrocenium
FT	fourier transformed
GS	ground state
HOMO	highest occupied molecular orbital
HR-MS	high resolution mass spectroscopy
IC	interconversion
LC	ligand-centred
IR	infrared
ISC	intersystem crossing
LF	ligand field
LLCT	ligand-to-ligand charge transfer
LMCT	ligand-to-metal charge transfer
LUMO	lowest unoccupied molecular orbital
MALDI-TOF	matrix-assisted laser desorption/ionization time-of-flight spectroscopy
Me	methyl
4,4′-(Me_2N)bpy	4,4′-di(dimethylamino)2,2′-bipyridine
MeOH	methanol
MLCT	metal-to-ligand charge transfer

MO	molecular orbital
MS	mass spectroscopy
NMR	nuclear magnetic resonance
OLED	organic light emitting diode
PC	photocatalyst
PCET	proton coupled electron transfer
Ph	phenyl
pin	pinacolato
ppm	parts per million
ppy	2-phenylpyridine
SET	single electron transfer
SCE	saturated calomel electrode
SCRIP	singlet contact ion radical pair
TADF	thermally activated delayed fluorescence
TBA	tetra(*n*-butyl)ammoinum
TCRIP	triplet contact ion radical pair
THF	tetrahydrofuran
TMP	2,2,6,6-tetramethylpiperidine
TON	turnover number
USD	US dollar
UV	ultraviolet
Vis	visible

I General Introduction

Progressing technological development and a growing world population lead to a steady increase of the overall energy consumption. The limited availability and the consequently increasing price of fossil fuels are major concerns of industries today, since the majority of energy is still obtained from fossil fuels. Additionally, the combustion of fossil fuels accounts for a major part of the overall CO_2 emission, which is known to be a greenhouse gas.[1] Over the last two decades, research focused on the development of more energy-efficient processes, as well as the development of sustainable fuels for energy generation and storage. If one compares the overall amount of energy, which could be harvested from natural resources such as wind, water and sun, the latter is the most powerful source, providing a theoretical amount of 23,000 TW per annum on earth. This amount exceeds today's world energy consumption by a factor of 1,500.[2]

The most prominent example, in which nature utilizes sunlight to drive challenging reactions under mild conditions, is photosynthesis. In this process, plants use sunlight to reduce CO_2 to more complex organic molecules, which then serve as an energy source and storage. The concept of artificial photosynthesis is in analogy with this intriguing process. In principle, when a photocatalyst is brought in contact with small, inert molecules such as carbon dioxide, nitrogen or water, it transforms them into valuable products, such as solar fuels or fine chemicals (Fig. I.1). Since these reactions usually proceed under very mild conditions (e.g. visible light irradiation at room temperature), photocatalysis more and more develops into a versatile tool to access complex organic structures bearing sensitive functionalities.

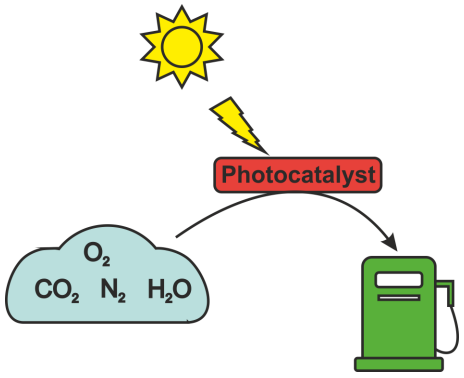

Figure I.1: General principle of artificial photosynthesis solar fuel production.

The most prominent class of photosensitizer are derivatives of ruthenium-tris(2,2′-bipyridine). Due to their high chemical robustness, as well as easily-tunable properties, these complexes

find application in a wide range of fields, from dye sensitized solar cells to photocatalysis in organic chemistry. Nevertheless, their redox potentials are limited to a certain range, resulting in a limited capability of driving demanding reduction reactions. Additionally, ruthenium is one of the rarest metals with an occurrence of 0.001 ppm in the earth's crust and is therefore rather expensive (1,350 USD/kg[3]) and only available in small quantities.[4] In this context, the development of new, stronger reducing photosensitizers made of earth-abundant metals is highly desirable. Under these premises, the exchange of the metal center to one of lower oxidation state appears favourable, since a lower oxidation state usually translates into a stronger reducing ground state. In the periodic table the neighbouring isoelectronic metal to ruthenium(II) would be technetium(I), which is radioactive, thus leaving molybdenum(0) as a suitable substitute for ruthenium(II). Molybdenum is approximately 10,000 times more earth-abundant than ruthenium with an occurrence of 14 ppm in the earth crust, leading to a much lower price on the world markets (15 USD/kg).[3,4] Therefore, the possible application of molybdenum(0) complexes as strong reducing analogues of ruthenium(II) complexes is investigated. In order to yield robust metal(0) complexes, strong π-acceptor ligands are required to stabilize metal centers in their low oxidation states via π-backbonding. Aryl isocyanide ligands are good candidates for this task since they are easy to modify to one's needs. The photophysical properties of molybdenum aryl isocyanide complexes with monodentate ligands have already been described in the 1970s.[5,6] However, these complexes did not appear to be suitable for any further applications, since they undergo rapid photosubstitution reactions from their ^{3}MLCT excited state, leading to short excited-state lifetimes (<20 ns) and fast decomposition. More recent studies on tungsten(0) aryl isocyanide complexes also employing monodentate ligands re-emphasized the outstanding reduction potentials of these complexes.[7,8]

The main project of this thesis aimed at the creation of strong photoreductants in form of molybdenum(0) complexes with sufficient excited state lifetimes and photostability by utilizing bidentate isocyanide ligands with a rigid, aromatic backbone (Fig. 2).

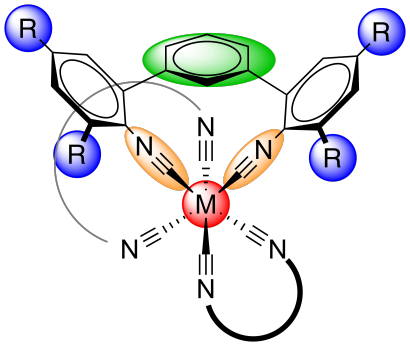

Figure I.2: General design concept of a low-valent d^6 metal complex bearing a bidentante isocyanide ligand. Different coloured compartments indicate sites of possible modification.

Figure I.2 shows the general design concept of a low-valent d^6 metal complex bearing a bidentante isocyanide ligand. The differently coloured compartments mark sites for possible modifications of the complex. The π-acceptor coordination sites are marked in orange. The substituents labelled in blue are supposed to shield the metal center and can be varied in size and electronic character. The backbone of the ligand scaffold (green) influences the bite angle of the coordination sites and therefore controls the torsion between the backbone and the two coordinating aryl rings. This torsion angle has a direct impact on the extent of conjugation over the entire ligand scaffold and determines the position of the ligand centred LUMO.
The metal center (red) could be any metal center in a low to intermediate oxidation state and different coordination geometries, such as octahedral or tetrahedral are accessible. In a side project, the scope of the developed ligand motive was investigated in order to access luminophores based on first row d^6 and d^{10} transition metals.

II Theoretical Introduction

2.1 Introduction to Photophysics of Transition Metal Complexes

In order to predict and tailor the photophysical properties of transition metal complexes for individual applications, such as photocatalysis, organic light emitting diodes (OLEDs) or dye-sensitized solar cells (DSSCs), a deeper understanding of the basic photophysics is required. The five d-orbitals of an unperturbed transition metal center are energetically degenerate, although they differ in their geometrical orientation. In theory, application of a spherical ligand field would lead to an equal rise of all d-orbitals in energy due to electrostatic repulsion between the d-electrons and the lone pair electrons of the ligand. However, the d-orbitals have different spatial orientations and therefore interact not equally strong with the ligands, resulting in a different ligand field splitting for each coordination geometry. Figure II.1 shows the relevant ligand field splittings found for complexes presented within this thesis.

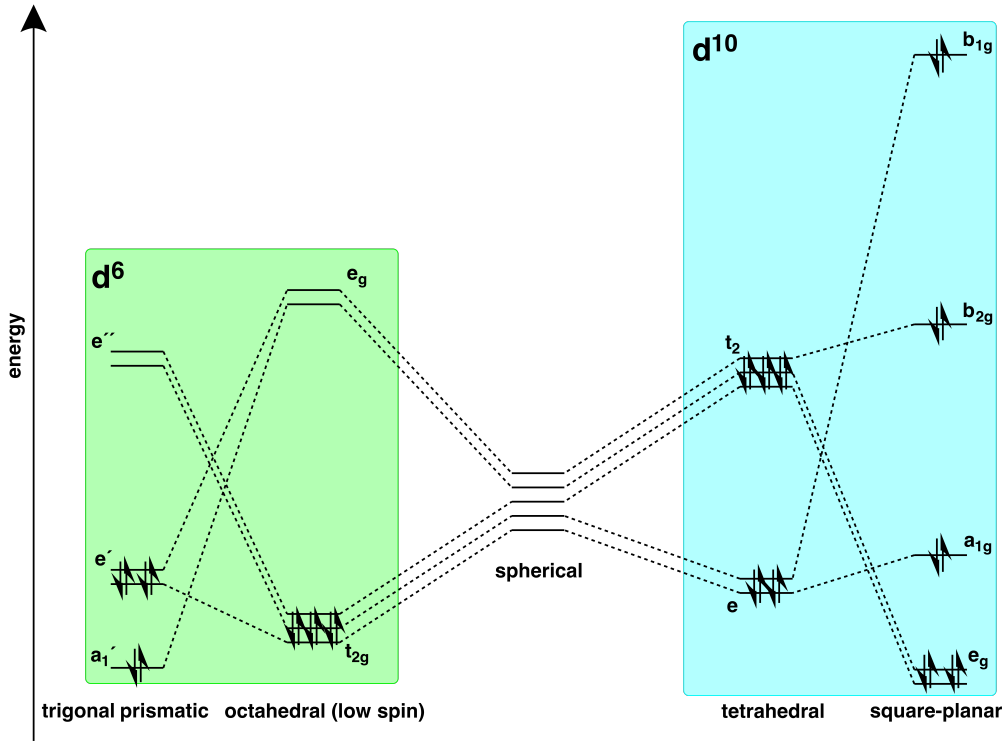

Figure II.1: Simplified ligand field splitting of the d-orbitals for different coordination geometries in d^6 and d^{10} metal complexes.

Complexes with the coordination number 6 usually adopt an octahedral ligand field, with three energetically low lying t_{2g} orbitals and two e_g orbitals that are higher in energy. In a low-spin configuration all electrons are paired. This is preferred over the high-spin configuration, as long as the metal center is a late transition metal and/or the ligand induces a strong ligand field splitting itself. All complexes discussed in this thesis are low-spin complexes, since the used ligands are strong field ligands. In case of d^6 metal complexes (II.1, green box) the t_{2g} orbitals are fully occupied while the e_g orbitals remain unoccupied.
A second, less common ligand field splitting found in d^6 metal complexes is trigonal prismatic. This geometry results from a trigonal twist of the octahedral geometry. The angles between the neighbouring ligands are not 90° anymore, but 85° and 95°. Although this geometry is usually found for complexes of d^0 to d^2 metals, it was reported that homoleptic molybdenum(0) and tungsten(0) complexes with 2,2′-biphosphinine ligands adopt geometries between octahedral and trigonal prismatic.[9]
The d^{10} metal complexes investigated in this thesis are tetra-coordinated, and the d-orbital splittings of the relevant coordination geometries are shown in the blue box in Figure II.1. Complexes with the coordination number 4 are most frequently found to be tetrahedral. The tetrahedral geometry is flattened in some cases due to steric or electronic reasons, which leads to a square-planar structure.[10]
As the coordination geometry dictates the d-orbital splitting, it also determines the chemical and photophysical properties of the complex.

2.1.1 The Excited State

In context of transition metal complexes, the concept of absorbing and emitting light is of fundamental importance to a vast majority of research fields, e.g. the development of luminescent materials, photocatalysts and energy conversion devices. The relevant physical processes usually involve the absorption of a photon of a certain energy to trigger the transition of an electron from an occupied to an unoccupied state. These electronic transitions generally require light from the UV to visible part of the electromagnetic spectrum (200 - 800 nm).
The observed intensity ε of a transition band in an absorption spectrum depends on the nature of the states between which the transition occurs. There are two general selection rules which determine if a electronic transition is allowed or forbidden. First, the spin multiplicity of the system has to remain unchanged upon transition. Therefore, transitions between singlet and triplet states are spin-forbidden (e.g. ^{1}GS-^{3}MLCT). Second, the so-called Laporte rule states that in centrosymmetric molecules, for example octahedral complexes, transitions between states of the same parity are forbidden (e.g. d-d transitions). In reality even forbidden transitions are observed, but with much smaller extinction coefficients (ε) than their allowed counterparts.[11]
The Jablonski diagram in Figure II.2 depicts the most relevant transitions in a given

molecule upon photon absorption. If the wavelength of a photon matches the energy difference between the singlet ground state S_0 and one of the excited singlet states S_1 or S_2, an electron will be transferred from S_0 to an excited state with the same spin multiplicity. These kind of transitions result in strong absorption bands since they are spin and LAPORTE allowed.

If the electron is excited to the S_2 state (solid, black arrow), usually fast non-radiative interconversion (IC), with the rate constant k_{IC}, to the S_1 state will take place (black, dashed arrow). From the S_1 state, three decay processes are now in competition. First, radiationless relaxation to the ground state via a multiphonon pathway with a rate constant k_{nr}^1 can occur (black, dashed arrow). Second, relaxation via emission of a photon with the energy of ΔE, with the rate constant k_F (solid, red arrow), can occur. Since the photon results from a transition between two states of the same spin multiplicity this process is called fluorescence. The third possible process is an intersystem crossing process (ISC), which, in general, is a spin-forbidden process, but might be favoured in metal complexes that exhibit a pronounced heavy atom effect.

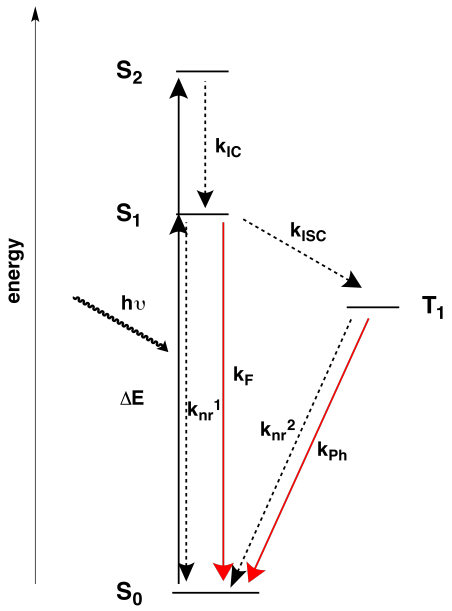

Figure II.2: General JABLONSKI diagram illustrating the most relevant electronic transitions upon light excitation.

Especially in late transition metal complexes, ISC competes efficiently with fluorescence and the energetically lowest excited state to be populated is the triplet state T_1. Since relaxation to the singlet ground state S_0 via phosphorescence is spin forbidden, these excited state usually exhibit significantly prolonged radiative lifetimes compared to singlet excited states. The lifetime of the singlet excited state S_1 results from the inverse of the sum over all depletion pathway rate constants (Eq. II.1).

$$\tau_{S_1} = \frac{1}{(k_F + k_{nr}^1 + k_{ISC})} \tag{II.1}$$

The same is valid for the lifetime of the triplet excited state, were k_{nr}^2 is attributed to multiphonon relaxation pathways and k_{ph} accounts for relaxation by emission of a photon (Eq. II.2).

$$\tau_{T_1} = \frac{1}{(k_{ph} + k_{nr}^2)} \tag{II.2}$$

In general, one expects transition metal complexes to follow KASHA's rule, which implies that emission is only observed from the energetically lowest excited state. In late transition metal complexes with inaccessible ligand field states (LF), efficient spin-orbit coupling usually leads to fast ISC processes resulting in the population of the energetically lowest triplet excited state T_1. Nevertheless, the spin-orbit coupling constant depends on the metal atom and especially for first-row transition metals it is not always sufficiently high to provide efficient ISC. Additional to the multiplicity of an excited state, the symmetry of this state is also vital to its photophysical and photochemical behaviour. In an absorption spectrum, three different kinds of transition bands leading to three different excited states can be found. The kind of state which is the lowest in energy will determine the emission behaviour of the complex. The first form of transitions are symmetry forbidden transitions between two orbitals with strong d-orbital character which lead to the population of the so-called ligand-field states. The corresponding absorptions show only small extinction coefficients of up to 1000 $M^{-1}cm^{-1}$. The population of these metal centred states does not lead to a charge redistribution between metal and ligand, but may give rise to excited state reactions such as ligand dissociation, isomerization or substitution.[12]

The second kind of transitions take place between two MOs that are ligand based. One commonly observed transition of this kind are $\pi \rightarrow \pi^*$ transitions which cause intense absorption bands in the ultraviolet to blue spectral range. Since these bands are purely ligand based, the nature of the metal, or the oxidation state of it, have only a minor influence on them.

The third, and in many photo-related applications most relevant kind, are the so-called charge-transfer transitions. The two commonly observed charge-transfers are a transition from a metal centred orbital to a ligand centred one, which is called a metal-to-ligand charge transfer (MLCT), or a so-called ligand-to-metal charge transfer (LMCT), in which an electron is transferred from a ligand orbital to a metal orbital. They are symmetry allowed transitions of an electron between a metal centred and a ligand centred orbital, and therefore rather intense absorption bands are found. These transitions cause a change in the electron distribution within the complex and result in a formally reduced or oxidized metal center, depending on the direction of electron transfer.

Which of these three possible excited states are relevant for the photophysical behaviour of a complex depends strongly on the nature of the ligand as well as the metal itself. In the

following sections the excited state behaviour of the two kinds of metal centres relevant for this thesis will be discussed.

2.1.2 Excited State Behaviour of First-Row d^{10} Metal Complexes

In the case of d^{10} metal complexes, all five d-orbitals are fully occupied, hence no ligand field transitions or ligand-to-metal charge transfers are observed, leaving MLCT and ligand-centred transitions (LT). The d^{10} metal complexes investigated in this thesis have the coordination number 4, and are expected to be tetrahedral. Intra-ligand transitions often occur at higher energies than MLCT transitions, leaving the MLCT state as the lowest excited state. The excitation of an electron from a metal-centred orbital to a ligand-centred π^* orbital leads to a formally reduced ligand and oxidized metal center. Consequently, in the excited state, the metal center can be considered a d^9 metal, which prefers a square-planar coordination geometry over a tetrahedral one. This usually leads to a fast flattening of the complex upon excitation.

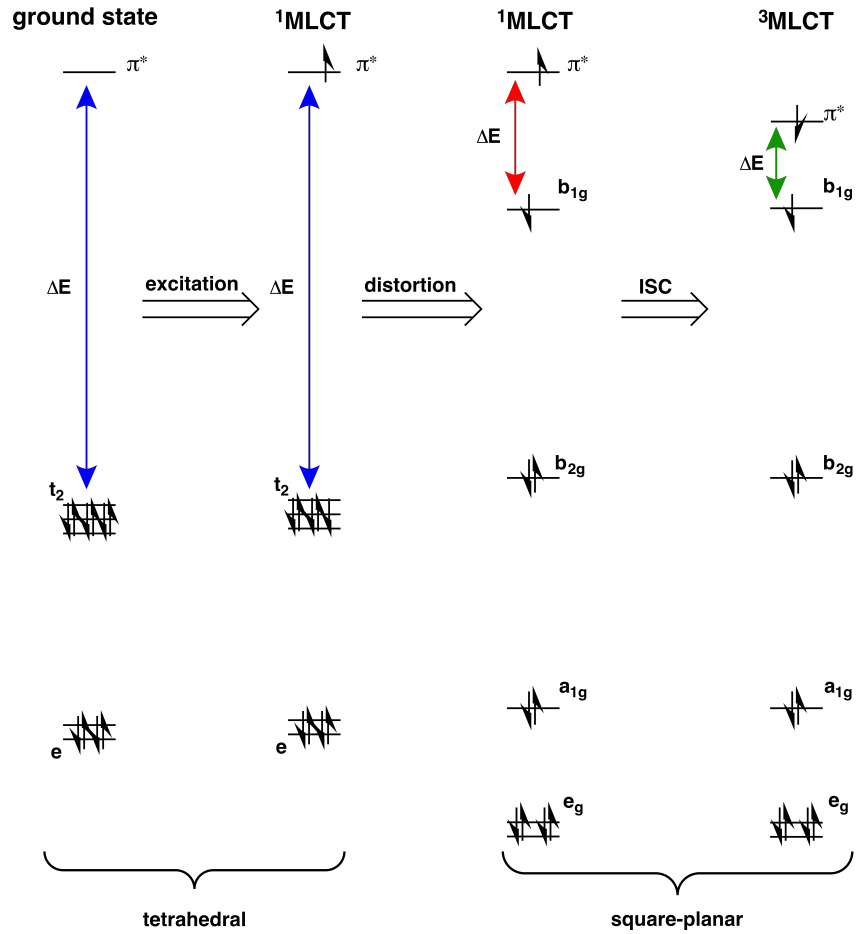

Figure II.3: Simplified Jablonski diagram illustrating the distortion of the coordination geometry in a d^{10} metal complex upon excitation. Intersystem crossing is assumed to occur significantly slower than the distortion.

Figure II.3 illustrates this process under the assumption that intersystem crossing occurs slower than the geometrical distortion, as was shown by IWAMURA et. al. for a series of copper(I) complexes.[13] First, an electron is excited from a t_2 orbital into the π^* orbital of the ligand, giving the ^{1}MLCT. The energy (ΔE) needed for this transition is marked with a blue arrow. If the lifetime of this state is rather short and fluorescence is faster than the geometrical distortion, emission of light with the energy ΔE shown in blue is observed. This would lead to the observation of a small to moderate STOKES shift. If the distortion towards a square-planar geometry is faster than relaxation to the ground state, the energy gap between the excited ^{1}MLCT and the t_2 is significantly decreased (red arrow), resulting in a significant STOKES shift of the observed emission. This is caused by a change of the d-orbitals in relative energy and the resulting decrease of the energy gap ΔE. The energy of the emitted light (green arrow) is even lower if intersystem crossing to the energetically lower lying ^{3}MLCT is faster than relaxation to the ground state. This leads to emission maxima that are commonly located in the red part of the visible spectrum and makes the design of blue emitters much more complicated. Additionally, a decrease of the energy gap leads to an increase in non-radiative relaxation processes according to the energy gap law and therefore to significantly shorter lifetimes and luminescence quantum yields. Hence, prevention of distortion towards square-planar structures is vital to the design of efficient d^{10} metal based luminophores. One way to achieve this is the design of interlocked structures via introduction of bulky substituents to rigid ligands.[14]

Copper(I) complexes are a prominent class of d^{10} metal based luminophores and photosensitizers, which are known to exhibit some unusual photophysical behaviours. The major cause of these phenomena, such as thermally activated delayed fluorescence (TADF), is the much smaller spin-orbit coupling constant which is characteristic of first row transition metals. In recent years, researchers started to exploit the unique TADF process to carefully tailor the emission properties of copper complexes to the need of OLED devices. TADF allows for short lived luminescence with high quantum yields, which is essential for the design of efficient OLED devices.[15] A TADF process, in general, is a singlet-harvesting process since the emission originates from a singlet excited state. This is in contrast to the well established triplet-harvesting in which the emission originates from a short lived triplet excited state, which is only accessible in late transition metal complexes with high spin-obit coupling constants. Figure II.4 shows a simplified JABLONSKI diagram which illustrates the TADF process in a d^{10} metal complex. The complex is first excited to its singlet excited state S_1, followed by relaxation to the triplet excited state T_1.

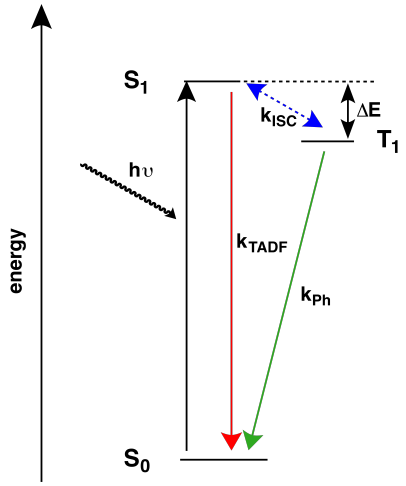

Figure II.4: Simplified JABLONSKI diagram illustrating thermally activated delayed fluorescence (TADF) in a d^{10} metal complex.

TADF was observed in compounds with energy differences ΔE between these two states ranging from 370 - 1000 cm^{-1}. This small energy difference ΔE allows for the S_1 to be thermally populated from the T_1 state. Due to a small spin-orbit coupling constant the transition from T_1 to the ground state S_0 is unlikely and phosphorescence with very long lifetimes is only observed at low temperatures when thermal population of S_1 does not occur. At room temperature, intersystem crossing is much faster than k_{Ph} and fluorescence from S_1 to S_0 occurs readily since the transition is spin-allowed. This leads to a prolonged fluorescence lifetime and high quantum yields, since singlet, as well as triplet excitons are harvested.[16]

2.1.3 Exploiting the Excited State of d^6 Metal Complexes

In contrast to d^{10} metal complexes, d^6 metal complexes, in addition to MLCT transitions, also allow for LMCT and LF transitions to occur since the e_g orbitals are unoccupied in the case of low spin complexes. In complexes of late transition metals, like ruthenium, rhenium or molybdenum, with ligands that have energetically low lying orbitals (e.g. π^* orbitals), ^{3}MLCT states usually dominate the excited state behaviour. In the case of first-row transition metals such as iron or possibly chromium, energetically low lying ligand field states might cause rapid relaxation of the excited states, preventing efficient light emission with sufficiently long lifetimes.

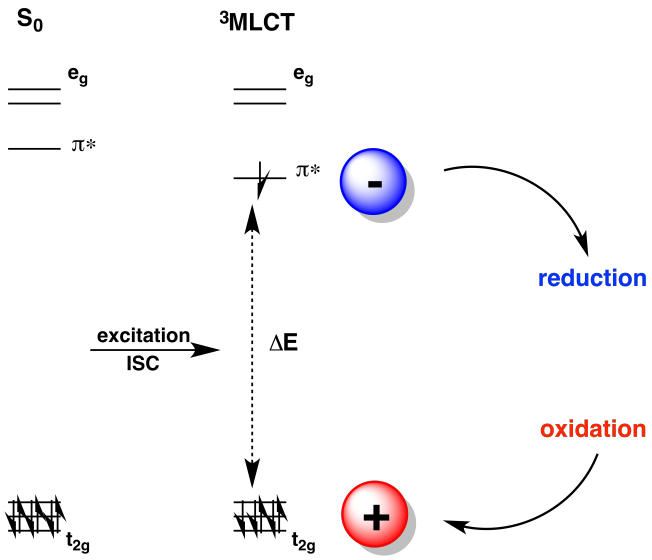

Figure II.5: Simplified JABLONSKI diagram illustrating the formation of an intramolecular charge separated state upon MLCT excitation of a octahedral d^6 metal complexes.

Octahedral d^6 metal complexes are commonly employed to drive electron transfer reactions from the excited state, since they do not undergo strong distortions and therefore offer relatively long excited state lifetimes. Theses are necessary to allow electron transfer kinetics to compete with other deactivation processes (vide supra). This is especially important for bimolecular reactions, since their kinetics tend to be limited by the diffusion-controlled formation of an encounter complex.[17] This part will focus on complexes in which the lowest excited state is a ^{3}MLCT state.

Upon excitation, an electron is transferred from a t_{2g} orbital to a ligand-centred orbital, such as π^*, which is lower in energy than the unoccupied e_g orbitals forming the excited ^{1}MLCT state (Fig. II.5). This process is followed by rapid intersystem crossing to the excited ^{3}MLCT state. As mentioned before, a MLCT state can be considered to be an intramolecular charge separated state consisting of a formally oxidized metal center and a formally reduced ligand.[18] Hence, the oxidation as well as the reduction of the excited metal complex proceeds by ΔE easier than in the ground state. The connection between the ground state and the excited state redox properties is most apparent in a LATIMER diagram as shown for $[Ru(bpy)_3]^{2+}$ (Fig. II.6).

The excited state oxidation potential (red value) can be calculated by subtracting the zero-phonon energy (2.1 eV for $[Ru(bpy)_3]^{2+}$) from the ground state oxidation potential. Analogously, the excited state reduction potential (blue value) is obtained by adding the zero-phonon energy to the ground state reduction potential. Thus, a metal complex in its excited charge separated state is simultaneously a stronger reductant as well as a stronger oxidant than in its ground state.

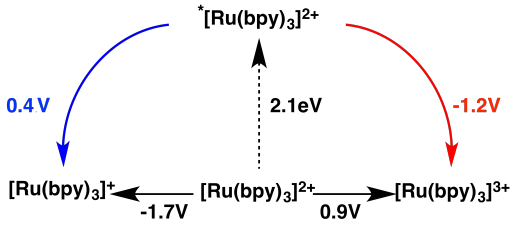

Figure II.6: The LATIMER diagram of $[Ru(bpy)_3]^{2+}$. Redox potentials are reported versus $Fc^{+/0}$ in acetonitrile.[19]

There are two options to tune the excited state redox potential to one's needs. One, the energy gap between the ground state and the ^{3}MLCT excited state can be varied, or second, the ground state potential can be altered by variation of the ligand or the metal. Increasing the energy gap will result in a blue shift of the excitation energy, which is unfavourable for photocatalytic applications. Therefore, the excited state redox potential is commonly altered by the manipulation of the ground state redox potentials.

2.2 Photoinduced Electron Transfer Catalysis

Nowadays, the term photocatalysis is used for a wide range of photo-related processes, such as organic reactions that are triggered by light, reactions that involve activation by light induced energy transfer or redox reactions proceeding from the excited state.
This thesis focuses on photoinduced electron transfer reactions, for which three different classes can be distinguished.[20] The first class are reactions in which the substrate forms a catalytic species upon light irradiation and the reaction then proceeds via a chain reaction without further irradiation. In the second class, the active catalyst is formed upon light excitation but requires no more photons to drive the catalysis. The photocatalytic reactions studied in the course of this thesis belong to the third class, redox photosensitization. This third class describes systems in which an excited photosensitizer transfers an electron to the substrate which then undergoes multiple step transformations to the desired product. In one of these subsequent steps the photosensitizer is reformed, either by a reaction intermediate or by a sacrificial reagent and re-enters the catalytic cycle.
From a mechanistic point of view this process is an outer-sphere electron transfer mechanism (Fig. II.7).

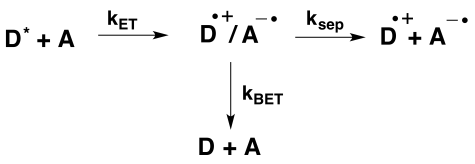

Figure II.7: Simplified outer-sphere mechanism for excited state electron transfer.

The excited donor species D* forms an encounter complex with the acceptor molecule A followed by electron transfer (ET) to give $D^{\bullet+}$ and $A^{\bullet-}$. These two ground state species can now separate to give the redox products $D^{\bullet+}$ and $A^{\bullet-}$, which perform further reactions, or back electron transfer (BET) occurs, yielding the ground state species D and A.[21] After electron transfer occurrs, the separation of the ion pair (k_{sep}) is in competition with back electron transfer (k_{BET}). The rate constant for ET(k_{ET}) and BET (k_{BET}) depends on several factors, such as the driving force, electronic coupling between A and D, reorganization energy of the solvent and the distance between A and D. These dependencies are described by the MARCUS equation.[22]

An additional factor influencing the rate of electron back transfer kinetics is the spin multiplicity of the excited state from which electron transfer occurs. This was primarily discussed in context of organic redox photosensitizers, but is relevant for any system that might operate from an excited singlet state (e.g. first-row transition metal complexes).[23]

Figure II.8 illustrates the different steps involved in a photoinduced oxidation reaction. The ground state catalyst is excited to its first excited singlet state ^{1}cat* via absorption of a photon (yellow arrow). If there is significant spin-orbit coupling present in the catalyst complex, fast intersystem crossing to the excited triplet state ^{3}cat* occurs. An encounter complex with the ground state substrate (sub) is formed, and electron transfer occurs from the HOMO of the substrate to the singly occupied HOMO of the catalyst. In the resulting triplet contact ion radical pair (TCRIP), cage escape (green arrow) and formation of the desired free ions is much faster than the undesired back electron transfer (dashed blue arrow) which yields the initial catalyst and substrate. These favourable kinetics result from the spin forbidden character of the back electron transfer reaction (BET) (dashed red arrow).

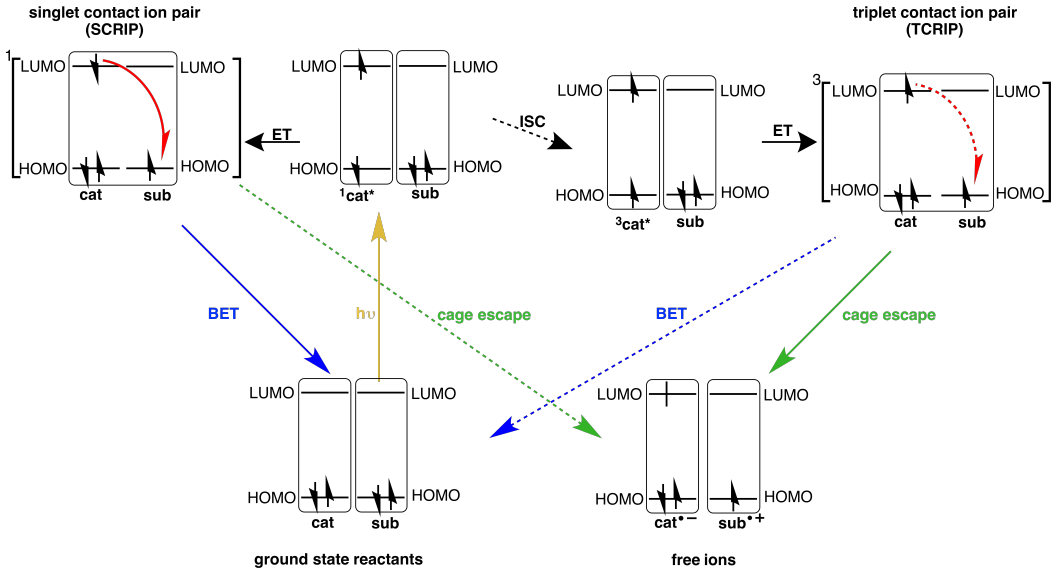

Figure II.8: Back electron transfer (BET) and cage escape in singlet and triplet contact (radical) ion pairs.

Although the excited singlet state ^{1}cat* is more oxidizing than the triplet state ^{3}cat*, its employment might lead to less efficient reactions, since the back electron transfer in the singlet contact radical ion pair (SCRIP) is spin allowed (red arrow) and effectively competes with the desired cage escape (dashed green arrow). The same procedure is applicable if the catalyst is oxidized by the substrate.[23]

Three different cases of photoinduced electron transfer catalysis can be distinguished. Since the process is related to electrochemical transformations, which also rely on single electron transfers (SET), one can observe two reactions that perform either an overall reduction reaction or an oxidation reaction. In the first case the catalysis is considered to be net reductive (Fig. II.9, blue box), in the second to be net oxidative (Fig. II.9, red box).[23]

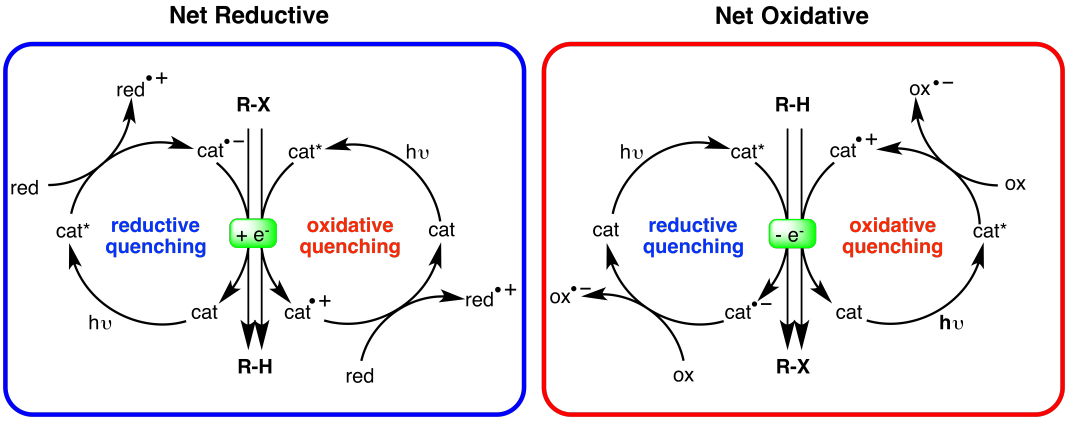

Figure II.9: Catalytic cycles for net reductive and net oxidative photoinduced electron transfer reactions. Reproduced from ref. [23].

Both kinds of reactions can either be driven via a reductive quench cycle or an oxidative quench cycle. In a reductive quenching process, the excited state of the catalyst cat* is quenched by electron transfer to the catalyst, yielding the reduced catalyst in its ground state cat$^{\bullet-}$. In case of a net oxidative process, the electron utilized in a reductive quenching event might originate from the substrate. In a net reductive process, the electron donor in a reductive quenching cycle is a reactant that is not related to the reaction itself, such as a sacrificial agent. The indirect generation of a strong ground state reductant from an excited catalyst can be used to drive reactions with relatively small driving force, which do not occur on the time scale of excited state electron transfers.[12]

If the excited state of the catalyst is quenched in a process in which it is oxidized to its ground state cat$^{\bullet+}$, the process is called an oxidative quench cycle. This process is commonly used to drive catalytic reduction reactions in which the electron transfer to the substrate proceeds on the time scale of the excited state lifetime. In order to perform oxidative reactions with small driving forces, one uses a similar flash-quench approach as already described for slow reductions. The excited state of the catalyst is oxidatively quenched by a suitable electron acceptor, giving the oxidized ground state of the catalyst. The oxidized catalyst can now be

re-reduced by the substrate on much longer time scales.[12]
The net reductive reaction, as well as the net oxidative reaction, are not redox neutral and therefore the reformation of the initial catalyst requires the addition of an external electron donor or acceptor, respectively. This can be achieved by either adding a sacrificial electron donor/acceptor, or by coupling the reaction to a second reaction of complementary redox character - similar to the design of an electrochemical cell.

2.2.1 Electron-Catalyzed Reactions

The third category of photoinduced electron transfer catalyzed reactions are redox neutral reactions. These kinds of reactions are initiated by either electron injection, or abstraction from the catalyst, followed by a reaction cascade in which at some point the catalyst is reformed by a reaction intermediate.

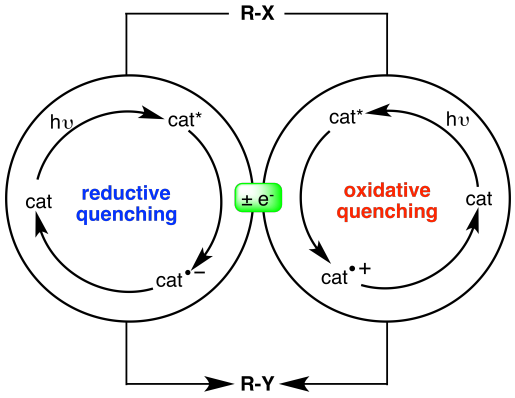

Figure II.10: Schematic illustration of a redox neutral photoinduced electron transfer catalyzed reaction. Reproduced from ref. [23].

Such a redox neutral process is illustrated in Figure II.10. This process can either be initiated via oxidative or reductive quenching of the excited catalyst cat*, which forms then the oxidized ($cat^{\bullet+}$) or reduced ($cat^{\bullet-}$) ground state species, respectively. The initial catalyst is regenerated from a reverse redox process between the oxidized/reduced catalyst and a reactive intermediate present in the catalytic cycle. Hence, these processes do not rely on any sacrificial agent but are indeed closed catalytic cycles, they can be considered as photocatalytic versions of electron-catalyzed reactions.[24] This class of reactions is well suited to be performed in a photocatalytic fashion.

Base-Promoted Homolytic Aromatic Substitution

The analogy between acid/base and redox catalysis was pointed out by Studer and Curran in 2014.[24] One electron-catalyzed reaction which should be discussed in more detail is the base-promoted homolytic aromatic substitution (BHAS).[25] This reaction class includes the formation of biaryls via intra- and intermolecular coupling of arenes with aryl halides, as well

as the formation of aryl-substituted alkenes via a HECK-type coupling between aryl halides and olefins.[26–36] These reactions are less common to be performed under light irradiation.[37–40] To the best of my knowledge, only one example in which an transition metal catalyst was employed is reported.[41] In the context of this thesis, a related reaction in the presence of moderately strong base was used as a photocatalytic benchmark reaction.

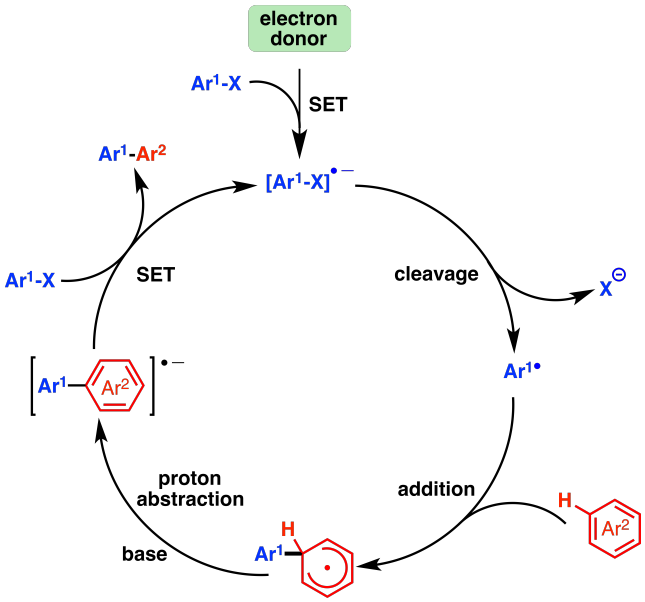

Figure II.11: General mechanism of a base-promoted homolytic aromatic substitution (BHAS). Reproduced from ref. [42].

In a non-photocatalytic system, a BHAS reaction is usually performed with three equivalents of KO^{t}Bu and a catalytic amount of ligand such as phenanthroline at elevated temperatures (80-155°C).[25] A general mechanism of a BHAS reaction is shown in Figure II.11. Although the exact mechanism for the initial SET unknown, the following steps of the radical chain mechanism are well established.[42] Initial SET transfer to the aryl halide gives the aryl halide radical anion [Ar^1-X]$^{\bullet-}$, which dissociates to the corresponding halide anion and aryl radical.[43] The aryl radical then adds to the arene, yileding the neutral biaryl radical. Since KO^{t}Bu is a strong base, proton abstraction is rapid and the biaryl radical anion is formed. This radical anion performs a second SET to an aryl halide, forming the biaryl product Ar^1-Ar^2 and another aryl halide radical anion, which re-starts the catalytic cycle.
In case of a photocatalytic experiment, the BHAS reaction will proceed via a different mechanism than the afore described radical chain mechanism. A significant advantage of a catalytic photoinduced electron transfer reaction pathway employing a photocatalyst of sufficient reduction power is the possibility to run the reaction at room temperature and to avoid an excess of very strong base. This approach extends the scope of the reaction to substrates that are not stable at elevated temperature or under very basic conditions. Additionally, one is no longer limited to polar solvents since KO^{t}Bu can be substituted by a weaker organic base

that is soluble in apolar solvents.

2.3 Challenges in the Design of Strong Photoreductants

In recent years, photoredox catalysis developed into a major research field. Besides the development of new purely organic photoredox catalysts that no longer depend on expensive and toxic metal complexes[23,44], and the design of new reaction pathways to facilitate more sophisticated reactions[45,46], a lot of investigations are set on exploring new areas for potential applications (e.g. synthesis of macro molecules and polymers[47,48]). Especially in synthetic strategies aiming at strained molecules with sensitive functionalities, photoredox catalysis developed into a versatile tool of organic chemists, as it provides significant chemical energy under very mild and well-controllable conditions.[49]

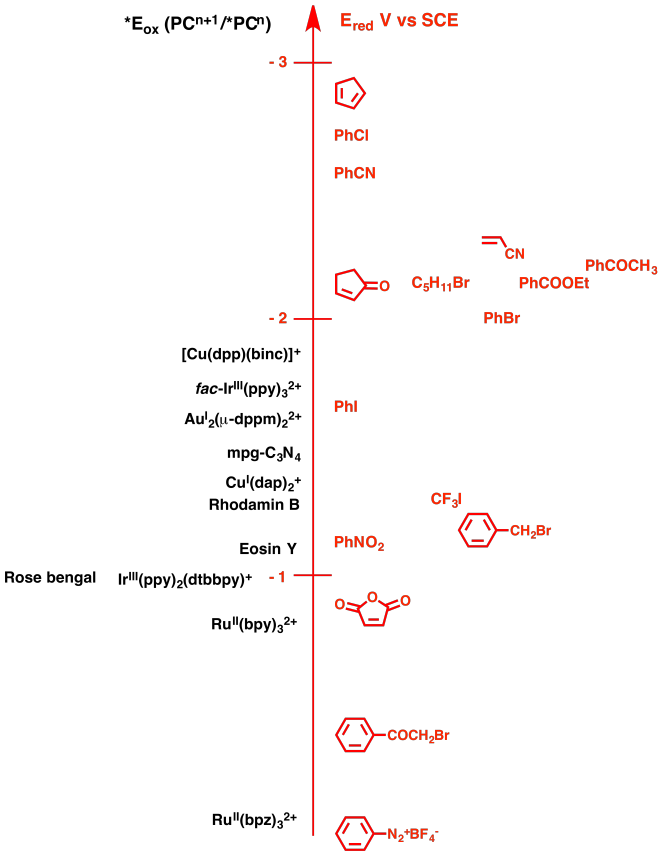

Figure II.12: Selected reduction potentials of organic molecules and excited state oxidation potentials of common photocatalysts (PCs). Reproduced and modified from ref. [50].

One remaining challenge in the design of photocatalysts is the realization of sensitizers that are powerful reductants in the excited state. Strong photoreductants are employed in e.g. atom transfer radical additions (ATRA), which describes the addition of a halocarbon to a

double bond by formation of a C-C and C-halogen bond.[51] Since these reactions are initialized via a carbon-halogen bond cleavage, photocatalysts with rather low excited state oxidation potentials are required.[50] Figure II.12 gives a qualitative overview of the excited state oxidation potentials of commonly used photocatalysts and the reduction potentials of organic molecules.
It is easily seen that a variety of organic molecules such as acetophenone are out of the application range of well-established reducing photocatalysts (e.g. $[Ir(ppy)_3]$). Organic photocatalyst are usually weak to intermediate strong photoreductants, except they are used in a two excitation process which mimics the Z-scheme of photosynthesis.[52] The majority of strongly reducing catalysts are based on precious metals (Ir, Au).
The development of strongly reducing photocatalysts is desirable for a wide range of applications, to do so there are two general options:

1. Increasing the HOMO-LUMO gap of the complex
2. Decreasing the ground state oxidation potential

Since an increase of the HOMO-LUMO gap inevitably leads to an unfavourable blue shift of the ^{1}MLCT absorption band, as discussed earlier in this chapter, the more promising approach is a decrease of the ground state potential. This may be achieved in two different strategies. The commonly applied approach is based on the introduction of electron donating groups to the ligand scaffold, which results in the desired cathodic shift of the oxidation potential. This is advantageous in terms of relatively simple system design, as the general chemical and photophysical behaviour are only weakly affected. On the other hand, the possible alteration of the potentials is still limited to a relatively narrow range around the potential of the parent complex. The second strategy is the alteration of the metal centre to an isoelectronic metal in a lower oxidation state. Since a change of the metal centre basically implies the development of a completely new catalyst, this approach allows for much bolder alterations in the relevant properties, but also requires a more advanced system design. Facing the additional challenge of abandoning precious metals as an inevitable part of strong photoreductants, a low-valent earth-abundant d^6 metal as a suitable new analogue to rhenium(I), ruthenium(II) and iridium(III) has to be identified.
The elements of the transition metal group 6 meet the above listed requirements. In the oxidation state 0, they are isoelectronic to elements of the transition metal group 8 in the oxidation state II (iron to osmium). Molybdenum(0), which is the direct analogue of ruthenium(II), is 10,000 times more earth-abundant than ruthenium.[4] This translates to a difference in price by a factor of approx. 100 on the world market.[3]
In order to obtain stable metal(0) complexes, it is necessary to stabilize the high electron density of the metal center by introducing ligands that are strong π-acceptors. These ligands will help to stabilize the metal in its zero-valent state via π-backbonding. Suitable ligands would, for example, be carbonyls or isocyanides. In contrast to carbonyls, isocyanides have

the advantage that they can be introduced to larger ligand scaffolds, like aryl systems, which have energetically low lying ligand orbitals to allow for MLCT transitions to occur.

2.3.1 Photophysics of Hexakis(aryl isocyanide) M(0) complexes (M: Cr, Mo and W)

Besides the economical advantages, studies from the 1970s showed that homoleptic hexa(aryl isocyanide) group 6 metal complexes exhibit favourable photophysical properties, such as ^{1}MLCT absorption bands in the visible range of the spectrum, as well as, at least in the case of tungsten complexes, acceptable excited state lifetimes of around 70 ns.[5,6,53] The prospect of tungsten(0) hexa(aryl isocyanide) complexes being potential candidates for strong photoreductants was recently re-emphasized by Sattler et al..[7,8] The major obstacle preventing the application of these promising complexes in photocatalytic reactions is their tendency to undergo photosubstitution reactions. This tendency decreases when moving from 3d (Cr) to 5d (W) metals. In order to gain a better understanding of the operating photophysical mechanisms a short summary of the relevant differences between the complexes of chromium(0), molybdenum(0) and tungsten(0) in terms of their photophysical properties is given in the following sections.

Hexakis(aryl Isocyanide) Tungsten(0) Complexes

After Sattler et al. reported hexakis(aryl isocyanide) complexes with oligoaryl backbones to show significantly prolonged excited state lifetimes (up to 1.7 μs) and high quantum yields (up to 42%), Kvapilová et al. published a study investigating the nature of the excited state of these complexes (Fig. II.13) by a combination of computational and experimental methods.[54]

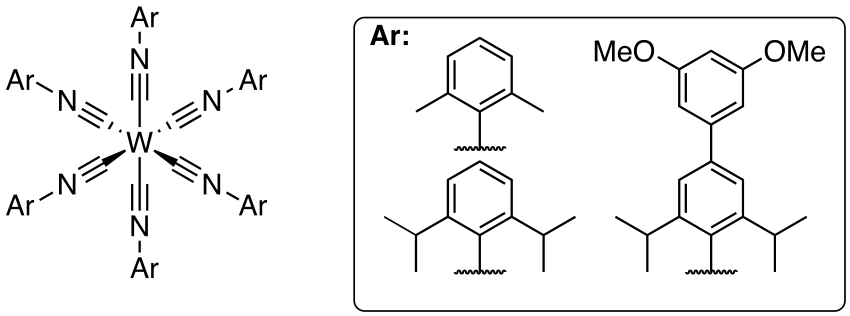

Figure II.13: Molecular structure of the complexes investigated in reference [54].

The complexes were found to be pseudooctahedral and exist in two configurations, in which the axial aryl rings stand either co-planar or orthogonal to each other. The ratio between these two configurations in solution determines the intensity distribution of the observed electronic transitions in the absorption spectrum. Both conformers exhibit transitions that

are similar in their character but shift in energy depending on the conformer. For each compound they found a set of three degenerate HOMO orbitals, which have 5dπ and π^* (C≡N) character. A corresponding set of three LUMO orbitals was identified to have π^* (C≡N)/π(N-C(Aryl))/π^*(Aryl) character. In general, the excited state properties are rather complex. Typical d-d transitions are expected to occur at very high energies and to be therefore negligible in the excited state behaviour. Beside this, all kinds of transitions like MLCTs into C≡N moieties or aryl rings, as well as $\pi\pi^*$ transitions within the ligands are likely.

ISC from an excited singlet state to the lowest excited triplet state proceeds in an ultrafast time regime (<200 fs). The populated triplet state was found to be localized along a molecular axis over two *trans* standing aryl isocyanide ligands. It contains contributions from $\pi\pi^*$ (C≡N -C), ligand-ligand charge transfer from the equatorial ligands to the axial ligand pair (LLCT), and MLCT. The MLCT occurs mainly to the two *trans* standing aryl rings and only very little to the isocyanide moiety. This leads to no significant weakening of the W-C bond, and hence no efficient ligand dissociation is observed. It was also shown that the increased delocalization of the excited electron over the extended π-system of oligoaryl ligands slows down the non-radiative decay, since it prevents pronounced excited state distortion.

The localization of the lowest excited triplet state has a very important implication for the design of bimolecular electron transfer reactions. Since the electron transfer will occur from the electron-rich axial aryl rings, an extension of the π-system combined with the introduction of bulky substituents will slow down the electron transfer kinetics, since the interaction between the excited state orbital and the oxidant is hampered. Also, in the design of molecular dyads and triads one needs to consider the axial charge distribution in the excited state to assure sufficient electron transfer rates.

Hexakis(aryl Isocyanide) Molybdenum(0) Complexes

While W(0) and Mo(0) hexakis(aryl isocyanide) complexes are luminescent at room temperature, Cr(0) hexakis(aryl isocyanide) complexes undergo ultrafast photosubstitution reactions. The difference in excited state behaviour between Cr(0) hexakis(aryl isocyanide) complexes and the corresponding W(0) and Mo(0) complexes challenged researchers for nearly 25 years. Early studies of Mann and Gray suggested that the photosubstitution in chromium complexes follows a dissociative pathway, whereas in tungsten and molybdenum complexes an associative pathways is operative.[5,6]

In 2002, Shaw et al. re-investigated the photochemical behaviour of [Mo(CNPh)$_6$].[53] First they found that the emission originates from a thermally equilibrated excited state, since no significant Stokes shift was observed and the luminescence quantum yield is independent of the excitation wavelength. They observed an excitation wavelength independent photosubstitution rate constant. Additionally, the quantum yield of the photosubstitution was also independent of the nucleophilicity of the nucleophile, as well as the concentration of it. From

these surprising results they excluded the afore-ascribed associative pathway. The photosubstitution proceeds rapidly and no reaction intermediates were observed in transient absorption spectroscopy. In combination with the independence of the excitation energy, this leads to the conclusion that photosubstitution occurs via population of ligand field states (LF) from the thermally equilibrated MLCT state, which has nearly no anti-bonding character itself. Since the LF states of the molybdenum complex are higher in energy than the ones of the chromium compound, photosubstitution is less favoured and luminescence is observed at room temperature.[53]
In the case of electron transfer reactions, they observed a pronounced excitation wavelength dependency. The electron transfer kinetics increase with decreasing excitation wavelength. This points to an electron transfer occurring from thermally non-equilibrated MLCT states, which is referred to as hot electron transfer. This hot electron transfer is in direct competition with vibrational relaxation to the thermally equilibrated excited state.[53]

Hexakis(aryl Isocyanide) Chromium(0) Complexes

Hexakis(aryl isocyanide) chromium(0) complexes exhibit no significant luminescence at room temperature, in analogy with isoelectronic polypyridine iron(II) complexes.[55,56] In both complex classes, this is attributed to energetically accessible LF states. The chromium compounds show photosubstitution kinetics that are independent of the sterical demand of the *ortho* substituents of the ligand. In combination with the independence of the photosubstitution rates of concentration and nucleophilicity of the nucleophile, this classifies this process as a dissociative one.[57]
Since electron-transfer reactions are observed upon light excitation, it can be concluded that these occur from a thermally non-equilibrated state, since photosubstitution was found to proceed on the ultrafast time scale (<20 ps). In contrast to the tungsten and molybdenum homologues, the quantum yields for photosubstitution, as well as electron transfer, depend on the excitation wavelength. While the quantum yield for photosubstitution decreases with increasing excitation wavelength, the quantum yield for electron transfer shows the reverse behaviour. This indicates that electron transfer originates from an excited state that is low in energy. Apparently, this state is not sufficiently populated upon excitation at higher energy. Resonance Raman experiments illustrated that strong geometrical distortions of the excited state occur upon excitation in the low energy part of the MLCT absorption band.[58] Additionally, the concentration dependence of electron-transfer reactions showed that these reactions do not occur from an excited state, but rather from an initially formed photoproduct.
These observations were rationalized by Shaw et al. under consideration of two kinds of excited states. The one at lower energy is reactive towards electron transfer reactions, whereas the ones at higher energies are apparently labile, and photosubstitution is favoured over

electron-transfer.[57]

The presence of these two states leads to two separate photochemical behaviours, of which one occurs at higher and the other at lower excitation energies. The process triggered with high energy excitation is charge neutral photosubstitution via a heterolytic cleavage of the Cr-CNAr bond. The second one is an electron-transfer mediated photosubstitution, which is initiated by a homolytic Cr-CNAr bond cleavage leading to a ligand radical anion, which then induces further electron transfer reactions. Based on these observations and their interpretation, Shaw et al. suggested the MO-Diagram of $[Cr(CNAr)_6]$ to be as shown in Figure II.14.[57]

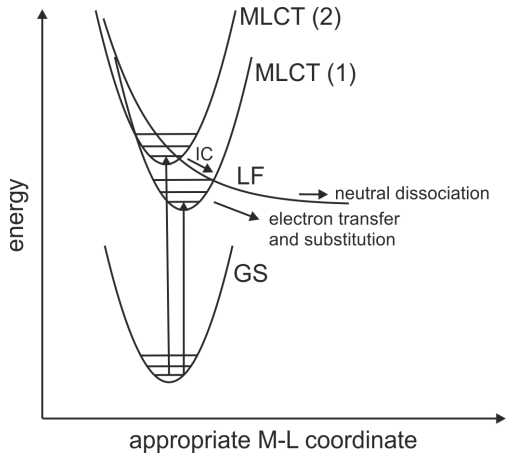

Figure II.14: Schematic potential energy curves of $Cr(CNAr)_6$, reproduced from ref. [57].

High energy excitation leads to population of the higher MLCT state (MLCT(2)), from which interconversion (IC) to lower ligand field states (LF) occurs. The LF states are expected to be much higher in energy than the MLCT states, but decrease rapidly in energy upon minor elongation of the Cr-C bond, which makes them accessible for IC processes. Population of these states results in ultrafast neutral ligand dissociation. If light of lower energies is used to excite the complex, the MLCT(2) is inaccessible, and the less energetic MLCT(1) is populated. Population of this state leads to significant excited state distortion, resulting in electron transfer to the ligand, followed by substitution reactions. The origin of the coupled electron transfer-substitution mechanism is not completely understood, but might be related to the strong distortion of the metal-isocyanide unit observed in the resonance raman experiments.[58]

2.3.2 Chelating Isocyanide Ligands

Isocyanide ligands are usually considered to be isolobal to CO, although they are stronger σ-donors and weaker π-acceptors.[59] This gives them the capacity to stabilize low oxidation state metal centers as well as higher oxidation states, whereas carbonyls preferably stabilize low oxidation states. This apparently minor difference in their electronic properties has significant

impact if one aims to alter their σ-donor/π-acceptors capacity.[60] Their main advantage over CO ligands is that they can easily be tuned or extended to chelating systems by modifying the (aryl) backbone.

The extent of π-backbonding in an isocyanide complex is reflected in the shift of the C≡N stretching vibrational band within the complex compared to the free ligand. Since efficient π-backbonding populates an antibonding π^* orbital, the C≡N bond is weaker and the vibrational band shifts to lower wavenumbers.[61] In the case of a charged metal center, the σ-donation is dominant and a smaller shift, or even a shift in the opposite direction, might be observed. In general, chelating ligands are known to enhance the robustness of complexes by prevention of ligand loss or nucleophilic attacks on the metal center, as well as reducing the vibrational modes of freedom. In the case of isocyanides, the linear geometry of these moieties makes the design of ligands with suitable bite angles rather challenging. Figure II.15 shows some examples of chelating isocyanides reported in literature.[62–70]

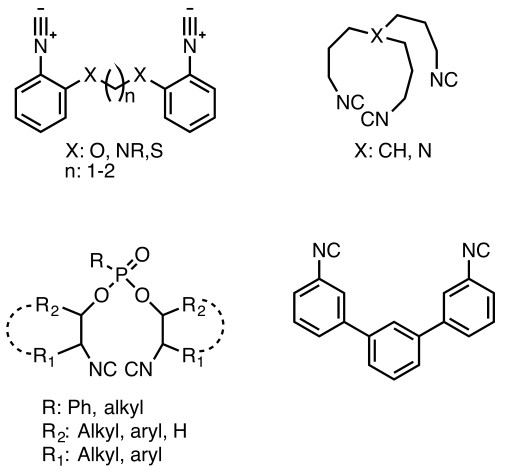

Figure II.15: Examples of chelating isocyanide ligands.[62–70]

Due to the challenging geometry of the isocyanide unit, the separation between the coordination sites within the chelating ligand needs to be equivalent to at least seven carbon atoms.[71] The resulting rather large chelate rings lead to a less pronounced chelate effect in these compounds. This gives rise to an efficient competition between the formation of polynuclear complexes via bridging isocyanide units and formation of chelate complexes. Which product is favoured can be controlled by careful adjustment of the reaction conditions. The relatively small tendency to actually form chelate complexes lead to the development of ligands with primarily flexible backbones, to allow for fast ring formation with little steric hindrance. To the best of my knowledge, only one chelating isocyanide ligand with a fully aromatic scaffold has been reported (Fig. II.15, lower right side).[70] In terms of synthetic strategies, the formation of chelates is favoured if a metal precursor with labile ligands such as THF, acetonitrile or COD is used. This allows for fast ligand exchange reactions, favouring intramolecular chelate

ring closure over intermolecular bridge formation.

2.4 System Design

Although Sattler et al. were able to prepare stable, brightly luminescent tungsten(0) complexes by using monodentate oligoaryl isocyanide ligands, accessing luminescent molybdenum or chromium complexes strongly relies on the shielding of these metal centres against nucleophilic attacks in their oxidized states, as well as the prohibition of fast ligand dissociation processes from the excited-state. Therefore, zero-valent metal complexes bearing chelating isocyanide ligands with rigid, conjugated scaffolds were designed (Fig. II.16).

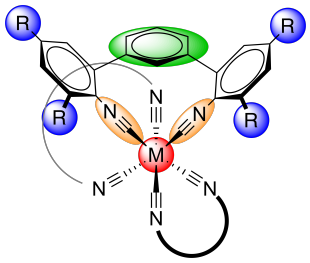

Figure II.16: General design of a homoleptic bis(isocyanide) complex with a low-valent metal centre. The different colors indicate relevant structural elements.

The challenging sterical demands of the isocyanide units (orange) can be met with a 1,3-bis(2-arylisocyanide) benzene scaffold. The chelate formation induces a torsion between the chelating aryl rings and the backbone aryl ring (green). In general, it is possible to control the extent of conjugation over the full ligand via variation of the bite angle, which is determined by the backbone (green). The substituents on the ligand scaffold (blue) are crucial to the photophysical performance of the complexes, since they are intended to protect the metal against attacks of potential ligands and therefore are of key importance to achieve robust and emissive zero-valent metal complexes. These kinds of ligands should be applicable to different metal centres (red) in a wide range of oxidation states, since isocyanides act as σ-donors as well as π-acceptors.

The combination of easily accessible modifications on several sides of the ligand scaffold, as well as the wide application potential, makes these a very intriguing ligand class. In order to access earth-abundant luminophores and photocatalysts, different ligands of this concept were introduced to zero-valent d^6 metals, as well as first-row transition metals.

III Results

3.1 d^6 Metal Complexes Bearing Tetramethoxy-Bipyridine Ligands

Many challenging reduction reactions would be favoured to be light driven, like CO_2 reduction or even reactions relevant to organic synthetic chemistry. As already discussed in Chapter 2.3, it is rather challenging to obtain photosensitizers that exhibit sufficient reduction power to drive these kind of reactions, while at the same time remaining chemically robust. The established approach to this challenge is the introduction of electron donating groups to the ligand backbone. Following this approach the following paper was published during the course of these PhD studies:

- Büldt, L. A.; Prescimone, A.; Neuburger, M.; Wenger, O. S. "Photoredox Properties of Homoleptic d^6 Metal Complexes with the Electron-Rich 4,4',5,5'-Tetramethoxy-2,2'-bipyridine Ligand" *Eur. J. Inorg. Chem.* **2015**, *28*, 4666-4677.

In order to access d^6 metal-based photosensitizers with pronounced reduction power, 4,4′,5,5′-tetramethoxy-2,2′-bipyridine was synthezied via a new synthetic route and used the first time as a ligand in homoleptic Fe(II), Ru(II) and Os(II) complexes (Fig. III.1).

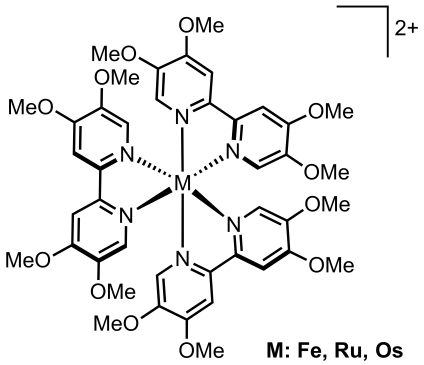

Figure III.1: Molecular structure of the investigated complexes.

The ^{1}MLCT absorption bands around 450 nm of the obtained complexes are similar to one another and reversible single-electron oxidation waves were found for all complexes in cyclic voltammetry experiments. The ground state oxidation potentials shifted by approximatly 0.4 V compared to the unsubstituted bipyridine parent complexes. Both, the ruthenium as

well as the osmium complex, showed ^{3}MLCT emission in aerated and deaerated acetonitrile solutions at room temperature with lifetimes < 100 ns.
From low temperature emission spectroscopy we concluded that the energy of the ^{3}MLCT excited state is similar to the corresponding parent complex. This leads to an excited state oxidation potential of -1.6 V vs $Fc^{+/0}$ for the ruthenium and -1.7 V vs $Fc^{+/0}$ in case of the osmium complex.
The reduction power of the excited state of the ruthenium complex was further investigated by Stern-Volmer experiments using 1-chloro-4-nitro-benzene as a moderately poor electron acceptor. The electron transfer proceeds with kinetics close to the diffusion limit in acetonitrile (k_q: 4.8×10^9 $M^{-1}s^{-1}$) and exceeds the rate constant obtained with $[Ru(bpy)_3]^{2+}$ by a factor of 600.
In order to access even more demanding reactions such as the reduction of acetophenone, which exhibits a reduction potential similar to CO_2, one could employ proton-coupled electron transfer reactions. In case of acetophenone a proton and electron are transferred to the keto function in concerted fashion, avoiding charged intermediates and therefore lowering the energy demand of the process. Since this strategy relies on acidic media, one has to ensure the acid stability of the photosensitzer, which turns out to be a rather challenging task with electron donating substituents on the ligand backbone.
The ruthenium tetramethoxy-bipyridine complex proved to tolerate acidic media and gave a quenching constant of 6.6×10^7 $M^{-1}s^{-1}$ in Stern-Volmer experiments.
In this study we were able to establish a ruthenium-tris(bipyridine) complex, which acts as a strong and robust photoreductant even in acidic media. This allows to access light-triggered, challenging PCET reactions, like the proton coupled reduction of acetophenone.

Author Contributions

- L. A. B. carried out the synthesis, data analysis and contributed equally to the preparation of the manuscript.
- A. P. and M. N. provided the crystal structures.
- O. S. W. made the molecular design and contributed equally to the analysis of data as well as their interpretation and the preparation of the manuscript.

EurJIC European Journal of Inorganic Chemistry
ChemPubSoc Europe
FULL PAPER

DOI:10.1002/ejic.201500670

Photoredox Properties of Homoleptic d^6 Metal Complexes with the Electron-Rich 4,4′,5,5′-Tetramethoxy-2,2′-bipyridine Ligand

Laura A. Büldt,[a] Alessandro Prescimone,[a] Markus Neuburger,[a] and Oliver S. Wenger*[a]

Keywords: Photochemistry / Charge transfer / Electron transfer / Nitrogen heterocycles / N ligands

A synthetic procedure leading to 4,4′,5,5′-tetramethoxy-2,2′-bipyridine [$(MeO)_4$bpy] was developed, and the first three metal complexes with this ligand were synthesized. A few ligand precursor compounds, the final ligand, and its homoleptic iron(II) complex were characterized structurally by X-ray diffraction. The combination of cyclic voltammetry, optical absorption, luminescence, and transient absorption spectroscopy provided detailed insight into the electronic structure of the entire series of homoleptic Fe^{II}, Ru^{II}, and Os^{II} complexes. The ruthenium(II) complex is a more potent photoreductant than the $[Ru(bpy)_3]^{2+}$ parent compound by approximately 0.4 V as confirmed by ^{3}MLCT excited-state quenching experiments with a relatively mild oxidant, 1-chloro-4-nitrobenzene. In the presence of methanesulfonic acid in CH_3CN, the photoexcited $[Ru\{(MeO)_4bpy\}_3]^{2+}$ complex is able to undergo proton-coupled electron transfer (PCET) with acetophenone to yield a ketyl radical. Chemically robust and potent photoreductants are of interest for the phototriggering of electron-transfer reactions, for example, in photoredox catalysis, in dye-sensitized solar cells, in fundamental studies of (proton-coupled) electron transfer, or for the generation of solvated electrons.

Introduction

Complexes of d^6 metals with α-diimine ligands are a very well-investigated class of materials.[1] From a photophysical and photochemical perspective, ruthenium(II) and osmium(II) α-diimines are attractive owing to their relatively long-lived and emissive triplet metal–ligand charge transfer (^{3}MLCT) excited states in which the redox properties are drastically altered relative to the electronic ground state.[2] Cyclometalated iridium(III) complexes and rhenium(I) tricarbonyl diimines exhibit similarly favorable electronic structures in many cases.[3] Consequently, such d^6 metal complexes have found use in various applications, ranging for example from luminescent materials to sensors,[4] dyes for solar cells,[5] DNA intercalators,[6] and photosensitizers for electron- or energy-transfer processes.[7] Recently, these types of complexes have received significant attention in the context of photoredox catalysis and small-molecule activation.[8] Furthermore, electron-rich $[Ru(\alpha\text{-diimine})_3]^{2+}$ complexes have become of interest for the photogeneration of solvated electrons.[9]

As part of our research program on long-range electron tunneling and proton-coupled electron transfer (PCET) we were interested in robust d^6 metal–diimine complexes, which are potent electron donors in their long-lived ^{3}MLCT excited states.[10] The electrochemical potentials and MLCT energies of such complexes are commonly tuned by ligand variation. A very simple strategy is to introduce electron-donating or -withdrawing substituents,[1] and there has been much fundamental work on how such ligand modifications alter the electrochemical and photophysical properties.[11] The largest and most important ligand family in this context is based on the 2,2′-bipyridine (bpy) parent ligand. Numerous variants of bpy are known, and most of them are symmetrical 4,4′-, 5,5′-, or 6,6′-disubstituted ligands whereas tetrasubstituted versions are less common.[1] To the best of our knowledge, the 4,4′,5,5′-tetramethoxy-2,2′-bipyridine [$(MeO)_4$bpy] molecule, although reported in 1995 as part of a synthetic effort on pyridines,[12] has never been used as a ligand to any metal until now. Given the electron-donating nature of methoxy substituents and their high chemical robustness (for example, when compared to dimethylamino groups),[13] we anticipated d^6 metal complexes with comparatively low oxidation potentials that might be particularly potent reductants in their long-lived ^{3}MLCT excited states.

We report here an efficient new procedure for the synthesis of $(MeO)_4$bpy and present the first complexes made with this ligand. Specifically, we focused on the homoleptic complexes of iron(II), ruthenium(II), and osmium(II). Crystal structures of the free ligand, the $[Fe\{(MeO)_4bpy\}_3]^{2+}$ complex, and some ligand precursor molecules have been obtained. The electrochemical and photophysical properties of

[a] Department of Chemistry, University of Basel,
St. Johanns-Ring 19, 4056 Basel, Switzerland
E-mail: oliver.wenger@unibas.ch
http://www.chemie.unibas.ch/~wenger/

Supporting information for this article is available on the WWW under http://dx.doi.org/10.1002/ejic.201500670.

EurJIC European Journal of Inorganic Chemistry
www.eurjic.org FULL PAPER

the complexes were explored in detail, and we find that $[Ru\{(MeO)_4bpy\}_3]^{2+}$ is indeed a very potent excited-state electron donor. The redox and photophysical properties of the new complexes are rationalized by comparison with existing data of related bpy-based complexes.

Results and Discussion

Synthesis

Commercial 5-amino-2-chloropyridine (**1**) was treated with $NaNO_2$ in diluted sulfuric acid, and after neutralization with aqueous Na_2CO_3 2-chloro-5-hydroxypyridine (**2**) was isolated (Scheme 1).[14] The latter was converted to 2-chloro-5-methoxypyridine (**3**) with iodomethane in the presence of K_2CO_3. Using the urea·H_2O_2 adduct and trifluoroacetic anhydride, conversion to 2-chloro-5-methoxypyridine *N*-oxide (**4**) occurred.[15] Subsequent reaction in nitrating acid gave 2-chloro-4-nitro-5-methoxypyridine (**5**), that is, nitration and loss of the *N*-oxide occurred in the same reaction step. Treatment of molecule **5** with tetrabutylammonium methoxide in THF afforded 2-chloro-4,5-dimethoxypyridine (**6**).[16] A homocoupling reaction catalyzed by $[Ni(PPh_3)_2Cl_2]$ in the presence of Zn powder and tetrabutylammonium iodide gave the final 4,4′,5,5′-tetramethoxy-2,2′-bipyridine ligand [**7**, $(MeO)_4bpy$].[17] The overall yield for the six reaction steps from molecule **1** to ligand **7** was 6%. This newly developed procedure is significantly different from the only previously published protocol for the synthesis of 4,4′,5,5′-tetramethoxy-2,2′-bipyridine and in our hands proved to be more effective.[12]

The metal complexes were synthesized with standard methods, using $Fe(BF_4)_2·6H_2O$, $RuCl_3·0.5H_2O$, and $[(NH_4)_2OsCl_6]$ as metal sources. The final complexes as well as ligand **7** [$(MeO)_4bpy$] were fully characterized by ^1H and ^{13}C NMR spectroscopy, high-resolution mass spectrometry, and elemental analysis. Complete synthetic protocols and product characterization data are in the Experimental Section. ^1H NMR spectra of all compounds are in the Supporting Information (Figures S1–S9).

Crystallographic Studies

In Figure 1a two molecules of 2-chloro-4,5-dimethoxypyridine (**6**) as found in the asymmetric unit of an X-ray crystal structure are shown. The crystallographic structure of 4,4′,5,5′-tetramethoxy-2,2′-bipyridine [**7**, $(MeO)_4$-bpy] is shown in Figure 1b. In both structures the methoxy groups are nearly coplanar with the pyridine rings, and in $(MeO)_4bpy$ the two pyridine moieties are essentially coplanar with one another, but with N atoms on opposite sides, as commonly observed for bpy ligands. An X-ray crystal

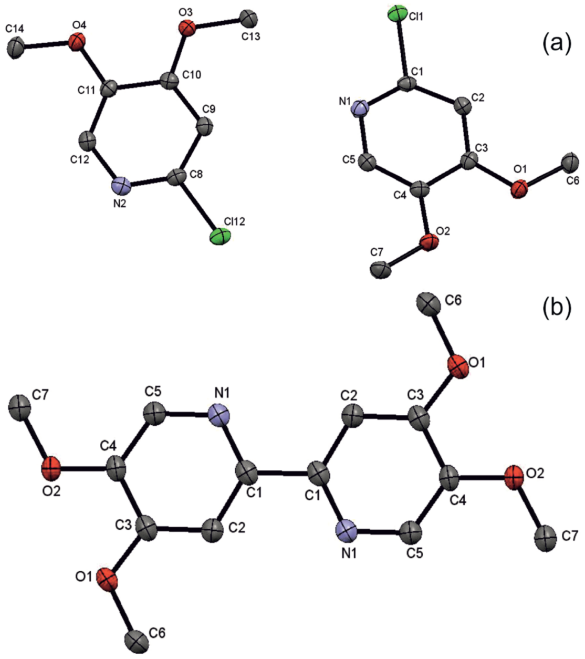

Figure 1. (a) Crystallographic structure of two 2-chloro-4,5-dimethoxypyridine (**6**) molecules forming the asymmetric unit. (b) Crystallographic structure of the 4,4′,5,5′-tetramethoxy-2,2′-bipyridine ligand [**7**, $(MeO)_4bpy$]. Anisotropic displacement parameters are drawn at the 50% probability level.

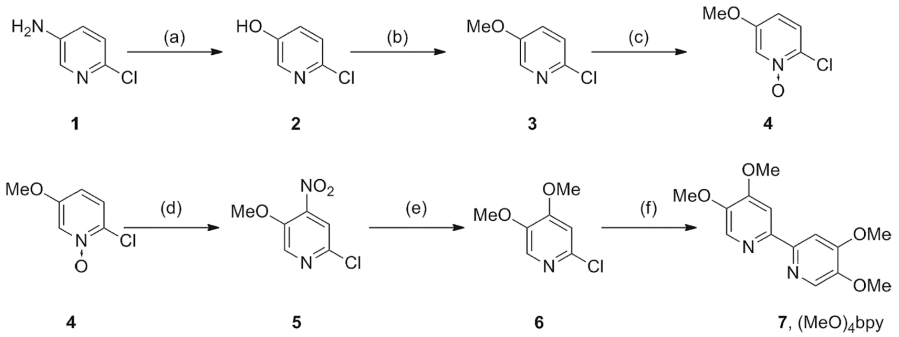

Scheme 1. Synthetic steps leading to the 4,4′,5,5′-tetramethoxy-2,2′-bipyridine ligand [**7**, $(MeO)_4bpy$]. (a) $NaNO_2$, dil. H_2SO_4, concd. AcOH, then aq. Na_2CO_3; (b) CH_3I, K_2CO_3, dry CH_3CN; (c) urea·H_2O_2, trifluoroacetic anhydride, CH_2Cl_2; (d) concd. H_2SO_4, concd. HNO_3; (e) $TBAOCH_3$, THF; (f) $[Ni(PPh_3)_2Cl_2]$, Zn, Et_4NI, THF.

EurJIC European Journal of Inorganic Chemistry
www.eurjic.org
FULL PAPER

structure of 2-chloro-4-nitro-5-methoxypyridine (**5**) is shown in the Supporting Information (Figure S10).

The homoleptic d^6 metal complexes with $(MeO)_4$bpy were more tricky to crystallize. With BF_4^- and PF_6^- anions the resulting crystals were not of sufficient quality for X-ray diffraction experiments; only with triflate did we obtain a satisfactory result. The respective crystals were obtained by diffusion of diethyl ether vapor into a solution of the compound in acetonitrile. In Figure 2 the crystallographic structure of the $[Fe\{(MeO)_4bpy\}_3]^{2+}$ cation is shown. The methoxy substituents remain essentially coplanar with the pyridine rings to which they are attached. Complete crystallographic details are included in the Experimental Section and in the Supporting Information.

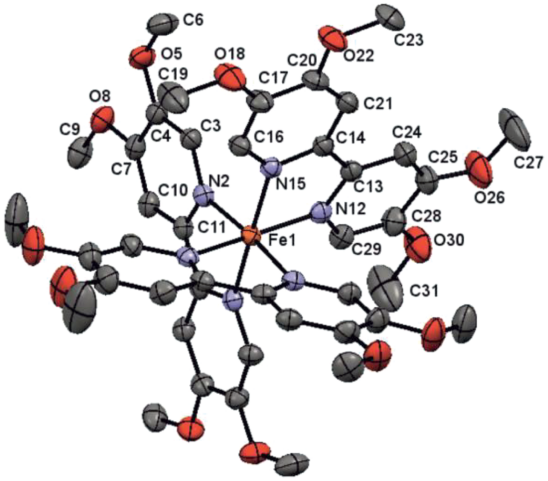

Figure 2. Crystallographic structure of the $[Fe\{(MeO)_4bpy\}_3]^{2+}$ cation. Anisotropic displacement parameters are drawn at the 50% probability level.

Electrochemistry

Cyclic voltammetry of the $[Fe\{(MeO)_4bpy\}_3]^{2+}$, $[Ru\{(MeO)_4bpy\}_3]^{2+}$, and $[Os\{(MeO)_4bpy\}_3]^{2+}$ complexes was performed in dry CH_3CN with 0.1 M $TBAPF_6$. The results are shown in Figure 3 (solid lines). Voltammograms recorded for the $[Fe(bpy)_3]^{2+}$, $[Ru(bpy)_3]^{2+}$, and $[Os(bpy)_3]^{2+}$ reference complexes were measured under identical conditions and are included in Figure 3 (dotted lines). All redox potentials extracted from Figure 3 are summarized in Table 1 along with those of some related homoleptic Ru^{II} complexes (values taken from the literature). For all three metals (M) considered here, the M^{3+}/M^{2+} reduction potential is roughly 0.4 V lower for L = $(MeO)_4$bpy than for L = bpy (second column of Table 1). The $[Fe\{(MeO)_4bpy\}_3]^{2+}$ complex becomes unstable upon reduction hence the observation of only one irreversible reduction wave instead of three reversible waves, as is usually the case for homoleptic d^6 metal complexes with bpy ligands. For the Ru^{II} and Os^{II} complexes each of the three consecutive one-electron reductions of individual ligands occurs at potentials more negative by about 0.3 V in complexes with L = $(MeO)_4$bpy relative to L = bpy.

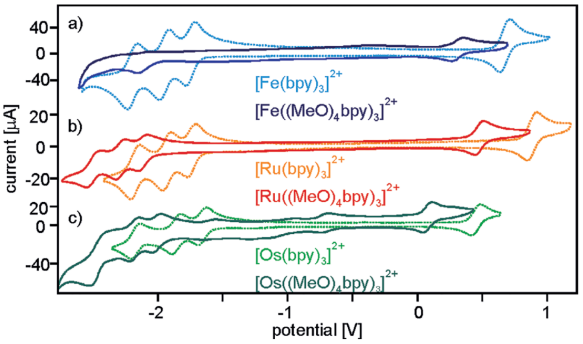

Figure 3. Cyclic voltammograms of the $[M\{(MeO)_4bpy\}_3]^{2+}$ and $[M(bpy)_3]^{2+}$ complexes in CH_3CN with 0.1 M $TBAPF_6$. The scan rate was 0.2 $V s^{-1}$, the potential is reported versus the ferrocenium/ferrocene (Fc^+/Fc) couple.

Table 1. Reduction potentials (in V vs. Fc^+/Fc) for the various metal- and ligand-based electrochemical processes of the three key complexes and some relevant reference complexes.

Complex	$E^0(M^{3+/2+})$	$E^0(L/L^-)$[a]	$E^0(L^-/L^{2-})$[b]	$E^0(L^{2-}/L^{3-})$
$[Fe(bpy)_3]^{2+}$	0.71[c]	–1.75[c]	–1.95[c]	–2.19[c]
$[Fe\{(MeO)_4bpy\}_3]^{2+}$	0.31[c]	–	–	–
$[Ru(bpy)_3]^{2+}$	0.89[c]	–1.72[c]	–1.91[c]	–2.15[c]
$[Ru(4,4'\text{-}Me_2bpy)_3]^{2+}$	0.75[a]	–1.75[a]	–1.92[a]	–2.18[a]
$[Ru(4,4'\text{-}tBu_2bpy)_3]^{2+}$	0.73[b]	–1.82[b]	–	–
$[Ru(4,4',5,5'\text{-}Me_4bpy)_3]^{2+}$	0.68[a]	–1.87[a]	–2.08[a]	–2.37[a]
$[Ru\{4,4'\text{-}(MeO)_2bpy\}_3]^{2+}$	0.56[d]	–1.87[d]	–2.04[d]	–2.24[d]
$[Ru\{(MeO)_4bpy\}_3]^{2+}$	0.47[c]	–2.01[c]	–2.18[c]	–2.46[c]
$[Ru\{(4,4'\text{-}Me_2N)_2bpy\}_3]^{2+}$	–0.05[c]	–	–	–
$[Os(bpy)_3]^{2+}$	0.45[c]	–1.67[c]	–1.86[c]	–2.16[c]
$[Os\{(MeO)_4bpy\}_3]^{2+}$	0.08[c]	–2.01[c]	–2.18[c]	–2.46[c]

[a] From the literature.[18] [b] From the literature.[19] [c] Measured in this work (Figure 3) in CH_3CN with 0.1 M $TBAPF_6$ using scan rates of 0.2 $V s^{-1}$. [d] From the literature.[13a] [e] From the literature.[20] Literature potentials reported against reference electrodes other than Fc^+/Fc were converted to Fc^+/Fc by using the conversion constants reported earlier.[21]

Several Ru^{II} complexes with 4,4′-disubstituted and 4,4′,5,5′-tetrasubstituted bpy ligands have been previously characterized electrochemically, hence for this metal one can put the effect of the fourfold methoxy substitution into broader and more quantitative perspective (Table 1). Substitution at the 4- and 4′-positions with methyl- and *tert*-butyl groups lowers the M^{3+}/M^{2+} reduction potential by roughly 0.15 V compared to ordinary bpy,[18,19] while the use of two methoxy groups causes a lowering by 0.3 V.[13a] The effect of additional substitution at the 5- and 5′-positions in $(MeO)_4$bpy therefore is relatively small, only about 0.1 V, to cause a total shift of 0.4 V. This is not unexpected as substituents in a *para* position to the coordinating N atoms are known to have a stronger effect on the electron density at the metal center than substituents in an *ortho* position.[11a–11c] Compared to the Ru^{II} complex with 4,4′,5,5′-tetramethylated bpy (Me_4bpy),[18] metal oxidation in $[Ru\{(MeO)_4bpy\}_3]^{2+}$ is easier by about 0.2 V. However,

EurJIC European Journal of Inorganic Chemistry www.eurjic.org FULL PAPER

the very electron-rich 4,4′-bis(dimethylamino)-substituted bpy ligand [4,4′-$(Me_2N)_2$bpy] leads to an oxidation potential that is roughly 0.5 V lower than that of $[Ru\{(MeO)_4bpy\}_3]^{2+}$.[20] However, the new $[Ru\{(MeO)_4bpy\}_3]^{2+}$ and $[Os\{(MeO)_4bpy\}_3]^{2+}$ complexes seem to be chemically significantly more robust than the $[Ru\{4,4'\text{-}(Me_2N)_2bpy\}_3]^{2+}$ complex.

UV/Vis Absorption and Photoluminescence

The solid lines in Figure 4 are the optical absorption spectra of the $[M\{(MeO)_4bpy\}_3]^{2+}$ complexes and $[M(bpy)_3]^{2+}$ reference compounds in CH_3CN at 22 °C. The lowest-energy absorption bands that are observable on this extinction scale are due to MLCT transitions in all six cases. For a given metal, the MLCT energy is similar in $[M\{(MeO)_4bpy\}_3]^{2+}$ and $[M(bpy)_3]^{2+}$ complexes. This makes sense because metal oxidation was found to be roughly 0.4 V easier in the complexes with $(MeO)_4$bpy but at the same time ligand reduction was about 0.3 V more difficult than in the bpy complexes. The ligand-based π–π* absorptions of $(MeO)_4$bpy near 300 nm are broadened with respect to those of ordinary bpy.

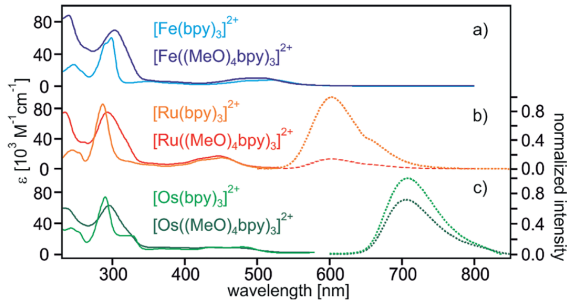

Figure 4. Optical absorption (solid lines) and luminescence spectra (dotted lines) of the $[M\{(MeO)_4bpy\}_3]^{2+}$ and $[M(bpy)_3]^{2+}$ complexes in aerated CH_3CN at 22 °C. Excitation occurred at 455 nm for all complexes. The luminescence intensities were normalized to the luminescence emitted by the $[Ru(bpy)_3]^{2+}$ and $[Os(bpy)_3]^{2+}$ parent complexes, by taking into account differences in absorbance at the excitation wavelength.

The dotted lines in Figure 4 are luminescence spectra recorded after excitation of the Ru^{II} and Os^{II} complexes in aerated CH_3CN at 455 nm. The Fe^{II} complexes are nonemissive owing to energetically low-lying d–d excited states. For the Ru^{II} and Os^{II} complexes the intensity has been normalized to that of the respective $[M(bpy)_3]^{2+}$ reference compounds to visualize the relative photoluminescence intensities of the new $[M\{(MeO)_4bpy\}_3]^{2+}$ complexes and the known parent compounds. In the last column of Table 2 the luminescence quantum yields of the various complexes in aerated CH_3CN are reported. These quantum yields were estimated on the basis of the measured relative emission intensities and the known luminescence quantum yield for $[Ru(bpy)_3]^{2+}$ under identical conditions (Figure S11 in the Supporting Information).[22] The $[M\{(MeO)_4bpy\}_3]^{2+}$ complexes exhibit weaker luminescence than the $[M(bpy)_3]^{2+}$ parent compounds, possibly because of additional multiphonon relaxation pathways that come into play with molecular vibrations involving the methoxy substituents.

Table 2. Lifetimes (τ_0) of the lowest-energetic ^{3}MLCT excited states and luminescence quantum yields (ϕ) in CH_3CN at 22 °C.

Complex	τ_0 (aerated) [ns]	τ_0 (deaerated) [ns]	ϕ (aerated)
$[Ru(bpy)_3]^{2+}$	173	830[a]	0.018[b]
$[Ru\{(MeO)_4bpy\}_3]^{2+}$	33	57	0.002[c]
$[Os(bpy)_3]^{2+}$	42	56[d]	0.010[c]
$[Os\{(MeO)_4bpy\}_3]^{2+}$	35	73	0.006[c]

[a] From the literature.[23] [b] From the literature.[22] [c] Determined from luminescence intensity measurements relative to $[Ru(bpy)_3]^{2+}$, corrected for differences in absorbance at excitation wavelengths. [d] From the literature.[23a]

Luminescence lifetimes (τ_0) measured after excitation at 532 nm with laser pulses of approximately 10 ns duration were detected at 600 nm for the Ru^{II} complexes and at 700 nm for the Os^{II} complexes (Figure S12 in the Supporting Information). The lifetimes in aerated and de-oxygenated CH_3CN at 22 °C are reported in Table 2. The luminescence lifetime of $[Ru\{(MeO)_4bpy\}_3]^{2+}$ is roughly a factor of five shorter than that of $[Ru(bpy)_3]^{2+}$ in aerated CH_3CN, whereas the luminescence quantum yields differ by a factor of nine under identical conditions. This suggests that the radiative ^{3}MLCT decay rate constants differ by a factor of two between these two complexes. For the two Os^{II} complexes the correlation between luminescence quantum yield and luminescence lifetime is closer than in the case of the Ru^{II} complexes, which indicates that the radiative ^{3}MLCT decay rate constants are very similar for $[Os\{(MeO)_4bpy\}_3]^{2+}$ and $[Os(bpy)_3]^{2+}$. The change from aerated to deoxygenated CH_3CN is associated with significant increases in luminescence lifetimes owing to the suppression of ^{3}MLCT relaxation by means of energy transfer to O_2 (third column of Table 2). However, even under these conditions the ^{3}MLCT lifetimes of $[Ru\{(MeO)_4bpy\}_3]^{2+}$ and $[Os\{(MeO)_4bpy\}_3]^{2+}$ stay well below 100 ns, which is significantly shorter than what is measured for $[Ru(bpy)_3]^{2+}$ under identical conditions.

Transient Absorption Spectroscopy

The $[Ru\{(MeO)_4bpy\}_3]^{2+}$ and $[Os\{(MeO)_4bpy\}_3]^{2+}$ complexes in aerated CH_3CN were excited at 532 nm with laser pulses of approximately 10 ns duration, and transient differences in optical absorption were probed with the white-light output of a high-pressure xenon lamp. Time integration over the first 200 ns after the excitation pulses afforded the transient difference spectra shown in Figure 5. The two spectra are rather similar to one another because the same type of ^{3}MLCT excited state is probed in both cases. The most important difference is a redshift of the MLCT bleach when going from the Ru^{II} to the Os^{II} complex owing to the lower MLCT energy of the latter. Both spectra from Figure 5 are similar to the transient difference spectrum of the $[Ru(bpy)_3]^{2+}$ parent complex,[24] with a bleach around 300 nm caused by (partial) disappearance of π–π* absorp-

EurJIC European Journal of Inorganic Chemistry
www.eurjic.org
FULL PAPER

tion from neutral $(MeO)_4bpy$ and an increase in absorbance between 320 and 430 nm caused by reduced $(MeO)_4bpy$. The negative signal at 600 nm in Figure 5 (b) is a fairly common artefact caused by difficulties in baseline calibration.

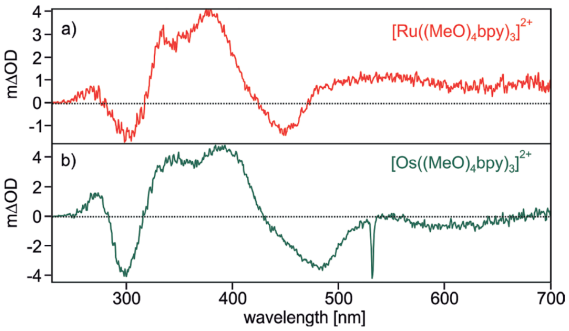

Figure 5. Transient difference spectra for ^{3}MLCT-excited $[Ru\{(MeO)_4bpy\}_3]^{2+}$ and $[Os\{(MeO)_4bpy\}_3]^{2+}$ in aerated CH_3CN at 22 °C. Excitation occurred with laser pulses of approximately 10 ns duration at 532 nm. The spectra were time-integrated over 200 ns. Sample concentrations were 1.4×10^{-5} and 0.9×10^{-5} M for Ru^{II} and Os^{II}, respectively.

The decays of the transient absorption signals of the $[Ru\{(MeO)_4bpy\}_3]^{2+}$ complex at 300, 380, and 448 nm are within experimental accuracy the same as the decay of the ^{3}MLCT luminescence detected at 600 nm (Figure S13a in the Supporting Information), which indicates that the same excited state is indeed being probed in transient absorption and photoluminescence experiments. This is also the case for the $[Os\{(MeO)_4bpy\}_3]^{2+}$ complex (Figure S13b).

Photoredox Properties

Having established that $[Ru\{(MeO)_4bpy\}_3]^{2+}$ and $[Os\{(MeO)_4bpy\}_3]^{2+}$ exhibit similar ^{3}MLCT excited-state structures (Figure 5), similar ^{3}MLCT energies (Figure 4) but significantly lower ground-state oxidation potentials (Figure 3, Table 1) than the $[Ru(bpy)_3]^{2+}$ and $[Os(bpy)_3]^{2+}$ parent complexes, we were curious to check whether the new methoxylated complexes are indeed better photoreductants than the parent compounds. To test this hypothesis, luminescence-quenching experiments with $[Ru\{(MeO)_4bpy\}_3]^{2+}$ and 1-chloro-4-nitrobenzene were performed. The latter exhibits an electrochemical potential for one-electron reduction of –1.44 V versus Fc^+/Fc and therefore is a comparatively weak electron acceptor.[25] 1-Chloro-4-nitrobenzene has been reported to quench the ^{3}MLCT excited state of $[Ru(bpy)_3]^{2+}$ very inefficiently with a rate constant for bimolecular electron transfer of 8.0×10^6 $M^{-1} s^{-1}$ in CH_3CN at 22 °C,[26] and we were able to reproduce this number. When performing the same experiment with $[Ru\{(MeO)_4bpy\}_3]^{2+}$ the luminescence data in Figure 6 (a, b) were obtained. The gradual increase in 1-chloro-4-nitrobenzene

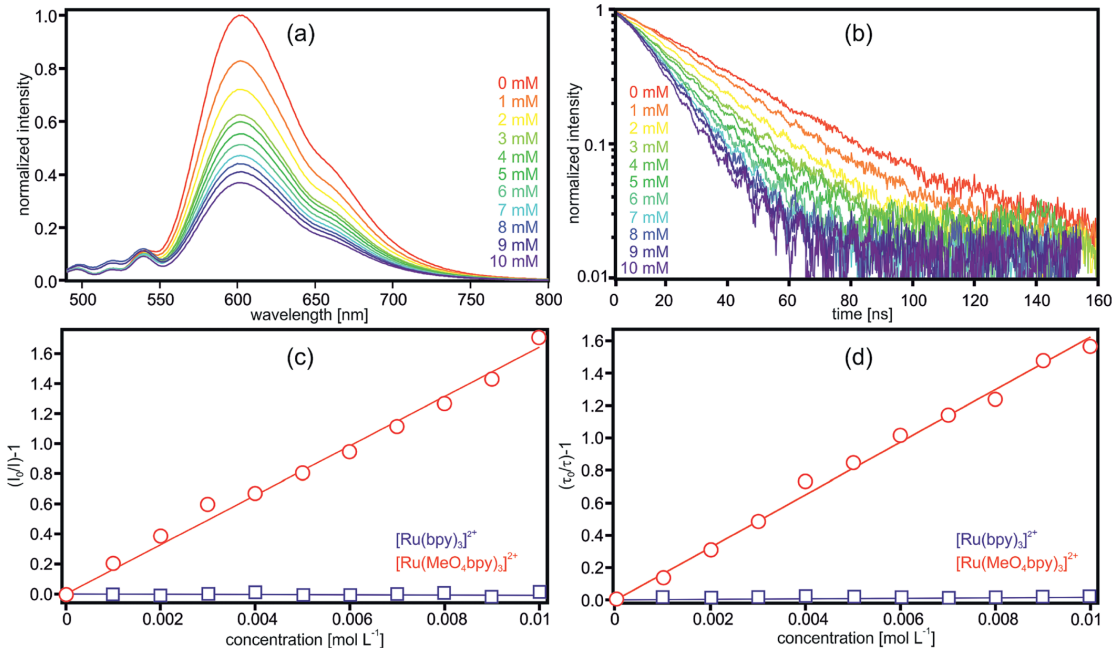

Figure 6. (a) Luminescence spectra of a 6.7×10^{-6} M solution of $[Ru\{(MeO)_4bpy\}_3]^{2+}$ in aerated CH_3CN as a function of increasing concentrations of 1-chloro-4-nitrobenzene (see inset). Excitation occurred at 455 nm, that is, at a wavelength at which 1-chloro-4-nitrobenzene does not absorb significantly in the relevant concentration range. (b) Luminescence decays detected at 610 nm after excitation of the same solutions at 532 nm with laser pulses of approximately 10 ns duration. (c) Stern–Volmer plot based on the steady-state luminescence data from (a) (red circles); analogous data for the $[Ru(bpy)_3]^{2+}$ reference complex is also included (purple squares) (luminescence spectra not shown). (d) Stern–Volmer plot based on the decay data from (b) (red circles); analogous data for the $[Ru(bpy)_3]^{2+}$ reference complex is also included (purple squares) (luminescence decays not shown).

EurJIC European Journal of Inorganic Chemistry www.eurjic.org FULL PAPER

concentration between 0 and 10 mM clearly induces significant luminescence quenching both with regard to luminescence intensity (Figure 6, a) and luminescence lifetime (Figure 6, b).

Based on the two sets of data in Figure 6 (a, b) the Stern–Volmer plots shown in Figure 6 (c, d) were established (red circles). Analogous data for the $[Ru(bpy)_3]^{2+}$ reference complex were also included (purple squares). The similarity of the Stern–Volmer plots for intensity and lifetime data for a given complex indicates that the excited-state quenching is dynamic. From the slopes of linear regression fits to the data in Figure 6 (c, d) and taking into account the ^{3}MLCT lifetimes of the $[Ru\{(MeO)_4bpy\}_3]^{2+}$ and $[Ru(bpy)_3]^{2+}$ complexes, one obtains the rate constants (k_q) for oxidative excited-state quenching as reported in Table 3. For $[Ru\{(MeO)_4bpy\}_3]^{2+}$ we found $k_q = 4.8 \times 10^9$ M^{-1} s^{-1}, which is a value that is a factor of 600 higher than what is found for $[Ru(bpy)_3]^{2+}$. For the parent complex, similarly rapid bimolecular quenching with nitroaromatic compounds was only observed for substances that have roughly 0.3 V more oxidative power.[25,26]

Table 3. Rate constants (k_q) for oxidative ^{3}MLCT excited-state quenching by 1-chloro-4-nitrobenzene in aerated CH_3CN at 22 °C.

Complex	k_q [M^{-1} s^{-1}]
$[Ru(bpy)_3]^{2+}$	8.0×10^6 [a]
$[Ru\{(MeO)_4bpy\}_3]^{2+}$	4.8×10^9 [b]

[a] From the literature.[26] [b] This work (Figure 6).

In Figure 7 (a) the known Latimer diagram for $[Ru(bpy)_3]^{2+}$ is shown.[25] The Latimer diagram for $[Ru\{(MeO)_4bpy\}_3]^{2+}$ established on the basis of our new data is shown in Figure 7 (b). The electrochemical potentials for one-electron reduction and oxidation in the electronic ground state were taken from Table 1 (Figure 3), and the ^{3}MLCT excited-state energy was estimated to be identical to that in $[Ru(bpy)_3]^{2+}$ (Figure 7, b). This approximation makes sense because the ^{1}MLCT absorption bands are detected at similar wavelengths in $[Ru\{(MeO)_4bpy\}_3]^{2+}$ and $[Ru(bpy)_3]^{2+}$ (Figure 4). Moreover we found that metal oxidation is about 0.4 V more favorable for the new methoxylated complexes but reduction of their ligands is roughly 0.3 V less favorable (Table 1). Thus, we assume that the error in ^{3}MLCT energy estimated in this manner is on the order of ±0.1 V. Figure 7 illustrates that ^{3}MLCT-excited $[Ru\{(MeO)_4bpy\}_3]^{2+}$ is indeed a significantly better photoreductant with a potential of –1.6 V (vs. Fc^+/Fc) for oxidation in the ^{3}MLCT excited state compared to –1.2 V (vs. Fc^+/Fc) for $[Ru(bpy)_3]^{2+}$. This explains why 1-chloro-4-nitrobenzene with a reduction potential of –1.44 V (vs. Fc^+/Fc) reacts efficiently with ^{3}MLCT-excited $[Ru\{(MeO)_4bpy\}_3]^{2+}$.

As far as the osmium complexes are concerned, the $[Os\{(MeO)_4bpy\}_3]^{2+}$ compound is a stronger photoreductant than the $[Os(bpy)_3]^{2+}$ parent complex, too, because metal oxidation is significantly facilitated by the electron-donating methoxy substituents. The ^{3}MLCT energy in this case is only approximately 1.8 eV, hence we estimate a potential of –1.7 V (vs. Fc^+/Fc) for oxidation in the long-lived ^{3}MLCT excited state of $[Os\{(MeO)_4bpy\}_3]^{2+}$. Thus, photoexcited $[Ru\{(MeO)_4bpy\}_3]^{2+}$ and $[Os\{(MeO)_4bpy\}_3]^{2+}$ are both relatively potent photoreductants, as the comparison with other metal complexes in Table 4 shows. To put our results into somewhat greater perspective, Table 4 includes the excited-state oxidation potentials of some of the most potent photoreductants known to date.

Table 4. Electrochemical potentials for one-electron oxidation of selected metal complexes in their long-lived excited states (in V vs. Fc^+/Fc).

Complex	E^0 (M^+/M^*)
$[Ru(bpy)_3]^{2+}$	–1.2 [a]
$[Ru\{(MeO)_4bpy\}_3]^{2+}$	–1.6 [b]
$[Os(bpy)_3]^{2+}$	–1.4 [c]
$[Os\{(MeO)_4bpy\}_3]^{2+}$	–1.7 [b]
$W(CNAr)_6$	< –2.7 [d]
$[Ir(\mu\text{-pz})(cod)]_2$	–2.2 [e]

[a] From the literature.[26] [b] This work. [c] Estimated on the basis of the ground-state oxidation potential reported in the literature[11a] and the ^{3}MLCT energy reported in the literature.[27] [d] From the literature[28] (CNAr = arylisocyanides). [e] From the literature[29] (μ-pz = μ-pyrazolyl; cod = 1,5-cyclooctadiene).

Proton-Coupled Electron Transfer

Evidently, the $[Ru\{(MeO)_4bpy\}_3]^{2+}$ complex is a strong reductant in its ^{3}MLCT excited state, yet the previously explored $[Ru\{4,4'\text{-}(Me_2N)_2bpy\}_3]^{2+}$ complex is an even stronger (photo)reductant (Table 1).[20] However, unlike the 4,4′-bis(dimethylamino)-substituted bpy ligands of the latter, the 4,4′,5,5′-tetramethoxy-2,2′-bipyridine ligands of $[Ru\{(MeO)_4bpy\}_3]^{2+}$ are not easily protonatable, and therefore this complex continues to exhibit its photoredox activity in acidic solution. This property is of interest for pho-

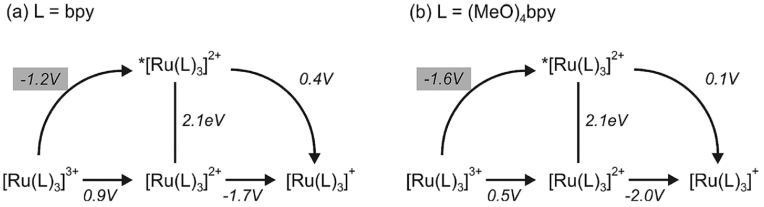

Figure 7. Latimer diagrams for $[Ru(bpy)_3]^{2+}$ and $[Ru\{(MeO)_4bpy\}_3]^{2+}$. The asterisks mark the ^{3}MLCT-excited species. Potentials are for solutions in CH_3CN in V vs. Fc^+/Fc.

EurJIC European Journal of Inorganic Chemistry
www.eurjic.org
FULL PAPER

toinduced PCET chemistry in which a substrate is reduced by the photoexcited $[Ru\{(MeO)_4bpy\}_3]^{2+}$ complex and protonated by an acid that is simultaneously present. Ketones are particularly interesting substrates in this context because they are not easily reduced unless electron transfer is coupled with proton transfer to yield neutral ketyl radicals.[30] Recent studies have reported on ketyl-olefin cyclization enabled by PCET, and this method proved to be of interest for organic synthesis.[31] The PCET reaction occurred between photogenerated $[Ru(bpy)_3]^+$, a series of Brönsted acids, and a variety of ketones. The ^{3}MLCT excited state of $[Ru(bpy)_3]^{2+}$ was unable to engage directly in PCET chemistry because it is not reducing enough, and therefore $[Ru(bpy)_3]^+$ had to be photogenerated by reductive ^{3}MLCT excited-state quenching with a Hantzsch dihydropyridine. Against this background we explored whether the ^{3}MLCT excited state of $[Ru\{(MeO)_4bpy\}_3]^{2+}$ in acidic media could directly engage in PCET chemistry with ketones, without the use of Hantzsch dihydropyridine or other sacrificial electron donors.

Acetophenone was used as a model ketone for the subsequent PCET studies, and methanesulfonic acid was employed as a proton source. In pure CH_3CN without acid, acetophenone is unable to quench the ^{3}MLCT excited state of $[Ru\{(MeO)_4bpy\}_3]^{2+}$ because electron-transfer and triplet-triplet energy-transfer processes are energetically unfavorable. The reduction potential of acetophenone in CH_3CN is –2.48 V (vs. Fc^+/Fc),[32] and its triplet energy is 3.21 eV;[33] the excited-state oxidation potential of $[Ru\{(MeO)_4bpy\}_3]^{2+}$ in CH_3CN is –1.6 V (vs. Fc^+/Fc) and the ^{3}MLCT energy is 2.1 eV (see above). Consequently, electron transfer and triplet–triplet energy transfer are both endergonic by more than 0.8 eV. However, upon addition of increasing amounts of methanesulfonic acid to an aerated CH_3CN solution containing 1.15×10^{-5} M $[Ru\{(MeO)_4bpy\}_3]^{2+}$ and 0.5 M acetophenone, increasingly strong luminescence quenching is observed (Figure 8). Addition of 0.5 M methanesulfonic acid leads to a decrease in the luminescence intensity by roughly 50% (Figure 8, a), and this is accompanied by a decrease in ^{3}MLCT luminescence lifetime from 35 ns in the absence of acid to 11 ns in the presence of 0.5 M methanesulfonic acid (Figure 8, b). When performing the exact same experiment with the $[Ru(bpy)_3]^{2+}$ reference complex, the luminescence intensity decreases by only approximately 20% (Figure 8, c), and the lifetime shortens only from 173 to 133 ns (Figure 8, d). In the lifetime data from Figure 8d, instrumentally limited decay components become visible; these are due to a fluorescence that is observed as soon as methanesulfonic acid is added to 0.5 M acetophenone in CH_3CN (Figure S14 in the Supporting Information). In the luminescence spectra of Figure 8a,c the respective (comparatively weak) fluorescence signal has been subtracted as described in the Supporting Information. Control experiments in which 0.5 M methanesulfonic acid has been added to aerated CH_3CN solutions containing $[Ru\{(MeO)_4bpy\}_3]^{2+}$ or $[Ru(bpy)_3]^{2+}$ but no acetophenone did not reveal any significant luminescence quenching (data not shown). Thus it is clear that acetophenone and methanesulfonic acid must be simultaneously present to induce excited-state quenching.

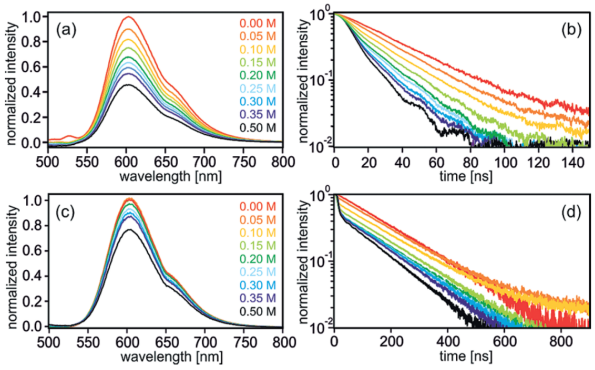

Figure 8. Luminescence of $[Ru\{(MeO)_4bpy\}_3]^{2+}$ and $[Ru(bpy)_3]^{2+}$ in aerated CH_3CN at 22 °C in the presence of 0.5 M acetophenone and increasing amounts of methanesulfonic acid (see insets). Excitation for the steady-state experiments (a, c) occurred at 455 nm. In the time-resolved experiments, excitation occurred at 532 nm with laser pulses of approximately 10 ns duration, and detection was at 610 nm. (a) and (b) $[Ru\{(MeO)_4bpy\}_3]^{2+}$ (concd. 1.15×10^{-5} M); (c) and (d) $[Ru(bpy)_3]^{2+}$ (concd. 0.85×10^{-5} M).

Direct observation of the ketyl radical of acetophenone by transient absorption spectroscopy is complicated by the fact that in the visible portion of the spectrum this particular ketyl exhibits only two comparatively weak absorption bands, the first one with a maximum at approximately 405 nm and the second at approximately 440 nm, both with extinction coefficients of approximately 2000 $M^{-1}\,cm^{-1}$.[34] In the UV region there are stronger ketyl absorptions, but detection in this range is hampered by the large excess amount of absorbing acetophenone present in solution. Nonetheless, the transient absorption spectrum shown in Figure S15 in the Supporting Information is compatible with the formation of ketyl, although the spectrum is dominated by the more intense spectral features of the oxidized ruthenium complex (see the Supporting Information for further details).

Figure 9 shows a Stern–Volmer plot based on the luminescence intensity data from Figure 8 (a,c). Using ^{3}MLCT lifetimes (τ_0) of 33 and 173 ns in aerated CH_3CN (Table 2), excited-state quenching constants ($k_{q,acid}$) of $(6.6 \pm 0.1) \times 10^7$ and $(2.6 \pm 0.3) \times 10^6$ $M^{-1}\,s^{-1}$ are extracted for $[Ru\{(MeO)_4bpy\}_3]^{2+}$ and $[Ru(bpy)_3]^{2+}$, respectively (Table 5). More quantitatively correct models would take the hydrogen-bonding equilibrium between methanesulfonic acid and acetophenone in CH_3CN into account,[30,35] but the currently available data do not permit this treatment (see the Supporting Information for further details). Note that acetophenone is only a very weak base in CH_3CN (pK_a = –0.1),[31a] which is not easily protonated even by methanesulfonic acid (pK_a = 10.0).[36] Based on these pK_a values, at the highest concentration of methanesulfonic acid used in Figure 9 (0.5 M acid in the presence of 0.5 M of acetophenone), the concentration of protonated acetophenone is only 5×10^{-6} M.

EurJIC European Journal of Inorganic Chemistry www.eurjic.org FULL PAPER

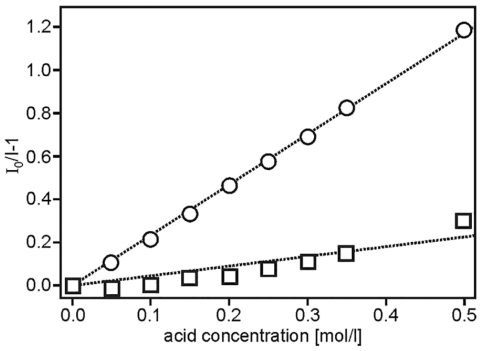

Figure 9. Stern–Volmer plot based on the luminescence intensity data from Figure 8 (a,c), measured for $[Ru\{(MeO)_4bpy\}_3]^{2+}$ (circles) and $[Ru(bpy)_3]^{2+}$ (squares) in aerated CH_3CN at 22 °C in the presence of 0.5 M acetophenone and increasing amounts of methanesulfonic acid.

Table 5. Rate constants ($k_{q,acid}$) for ^{3}MLCT excited-state quenching by methanesulfonic acid in CH_3CN at 22 °C in the presence of 0.5 M acetophenone; formal bond-dissociation free energies (*f*BDFEs) for the reaction couples comprised of the photoexcited Ru^{II} complex and methanesulfonic acid in CH_3CN (see the text for details).

Complex	$k_{q,\,acid}$ [$M^{-1}s^{-1}$]	*f*BDFE [kcal mol^{-1}]
$[Ru(bpy)_3]^{2+}$	$(2.6 \pm 0.3) \times 10^6$	40.9
$[Ru\{(MeO)_4bpy\}_3]^{2+}$	$(6.6 \pm 0.1) \times 10^7$	31.6

The hydrogen-bonding equilibrium between methanesulfonic acid and acetophenone is largely independent of which one of the two ruthenium(II) complexes is present, particularly because the concentrations of the latter are only in the micromolar range. Consequently, in both experiments from Figure 9 essentially identical concentrations of hydrogen-bonded acetophenone/methanesulfonic acid couples are present at the individual acid concentrations, and we conclude from the data in Table 5 that the ^{3}MLCT excited state of $[Ru\{(MeO)_4bpy\}_3]^{2+}$ reacts with acetophenone in acidic CH_3CN roughly 25 times more rapidly than the ^{3}MLCT excited state of $[Ru(bpy)_3]^{2+}$. This is attributed to the stronger reducing power of the $[Ru\{(MeO)_4bpy\}_3]^{2+}$ complex. However, the reduction must evidently occur in a proton-coupled fashion, and the driving force for the overall PCET process is a function not just of reducing power but also of acid strength.[37] For the $[Ru\{(MeO)_4bpy\}_3]^{2+}$/methanesulfonic acid reaction couple in CH_3CN one can estimate a formal bond-dissociation free energy (*f*BDFE) according to Equation (1).[37a,38] In this equation, pK_a is the acidity constant of the acid in CH_3CN, E^0 is the standard oxidation potential of the electron donor (in V vs. Fc^+/Fc in CH_3CN), and the $C_{G,sol}$ term describes the free energies for formation and solvation of H· (in CH_3CN).

$$f\text{BDFE [kcal mol}^{-1}] = 1.37\,pK_a + 23.06\,E^0 + C_{G,sol} \quad (1)$$

The *f*BDFE is a measure of the energetic cost associated with the coupled oxidation of ^{3}MLCT-excited $[Ru\{(MeO)_4bpy\}_3]^{2+}$ and the deprotonation of methanesulfonic acid. The *f*BDFE relies on the fact that even though the electron and proton may come from different sources, the overall PCET thermochemistry is equivalent to a reaction in which there is a single hydrogen-atom source (donating both an electron and a proton). Using $pK_a = 10.0$,[36] $E^0 = -1.6$ V vs. Fc^+/Fc (Figure 7), and $C_{G,sol} = 54.9$ kcal mol^{-1},[37a,38] one obtains *f*BDFE = 31.6 kcal mol^{-1} for the reaction couple consisting of ^{3}MLCT-excited $[Ru\{(MeO)_4bpy\}_3]^{2+}$ and methanesulfonic acid in CH_3CN. For the O–H bond in the ketyl radical of acetophenone, a BDFE of 26 kcal mol^{-1} has been reported.[31] Using this value, we estimate that intermolecular PCET involving photoexcited $[Ru\{(MeO)_4bpy\}_3]^{2+}$, methanesulfonic acid, and acetophenone is endergonic by 5.6 kcal mol^{-1}. The analogous PCET reaction involving photoexcited $[Ru(bpy)_3]^{2+}$ ($E^0 = -1.2$ V vs. Fc^+/Fc) is estimated to be endergonic by 14.9 kcal mol^{-1} (*f*BDFE = 40.9 kcal mol^{-1}, Table 5). Both of these estimates are associated with uncertainties on the order of 2–3 kcal mol^{-1}, yet it is clear that there is a significant difference in PCET driving forces between the $[Ru\{(MeO)_4bpy\}_3]^{2+}$ and $[Ru(bpy)_3]^{2+}$ systems. This interpretation is compatible with the observed reaction kinetics (Table 5).

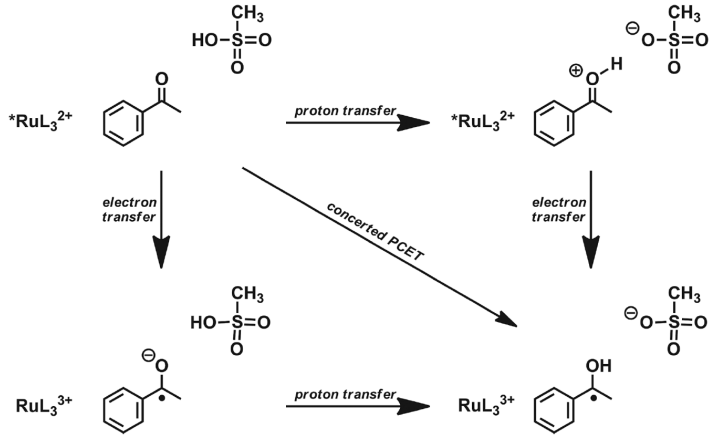

Scheme 2. Mechanistic pathways for PCET (L = MeO_4bpy). The asterisk denotes the photoexcited complex.

EurJIC European Journal of Inorganic Chemistry www.eurjic.org FULL PAPER

Concerted proton-electron transfer (CPET) is likely to be the prevalent reaction mechanism in the phototriggered reaction between $[Ru\{(MeO)_4bpy\}_3]^{2+}$, acetophenone, and methanesulfonic acid (Scheme 2). A mechanism with consecutive electron- and proton-transfer steps (ET-PT) can be excluded on the basis of the unfavorable reaction free energy for the initial electron-transfer event (ΔG^0_{ET} = 0.9 eV based on the potentials reported above); the lack of any significant $[Ru\{(MeO)_4bpy\}_3]^{2+}$ luminescence quenching even in presence of 0.5 M acetophenone (in absence of acid) strongly supports this argument. A stepwise proton-transfer, electron-transfer (PT-ET) sequence with a proton-transfer pre-equilibrium preceding a fast electron-transfer step is unlikely because the concentration of protonated acetophenone is very small. As noted above, even in the presence of 0.5 M acetophenone and 0.5 M methanesulfonic acid, the concentration of protonated acetophenone is only 5×10^{-6} M. This leaves us with concerted proton–electron transfer as the most plausible mechanism for PCET in this case.

Conclusion

4,4′,5,5′-Tetramethoxy-2,2′-bipyridine [$(MeO)_4bpy$] had been reported in the literature only once as part of a broad (organic) synthetic study of pyridines,[12] but to the best of our knowledge it had never been used as a ligand to any metal until now. We developed a new synthetic procedure to make $(MeO)_4bpy$ in six steps from commercial 2-chloro-5-hydroxypyridine. The presence of twelve electron-donating methoxy substituents on homoleptic Fe^{II}, Ru^{II}, and Os^{II} complexes with $(MeO)_4bpy$ makes these complexes very strong electron donors. Both the $[Ru\{(MeO)_4bpy\}_3]^{2+}$ and the $[Os\{(MeO)_4bpy\}_3]^{2+}$ complex are significantly stronger excited-state electron donors than the $[Ru(bpy)_3]^{2+}$ and $[Os(bpy)_3]^{2+}$ parent compounds. As an example, ^{3}MLCT-excited $[Ru\{(MeO)_4bpy\}_3]^{2+}$ is able to reduce even relatively mild oxidants such as 1-chloro-4-nitrobenzene. Even in the presence of strong acids such as methanesulfonic acid (pK_a = 10.0 in CH_3CN),[36] the $[Ru\{(MeO)_4bpy\}_3]^{2+}$ complex is stable in CH_3CN for several hours and remains unprotonated. As a consequence, $[Ru\{(MeO)_4bpy\}_3]^{2+}$ can engage in proton-coupled electron transfer (PCET) chemistry with ketones to form (neutral) ketyl radicals directly from the ^{3}MLCT excited state, as demonstrated with the specific example of acetophenone. Analogous PCET chemistry with the $[Ru(bpy)_3]^{2+}$ parent complex is significantly less efficient. The two main disadvantages of $[Ru\{(MeO)_4bpy\}_3]^{2+}$ with respect to the $[Ru(bpy)_3]^{2+}$ complex are its comparatively short ^{3}MLCT lifetime (35 ns vs. 173 ns in aerated CH_3CN), and the fact that 4,4′,5,5′-tetramethoxy-2,2′-bipyridine has to be synthesized in six steps whereas the bpy parent ligand is commercially available. Nevertheless, our study demonstrates that $[Ru\{(MeO)_4bpy\}_3]^{2+}$ clearly outperforms the ordinary $[Ru(bpy)_3]^{2+}$ complex as a photoreductant, both in neutral and acidic CH_3CN.

Experimental Section

General: The yields reported in the following are average values of at least two attempts. All commercial compounds were used as received. The only exception is zinc powder, which was activated as described previously.[17a]

2-Chloro-5-hydroxypyridine (2): The following procedure was developed based on a previously published protocol.[14] An aqueous solution (5 mL) of $NaNO_2$ (3.22 g, 46.6 mmol, 1.2 equiv.) was added to an ice-cooled solution of commercial 5-amino-2-chloropyridine (**1**) (5 g, 38.8 mmol, 1 equiv.) in sulfuric acid (50 wt.-%, 74 mL) in such a manner that the temperature of the reaction mixture did not exceed 5 °C. After stirring at room temperature for 30 min, the mixture was added to concentrated acetic acid (100 mL) at 100 °C. Stirring was continued at this temperature overnight. Then the cooled reaction mixture was neutralized with saturated aqueous Na_2CO_3 solution and extracted with ethyl acetate (5 × 200 mL). The combined organic phases were dried with anhydrous Na_2SO_4 and the solvents evaporated. The resulting orange solid was purified by column chromatography on silica gel using a 4:1 (v/v) mixture of pentane and ethyl acetate as the eluent. The pure product was obtained in the form of colorless needles (54% yield). ^{1}H NMR (400 MHz, [D$_6$]acetone): δ = 9.01 (s, 1 H), 7.98 (dd, J = 2.9, 0.8 Hz, 1 H), 7.29 (dd, J = 8.6, 2.9 Hz, 1 H), 7.26 (dd, J = 8.6, 0.8 Hz, 1 H) ppm. ^{13}C NMR (101 MHz, [D$_6$]acetone): δ = 154.2, 141.8, 138.3, 126.9, 125.4 ppm. ESI-MS: m/z: 128.0. C_5H_4ClNO (129.55): calcd. C 46.36, H 3.11, N 10.81; found C 46.68, H 3.33, N 11.19.

2-Chloro-5-methoxypyridine (3): 2-Chloro-5-hydroxypyridine (**2**) (1 equiv.) was dissolved in dry acetonitrile (3 mL per mmol of **2**) and stirred with K_2CO_3 (1.5 equiv.) at room temperature for 15 min. Iodomethane (1.05 equiv.) was added to the orange solution. The reaction mixture turned dark yellow and stirring was continued overnight. Then the solvent was removed on a rotary evaporator, and the residue was vigorously stirred in a mixture of water and diethyl ether for 5 min. The aqueous and organic phases were separated, and the aqueous phase was extracted twice with diethyl ether. The combined ether phases were washed with brine and dried with anhydrous Na_2SO_4. After solvent evaporation the pure product was obtained as an orange-yellow liquid (63% yield). ^{1}H NMR (400 MHz, $CDCl_3$): δ = 8.06 (d, J = 2.9 Hz, 1 H), 7.23 (dd, J = 8.8, 0.7 Hz, 1 H), 7.18 (dd, J = 8.8, 2.9 Hz, 1 H), 3.85 (s, 3 H) ppm. ^{13}C NMR (101 MHz, $CDCl_3$): δ = 155.1, 142.7, 136.3, 124.6, 124.5, 56.1 ppm. ESI-MS: m/z: 144.0.

2-Chloro-5-methoxypyridine *N*-Oxide (4): The following procedure was adapted from a previously published protocol.[15] Urea·H_2O_2 adduct (2 equiv.) was added in one portion to an ice-cooled solution of 2-chloro-5-methoxypyridine (**3**) (1 equiv.) in dry dichloromethane (22 mL per mmol of **3**). Trifluoroacetic anhydride (1.8 equiv.) was added dropwise. Then the reaction was allowed to reach room temperature and stirring was continued overnight. An aqueous solution of sodium thiosulfate was added carefully to the reaction mixture to destroy unreacted peroxide and vigorous stirring was continued for one hour. Then the phases were separated and the aqueous phase was extracted three times with dichloromethane. The combined organic phases were dried with anhydrous Na_2SO_4 and the solvent was removed on a rotary evaporator. The pure product was obtained as a white solid after column chromatography on silica gel using a 75:1 (v/v) mixture of CH_2Cl_2 and CH_3OH as the eluent (69% yield). ^{1}H NMR (400 MHz, $CDCl_3$): δ = 8.13 (d, J = 2.6 Hz, 1 H), 7.36 (d, J = 9.1 Hz, 1 H), 6.88 (dd, J = 9.1, 2.6 Hz, 1 H), 3.84 (s, 3 H) ppm. ^{13}C NMR (101 MHz, $CDCl_3$): δ = 156.2, 133.9, 128.2, 126.0, 114.3, 56.3 ppm.

ESI-MS: *m/z*: 160.0. $C_6H_6ClNO_2$ (159.57): calcd. C 44.95, H 3.79, N 8.78; found C 44.95, H 3.95, N 8.95.

2-Chloro-4-nitro-5-methoxypyridine (5): 2-Chloro-5-methoxypyridine *N*-oxide (**4**) (1 equiv.) was dissolved in concentrated sulfuric acid (1.1 mL per mmol of **4**), and concentrated (65%) nitric acid (0.55 mL per mmol of **4**) was added. The reaction mixture was heated to 100 °C overnight. After cooling to room temperature, the mixture was poured on ice, and then aqueous NaOH solution (40 wt.-%) was added carefully to adjust the pH to 14. The resulting precipitate was dissolved in dichloromethane and the aqueous supernatant was extracted with dichloromethane four times (using 8.5 mL per mmol of **4**). The combined organic phases were dried with anhydrous Na_2SO_4, and then the solvent was removed on a rotary evaporator. The light yellow crude product was purified by column chromatography on silica gel using a 2:1 (v/v) mixture of pentane and ethyl acetate as the eluent. This afforded the pure product as a white solid (44% yield). ^{1}H NMR (400 MHz, $CDCl_3$): δ = 8.35 (s, 1 H), 7.66 (s, 1 H), 4.07 (s, 3 H) ppm. ^{13}C NMR (101 MHz, $CDCl_3$): δ = 146.6, 145.9, 143.1, 137.0, 118.5, 57.7 ppm. $C_6H_5ClN_2O_3$ (188.57): calcd. C 38.22, H 2.67, N 14.86; found C 38.41, H 2.79, N 14.50.

2-Chloro-4,5-dimethoxypyridine (6): This compound was prepared by following a method developed for related reactants.[16] 2-Chloro-4-nitro-5-methoxypyridine (**5**) (1 equiv.) was dissolved in dry THF (1.4 mL per mmol of **5**) and $TBAOCH_3$ (20 wt.-% in CH_3OH, 1 equiv.) was added. The mixture was stirred at room temperature until no starting material was left (as verified by TLC), which was usually the case after 2 to 3 h. Then the solvent was removed on a rotary evaporator. The crude product was purified by flash chromatography on silica gel using diethyl ether as the eluent. This afforded the pure product as a white solid (89% yield). ^{1}H NMR (400 MHz, $CDCl_3$): δ = 7.73 (s, 1 H), 6.69 (s, 1 H), 3.81 (s, 2×3 H) ppm. ^{13}C NMR (101 MHz, $CDCl_3$): δ = 156.7, 145.3, 143.9, 131.7, 106.7, 56.6, 56.1 ppm. ESI-MS: *m/z*: 174.0. $C_7H_8ClNO_2$ (173.60): calcd. C 48.43, H 4.64, N 8.07; found C 48.67, H 4.87, N 8.03.

4,4′,5,5′-Tetramethoxy-2,2′-bipyridine [7, (MeO)$_4$bpy]: This ligand was prepared by following a general procedure for the homocoupling of pyridines.[17] In our hands, the use of an excess amount of triphenylphosphine as described earlier proved to be problematic because of difficulties in the process of product purification.[12] $[Ni(PPh_3)_2Cl_2]$ (0.2 equiv.), activated Zn powder (1.7 equiv.) and Et_4NI (1 equiv.) were stirred at room temperature in dry THF (4 mL per mmol of Et_4NI) under an inert atmosphere for 1 h. The solution turned from dark blue through greenish to dark red during this time. 2-Chloro-4,5-dimethoxypyridine (**6**) (1 equiv.) was dissolved in dry THF (4 mL per mmol of **6**) and was then added to the dark red reaction mixture. The latter immediately turned brown. This mixture was stirred under an inert atmosphere at 50 °C overnight. After cooling to room temperature, the reaction mixture was poured into a mixture of 2 M aqueous NH_3 solution (30 mL per mmol of **6**) and dichloromethane (50 mL per mmol of **6**), and stirring was continued for 30 min. The resulting gray precipitate was removed by filtration, and the phases were separated. The organic phase was dried with anhydrous Na_2SO_4 and the solvent was removed on a rotary evaporator. The solid residue was purified by column chromatography on silica gel using a 97:3 (v/v) mixture of ethyl acetate and methanol as the eluent. This procedure afforded ligand **7** as an off-white solid (66% yield). ^{1}H NMR (400 MHz, $CDCl_3$): δ = 8.11 (s, 2 H), 7.92 (s, 2 H), 4.00 (s, 6 H), 3.95 (s, 6 H) ppm. ^{13}C NMR (101 MHz, $CDCl_3$): δ = 155.8, 151.0, 145.9, 132.1, 103.4, 56.7, 56.0 ppm. HR ESI-MS: calcd. 277.1186; found 277.1188 ($M+H^+$). $C_{14}H_{16}N_2O$ (+0.25 EtOAc) (298.32): calcd. C 60.39, H 6.08, N 9.29; found C 60.35, H 5.95, N 9.29.

[Fe{(MeO)$_4$bpy}](BF$_4$)$_2$: Commercial $Fe(BF_4)_2{\cdot}6H_2O$ (1 equiv.) was dissolved in a minimal amount of deoxygenated acetonitrile. A solution of ligand **7** [(MeO)$_4$bpy] (3 equiv.) in a minimal amount of chloroform was added. The initially colorless iron solution turned dark red, and stirring at room temperature was continued for 20 min. Then the solvent was evaporated under reduced pressure and the residue was redissolved in acetonitrile. The product was crystallized from acetonitrile by diffusion of diethyl ether vapor (96% yield). For elemental analysis, the NMR spectroscopy sample was dried at 80 °C under reduced pressure overnight. ^{1}H NMR (400 MHz, [D$_6$]acetone): δ = 8.40 (s, 6 H), 6.99 (s, 6 H), 4.09 (s, 18 H), 3.59 (s, 18 H) ppm. ^{13}C NMR spectra could not be measured because the complex was unstable over the time required for the acquisition of such spectra. HR ESI-MS: calcd. 442.1335; found 442.1341 [M^{2+}]. $C_{42}H_{48}N_6O_{12}B_2F_8Fe$ + 0.45 $C_4H_{10}O$ + 2 H_2O (1127.71): calcd. C 46.65, H 5.05, N 7.45; found C 46.52, H 5.18, N 7.51.

[Fe{(MeO)$_4$bpy}$_3$](SO$_3$CF$_3$)$_2$: This compound was prepared in an analogous manner to the tetrafluoroborate salt but with $Fe(OTf)_2$ instead of $Fe(BF_4)_2{\cdot}6H_2O$ as a starting material. The triflate salt of $[Fe\{(MeO)_4bpy\}]^{2+}$ was made in the course of crystallization attempts. Slow diffusion of diethyl ether vapor into an acetonitrile solution afforded crystals that were used to obtain the X-ray diffraction data shown in Figure 2.

[Ru{(MeO)$_4$bpy}](PF$_6$)$_2$: $RuCl_3{\cdot}0.5H_2O$ (1 equiv.) and 4,4′,5,5′-tetramethoxy-2,2′-bipyridine [**7**, (MeO)$_4$bpy] (3.5 equiv.) were heated to 190 °C in ethylene glycol (2 mL) under an inert atmosphere for 4 h. The cooled orange solution was treated with several portions of diethyl ether until the product stuck to the walls of the flask. The solid residue was then dissolved in acetonitrile and added dropwise to diethyl ether. The resulting suspension was filtered, washed with diethyl ether, and the solid was redissolved in deionized water. Purification occurred by column chromatography on silica gel using a 100:10:1 (v/v/v) mixture of acetone, deionized water, and saturated aqueous KNO_3 as the eluent. Acetone was evaporated from the desired chromatography fractions, and the pure complex was precipitated as a hexafluorophosphate salt by adding saturated aqueous KPF_6 solution. The precipitate was dissolved in dichloromethane. After drying over anhydrous Na_2SO_4, the solvent was removed by using a rotary evaporator. The product was obtained as a red solid (72% yield), which was redissolved in acetonitrile to transfer it to a smaller flask. Then the solvent was removed by using a rotary evaporator. ^{1}H NMR (400 MHz, CD_3CN): δ = 7.84 (s, 6 H), 7.03 (s, 6 H), 4.08 (s, 18 H), 3.56 (s, 18 H) ppm. ^{13}C NMR (101 MHz, CD_3CN): δ = 157.2, 153.2, 148.6, 134.3, 107.7, 57.8, 57.3 ppm. HR ESI-MS: calcd. 465.1182; found 465.1194 [M^{2+}]. $C_{42}H_{48}N_6O_{12}F_{12}RuP_2$ + 0.5 CH_3CN + 1.5 CH_3COCH_3 (1327.53): calcd. C 42.98, H 4.44, N 6.86; found C 43.15, H 4.52, N 6.84.

[Os{(MeO)$_4$bpy}](PF$_6$)$_2$: This compound was prepared in an analogous manner as $[Ru\{(MeO)_4bpy\}](PF_6)_2$ using $(NH_4)_2OsCl_6$ as a metal source instead of $RuCl_3{\cdot}0.5H_2O$. The product was obtained as a dark green to blackish solid (64% yield). ^{1}H NMR (400 MHz, CD_3OD): δ = 9.49 (s, 6 H), 8.49 (s, 6 H), 5.34 (s, 18 H), 4.86 (s, 18 H) ppm. ^{13}C NMR (101 MHz, CD_3OD): δ = 176.0, 174.6, 168.3, 127.1, 119.2, 76.5, 76.3 ppm. HR ESI-MS: calcd. 510.1467; found 510.1476 [M^{2+}]. $C_{42}H_{48}N_6O_{12}F_{12}OsP_2$ + 2 CH_3COCH_3 (1425.20): calcd. C 40.45, H 4.24, N 5.90; found C 40.09, H 4.58, N 6.20.

X-ray Crystallography: The crystals were measured on a Bruker Kappa Apex2 diffractometer at 123 K using graphite-mono-

chromated Cu-K_α radiation with λ = 1.5418 Å. The Apex software was used for data collection and integration.[39] The structures were solved by the charge-flipping method using the program Superflip.[40] Least-squares refinement against F was carried out on all non-hydrogen atoms using the program Crystals.[41] Plots were produced using Mercury.[42] CCDC-1037160 (for **7**), -1037161 (for **5**), -1037162 (for $[Fe\{(MeO)_4bpy\}_3](SO_3CF_3)_2$), and -1037163 (for **6**) contain the supplementary crystallographic data for this paper. These data can be obtained free of charge from The Cambridge Crystallographic Data Centre via www.ccdc.cam.ac.uk/data_request/cif.

Methods and Equipment: ^{1}H and ^{13}C NMR spectra were measured on a 400 MHz Bruker Avance III instrument. ^{1}H NMR spectra of all relevant compounds are shown in the Supporting Information (Figures S1–S9). High-resolution mass spectrometry was performed with a Bruker maxis 4G QTOF ESI spectrometer. Low-resolution mass spectra were measured on a Bruker esquire 3000 plus instrument. Elemental analysis occurred with a Varia Micro Cube instrument from Elementar and was conducted by Ms. Sylvie Mittelheisser in the Department of Chemistry at the University of Basel. A Cary 5000 UV/Vis-NIR spectrophotometer from Varian was employed for optical absorption spectroscopy, and a Fluorolog-322 instrument from Horiba Jobin–Yvon was used for steady-state luminescence spectroscopy. Time-resolved luminescence and transient absorption spectroscopy was performed with an LP920-KS spectrophotometer from Edinburgh Instruments using the frequency-doubled output of a Quantel Brilliant b laser for excitation and either a R928 photomultiplier tube or an iCCD camera from Andor for detection. The duration of the laser pulses was approximately 10 ns and the pulse frequency was 10 Hz. Transient absorption (difference) spectra were time-averaged over a duration of 200 ns. Quartz cuvettes from Starna were used for all optical spectroscopic studies. Cyclic voltammetry was performed in a conventional setup with three electrodes using a Versastat3-200 potentiostat from Princeton Applied Research. A glassy carbon disk served as a working electrode, and two silver wires were used as counter and quasi-reference electrodes, respectively. Internal potential calibration occurred by addition of small amounts of ferrocene. The measurements were performed in dry acetonitrile with 0.1 M tetrabutylammonium hexafluorophosphate ($TBAPF_6$) as supporting electrolyte.

Acknowledgments

This work was supported by the Swiss National Science Foundation through grant number 200021_156063/1. Support from the European Union, COST action, CM1202, PERSPECT-H_2O is acknowledged.

[1] A. Juris, V. Balzani, F. Barigelletti, S. Campagna, P. Belser, A. Von Zelewsky, *Coord. Chem. Rev.* **1988**, *84*, 85–277.
[2] T. J. Meyer, *Pure Appl. Chem.* **1986**, *58*, 1193–1206.
[3] a) M. S. Lowry, S. Bernhard, *Chem. Eur. J.* **2006**, *12*, 7970–7977; b) K. S. Schanze, D. B. MacQueen, T. A. Perkins, L. A. Cabana, *Coord. Chem. Rev.* **1993**, *122*, 63–89; c) K. N. Swanick, S. Ladouceur, E. Zysman-Colman, Z. F. Ding, *Chem. Commun.* **2012**, *48*, 3179–3181; d) R. D. Costa, E. Orti, H. J. Bolink, F. Monti, G. Accorsi, N. Armaroli, *Angew. Chem. Int. Ed.* **2012**, *51*, 8178–8211; *Angew. Chem.* **2012**, *124*, 8300.
[4] a) V. Balzani, A. Juris, M. Venturi, S. Campagna, S. Serroni, *Chem. Rev.* **1996**, *96*, 759–833; b) M. H. Keefe, K. D. Benkstein, J. T. Hupp, *Coord. Chem. Rev.* **2000**, *205*, 201–228; c) H. Yersin, A. F. Rausch, R. Czerwieniec, T. Hofbeck, T. Fischer, *Coord. Chem. Rev.* **2011**, *255*, 2622–2652; d) M. Cattaneo, F. Fagalde, C. D. Borsarelli, N. E. Katz, *Inorg. Chem.* **2009**, *48*, 3012–3017; e) A. Breivogel, M. Park, D. Lee, S. Klassen, A. Kuhnle, C. Lee, K. Char, K. Heinze, *Eur. J. Inorg. Chem.* **2014**, 288–295.
[5] a) A. Hagfeldt, M. Grätzel, *Chem. Rev.* **1995**, *95*, 49–68; b) A. Hagfeldt, G. Boschloo, L. C. Sun, L. Kloo, H. Pettersson, *Chem. Rev.* **2010**, *110*, 6595–6663; c) R. Argazzi, C. A. Bignozzi, T. A. Heimer, F. N. Castellano, G. J. Meyer, *Inorg. Chem.* **1994**, *33*, 5741–5749.
[6] a) A. E. Friedman, J. C. Chambron, J. P. Sauvage, N. J. Turro, J. K. Barton, *J. Am. Chem. Soc.* **1990**, *112*, 4960–4962; b) K. E. Erkkila, D. T. Odom, J. K. Barton, *Chem. Rev.* **1999**, *99*, 2777–2795; c) Y. Sun, D. A. Lutterman, C. Turro, *Inorg. Chem.* **2008**, *47*, 6427–6434; d) E. Baggaley, M. R. Gill, N. H. Green, D. Turton, I. V. Sazanovich, S. W. Botchway, C. Smythe, J. W. Haycock, J. A. Weinstein, J. A. Thomas, *Angew. Chem. Int. Ed.* **2014**, *53*, 3367–3371; *Angew. Chem.* **2014**, *126*, 3435.
[7] a) O. S. Wenger, *Coord. Chem. Rev.* **2009**, *253*, 1439–1457; b) S. Van Wallendael, D. P. Rillema, *Coord. Chem. Rev.* **1991**, *111*, 297–318; c) L. De Cola, P. Belser, *Coord. Chem. Rev.* **1998**, *177*, 301–346; d) A. I. Baba, J. R. Shaw, J. A. Simon, R. P. Thummel, R. H. Schmehl, *Coord. Chem. Rev.* **1998**, *171*, 43–59; e) A. Vlček, M. Busby, *Coord. Chem. Rev.* **2006**, *250*, 1755–1762.
[8] a) J. M. R. Narayanam, C. R. J. Stephenson, *Chem. Soc. Rev.* **2011**, *40*, 102–113; b) C. K. Prier, D. A. Rankic, D. W. C. MacMillan, *Chem. Rev.* **2013**, *113*, 5322–5363; c) C. D. Windle, R. N. Perutz, *Coord. Chem. Rev.* **2012**, *256*, 2562–2570; d) B. Kumar, M. Llorente, J. Froehlich, T. Dang, A. Sathrum, C. P. Kubiak, *Annu. Rev. Phys. Chem.* **2012**, *63*, 541–569; e) X. Sala, S. Maji, R. Bofill, J. Garcia-Anton, L. Escriche, A. Llobet, *Acc. Chem. Res.* **2014**, *47*, 504–516.
[9] M. Goez, C. Kerzig, R. Naumann, *Angew. Chem. Int. Ed.* **2014**, *53*, 9914–9916; *Angew. Chem.* **2014**, *126*, 10072.
[10] a) O. S. Wenger, *Acc. Chem. Res.* **2011**, *44*, 25–35; b) O. S. Wenger, *Acc. Chem. Res.* **2013**, *46*, 1517–1526.
[11] a) A. B. P. Lever, *Inorg. Chem.* **1990**, *29*, 1271–1285; b) E. S. Dodsworth, A. B. P. Lever, *Chem. Phys. Lett.* **1986**, *124*, 152–158; c) A. B. P. Lever, *Inorg. Chem.* **1991**, *30*, 1980–1985; d) N. H. Damrauer, T. R. Boussie, M. Devenney, J. K. McCusker, *J. Am. Chem. Soc.* **1997**, *119*, 8253–8268; e) S. L. Howell, K. C. Gordon, *J. Phys. Chem. A* **2006**, *110*, 4880–4887; f) C. M. Elliott, E. J. Hershenhart, *J. Am. Chem. Soc.* **1982**, *104*, 7519–7526; g) M. Wachtler, M. Maiuri, D. Brida, J. Popp, S. Rau, G. Cerullo, B. Dietzek, *ChemPhysChem* **2013**, *14*, 2973–2983.
[12] O. Mongin, P. Rocca, L. Thomas-dit-Dumont, F. Trécourt, F. Marsais, A. Godard, G. Quéguiner, *J. Chem. Soc. Perkin Trans. 1* **1995**, 2503–2508.
[13] a) M. J. Fuentes, R. J. Bognanno, W. G. Dougherty, W. J. Boyko, W. S. Kassel, T. J. Dudley, J. J. Paul, *Dalton Trans.* **2012**, *41*, 12514–12523; b) S. Klein, W. G. Dougherty, W. S. Kassel, T. J. Dudley, J. J. Paul, *Inorg. Chem.* **2011**, *50*, 2754–2763.
[14] Production of 2-chloro-5-hydroxypyridine: Y. Takuma, Y. Kasuga, Mitsubishi Chem. Corp., Patent IPC: C07B61/00 C07D213/65, Mitsubishi Chem. Corp. **1998**.
[15] M. Ando, N. Sato, T. Nagase, K. Nagai, S. Ishikawa, H. Takahashi, N. Ohtake, J. Ito, M. Hirayama, Y. Mitobe, H. Iwaasa, A. Gomori, H. Matsushita, K. Tadano, N. Fujino, S. Tanaka, T. Ohe, A. Ishihara, A. Kanatani, T. Fukami, *Bioorg. Med. Chem.* **2009**, *17*, 6106–6122.
[16] S. D. Kuduk, R. M. DiPardo, M. G. Bock, *Org. Lett.* **2005**, *7*, 577–579.
[17] a) A. Jutand, A. Mosleh, *J. Org. Chem.* **1997**, *62*, 261–274; b) S. A. McFarland, F. S. Lee, K. Cheng, F. L. Cozens, N. P. Schepp, *J. Am. Chem. Soc.* **2005**, *127*, 7065–7070.
[18] C. M. Elliott, R. A. Freitag, D. D. Blaney, *J. Am. Chem. Soc.* **1985**, *107*, 4647–4655.
[19] A. Juris, V. Balzani, P. Belser, A. Von Zelewsky, *Helv. Chim. Acta* **1981**, *64*, 2175–2182.
[20] S. J. Slattery, N. Gokaldas, T. Mick, K. A. Goldsby, *Inorg. Chem.* **1994**, *33*, 3621–3624.

[21] V. V. Pavlishchuk, A. W. Addison, *Inorg. Chim. Acta* **2000**, *298*, 97–102.
[22] K. Suzuki, A. Kobayashi, S. Kaneko, K. Takehira, T. Yoshihara, H. Ishida, Y. Shiina, S. Oishic, S. Tobita, *Phys. Chem. Chem. Phys.* **2009**, *11*, 9850–9860.
[23] a) A. A. Abdel-Shafi, D. R. Worrall, A. Y. Ershov, *Dalton Trans.* **2004**, 30–36; b) J. Hankache, M. Niemi, H. Lemmetyinen, O. S. Wenger, *Inorg. Chem.* **2012**, *51*, 6333–6344.
[24] a) A. Yoshimura, M. Z. Hoffman, H. Sun, *Photochem. Photobiol.* **1993**, *70*, 29–33; b) P. Müller, K. Brettel, *Photochem. Photobiol. Sci.* **2012**, *11*, 632–636.
[25] D. M. Roundhill, *Photochemistry and Photophysics of Metal Complexes*, Plenum Press, New York, **1994**, p.
[26] C. R. Bock, J. A. Connor, A. R. Gutierrez, T. J. Meyer, D. G. Whitten, B. P. Sullivan, J. K. Nagle, *J. Am. Chem. Soc.* **1979**, *101*, 4815–4824.
[27] A. El-ghayoury, A. Harriman, R. Ziessel, *Chem. Commun.* **1999**, 2027–2028.
[28] W. Sattler, L. M. Henling, J. R. Winkler, H. B. Gray, *J. Am. Chem. Soc.* **2015**, *137*, 1198–1205.
[29] D. C. Smith, H. B. Gray, *Coord. Chem. Rev.* **1990**, *100*, 169–181.
[30] D. Shukla, R. H. Young, S. Farid, *J. Phys. Chem. A* **2004**, *108*, 10386–10394.
[31] a) K. T. Tarantino, P. Liu, R. R. Knowles, *J. Am. Chem. Soc.* **2013**, *135*, 10022–10025; b) H. G. Yayla, R. R. Knowles, *Synlett* **2014**, *25*, 2819–2826.
[32] S. Fukuzumi, K. Ishikawa, K. Hironaka, T. Tanaka, *J. Chem. Soc. Perkin Trans. 2* **1987**, 751–760.
[33] S. K. Ghoshal, S. K. Sarkar, G. S. Kastha, *Bull. Chem. Soc. Jpn.* **1981**, *54*, 3556–3561.
[34] H. Lutz, E. Breheret, L. Lindqvist, *J. Phys. Chem.* **1973**, *77*, 1758–1762.
[35] a) L. Biczok, N. Gupta, H. Linschitz, *J. Am. Chem. Soc.* **1997**, *119*, 12601–12609; b) L. Biczók, H. Linschitz, *J. Phys. Chem.* **1995**, *99*, 1843–1845; c) J. Nomrowski, O. S. Wenger, *Inorg. Chem.* **2015**, *54*, 3680–3687.
[36] J. T. Muckerman, J. H. Skone, M. Ning, Y. Wasada-Tsutsui, *Biochim. Biophys. Acta Bioenerg.* **2013**, *1827*, 882–891.
[37] a) J. J. Warren, T. A. Tronic, J. M. Mayer, *Chem. Rev.* **2010**, *110*, 6961–7001; b) D. R. Weinberg, C. J. Gagliardi, J. F. Hull, C. F. Murphy, C. A. Kent, B. C. Westlake, A. Paul, D. H. Ess, D. G. McCafferty, T. J. Meyer, *Chem. Rev.* **2012**, *112*, 4016–4093; c) S. Y. Reece, D. G. Nocera, *Annu. Rev. Biochem.* **2009**, *78*, 673–699; d) C. Costentin, M. Robert, J.-M. Savéant, *Acc. Chem. Res.* **2010**, *43*, 1019–1029; e) L. Hammarström, S. Styring, *Energy Environ. Sci.* **2011**, *4*, 2379–2388; f) T. T. Eisenhart, J. L. Dempsey, *J. Am. Chem. Soc.* **2014**, *136*, 12221–12224; g) T. Irebo, M.-T. Zhang, T. F. Markle, A. M. Scott, L. Hammarström, *J. Am. Chem. Soc.* **2012**, *134*, 16247–16254.
[38] C. R. Waidmann, A. J. M. Miller, C. W. A. Ng, M. L. Scheuermann, T. R. Porter, T. A. Tronic, J. M. Mayer, *Energy Environ. Sci.* **2012**, *5*, 7771–7780.
[39] *Apex2*, Ion 2 user manual, M86-E01078, Bruker Analytical X-ray Systems Inc. **2006**, Madison, WI, USA.
[40] L. Palatinus, G. Chapuis, *J. Appl. Crystallogr.* **2007**, *40*, 786–790.
[41] P. W. Betteridge, J. R. Carruthers, R. I. Cooper, K. Prout, D. J. Watkin, *J. Appl. Crystallogr.* **2003**, *36*, 1487–1487.
[42] C. F. Macrae, I. J. Bruno, J. A. Chisholm, P. R. Edgington, P. McCabe, E. Pidcock, L. Rodriguez-Monge, R. Taylor, J. van de Streek, P. A. Wood, *J. Appl. Crystallogr.* **2008**, *41*, 466–470.

Received: June 16, 2015
Published Online: September 4, 2015

3.2 Tris(bis(isocyanide)triaryl) Molybdenum(0) Complexes as $[Ru(bpy)_3]^{2+}$ Analoga

Since the approach to strongly reducing photosensitizers discussed before, namely the introduction of electron donating groups in the ligand scaffold, has its limitations in terms of stability as well as the range of potentials accessible, an alternative strategy was developed. As shown in Chapter 2.1.3, the excited state oxidation potential of a complex is tunable by variation of the ground state oxidation potential. This potential is limited to a certain range for each metal in a specific oxidation state. Thus a significant lowering of the ground state oxidation potential is only accessible via a replacement of the metal center by one with a lower oxidation state.

Ruthenium itself is a precious metal with one of the lowest abundances in the earths crust (approx. 0.001 ppm).[4] This leads to a relatively high price on the world market (1350 USD/kg[3]). Therefore it is desirable to substitute ruthenium with other metals, which are more earth-abundant and stable in a lower oxidation state. Considering that the metal should be isoelectronic to ruthenium(II) one could think of its neighbouring atom in the periodic table, which would be technetium(I). However, Tc(I) is radioactive and therefore not a suitable substitute. Molybdenum(0) appeared to be a suitable choice for this task. Additional to its electronic similarity to Ru(II) molybdenum is approximately 10000 times more earth-abundant than ruthenium (14 ppm)[4], which results in a much lower price (15 USD/kg[3]).

In general, ligands which are strong π-acceptors help to stabilize metals in low oxidation states. These complexes tend to be rather robust and to some extent air stable. In order to obtain an air stable and robust molybdenum(0) complex a suitable ligand with significant π-accepting capability is needed. Aryl isocyanides are known to be strong π-acceptors and, similar to carbonyl ligands, to stabilize zero-valent metal complexes.

Molybdenum(0) complexes with monodentate aryl isocyanide ligands are known to exhibit ^{3}MLCT emission, but undergo rapid photosubstitution reactions in the excited state (s. Chapter 2.3.1), disqualifying them as photosensitizers.[6] In avoidance of these reactions, a chelating aryl isocyanide ligand was designed and the new complex $[Mo(CNAr_3NC)_3]$ (Fig. III.2) synthesized.

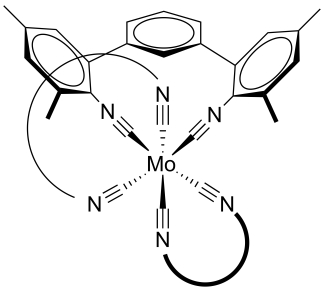

Figure III.2: Molecular structure of the complex $[Mo(CNAr_3NC)_3]$.

The introduction of sterically demanding chelating isocyanide ligands should shield the metal center against nucleophilic attacks in its oxidized state and prevent photosubstitution. In addition, the rigid, aromatic scaffold is supposed to minimize non-radiative relaxation processes by rising the energy of accessible vibrational modes: This should result in prolonged ^{3}MLCT excited state lifetimes and higher quantum yields, which are essential to perform efficient electron transfer reactions from the excited state.
The new complex was found to have broad ^{1}MLCT transition bands between 340 nm and 520 nm and exhibit significantly longer ^{3}MLCT excited state lifetimes, ranging from 70 ns (THF) to 220 ns (n-hexane), when compared to monodentate hexakis(isocyanide aryl) complexes ($<$ 20 ns).
The new complex remained sufficiently inert to substitution reactions under light irradiation and showed a reversible one electron oxidation wave at a potential of -0.4 V vs. Fc^+/Fc in cyclic voltammetry experiments. With an estimated excited state energy of 2.2 eV, the excited state oxidation potential is expected to be -2.6 V vs. $Fc^{+/0}$.
Stern-Volmer experiments were performed with the complex in THF using acetophenone (-2.52 V vs. Fc^+/Fc) as a quencher. The electron transfer from the excited complex to acetophenone was determined to proceed with kinetics close to the diffusion limit (k_q: 3.1$\pm$ 0.4 $\times$ 10^9 $M^{-1}s^{-1}$). The potential application of this complex as a photocatalyst was put to proof by a vinyl-cyclopropane-cyclopentene-like rearrangement reaction. The electron-catalyzed rearrangement reaction of an acyl-cyclopropane to a 2,3-dihydrofuran was chosen as a benchmark reaction since the initiation of the reaction requires a very negative oxidation potential of the photocatalyst. The reaction proceeds in benzene under very mild reaction conditions (r.t., λ_{ex}: 455 nm) and yields the desired product in 84% yield with close to maximum TON of 17 ($TON_{theo.max.}$: 20). In contrast, the well-established [Ir(ppy)$_3$] ($E^{IV/III*}$: -2.1 V vs $Fc^{+/0}$) was not able to catalyse this reaction.

Author Contributions

- L. A. B. carried out the molecular design, synthesis and data analysis, as well as contributed equally to the preparation of the manuscript.
- X. G. conducted the design of the photocatalytic experiments and the interpretation of their results. He also contributed equally to the preparation of the manuscript.
- A. P. contributed the crystal structure.
- O. S. W. contributed equally to the molecular and system design, as well as the interpretation of data and preparation of the manuscript.

GDCh Communications Angewandte International Edition Chemie

Photoredox Catalysis

International Edition: DOI: 10.1002/anie.201605571
German Edition: DOI: 10.1002/ange.201605571

A Molybdenum(0) Isocyanide Analogue of Ru(2,2′-Bipyridine)$_3^{2+}$: A Strong Reductant for Photoredox Catalysis

*Laura A. Büldt, Xingwei Guo, Alessandro Prescimone, and Oliver S. Wenger**

Abstract: *We report the first homoleptic Mo^0 complex with bidentate isocyanide ligands, which exhibits metal-to-ligand charge transfer (^{3}MLCT) luminescence with quantum yields and lifetimes similar to $Ru(bpy)_3^{2+}$ (bpy = 2,2′-bipyridine). This Mo^0 complex is a very strong photoreductant, which manifests in its capability to reduce acetophenone with essentially diffusion-limited kinetics as shown by time-resolved laser spectroscopy. The application potential of this complex for photoredox catalysis was demonstrated by the rearrangement of an acyl cyclopropane to a 2,3-dihydrofuran, which is a reaction that requires a reduction potential so negative that even the well-known and strongly reducing Ir(2-phenylpyridine)$_3$ photosensitizer cannot catalyze it. Our study thus provides the proof-of-concept for the use of chelating isocyanides to obtain Mo^0 complexes with long-lived ^{3}MLCT excited states that are applicable to unusually challenging photoredox chemistry.*

Ru(bpy)$_3^{2+}$ is the prototype of a very large class of metal complexes with long-lived metal-to-ligand charge transfer (^{3}MLCT) excited states,[1] which comprises many examples based on the precious metals Ru^{II},[2] Os^{II},[3] Re^{I},[4] and Ir^{III}.[5] Aside from such d^6 metal diimines, many Pt^{II} and $Au^{I/III}$ complexes have favorable luminescence properties,[6] but emissive complexes made from earth-abundant metals are more difficult to obtain.[7] Notable exceptions are complexes based on Zn^{II} or Cu^{I},[8] but their MLCT excited states often undergo strong geometrical distortion,[9] and nonradiative relaxation to the ground state can be rapid.

Many of the above-mentioned metal complexes have found applications, for example, as triplet harvesters in organic light emitting diodes (OLEDs),[10] photosensitizers in dye-sensitized solar cells (DSSCs),[11] or sensitizers of electron- and energy-transfer processes in artificial and biological systems.[12] In recent years, photoredox catalysis has received much attention in organic synthesis,[13] with Ru^{II} and Ir^{III} complexes playing a particularly prominent role. Furthermore, Ru(bpy)$_3^{2+}$ and related complexes are now frequently used for the production of solar fuels, for example, in the light-driven reduction of CO_2 or H_2O.[14] However, ruthenium is a precious metal with a natural abundance of approximately 10^{-3} ppm in the earth's crust, and even though the luminescence and photoredox properties of Ru(bpy)$_3^{2+}$-type complexes are tunable through ligand variation, there are limitations to this approach. In view of the continued great interest in the above-mentioned research areas ranging from synthetic organic chemistry to materials applications and solar-energy conversion, the development of new photosensitizers is highly desirable.

The photophysical and photochemical properties of Mo^0 complexes with monodentate arylisocyanide ligands were first explored nearly 40 years ago.[15] Some ^{3}MLCT luminescence was indeed observed, but these complexes become substitutionally labile upon photoexcitation, thus making them unsuitable for most applications.[15,16] Recently, W^0 complexes with monodentate arylisocyanides were found to be strong emitters and photoreductants, but as a 5d metal, W^0 is inherently more inert to substitution than the 4d metal Mo^0.[17] We hypothesized that by using chelating arylisocyanides rather than monodentate ligands, it might be possible to obtain robust Mo^0 complexes with long-lived ^{3}MLCT excited states and high reducing power.

Compared to α-diimine ligands such as 2,2′-bipyridine, there has been surprisingly little prior work on chelating isocyanide ligands,[18] particularly with regard to luminescent metal complexes.[19] We prepared the new 2,2″-diisocyano-3,5,3″,5″-tetramethyl-1,1′:3′,1″-terphenyl ($CNAr_3NC$) ligand and reacted it with $Mo(THF)_2Cl_4$ in the presence of Na/Hg to obtain the $Mo(CNAr_3NC)_3$ complex shown in Figure 1 (pages S2–S5 in the Supporting Information). X-ray diffraction on single crystals revealed Mo–C distances of 2.051(5) and 2.056(4) Å, as well as C-Mo-C bite angles between 82.9(2) and 94.2(4)° (pages S6–S7 in the Supporting Information). In each ligand, there are torsion angles of 51.2(7) and 55.8(7)° between the central benzene ring and the two flanking aryls.

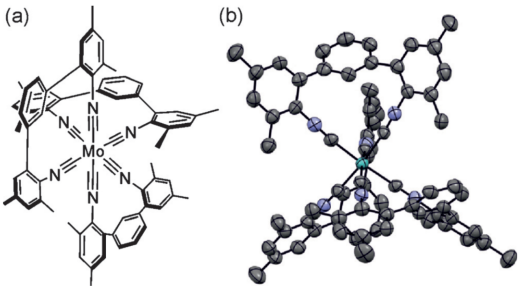

Figure 1. Molecular (a) and crystallographic (b) structures of the $Mo(CNAr_3NC)_3$ complex; thermal ellipsoids are drawn at the 50% probability level.[29] Hydrogen atoms are omitted for clarity.

[*] L. A. Büldt, Dr. X. Guo, Dr. A. Prescimone, Prof. Dr. O. S. Wenger
Department of Chemistry, University of Basel
St. Johanns-Ring 19 and Spitalstrasse 51, 4056 Basel (Switzerland)
E-mail: oliver.wenger@unibas.ch

Supporting information and the ORCID identification number(s) for the author(s) of this article can be found under http://dx.doi.org/10.1002/anie.201605571.

trans-Standing isocyanobenzene units are nearly orthogonal to each another. The methyl substituents help shield the metal center from the environment and thus presumably contribute to the overall stability of the complex. The C≡N stretch frequency in the complex is $\tilde{\nu} = 1939\ cm^{-1}$, compared to $\tilde{\nu} = 2113\ cm^{-1}$ in the free ligand, thus indicating substantial π backbonding (page S8 in the Supporting Information).[20]

In cyclic voltammetry, the Mo^0 center is oxidized reversibly to Mo^I at a potential (E^0) of −0.40 V vs. Fc^+/Fc in THF (page S9 in the Supporting Information), which is in line with a prior report of Mo^0 complexes with monodentate isocyanide ligands.[15a]

The UV/Vis absorption spectrum of $Mo(CNAr_3NC)_3$ in THF (Figure 2a) exhibits a broad band between λ = 350 and

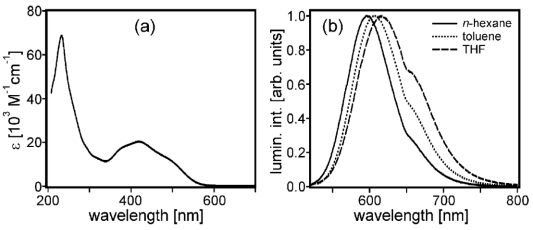

Figure 2. a) UV/Vis absorption spectrum of $Mo(CNAr_3NC)_3$ in THF at 20 °C. b) Luminescence spectra in different solvents at 20 °C ($\lambda_{exc} = 500$ nm).

λ = 560 nm, which is reminiscent of the MLCT absorption of $Ru(bpy)_3^{2+}$. At shorter wavelengths, there are ligand-based absorptions. The photoluminescence band maximum is blue-shifted when going from THF to toluene to *n*-hexane (Figure 2b), as expected for MLCT emission. The luminescence lifetime (τ) increases from 74 ± 7 (THF) to 166 ± 17 (toluene) to 225 ± 23 ns (*n*-hexane) in deaerated solutions at 20 °C (page S11 in the Supporting Information), and in parallel there is an increase of the luminescence quantum yield (ϕ) from 0.6 ± 0.1 to 2.3 ± 0.2 to 4.5 ± 0.4 % (page S11 in the Supporting Information). In frozen matrices at 77 K, there is a strong rigidochromic effect and emission decays are biexponential with lifetimes in the μs region (pages S12–S13 in the Supporting Information). From the 77 K emission spectra, we estimate an energy (E_{00}) of 2.2 eV for the emissive ^{3}MLCT state. The transient absorption spectra of the long-lived ^{3}MLCT excited state of $Mo(CNAr_3NC)_3$ in various solvents are very similar to the spectrum of the ^{3}MLCT state of $Ru(bpy)_3^{2+}$ (page S10 in the Supporting Information).

Given a potential of −0.40 V vs. Fc^+/Fc in the electronic ground state and an energy (E_{00}) of 2.2 eV for the emissive excited state (see above), a potential of around −2.6 V vs. Fc^+/Fc can be expected for oxidation of Mo^0 to Mo^I in the long-lived ^{3}MLCT state. In order to test this estimate of the excited-state redox potential, the possibility of photoinduced electron transfer with acetophenone (ACP) was explored. The redox potential for the ACP/ACP$^-$ couple in THF is −2.5 V vs. Fc^+/Fc,[21] and hence ^{3}MLCT-excited $Mo(CNAr_3NC)_3$ should be thermodynamically competent for the reduction of ACP to ACP$^-$. Indeed the luminescence of $Mo(CNAr_3NC)_3$ in THF is strongly quenched upon addition of ACP (page S14 in the Supporting Information), and a Stern–Volmer plot (Figure 3a) yields a quenching constant of $(3.1 \pm 0.4) \times 10^9\ M^{-1}\ s^{-1}$, which is near the diffusion limit.

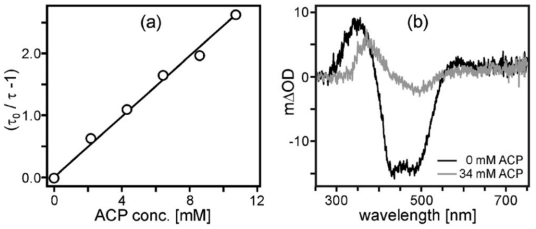

Figure 3. Stern–Volmer plot based on luminescence lifetimes ($\lambda_{det} = 615$ nm) of ca. 10^{-5} M $Mo(CNAr_3NC)_3$ in deaerated THF at 20 °C in presence of increasing concentrations of acetophenone (ACP). b) Transient absorption of ca. 10^{-5} M $Mo(CNAr_3NC)_3$ in the absence (black) and presence (gray) of 34 mM ACP. Excitation and detection was as described above. The disappearance of the bleach between 400 and 520 nm is caused by formation of the ACP radical anion (ACP$^-$); see text and pages S14–S16 in the Supporting Information.

The transient absorption data in Figure 3b are fully compatible with the formation of ACP$^-$ and $Mo(CNAr_3NC)_3^+$ (see pages S14–S16 in the Supporting Information for further details).

To assess the potential applicability of $Mo(CNAr_3NC)_3$ as a photoredox catalyst, we attempted to perform a rearrangement of an acyl cyclopropane (**1**) to a 2,3-dihydrofuran (**2**; Scheme 1), a reaction related to vinylcyclopropane-cyclopentene rearrangements that are important for organic synthesis.[22] 2,3-Dihydrofurans play key roles as structural

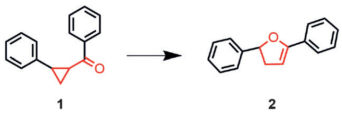

Scheme 1. Rearrangement of acyl cyclopropane (**1**) to 2,3-dihydrofuran (**2**) accomplished in 84 % yield through photoirradiation ($\lambda_{exc} = 455$ nm) of 5 % $Mo(CNAr_3NC)_3$ in dry [D_6]benzene (TON = 17).

elements of biologically active compounds such as aflatoxin B_1, and they are considered very useful synthetic intermediates.[23] We used the reaction in Scheme 1 as a benchmark for the utility of our complex. Thermally, the conversion of **1** into **2** is very difficult to perform because very harsh conditions or activating groups are necessary.[24]

When irradiating a mixture of substrate **1** and 5 % $Mo(CNAr_3NC)_3$ in dry [D_6]benzene with a blue LED at λ = 455 nm in an evacuated sealed NMR tube, product **2** is formed in 84 % yield (at room temperature). When attempting to perform the same reaction with the well-known $Ir(ppy)_3$ (ppy = 2-phenylpyridine) photosensitizer, no conversion is observed. We attribute this to the very negative potential required for one-electron reduction of **1**, which is

necessary to initiate pericyclic rearrangement through a diradical mechanism. This potential can reasonably be assumed to be similar to that of acetophenone (−2.5 V vs. Fc^+/Fc), and our Mo^0 complex has sufficient reducing power (−2.6 V vs. Fc^+/Fc) to undergo photoinduced electron transfer with nearly diffusion-limited kinetics (see above). By contrast, the $Ir(ppy)_3$ photosensitizer has an excited-state reduction potential of only −2.1 V vs. Fc^+/Fc[13c] and is therefore unable to reduce **1** efficiently.

The proposed reaction mechanism for the conversion of **1** into **2** with $Mo(CNAr_3NC)_3$ is shown in Scheme 2. Initially only the *trans* isomer of **1** is present.[25] Electron transfer between photoexcited $Mo(CNAr_3NC)_3$ and *trans*-**1** produces radical intermediate $\mathbf{A}^{-\cdot}$ which can be oxidized to diradical **B**

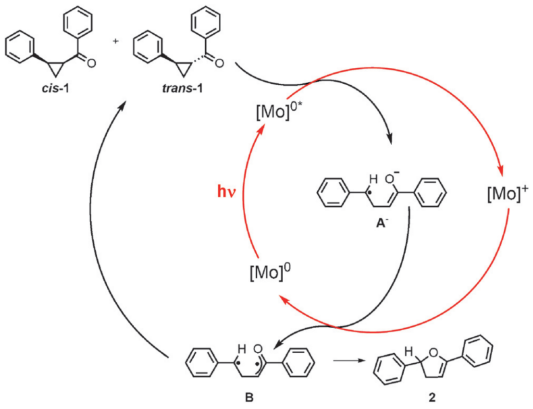

Scheme 2. Proposed reaction mechanism for the conversion of **1** into **2**. Mo^{0*} denotes the photoexcited $Mo(CNAr_3NC)_3$ complex.

by $Mo(CNAr_3NC)_3^+$ in the electronic ground state.[26] **B** can then either undergo intramolecular reaction to form product **2** or it can revert to substrate **1**, thereby producing a mixture of *cis* and *trans* isomers. Both diastereomers can then re-enter the catalysis cycle with photoexcited Mo^0 complex until conversion to **2** is complete. In principle, this can be considered an electron-catalyzed reaction.[27]

Owing to the ability of diradical **B** to undergo forward and backward reactions, the irradiation time to achieve complete conversion to **2** is relatively long, at approximately 80 hours. This is evidently an inherent property of the model reaction investigated here and is clearly not a shortcoming of the Mo^0 sensitizer. We were able to follow the isomerization of **1** and conversion to **2** as a function of irradiation time by NMR spectroscopy (page S17 in the Supporting Information). The overall yield of **2** is 84%, which corresponds to a TON of 17, which is close to the theoretical limit of 20 at a catalyst loading of 5%.

In summary, we have synthesized and characterized the first homoleptic Mo^0 complex with bidentate isocyanide ligands. Photoexcited $Mo(CNAr_3NC)_3$ has roughly 1.3 V more reducing power than ^{3}MLCT-excited $Ru(bpy)_3^{2+}$,[1a,2a,13c] and it is about 0.5 V more reducing than photoexcited $Ir(ppy)_3$,[13c,17a,28] thus making it one of the most potent visible-light absorbing photoreductants known to date. The application potential of Mo^0 complexes with chelating isocyanides for photoredox catalysis was illustrated in this study by using the example of a pericyclic rearrangement, which is a very challenging benchmark reaction because its initiation requires exceptionally strong reductants. The $Mo(CNAr_3NC)_3$ complex is able to act as a robust and efficient photoredox sensitizer for this reaction, clearly outperforming the widely used $Ir(ppy)_3$ complex.

In conclusion, our study provides a proof-of-concept for the use of chelating isocyanides to obtain Mo^0 complexes with long-lived ^{3}MLCT excited states, which emit visible light and are applicable to unusually challenging photoredox chemistry.

Acknowledgements

This research was supported by the Swiss National Science Foundation through grant number 200021_156063/1 and through the NCCR Molecular Systems Engineering.

Keywords: electron transfer · isocyanide ligands · luminescence · photocatalysis · photochemistry

How to cite: *Angew. Chem. Int. Ed.* **2016**, *55*, 11247–11250
Angew. Chem. **2016**, *128*, 11413–11417

[1] a) C. R. Bock, T. J. Meyer, D. G. Whitten, *J. Am. Chem. Soc.* **1974**, *96*, 4710–4712; b) R. Bensasson, C. Salet, V. Balzani, *J. Am. Chem. Soc.* **1976**, *98*, 3722–3724.
[2] a) A. Juris, V. Balzani, F. Barigelletti, S. Campagna, P. Belser, A. Von Zelewsky, *Coord. Chem. Rev.* **1988**, *84*, 85–277; b) J. K. McCusker, *Acc. Chem. Res.* **2003**, *36*, 876–887; c) J. England, C. C. Scarborough, T. Weyhermüller, S. Sproules, K. Wieghardt, *Eur. J. Inorg. Chem.* **2012**, 4605–4621.
[3] J.-P. Sauvage, J.-P. Collin, J.-C. Chambron, S. Guillerez, C. Coudret, V. Balzani, F. Barigelletti, L. De Cola, L. Flamigni, *Chem. Rev.* **1994**, *94*, 993–1019.
[4] a) K. S. Schanze, D. B. MacQueen, T. A. Perkins, L. A. Cabana, *Coord. Chem. Rev.* **1993**, *122*, 63–89; b) D. J. Stufkens, A. Vlcek, *Coord. Chem. Rev.* **1998**, *177*, 127–179.
[5] a) M. S. Lowry, S. Bernhard, *Chem. Eur. J.* **2006**, *12*, 7970–7977; b) J. Li, P. I. Djurovich, B. D. Alleyne, M. Yousufuddin, N. N. Ho, J. C. Thomas, J. C. Peters, R. Bau, M. E. Thompson, *Inorg. Chem.* **2005**, *44*, 1713–1727; c) K. N. Swanick, S. Ladouceur, E. Zysman-Colman, Z. F. Ding, *Angew. Chem. Int. Ed.* **2012**, *51*, 11079–11082; *Angew. Chem.* **2012**, *124*, 11241–11244; d) R. D. Costa, E. Orti, H. J. Bolink, F. Monti, G. Accorsi, N. Armaroli, *Angew. Chem. Int. Ed.* **2012**, *51*, 8178–8211; *Angew. Chem.* **2012**, *124*, 8300–8334.
[6] a) M. Hissler, J. E. McGarrah, W. B. Connick, D. K. Geiger, S. D. Cummings, R. Eisenberg, *Coord. Chem. Rev.* **2000**, *208*, 115–137; b) V. W. W. Yam, *Acc. Chem. Res.* **2002**, *35*, 555–563; c) T. T. Zou, C. T. Lum, C. N. Lok, J. J. Zhang, C. M. Che, *Chem. Soc. Rev.* **2015**, *44*, 8786–8801; d) F. N. Castellano, I. E. Pomestchenko, E. Shikhova, F. Hua, M. L. Muro, N. Rajapakse, *Coord. Chem. Rev.* **2006**, *250*, 1819–1828; e) M. A. Malwitz, S. H. Lim, R. L. White-Morris, D. M. Pham, M. M. Olmstead, A. L. Balch, *J. Am. Chem. Soc.* **2012**, *134*, 10885–10893; f) M. J. Irwin, J. J. Vittal, R. J. Puddephatt, *Organometallics* **1997**, *16*, 3541–3547.
[7] a) S. Otto, M. Grabolle, C. Förster, C. Kreitner, U. Resch-Genger, K. Heinze, *Angew. Chem. Int. Ed.* **2015**, *54*, 11572–11576; *Angew. Chem.* **2015**, *127*, 11735–11739; b) A. Vogler, H.

Kunkely, *Transition Metal and Rare Earth Compounds: Excited States, Transition, Interactions I*, *Vol. 213*, Springer, Berlin, **2001**, pp. 143 – 182; c) A. J. Lees, *Chem. Rev.* **1987**, *87*, 711 – 743.

[8] a) G. Cheng, G. K. M. So, W. P. To, Y. Chen, C. C. Kwok, C. S. Ma, X. G. Guan, X. Chang, W. M. Kwok, C. M. Che, *Chem. Sci.* **2015**, *6*, 4623 – 4635; b) D. G. Cuttell, S. M. Kuang, P. E. Fanwick, D. R. McMillin, R. A. Walton, *J. Am. Chem. Soc.* **2002**, *124*, 6 – 7.

[9] L. X. Chen, G. B. Shaw, I. Novozhilova, T. Liu, G. Jennings, K. Attenkofer, G. J. Meyer, P. Coppens, *J. Am. Chem. Soc.* **2003**, *125*, 7022 – 7034.

[10] a) A. Tsuboyama, H. Iwawaki, M. Furugori, T. Mukaide, J. Kamatani, S. Igawa, T. Moriyama, S. Miura, T. Takiguchi, S. Okada, M. Hoshino, K. Ueno, *J. Am. Chem. Soc.* **2003**, *125*, 12971 – 12979; b) H. Yersin, A. F. Rausch, R. Czerwieniec, T. Hofbeck, T. Fischer, *Coord. Chem. Rev.* **2011**, *255*, 2622 – 2652.

[11] A. Hagfeldt, G. Boschloo, L. C. Sun, L. Kloo, H. Pettersson, *Chem. Rev.* **2010**, *110*, 6595 – 6663.

[12] a) B. Geiss, C. Lambert, *Chem. Commun.* **2009**, 1670 – 1672; b) A. Magnuson, M. Anderlund, O. Johansson, P. Lindblad, R. Lomoth, T. Polivka, S. Ott, K. Stensjö, S. Styring, V. Sundström, L. Hammarström, *Acc. Chem. Res.* **2009**, *42*, 1899 – 1909; c) J. R. Winkler, H. B. Gray, *Chem. Rev.* **1992**, *92*, 369 – 379; d) L. De Cola, P. Belser, *Coord. Chem. Rev.* **1998**, *177*, 301 – 346; e) D. G. Brown, N. Sanguantrakun, B. Schulze, U. S. Schubert, C. P. Berlinguette, *J. Am. Chem. Soc.* **2012**, *134*, 12354 – 12357; f) A. J. Howarth, M. B. Majewski, M. O. Wolf, *Coord. Chem. Rev.* **2015**, *282*, 139 – 149; g) M. Goez, C. Kerzig, R. Naumann, *Angew. Chem. Int. Ed.* **2014**, *53*, 9914 – 9916; *Angew. Chem.* **2014**, *126*, 10072 – 10074.

[13] a) J. Svoboda, B. König, *Chem. Rev.* **2006**, *106*, 5413 – 5430; b) J. M. R. Narayanam, C. R. J. Stephenson, *Chem. Soc. Rev.* **2011**, *40*, 102 – 113; c) C. K. Prier, D. A. Rankic, D. W. C. MacMillan, *Chem. Rev.* **2013**, *113*, 5322 – 5363; d) T. P. Yoon, M. A. Ischay, J. N. Du, *Nat. Chem.* **2010**, *2*, 527 – 532; e) T. Bach, J. P. Hehn, *Angew. Chem. Int. Ed.* **2011**, *50*, 1000 – 1045; *Angew. Chem.* **2011**, *123*, 1032 – 1077; f) H. H. Huo, X. D. Shen, C. Y. Wang, L. L. Zhang, P. Rose, L. A. Chen, K. Harms, M. Marsch, G. Hilt, E. Meggers, *Nature* **2014**, *515*, 100 – 103; g) K. T. Tarantino, P. Liu, R. R. Knowles, *J. Am. Chem. Soc.* **2013**, *135*, 10022 – 10025; h) O. Gutierrez, J. C. Tellis, D. N. Primer, G. A. Molander, M. C. Kozlowski, *J. Am. Chem. Soc.* **2015**, *137*, 4896 – 4899; i) A. C. Bissember, R. J. Lundgren, S. E. Creutz, J. C. Peters, G. C. Fu, *Angew. Chem. Int. Ed.* **2013**, *52*, 5129 – 5133; *Angew. Chem.* **2013**, *125*, 5233 – 5237.

[14] a) J. L. Dempsey, B. S. Brunschwig, J. R. Winkler, H. B. Gray, *Acc. Chem. Res.* **2009**, *42*, 1995 – 2004; b) M. G. Pfeffer, B. Schäfer, G. Smolentsev, J. Uhlig, E. Nazarenko, J. Guthmüller, C. Kuhnt, M. Wachtler, B. Dietzek, V. Sundström, S. Rau, *Angew. Chem. Int. Ed.* **2015**, *54*, 5044 – 5048; *Angew. Chem.* **2015**, *127*, 5132 – 5136; c) D. J. Boston, C. D. Xu, D. W. Armstrong, F. M. MacDonnell, *J. Am. Chem. Soc.* **2013**, *135*, 16252 – 16255; d) A. Fihri, V. Artero, M. Razavet, C. Baffert, W. Leibl, M. Fontecave, *Angew. Chem. Int. Ed.* **2008**, *47*, 564 – 567; *Angew. Chem.* **2008**, *120*, 574 – 577; e) E. Reisner, D. J. Powell, C. Cavazza, J. C. Fontecilla-Camps, F. A. Armstrong, *J. Am. Chem. Soc.* **2009**, *131*, 18457 – 18466; f) J. F. Hull, Y. Himeda, W. H. Wang, B. Hashiguchi, R. Periana, D. J. Szalda, J. T. Muckerman, E. Fujita, *Nat. Chem.* **2012**, *4*, 383 – 388; g) S. Kato, J. U. Jung, T. Suenobu, S. Fukuzumi, *Energy Environ. Sci.* **2013**, *6*, 3756 – 3764; h) C. D. Windle, M. W. George, R. N. Perutz, P. A. Summers, X. Z. Sun, A. C. Whitwood, *Chem. Sci.* **2015**, *6*, 6847 – 6864; i) H. Takeda, O. Ishitani, *Coord. Chem. Rev.* **2010**, *254*, 346 – 354; j) J. H. Alstrum-Acevedo, M. K. Brennaman, T. J. Meyer, *Inorg. Chem.* **2005**, *44*, 6802 – 6827; k) C. Herrero, A. Quaranta, S. El Ghachtouli, B. Vauzeilles, W. Leibl, A. Aukauloo, *Phys. Chem. Chem. Phys.* **2014**, *16*, 12067 – 12072.

[15] a) K. R. Mann, H. B. Gray, *J. Am. Chem. Soc.* **1977**, *99*, 306 – 307; b) K. R. Mann, M. Cimolino, G. L. Geoffroy, G. S. Hammond, A. A. Orio, G. Albertin, H. B. Gray, *Inorg. Chim. Acta* **1976**, *16*, 97 – 101.

[16] L. E. Shaw, C. H. Langford, *Coord. Chem. Rev.* **2002**, *230*, 165 – 169.

[17] a) W. Sattler, M. E. Ener, J. D. Blakemore, A. A. Rachford, P. J. LaBeaume, J. W. Thackeray, J. F. Cameron, J. R. Winkler, H. B. Gray, *J. Am. Chem. Soc.* **2013**, *135*, 10614 – 10617; b) W. Sattler, L. M. Henling, J. R. Winkler, H. B. Gray, *J. Am. Chem. Soc.* **2015**, *137*, 1198 – 1205; c) H. Kvapilová, W. Sattler, A. Sattler, I. V. Sazanovich, I. P. Clark, M. Towrie, H. B. Gray, S. Zalis, A. Vlcek, *Inorg. Chem.* **2015**, *54*, 8518 – 8528.

[18] a) F. E. Hahn, *Angew. Chem. Int. Ed. Engl.* **1993**, *32*, 650 – 665; *Angew. Chem.* **1993**, *105*, 681 – 696; b) F. E. Hahn, M. Tamm, *Angew. Chem. Int. Ed. Engl.* **1991**, *30*, 203 – 205; *Angew. Chem.* **1991**, *103*, 213 – 215; c) D. T. Plummer, G. A. Kraus, R. J. Angelici, *Inorg. Chem.* **1983**, *22*, 3492 – 3497; d) M. L. Winzenburg, J. A. Kargol, R. J. Angelici, *J. Organomet. Chem.* **1983**, *249*, 415 – 428; e) A. Naik, T. Maji, O. Reiser, *Chem. Commun.* **2010**, *46*, 4475 – 4477; f) A. Naik, L. Meina, M. Zabel, O. Reiser, *Chem. Eur. J.* **2010**, *16*, 1624 – 1628; g) M. Knorn, E. Lutsker, O. Reiser, *Organometallics* **2015**, *34*, 4515 – 4520; h) D. Vicenzi, P. Sgarbossa, A. Biffis, C. Tubaro, M. Basato, R. A. Michelin, A. Lanza, F. Nestola, S. Bogialli, P. Pastore, A. Venzo, *Organometallics* **2013**, *32*, 7153 – 7162.

[19] a) F. Monti, A. Baschieri, E. Matteucci, A. Mazzanti, L. Sambri, A. Barbieri, N. Armaroli, *Faraday Discuss.* **2015**, *185*, 233 – 248; b) M. Knorn, T. Rawner, R. Czerwieniec, O. Reiser, *ACS Catal.* **2015**, *5*, 5186 – 5193; c) D. B. Bagal, G. Kachkovskyi, M. Knorn, T. Rawner, B. M. Bhanage, O. Reiser, *Angew. Chem. Int. Ed.* **2015**, *54*, 6999 – 7002; *Angew. Chem.* **2015**, *127*, 7105 – 7108.

[20] a) G. W. Margulieux, N. Weidemann, D. C. Lacy, C. E. Moore, A. L. Rheingold, J. S. Figueroa, *J. Am. Chem. Soc.* **2010**, *132*, 5033 – 5035; b) C. C. Mokhtarzadeh, G. W. Margulieux, A. E. Carpenter, N. Weidemann, C. E. Moore, A. L. Rheingold, J. S. Figueroa, *Inorg. Chem.* **2015**, *54*, 5579 – 5587.

[21] P. J. Wagner, R. J. Truman, A. E. Puchalski, R. Wake, *J. Am. Chem. Soc.* **1986**, *108*, 7727 – 7738.

[22] a) J. E. Baldwin, *Chem. Rev.* **2003**, *103*, 1197 – 1212; b) M. Rubin, M. Rubina, V. Gevorgyan, *Chem. Rev.* **2007**, *107*, 3117 – 3179.

[23] a) S. Son, G. C. Fu, *J. Am. Chem. Soc.* **2007**, *129*, 1046 – 1047; b) T. G. Kilroy, T. P. O'Sullivan, P. J. Guiry, *Eur. J. Org. Chem.* **2005**, 4929 – 4949.

[24] a) C. L. Wilson, *J. Am. Chem. Soc.* **1947**, *69*, 3002 – 3004; b) R. K. Bowman, J. S. Johnson, *Org. Lett.* **2006**, *8*, 573 – 576; c) V. K. Yadav, R. Balamurugan, *Org. Lett.* **2001**, *3*, 2717 – 2719.

[25] K. Miyazawa, T. Koike, M. Akita, *Chem. Eur. J.* **2015**, *21*, 11677 – 11680.

[26] The oxidation potential of A^- is estimated to be lower than −0.8 V vs. Fc^+/Fc, given the reported values for related enolates: M. Schmittel, M. Lal, R. Lal, M. Röck, A. Langels, Z. Rappoport, A. Basheer, J. Schlirf, H. J. Deiseroth, U. Florke, G. Gescheidt, *Tetrahedron* **2009**, *65*, 10842 – 10855.

[27] A. Studer, D. P. Curran, *Nat. Chem.* **2014**, *6*, 765 – 773.

[28] K. A. King, P. J. Spellane, R. J. Watts, *J. Am. Chem. Soc.* **1985**, *107*, 1431 – 1432.

[29] CCDC 1446591 contains the supplementary crystallographic data for this paper. These data are provided free of charge by The Cambridge Crystallographic Data Centre.

Received: June 8, 2016
Published online: July 27, 2016

3.2.1 Photo-Triggered Electron-Catalyzed Ring Closure Reaction of Halogenated Benzyl-Phenylethers

The general applicability of molybdenum(0) complexes bearing chelating isocyanide ligands as strongly reducing photocatalysts was illustrated using the aforementioned acyl-cyclopropane-2,3-dihydrofuran rearrangement reaction.[72] This proof of principle lead to a first attempt at approaching the challenge of cleaving relatively inert carbon-halogen bonds using photocatalysis. The application of the Mo(0) complex in the C-I bond cleavage and ring closure reaction of benzyl-2-iodo-phenylether was investigated (Figure III.3). This transformation is a well-known electron-catalyzed reaction initiated by a strong base and belongs to the class of base-promoted homolytic aromatic substitutions (BHAS).[24] There are only few reports of a photocatalytic approach to this reaction.[37–41]

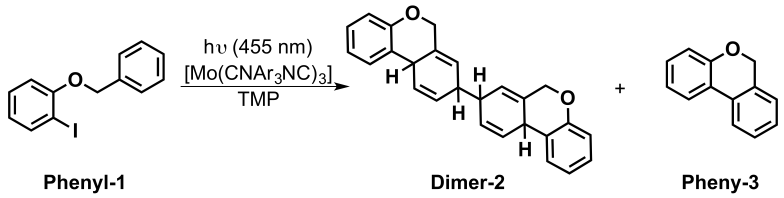

Figure III.3: Photo-triggered electron-catalyzed ring closure reaction of 1-(benzyloxy)-2-iodobenzene in benzene-d_6 using $[Mo(CNAr_3NC)_3]$ as a photocatalyst and TMP (2,2,6,6-tetramethylpiperidine) as base.

As a case study, a mixture of substrate **Phenyl-1**, 1 equivalent of 2,2,6,6-tetramethylpiperidine (TMP) and 14 mol% catalyst in deaerated benzene-d_6 was irradiated at 455 nm in a sealed NMR tube. ^{1}H-NMR spectra were recorded after 1 h and 13 h of irradiation.

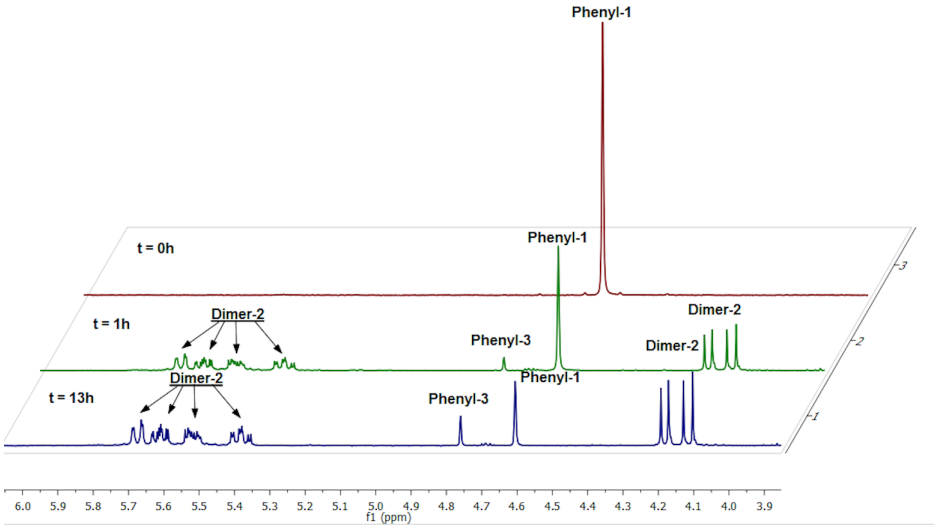

Figure III.4: ^{1}H-NMR (400 MHz) spectra of the reaction mixture in benzene-d_6 after different irradiation times.

^{1}H-NMR data obtained after 1 h of irradiation showed that the desired ring closure product **Phenyl-3** was indeed formed in 6% yield. The signal **Phenyl-3** corresponds to the singlet assigned to the two benzylic protons of the desired product **Phenyl-3**. Surprisingly, dimer **Dimer-2** was also formed in 48% yield as a major product, which was identified by the characteristic doublet of doublets signal at 4.15 ppm (**Dimer-2**) and multiple signals between 5.3 and 5.7 ppm (**Dimer-2**). After further irradiation over 12 h, the amount of remaining substrate **Phenyl-1** decreased from 46% to 24%. Product **Phenyl-3** was determined to be formed in 10% (TON: 0.7), and **Dimer-2** in 66% yield. The overall TON of the catalyst is calculated to be 5.5 after 13 h of irradiation. Figure III.5 illustrates the proposed mechanism of the photocatalytic ring closure reaction of 1-(benzyloxy)-2-iodobenzene. The desired productive catalytic cycle is depicted in red. Following the excitation of $[Mo]^0$ an electron is transferred from the complex to substrate **Phenyl-1**, which leads to the formation of radical **A** under elimination of iodide. Radical **A** undergoes a rapid ring closure reaction leading to the tricyclic intermediate radical **B**. The regeneration of the catalyst via electron transfer from intermediate **B** yielding the cation **C**, proves to be the rate determining step and seems to be in competition with the dimerization of **B** to dimer **Dimer-2**. The formation of cation **C** is followed by a fast proton transfer to TMP yielding aromatic product **Phenyl-3** and $TMPH^+$.

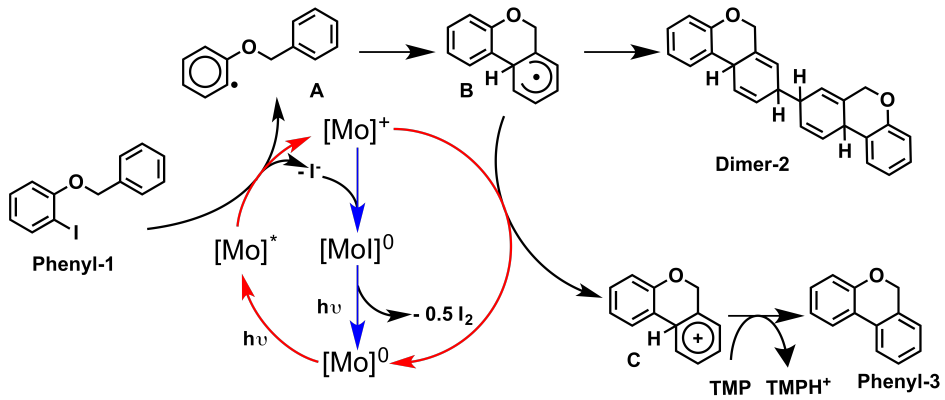

Figure III.5: Proposed mechanism of the photocatalytic ring closure reaction of 1-(benzyloxy)-2-iodobenzene with $[Mo(CNAr_3NC)_3]$.

According to the mechanism proposed above, the dimerization should lead to an accumulation of an equal amount of $[Mo]^+$ and eventually all of $[Mo]^0$ would be consumed when the dimerization product reaches 14% yield, since this equals the catalyst concentration. The observed yield of 48% for dimer **Dimer-2** after 1h of irradiation contradicts the proposed catalytic cycle (in red). In order to resolve this paradox, it is necessary to consider a second pathway to regenerate the catalyst without the formation of product **Phenyl-3**. This second pathway is marked in blue in Figure III.5. It includes the possibility of the formed $[Mo]^+$ species to react with an iodide anion and form the hepta-coordinated complex $[MoI]^0$.

The ability of Mo to form hepta-coordinated complexes is well-known and described in the literature[6,73,74]. This complex is assumed to be able to undergo a photo-triggered homolytic bond cleavage and regenerate the catalyst under formation of iodine. A pathway involving concerted iodide abstraction and electron transfer from substrate **Phenyl-1** within one step, leading to radical **A** and $[MoI]^0$ is unlikely since the electron is transferred from the molybdenum center to the π^* orbital of the aromatic ligand system, not to the antibonding orbital of the aryliodide bond. This should lead to much faster electron transfer than C-I bond cleavage transfer rates. Additionally, C-I bond cleavages triggered by electron injection are known to preferably proceed in a stepwise mechanism via an aryl halide radical anion.[43] Furthermore, the second cycle gives rise to a potential destruction of the catalyst, since an electron transfer from the $[MoI]^0$ species without release of iodine is also possible. This leads to the formation of the $[MoI]^+$ complex, which can certainly not act as an active catalyst since $[MoI]^+$, once it is formed, precipitates with I^- as a counter ion, which explains the slow down of reaction kinetics after the first hour of irradiation.

These results indicate two separate problems in the catalytic system. First, the dimerization appears to proceed faster than the reduction of the $[Mo]^+$ ground state species leading to an accumulation of this species. Second, the complex takes up an iodide ligand resulting in the formation of other reactive species and in a pathway leading to the decomposition of the catalyst. The latter process appears to proceed slower than the dimerization and to be a consequence of the accumulation of the oxidized molybdenum complex. If the dimerization of radical **B** would be shut down, the re-formation of $[Mo]^0$ should be more efficient, due to less competitive reaction pathways.
This hypothesis was investigated in the cyclization reaction of 1-((4-(*tert*-butyl)benzyl)oxy)-2-iodobenzene under similar reaction conditions (Fig. III.6). The introduction of a sterically demanding *tert*-butyl group in the *para* position to the phenylether, should prevent, or at least significantly slow down, the dimerization of the intermediate aryl radical.

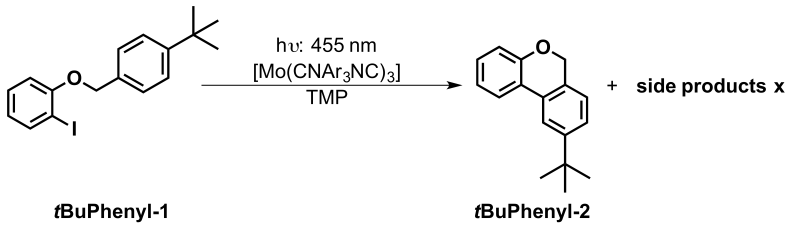

Figure III.6: Photo-triggered electron-catalyzed ring closure reaction of 1-((4-(*tert*-butyl)benzyl)oxy)-2-iodobenzene in benzene-d_6 using $[Mo(CNAr_3NC)_3]$ as a photocatalyst.

Similar to the aforementioned experiment, a mixture of the substrate, 1 equivalent of TMP and 6.6 mol% catalyst in benzene-d_6 was irradiated at 455 nm in a NMR tube, which was

sealed under vacuum. ^{1}H-NMR spectra were recorded after 1 and 16 hours of irradiation (Fig. III.7).

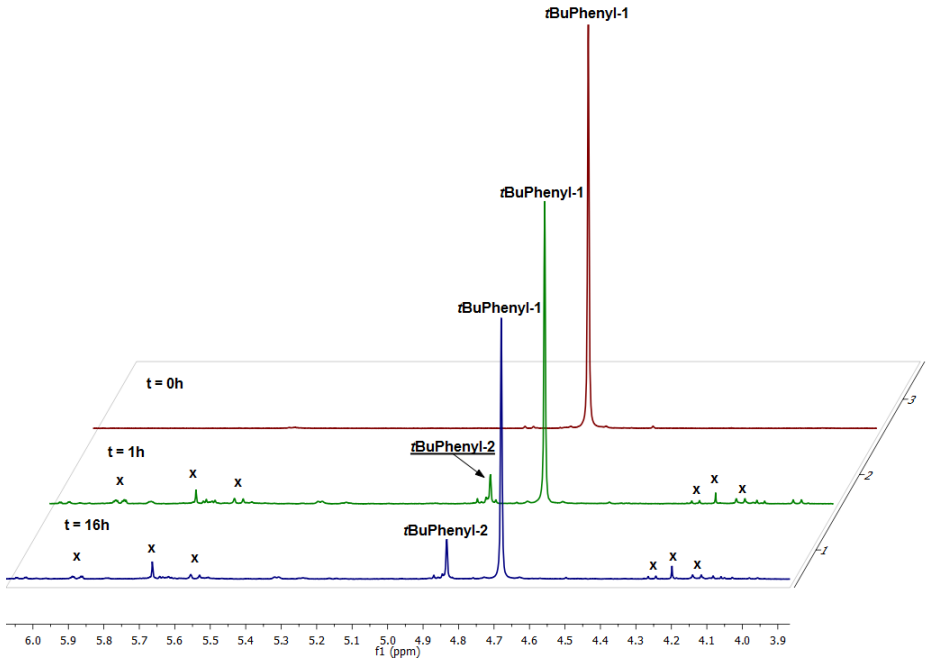

Figure III.7: ^{1}H-NMR (400 MHz) spectra of the reaction mixture in benzene-d_6 after different irradiation times.

After 1 h the desired product ***t*BuPhenyl-2** is formed in 8% yield, which corresponds to a TON of 1.2 compared to a TON of 0.4 for the previously described reaction. Even though the system reaches a final TON of only 1.8 after 16 h of irradiation, it already improved by a factor of 3 compared to the first catalytic system. In fact, it was possible to slow down the dimerization processes of the aryl radical by introducing sterically demanding groups, allowing the reformation of the $[Mo]^0$ species to efficiently compete with these processes. The multiple arising signals in the ^{1}H-NMR spectra, marked with **x**, could not be assigned to one specific compound, rather than to multiple side products probably formed from the aryl radical species. According to this observation the aryl radical is a rather reactive species, which at the same time is a relatively weak reductant. This leads to a low driving force for the reduction of the oxidized catalyst by the aryl radical and gives rise to the formation of various side products.

This experiment illustrates the possibility to slow down undesired dimerization of the aryl radical by introduction of sterically demanding substituents, which directly translates to an increase of the TON for the formation of the desired product by a factor of 3 compared to the initial substrate. However, the inefficiency of the reaction is not only due to dimerization reactions of the formed aryl radical which prevents efficient reformation of the catalyst, but additionally the iodine uptake by the catalyst and the low driving force of the catalyst re-

formation play a more pronounced role in the deactivation of the catalyst than previously expected.

3.2.2 A Structurally Improved Ligand Scaffold

In order to overcome the limitation of $[Mo(CNAr_3NC)_3]$ resulting from its ability to coordinate a seventh ligand, as discussed in the last paragraph, a more sterically demanding ligand was designed. Since the methyl groups seemed to fail to protect the metal center against coordination sufficiently, more sterically demanding *tert*-butyl groups were introduced. The more sterically demanding ligand **(*t*Bu)CNAr$_3$NC(*t*Bu)** was isolated in 50 % overall yield following the five step synthesis depicted in Figure III.8.

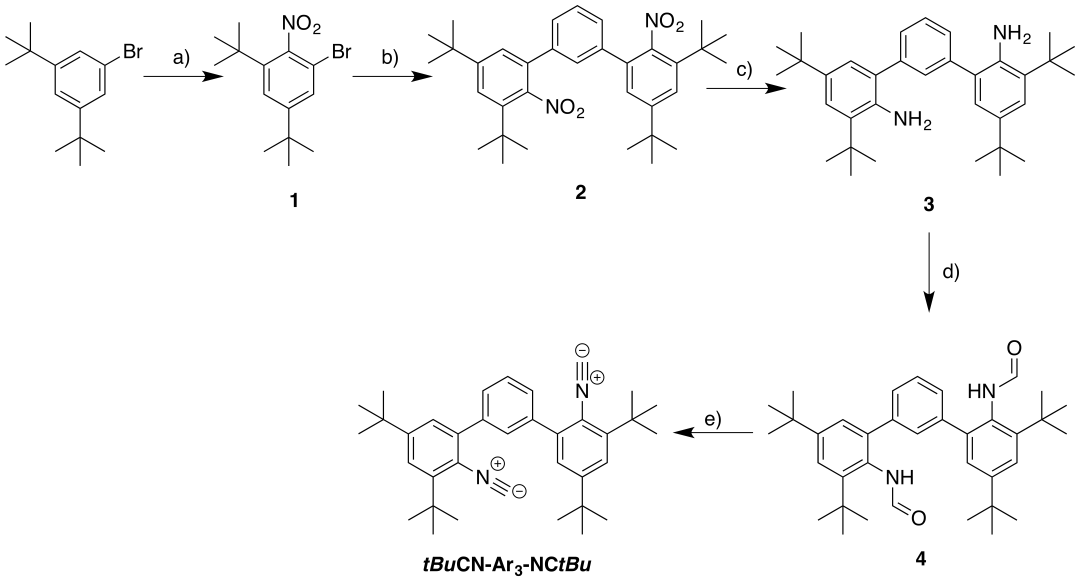

Figure III.8: Synthesis of the *tert*-butyl substituted ligand **(*t*Bu)CNAr$_3$NC(*t*Bu)**. *a)* AcOH, H_2SO_4, fum. HNO_3, 80 °C, 1.5 h; *b)* 1,3-(B(pin))$_2$benzene, dioxane/H_2O, K_2CO_3, $[Pd(dppf)Cl_2]$, 110°C, overnight; *c)* hydrazine, Zn powder, MeOH, reflux, overnight; *d)* acac, formic acid, 100°C, overnight; *e)* $POCl_3$, D*i*PA, r.t., overnight.

3,5-Di(*tert*-butyl)-bromobenzene was nitrated using fuming nitric acid in a mixture of acetic acid and concentrated sulfuric acid. The resulting nitrobenzene **1** was isolated in 77 % yield. The di(nitro)triaryl compound **2** was prepared in 85 % yield via Suzuki-Miyura coupling with 1,3-bis(Bpin)benzene in THF with potassium carbonate and $[Pd(dppf)Cl_2]\cdot CH_2Cl_2$.
Attempts to perform the reduction of **2** to the diamine **3** with H_2 gas under atmospheric pressure in presence of Pd/C catalyst were not successful. This was overcome by performing the reaction at 11 bar and elevated temperature over longer time. After four days the desired diamine **3** was isolated in 71% yield.
The reduction of the nitro groups to the desired diamine **3** was also achieved with Zn powder

and hydrazine over two steps in 88% yield. The reduction of one of the nitro groups proceeded overnight at reflux. The mono-reduced intermediate was isolated as a pure, bright yellow solid which was then subjected to the same reaction conditions as before, finally yielding the diamine in 88% yield. The pure product was isolated after filtration and removal of the solvent. The formamide was prepared by heating diamine **3** in freshly prepared acetic formic anhydride overnight, followed by dilution with water. The product was filtered and isolated in 91% yield. The crude product was used as obtained and stirred with $POCl_3$ to give the final ligand **(*t*Bu)CNAr$_3$NC(*t*Bu)** in 95% yield.

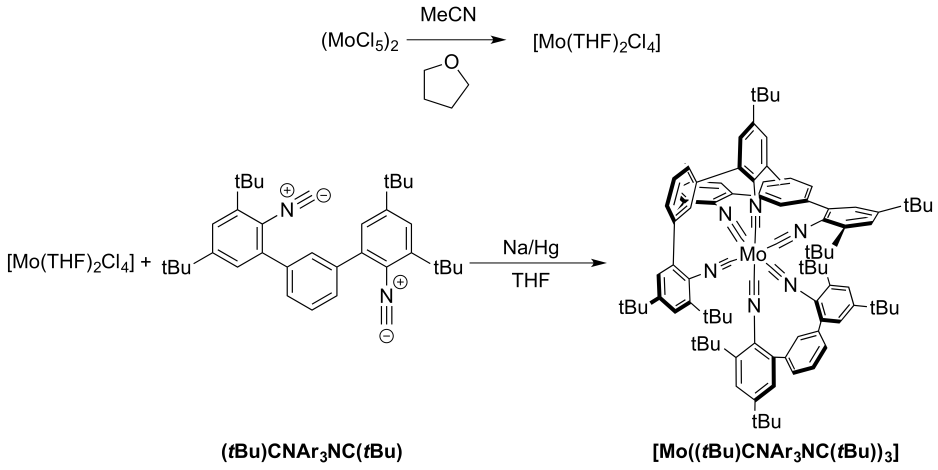

Figure III.9: Synthesis of $[Mo((t\text{Bu})CNAr_3NC(t\text{Bu}))_3]$.

The corresponding molybdenum(0) complex was synthesized by stirring a suspension of $[MoCl_4(THF)_2]$ and 3 equivalents of the ligand in THF over sodium amalgam (Fig. III.9). After stirring overnight, the solution was filtered and the solvent evaporated, giving $[Mo((t\text{Bu})CNAr_3NC(t\text{Bu}))_3]$ as dark red solid (70% yield).

IR-Spectroscopy

The IR-spectra of the free ligand $(t\text{Bu})CNAr_3NC(t\text{Bu})$ (upper spectrum) and $[Mo((t\text{Bu})CNAr_3NC(t\text{Bu}))_3]$ (lower spectrum) are shown in Figure III.10.

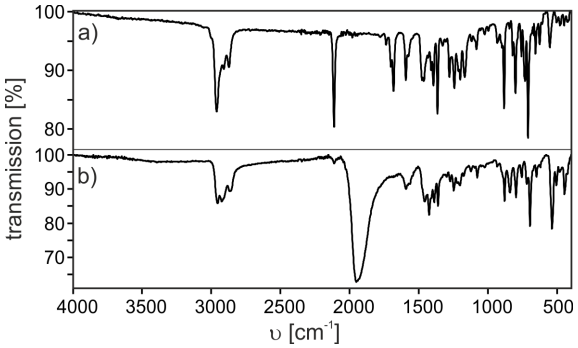

Figure III.10: Solid state FTIR-spectra of a) the free ligand (tBu)CNAr$_3$NC(tBu) and b) the new complex [Mo((tBu)CNAr$_3$NC(tBu))$_3$].

In the upper spectrum, the sharp band at 2112 cm^{-1} is assigned to the C≡N stretching vibration. In the complex this band is shifted towards lower wavenumber (1951 cm^{-1}), which is indicative of substantial π-backbonding and is in agreement with values reported for related compounds.[7,8] The very weak band at 2111 cm^{-1} is probably caused by a minimal amount of oxidized complex. This was already observed in the case of [Mo(CNAr$_3$NC)$_3$] and discussed in the supporting information of our publication in *Angew. Chem. Int. Ed.* **2016**, *55*, 11247 which is included in this chapter.

3.2.3 Electrochemistry

Cyclic voltammetry was performed in dry and deaerated THF with 0.1 M TBAPF$_6$ as supporting electrolyte. The potential was referenced versus the ferrocenium/ferrocene couple.[75] The compound exhibits a reversible one electron oxidation wave at -0.28 V vs. Fc$^{+/0}$ which is assigned to the Mo$^{+/0}$ redox couple (Fig. III.11).

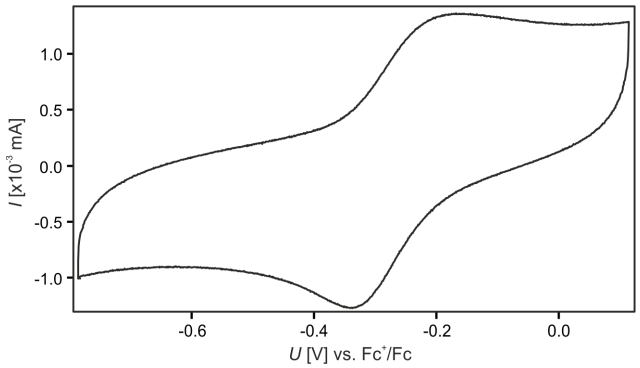

Figure III.11: Cyclic voltammogram of [Mo((tBu)CNAr$_3$NC(tBu))$_3$] in THF with 0.1 M TBAPF$_6$. A glassy carbon working electrode, and two silver wires as counter and quasi reference electrode were used. The scan rate was 0.1 V s^{-1}. The potential was referenced versus the Fc$^{+/0}$ couple.

The observed $Mo^{+/0}$ oxidation potential is slightly more positive than usually reported for this class of compounds[73,74,76] (Tab. III.1). The dependence of the oxidation potential on solvent polarity, electrolyte and steric effects was extensively studied in a series of Cr(0) hexaaryl isocyanide compounds by Bohling et. al..[77]

Table III.1: Redox potentials of different Mo(0) complexes vs. SCE

Compound	E^0 (M^+/M^0) [V] *vs.* SCE
$[Mo((t\text{Bu})CNAr_3NC(t\text{Bu}))_3]$	0.28[a]
$[Mo(CNAr_3NC)_3]$	0.16[a]
$[Mo(CNPh\text{-}4\text{-}Cl)_6]$	-0.07[b]
$[Mo(CNPh)_6]$	-0.21[b]
$[Mo(CNPh\text{-}2,6\text{-}DIP)_6]$	-0.29[b]
$[Mo(CNxylyl)_6]$	-0.35[b]

Potentials referenced vs. $Fc^{+/0}$ were converted to SCE according to ref. [75]; [a] in THF, *this work*; [b] in dichloromethane, from ref. [76].

Since the electronic and chemical structure of the Mo(0) and Cr(0) complexes are similar to one another, the same effects should be present in the systems presented herein. The slightly more positive potential of $[Mo(CNAr_3NC)_3]$ compared to related hexakis(aryl isocyanide) molybdenum complexes might result from a combination of solvent effect, better stabilization of the Mo(0) state by a more extended π-system of the ligand, as well as steric effects. The significant difference of 0.12 V between the two complexes prepared in this study have to be assigned to steric effects, since the measurement conditions and the electronic nature of the ligands are identical. The increase of the oxidation potential indicates either a stabilisation of the Mo(0) state or a destabilisation of the oxidized species due to increased repulsive steric interactions. Following the argumentation of Bohling et. al. and taking into account that the only difference in the two prepared complexes is the size of the substituentes, the latter appears to be more reasonable. The pronounced effect of the change of a methyl group to a *tert*-butyl group on the oxidation potential is most certainly caused by the chelating ligand in combination with the very bulky *ortho*-substituents, namely *tert*-butyl and the phenyl backbone, leading to a very rigid and compact coordination geometry. Upon oxidation the ion radius decreases and repulsive interligand interactions are increased giving rise to the observed anodic shift of the oxidation potential and indicating the destabilisation of the $[Mo]^+$ species. It was not possible to observe any reduction processes within the electrochemical window ($>$ -2.5 V).

3.2.4 UV/Vis Absorption and Photoluminescence

The UV/Vis absorption spectra (solid lines) and steady-state emission spectra (dashed lines) obtained in different deaerated solvents at 20°C are shown in Figure III.12. They differ only slightly from the ones obtained for $[Mo(CNAr_3NC)_3]$.

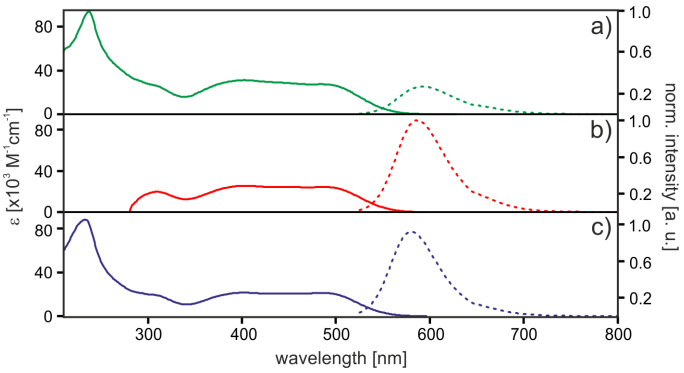

Figure III.12: Absorption- (solid lines) and steady-state emission spectra (dotted lines) of $[Mo((t\text{Bu})CNAr_3NC(t\text{Bu}))_3]$ in dry and deaerated a) THF (green traces), b) toluene (red traces) and c) *n*-hexane (blue traces). Excitation occurred at 500 nm.

The broad absorption bands from 350-550 nm are assigned to ^{1}MLCT transitions, whereas the intense bands below 350 nm originate from $\pi \rightarrow \pi^*$ transitions. Their extinction coefficient shows very little solvent dependency (Tab. III.2). In contrast the luminescence intensity decreases dramatically with increasing polarity of the solvent. While it remains nearly unchanged upon changing the solvent from toluene (red) to hexane (blue), the intensity drops to only 20% when changing the solvent to THF (green).

Table III.2: Absorption maxima with corresponding extinction coefficients and emission maxima λ_{em} of $[Mo((t\text{Bu})CNAr_3NC(t\text{Bu}))_3]$ in different deaerated solvents at 20°C. Measurements were performed with complex concentrations of 10^{-5} M.

solvent	λ_{abs} [nm]	$\varepsilon \times 10^3$ [$M^{-1}cm^{-1}$]	λ_{em} [nm]
THF	237 ($\pi - \pi^*$)	93.9	595
	400 (MLCT)	31.3	
	450 (MLCT)	28.6	
	485 (MLCT)	27.6	
toluene	400 (MLCT)	25.7	585
	450 (MLCT)	24.6	
	485 (MLCT)	24.5	
hexane	233 ($\pi - \pi^*$)	88.3	580
	400 (MLCT)	21.6	
	450 (MLCT)	20.8	
	485 (MLCT)	21.3	

The observed blue shift of the emission maximum in less polar solvents (Fig. III.13) is indicative of a MLCT excited state.

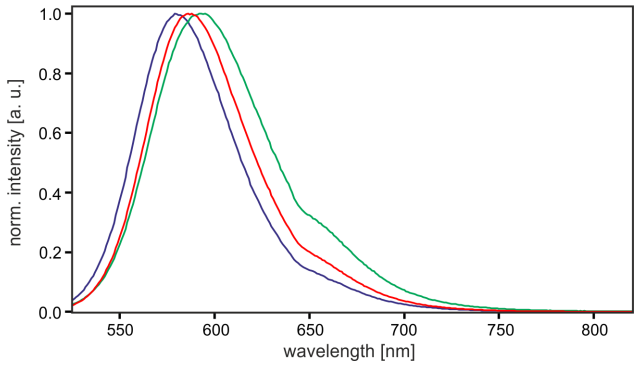

Figure III.13: Steady-state emission spectra of $[Mo((t\text{Bu})CNAr_3NC(t\text{Bu}))_3]$ in THF (green), toluene (red), hexane (blue). Excitation occurred at 500 nm.

Transient absorption spectra in different solvents were obtained from deaerated solutions of $[Mo((t\text{Bu})CNAr_3NC(t\text{Bu}))_3]$ (10^{-5}M) excited at 532 nm with laser pulses of approximately 10 ns duration. Differences in optical absorption were probed with the white-light output of a high-pressure xenon lamp. Time integration occurred over the first 200 ns after excitation. Figure III.14 shows the resulting transient absorption spectra. The positive signal at approx. 350 nm is assigned to the reduced ligand formed upon excitation, whereas the bleach at 500 nm is due to the vanishing of the $[Mo]^0$ ground state absorption.

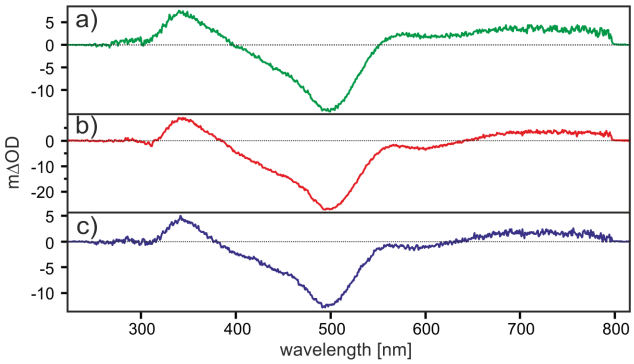

Figure III.14: Transient absorption spectra of 10^{-5} M solutions of $[Mo((t\text{Bu})CNAr_3NC(t\text{Bu}))_3]$ in deaerated THF (green), toluene (red) and hexane (blue). The spectra were obtained by time integration over 200 ns directly after excitation with a laser pulse of 10 ns duration at 532 nm.

The similarity of all three traces illustrates that in each solvent the same kind of excited state is probed.

Excited state lifetimes (τ_0) were determined at the emission maximum in the corresponding solvent (Tab. III.3).

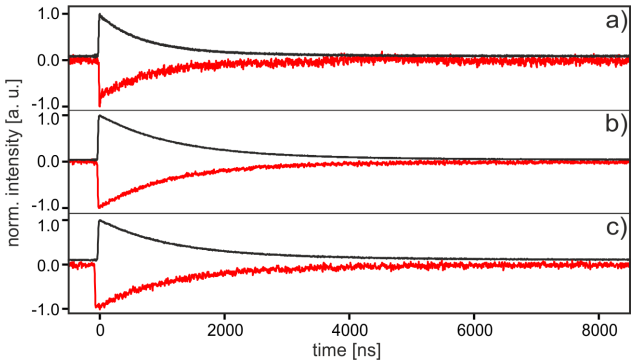

Figure III.15: Emission decay curves (black traces) were detected at the respective emission maximum and bleach recovery curves (red) at 500 nm in deaerated (a) THF, (b) toluene and (c) hexane recorded after exciting a 10^{-5} M solution of $[Mo((t\text{Bu})CNAr_3NC(t\text{Bu}))_3]$ at 532 nm with a laser pulse of approximately 10 ns duration at 20°C.

The emission decay (black traces) and bleach recovery (red) curves in (a) THF , (b) toluene and (c) hexane are shown in Figure III.15. Lifetimes (τ_0) were determined by fitting to a bi-exponential decay. The bi-exponential behaviour of the decay curves is attributed to the presence of several static conformations. For the less sterically demanding ligand **$CNAr_3NC$** this is only observed in solid matrices at 77K, indicating efficient interconversion between differnet conformers in solution at room temperature. This theory is supported by the ^{1}H-NMR spectra of the two complexes. While $[MoCNAr_3NC_3]$ shows only one signal for each proton set of the ligand, in case of $[Mo((t\text{Bu})CNAr_3NC(t\text{Bu}))_3]$ every single proton of the complex

gives a different signal leading to a rather complicated spectral signature.

Table III.3: Excited state lifetimes of $[Mo((t\text{Bu})CNAr_3NC(t\text{Bu}))_3]$ in different deaerated solvents at 20°C. Measurements were performed with complex concentrations of 10^{-5}M.

solvent	emission		absorption		
	τ_0^1 [ns]	τ_0^2 [ns]	τ_0^1 [ns]	τ_0^2 [ns]	quantum yield [%]
tetrahydrofuran	609 (75%)	1613 (25%)	609 (71%)	1613 (29%)	5.8
toluene	1112 (80%)	2327 (20%)	1112 (91%)	2327 (9%)	20.3
hexane	1040 (75%)	2369 (25%)	1040 (77%)	2369 (23%)	19

Table III.3 summarizes the excited state lifetimes in different solvents at room temperature. The ratio of the shorter to the longer lifetimes extracted from the bi-exponential fit of the decay curves is in all solvents similar. The average lifetime increases with decreasing polarity of the solvent. For example, the average lifetime in THF is 860 ns which increases to 1355 ns in toluene. This indicates a strong increase in non-radiative deactivation pathways upon increasing solvent polarity, most likely due to enhanced coupling with vibrational overtones. The lifetimes extracted from the bleach recovery curves are similar to the ones obtained from the decay data set (Fig. III.15).
The reported quantum yields were determined by using $[Ru(bpy)_3]^{2+}$ in deaerated acetonitrile as a reference and calculated using equation III.1.

$$\phi = \phi_r \cdot \frac{I \cdot A_r \cdot n}{I_r \cdot A \cdot n_r} \tag{III.1}$$

In this case ϕ_r corresponds to the quantum yield of $[Ru(bpy)_3]^{2+}$ in deareated acetonitrile (9.5%[78]), I to the integrated luminescence intensity, A to the absorption at the excitation wavelength and n to the refractive index of the solvent. The index r is indicative for the reference system ($[Ru(bpy)_3]^{2+}$). The obtained quantum yields show the same solvent dependency trend as discussed for the lifetimes consistent with the energy gap law. The lowest quantum yield of 5.8% is found in THF and the ones in toluene (20.3%) and hexane (19.0%) are significantly higher and similar to each other.
From low temperature steady-state emission spectroscopy it is possible to estimate the ^{3}MLCT excited state energy. It is expected that the energy is similar to the one determined for $[Mo(CNAr_3NC)_3]$. The emission spectrum obtained from $[Mo((t\text{Bu})CNAr_3NC(t\text{Bu}))_3]$ in a glass of 2-methyl-tetrahydrofuran at 77 K (black dashed trace) is shown in comparison to the emission spectrum in THF at 20°C (solid green trace) in Figure III.16.

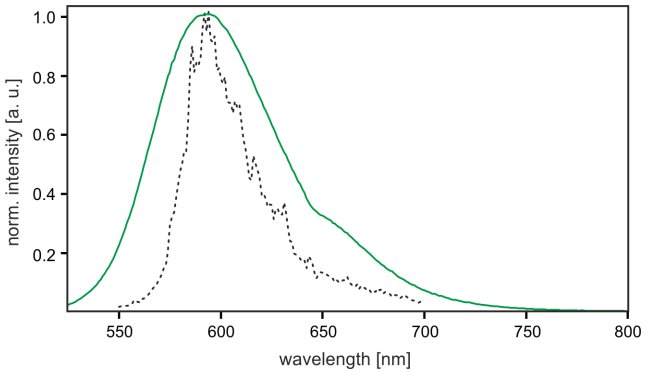

Figure III.16: Steady-state emission spectra of [Mo((*t*Bu)CNAr$_3$NC(*t*Bu))$_3$] recorded at 20°C in THF (green solid line) and 77 K in 2-methyl-tetrahydrofuran (black dashed trace) after excitation at 500 nm.

The emission spectrum obtained at low temperature is narrower than the one at room temperature, which is due to a minimization of vibrational grades of freedom and the prohibition of thermal population of vibrational states. Some of the sharp features present in the spectrum probably correspond to activated vibrational modes, which are resolved at low temperature. The emission maximum itself remains unchanged compared to room temperature and the energy of the emissive excited state is estimated to be 2.2 eV as already observed for [Mo(CNAr$_3$NC)$_3$].
From this excited state energy and the oxidation potential of the ground state, it is possible to estimate the oxdiation potential of the excited state by using equation III.2.

$$E^0(M^{+/0*}) = E^0(M^{+/0}) - E_{MLCT} \tag{III.2}$$

$E^0(M^{+/0*})$ denotes the excited state oxidation potential, $E^0(M^{+/0})$ the ground state oxidation potential obtained from cyclic voltammetry experiments and E_{MLCT} the estimated energy level of the emissive ^{3}MLCT state.
The resulting excited state oxidation potential is -2.48 V and therefore slightly higher than the one of [Mo(CNAr$_3$NC)$_3$] (-2.6 V). This is caused by the difference of 0.12 V in the ground state oxidation potential of the two complexes.

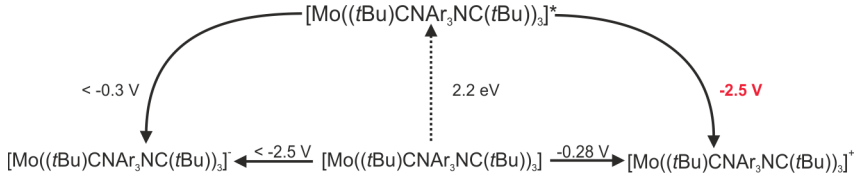

Figure III.17: LATIMER diagram for [Mo((*t*Bu)CNAr$_3$NC(*t*Bu))$_3$].

All potentials and energies of [Mo((*t*Bu)CNAr$_3$NC(*t*Bu))$_3$] relevant for the design of photocatalytic experiments are summarized in a so called LATIMER diagram (Fig. III.17).

3.2.5 Comparison of the New Molybdenum Catalysts to $[Ru(bpy)_3]^{2+}$

In order to gain a better overview of the improved photophysical properties of the molybdenum complex achieved by introduction of bulky groups in the ligand periphery and to put these properties in direct comparison with $[Ru(bpy)_3]^{2+}$, they are summarized in Table III.4.
It is obvious that, although the ground state oxidation potential as well as the excited state oxidation potential is slightly higher in $[Mo((t\text{Bu})CNAr_3NC(t\text{Bu}))_3]$ than in the first complex, the severely improved photophysical properties compensate this minor drawback. In fact the first Mo(0) complex prepared in this study showed the longest ^{3}MLCT lifetime ever reported for molybdenum(0) isocyanide complexes and enabled their use in photocatalytic reactions for the first time. Still it was not able to compete with $[Ru(bpy)_3]^{2+}$ in terms of lifetime and quantum yield.
The bulkier ligands lead to a much more rigid coordination sphere and thus the new complex now outperforms $[Ru(bpy)_3]^{2+}$ in many aspects.

Table III.4: Comparison of the new molybdenum complexes to $[Ru(bpy)_3]^{2+}$.

Compound	E^0 (M^{n+1}/M^n) *vs.* Fc^+/Fc [V]	E_{MLCT} [eV]	$E^0(M^{n+1}/M^{*n})$ *vs.* Fc^+/Fc [V]	τ_0 [ns]	ϕ_{Lum} [%]
$[Mo((t\text{Bu})CNAr_3NC(t\text{Bu}))_3]$	-0.28[a]	2.2	-2.48	1112 ± 110 (80%)[b] 2327 ± 230 (20%)[b]	20.3 ± 2[b]
$[Mo(CNAr_3NC)_3]$	-0.4[a]	2.2	-2.6	166 ±17[b]	2.3 ± 0.2[b]
$[Ru(bpy)_3^{2+}]$	0.9[c]	2.1[79]	-1.2[79]	855[d][78]	9.5[d][78]

Potentials vs. Fc^+/Fc. [a]in THF, *this work*. [b] in toluene, *this work*, [c] vs. Fc^+/Fc in acetonitrile *this work*, [d] in deaerated acetonitrile.

Although the new Mo(0) complex is 0.12 V less reducing than the first one, it still has 1.28 V more reduction power than $[Ru(bpy)_3]^{2+}$ and offers now comparable lifetimes in THF and even higher ones in less polar solvents. The determined quantum yields exceed the one of $[Ru(bpy)_3]^{2+}$ for apolar solvents such as benzene and hexane by a factor of 2.
These severely improved photophysical properties imply the presence of less accessible non-radiative deactivation pathways and probably a better protection of the metal center against environmental influences.

3.2.6 The Photocatalytic Electron-Catalyzed Ring Closure Reaction of Halogenated Benzyl-Phenylethers Revisited

The new complex is expected to catalyse the ring closure reaction of 1-((4-(*tert*-butyl)benzyl)oxy)-2-iodobenzene ***t*BuPhenyl-1** more efficiently than $[Mo(CNAr_3NC)_3]$ (Fig. III.18).

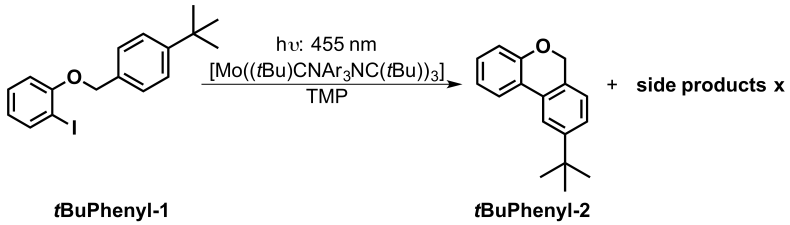

Figure III.18: Phototriggered electron-catalyzed ring closure reaction of 1-((4-(*tert*-butyl)benzyl)oxy)-2-iodobenzene using $[Mo((tBu)CNAr_3NC(tBu))_3]$ as photosensitizer.

As the initial electron transfer is not rate determining, the slightly higher oxidation potential relative to the original complex has very little effect on the overall system performance. The more important factor is an enhanced sterical shielding of the metal center against iodine uptake, as well as the improved re-formation of the catalyst by reduction of ground state $[Mo]^+$.

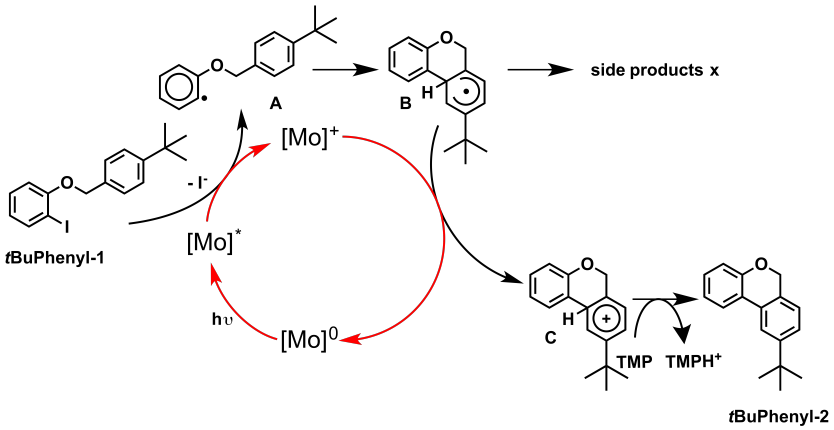

Figure III.19: Proposed mechanism for the photocatalytic ring closure reaction of 1-((4-(*tert*-butyl)benzyl)oxy)-2-iodobenzene.

The catalyst re-formation depends on the lifetime of the aryl radical species **B** (Fig. III.19), its oxidation potential, as well as the reduction potential of $[Mo]^+$. Since the ground state oxidation potential of $[Mo((tBu)CNAr_3NC(tBu))_3]$ is higher than that of the initially used complex, one expects the reduction of $[Mo]^+$ to be more exergonic and therefore to proceed easier compared to the previous catalyst, resulting in the catalysis to be more efficient.
A mixture of substrate ***t*BuPhenyl-1**, 1 equivalent of TMP and 4.7 mol% catalyst in deaerated benzene-d_6 was irradiated at 455 nm in a NMR tube, which was sealed under vacuum. ^{1}H-NMR spectra recorded after 1 h, 17 h and 33 h irradiation are shown in Figure III.20.

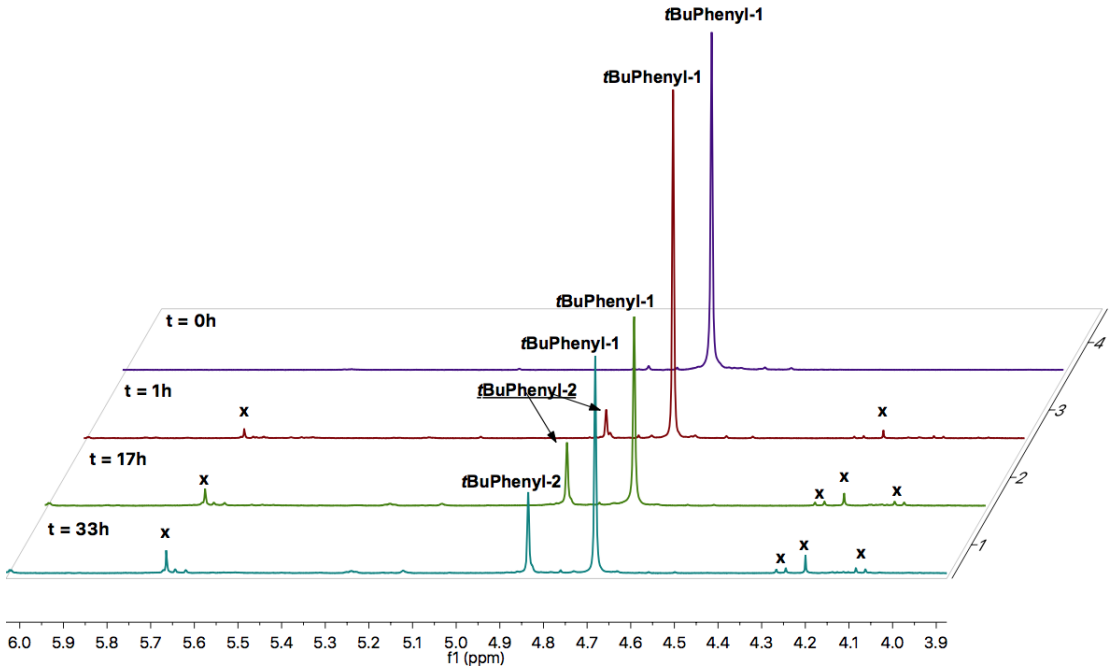

Figure III.20: ^{1}H-NMR (400 MHz) spectra of the reaction mixture in deaerated benzene-d_6 after different time intervals of irradiation at 455 nm.

After 1 h of irradiation, 8% of the desired product ***t*BuPhenyl-2** is formed, which corresponds to a TON of 1.7. In comparison, the first Mo(0) complex reached a TON of 1.8 under similar conditions after 16 h of irradiation. Additional 16 h of irradiation lead to a further increase in product concentration to 25%, giving a TON of 5.4. Continued irradiation up to 33 hours in total gives a final product yield of 29% and a maximum TON of 6.2.
These results are indeed an improvement compared to $[Mo(CNAr_3NC)_3]$, and from the relatively fast kinetics within the first hour it can be concluded that the electron transfer to the substrate ***t*BuPhenyl-1** is rapid despite the slightly less negative excited state oxidation potential of the new complex.
Control experiments with benzyl-2-iodo-phenylether as substrate that lacks the bulky *tert*-butyl group and allows for rapid dimerization (s. Chapter 3.2.1), gave an overall TON of 1.8 after 1 h of irradiation and the catalyst decomposed over the course of this reaction.
In general one would expect a higher yield of the desired product ***t*BuPhenyl-2** given the successful prevention of iodide uptake and subsequent catalyst decomposition, but since the driving force for the reduction of the $[Mo]^+$ species by the aryl radical **B** is still not large enough, the formation of undefined (probably dimeric) side products **x** from the aryl radical is in competition with the relatively slow reformation of the catalyst (Fig. III.20). This leads to a limitation of the product yield and hence is attributed to a problem in the design of the catalytic system rather than an intrinsic problem of the catalyst itself.

3.2.7 Photocatalytic Electron-Catalyzed Ring Closure Reaction of Halogenated Thiophenemethyl-Phenylethers

Because the side reactions arising from the slow reduction of the benzyl radical by the oxidzied catalyst limit the efficiency of the catalytic system, the benzyl ring was exchanged for a thiophene unit (Fig. III.21). The oxidation of the thiophene-derived radical is thought to proceed faster and therefore be able to compete sufficiently with potential side reactions.

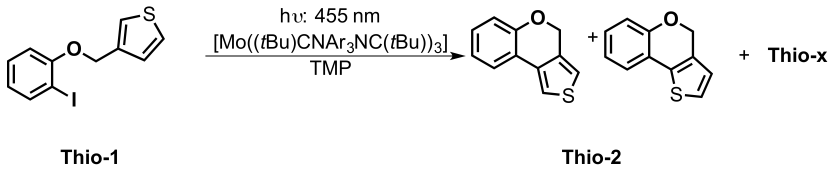

Figure III.21: Photo-triggered electron-catalyzed ring closure reaction of 3-((2-iodophenoxy)methyl)thiophene using $[Mo((t\text{Bu})CNAr_3NC(t\text{Bu}))_3]$ as photosensitizer.

The same experimental conditions as used in the experiment described before were employed. $[Mo((t\text{Bu})CNAr_3NC(t\text{Bu}))_3]$ was used as a photocatalyst (5 mol-%) and the reaction mixture was irradiated in a NMR tube which was sealed under vacuum. ^{1}H-NMR spectra were recorded after different time intervals of irradiation at 455 nm (Fig. III.22).

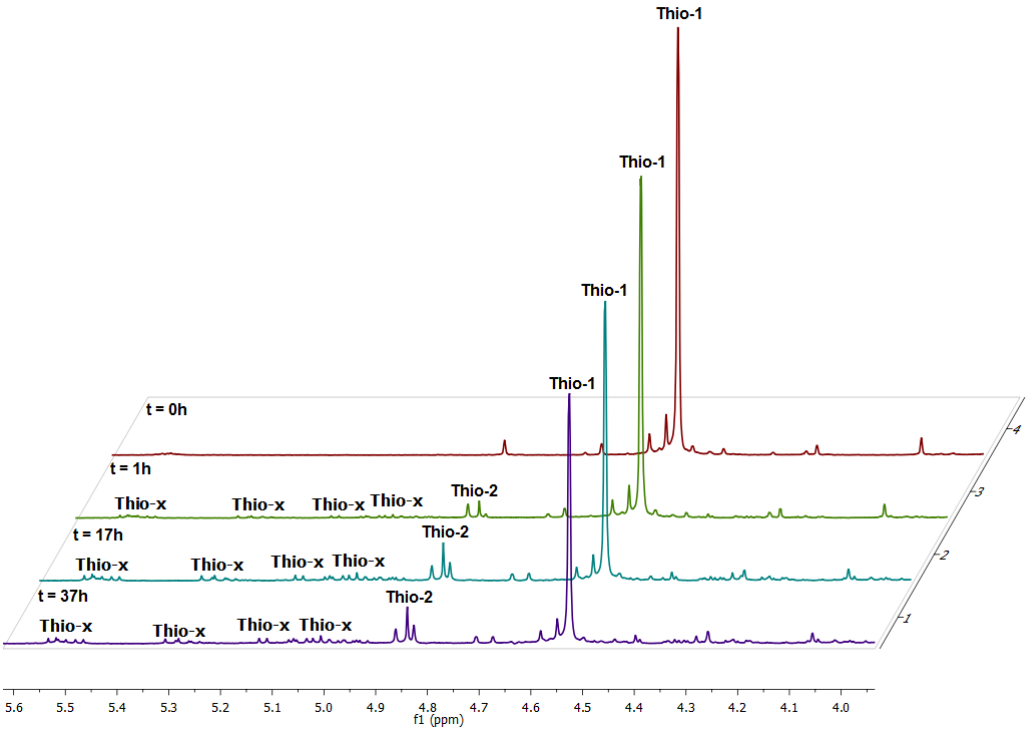

Figure III.22: ^{1}H-NMR (400 MHz) spectra of the reaction mixture in deaerated benzene-d_6 after different time intervals of irradiation at 455 nm.

After 1 h 4% of the desired product **Thio-2** was formed which corresponds to a TON of 0.8. Additional 16 hours of irradiation lead to a product concentration of 11% and a TON of 2.2. Further irradiation gave only a small increase in product yield to 12% (TON: 2.4). Additional signals labelled with **Thio-x** are assigned to dimeric side products.
Compared to the *tert*-butyl substituted substrate ***t*BuPhenyl-1** this catalytic system performed by a factor 3 less efficient. Even so, it gave better results than experiments using the unsubstituted substrate **Phenyl-1**. This substrate gave a final product yield of 1% with a TON of 0.2, and even the overall yield and TON of product and dimer formation were only 9% and 1.8 respectively.
The yields and TONs of the tested catalytic systems are summarized in Table III.5.

Table III.5: Product yields and TONs of the tested catalytic systems.

	catalyst			
	$[Mo(CNAr_3NC)_3]$		$[Mo((t\text{Bu})CNAr_3NC(t\text{Bu}))_3]$	
substrate	yield [%]	TON	yield [%]	TON
Phenyl-1	$10^a/66^b$	$0.7^a/5.5^b$	1/9	$0.2^a/1.8^b$
*t*BuPhenyl-1	12	1.8^a	29	6.2^a
Thio-1	-	-	12	2.4^a

[a] The yield and TON of formation of the desired product, [b] combined yield and TON of product and dimer.

It is evident that the efficiency of the catalytic systems depend on three factors. First, robustness of the catalyst itself against uptake of iodine plays an important role. Second, the tendency of the formed tricyclic radical species to dimerize, and third, the driving force of the reduction of the catalyst cation by the tricyclic radical species. From Table III.5 one has to conclude that although an enhanced driving force does improve the catalytic performance, the slow down of dimerization kinetics has the greater effect.
It is also apparent that the observed difficulties do not originate from the catalyst itself, but are of a general kind. That is the difficulty to balance a very low oxidation potential in the excited state with a moderate ground state reduction potential and to design a catalytic system in which intermediates are formed which are reactive enough to drive the re-formation of the catalyst, and at the same time are not prone to side reactions (e.g. dimerization).

3.2.8 Summary

The aim of this study was to further establish homoleptic molybdenum(0) complexes bearing chelating aryl isocyanide ligands as very strong and robust photosenstizers. In this context, the main challenge was to disable photosubstitution reactions on the metal core and to prevent the coordination of a seventh ligand. This was achieved by introducing sterically demanding *tert*-

butyl groups in *ortho* position to the isocyanide functionality in $[Mo((tBu)CNAr_3NC(tBu))_3]$. The new complex exhibits dramatically improved photophysical properties and outperforms the famous $[Ru(bpy)_3]^{2+}$ in many aspects, e.g. excited state lifetime and quantum yield.
The reduction power of this complex is slightly lower than the one of $[Mo(CNAr_3NC)_3]$, which was attributed to a destabilisation of the oxidized complex due to an increase in repulsive sterical interactions upon decrease of the radius of the metal center.
Although this lead to a minor decrease in excited state reduction power, the complex still performed more efficiently than its parent complex in the photocatalytic dehalogenation and cyclization reaction of 2-iodo-phenyl-benzylether derivates. This illustrates the successful shielding of the metal center against an uptake of the produced iodide as a seventh ligand.
With these results it was possible to completely establish molybdenum(0) tris(triaryl-bis(isocyanide)) complexes as $[Ru(bpy)_3]^{2+}$ analogues based on a relatively earth-abundant metal. The complexes offer extraordinary reduction power and long lived ^{3}MLCT states with high quantum yields while being relatively air-stable and robust under various reaction conditions. They enable a whole new range of challenging photocatalytic reactions which were not accessible before or needed harsh reaction conditions.

3.3 A New Cr(0) Based Luminophore

Nowadays, ruthenium(II) polypyridyl complexes are involved in nearly any research field concerning energy conversion using light, such as Dye Sensitized Solar Cells (DSSCs) or artifical photosynthesis.[80,80–83] Although these complexes excel in many applications due to their high stability, tunability and desirable photophysics, the scientific community strives to substitute the precious ruthenium metal by the more earth-abundant iron.[4,84,85] In contrast to ruthenium(II) polypyridyl complexes, some ligand field states of the homologous iron complexes are not higher in energy than the excited ^{3}MLCT state.[86,87] This leads to a rapid depopulation of the excited ^{3}MLCT state into the ligand field states on the femtosecond time scale.[55] However, ultra-fast electron injection from hot MLCT excited states into TiO_2 was observed for $[Fe(bpy)_3]^{2+}$. Nevertheless, the efficiencies of these devices were rather low, and a lot of effort was put into prolonging the MLCT excited state lifetime.[56,88] This eventually lead to the development of very few homoleptic iron(II) complex with high light-to-electron conversion rates of up to 92%.[89]
With this problem in mind, we set out to investigate the possibility to make use of our chelating isocyanide ligands in order to shift the ligand field states to higher energies, making them inaccessible from the excited ^{3}MLCT state.
Since the $[Mo((t\text{Bu})CNAr_3NC(t\text{Bu}))_3]$ complex was found to exhibit long lived ^{3}MLCT luminescence with high quantum yields and not to be prone to photosubstitution reactions, it is reasonable to assume that the homologous chromium(0) (Figure III.23) complex might be emissive as well.

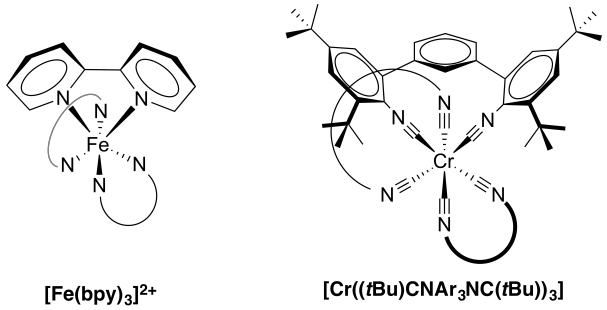

Figure III.23: Molecular structure of $[Fe(bpy)_3]^{2+}$ and the new complex $[Cr((t\text{Bu})CNAr_3NC(t\text{Bu}))_3]$.

The designed complex $[Cr((t\text{Bu})CNAr_3NC(t\text{Bu}))_3]$ is an isoelectronic analogue to $[Fe(bpy)_3]^{2+}$ just like $[Mo((t\text{Bu})CNAr_3NC(t\text{Bu}))_3]$ is one to $[Ru(bpy)_3]^{2+}$.

3.3.1 Synthesis

The synthesis of the ligand **$(t$Bu$)$CNAr$_3$NC$(t$Bu$)$** was already described in Chapter 3.2.2. Similar to the synthesis strategy applied to obtain the corresponding Mo(0) complex, the lig-

and was brought in contact with the precursor complex $[CrCl_3(THF)_3]$ in presence of Na/Hg. In contrast to the previously used procedure, the chromium precursor was prepared *in situ* by stirring $CrCl_3$ with activated zinc powder in dry THF at room temperature (Fig. III.24).

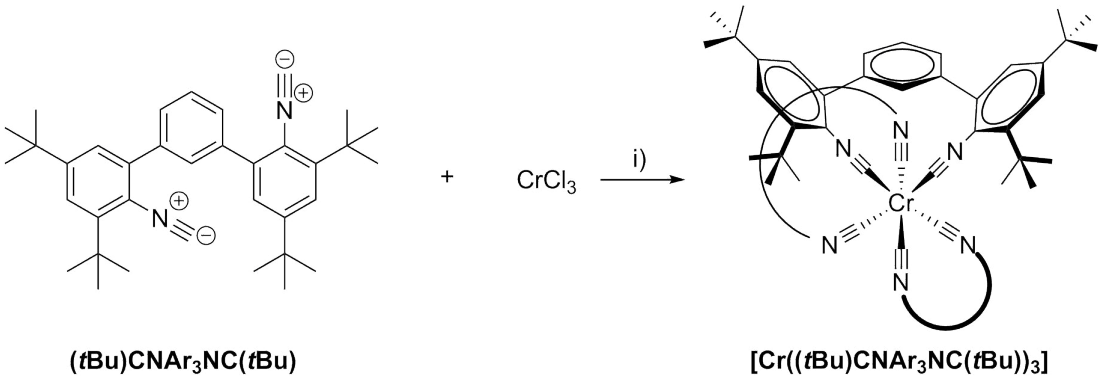

Figure III.24: Synthesis of the desired complex $[Cr((tBu)CNAr_3NC(tBu))_3]$.
i) Zn, THF, 2h; Na/Hg, THF, minutes.

The formation of the precursor is completed within 2 hours and the formation of the desired complex proceeds immediately during the addition of the ligand yielding 80% of an air-stable, red solid.

3.3.2 IR-Spectroscopy

Figure III.25 shows the IR-spectra of the free ligand $(tBu)CNAr_3NC(tBu)$ (top) and $[Cr((tBu)CNAr_3NC(tBu))_3]$ (bottom). The vibrational band assigned to the C≡N vibration shows a similar shift to lower wavenumbers when comparing the free ligand (2112 cm^{-1}) to the ligand bound to the Cr(0) center (1941 cm^{-1}).

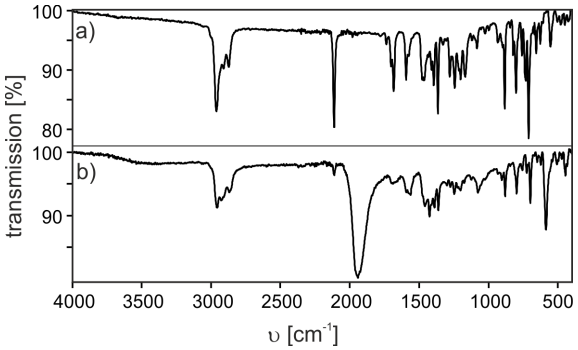

Figure III.25: Solid state FTIR-spectra of a) the free ligand $(tBu)CNAr_3NC(tBu)$ and b) the new complex $[Cr((tBu)CNAr_3NC(tBu))_3]$.

As discussed for the molybdenum complexes before, the shift of the C≡N streching frequency indicates significant π-backbonding and is in good agreement with previously reported values for hexakis(aryl isocyanide)Cr(0) complexes.[62]

3.3.3 Electrochemistry

The ground state oxidation potentials were determined via cyclic voltammetry. The measurement was performed in THF with 0.1 M $TBAPF_6$ as electrolyte and the potential was referenced vs. $Fc^{+/0}$.

Cr(0) isocyanide complexes are known to exhibit well-defined electrochemistry with three reversible oxidation waves.[62,90–94] The cyclic voltammogram is shown in Figure III.26. All three oxidation waves are reversible one electron oxidations.

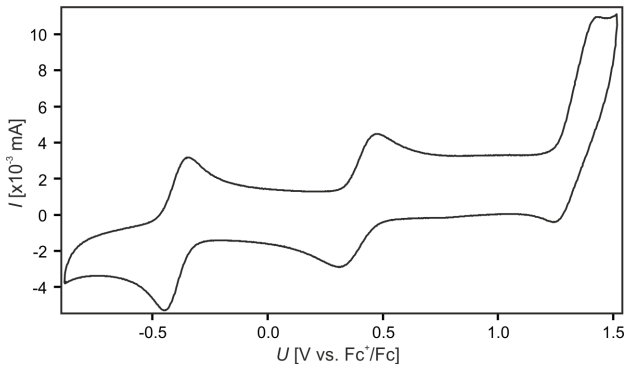

Figure III.26: Cyclic voltammogram of $[Cr((t\text{Bu})CNAr_3NC(t\text{Bu}))_3]$ in THF with 0.1 M $TBAPF_6$ as supporting electrolyte at 20°C. A glassy carbon working electrode, and two silver wires as counter and quasi reference electrode were used. The scan rate was 0.1 V s^{-1}. The potential was referenced versus the $Fc^{+/0}$ couple.

The first oxidation occurs at -0.38 V and is assigned to the Cr^+/Cr^0 couple, the second at 0.40 V corresponds to Cr^{2+}/Cr^+, whereas the oxidation from Cr^{2+} to Cr^{3+} is found to occur at 1.33 V.

These potentials are compared to those of different Cr(0) hexaaryl isocyanide complexes in Table III.6.

Table III.6: Redox potentials of different (aryl isocyanide) Cr(0) complexes vs. $Fc^{+/0}$.

Compound	E^0 (M^+/M^0) [V]	E^0 (M^{2+}/M^+) [V]	E^0 (M^{3+}/M^{2+}) [V]
$[Cr((t\text{Bu})CNAr_3NC(t\text{Bu}))_3]^a$	-0.38	0.40	1.33
$[Cr(2,6\text{-diisopropyl-CNPh})_6]^b$	-0.78	0.16	1.27
$[Cr(2,6\text{-dimethyl-CNPh})]^b$	-0.78	0.01	0.82
$[Cr(CNAr)_6]^b$	-0.67	-0.05	0.73
$[Cr(p\text{-MeO-CNPh})_6]^b$	-0.78	-0.21	0.59
$[Cr(p\text{-Cl-CNPh})_6]^b$	-0.53	0.00	0.77

Potentials referenced vs. $Fc^{+/0}$. [a] in THF, *this work*. [b] in dichloromethane from ref. [77].

As already discussed in Chapter 3.2.3 the observed aniodic shift for $[Cr((tBu)CNAr_3NC(tBu))_3]$ compared to the reported potentials of related compounds is most certainly caused by the increase of repulsive interligand interactions upon oxidation of the metal center due to a decreased ionic radius.[77]

3.3.4 UV/Vis and Photoluminescence

The UV/Vis absorption spectra and steady-state emission spectra of $[Cr((tBu)CNAr_3NC(tBu))_3]$ in different solvents at room temperature are shown in Figure III.27.

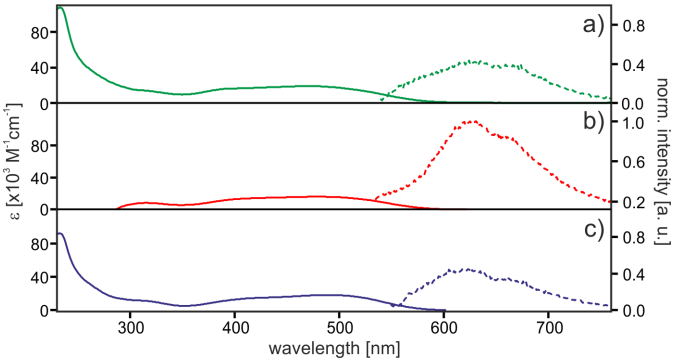

Figure III.27: Absorption (solid trace) and steady-state emission spectra (dashed trace) of $[Cr((tBu)CNAr_3NC(tBu))_3]$ in dry and deaerated a) THF (green), b) toluene (red) and c) hexane (blue) at 20°C.

The absorption spectra show broad and intense bands below 350 nm which are assigned to ligand based $\pi \rightarrow \pi^*$ transitions. In toluene theses absorption overlap with intense absorption bands of the solvent. The broad absorption band from 350 - 550 nm is caused by ^{1}MLCT transitions and is similar in structure and intensity as the one observed in the molybdenum analogue. The extinction coefficients in different solvents differ only slightly (Tab. III.7).
Up to now, there are no reports on homoleptic Cr(0) complexes which exhibit emission in liquid solution at room temperature. Earlier studies on homoleptic Cr(0) hexakis(aryl isocyanide) complexes report weak and rather short lived emission in organic glass matrices at 77 K. Since this emission showed much shorter life times ($<$ 10 ns) than the analogous Mo(0) and W(0) complexes under identical conditions, it was assigned to an allowed singlet-singlet transition from the ligand centred π^* to a dπ state.[6]
The new complex $[Cr((tBu)CNAr_3NC(tBu))_3]$ is the first of its kind to be emissive in solution at room temperature.
As expected, the emission is rather weak compared to that of the corresponding molybdenum complex. It shows, like the emission of the molybdenum complexes, a certain solvent dependency. The strongest emission is observed in toluene, while it is less intense in hexane and THF. Usually one would expect an increase in luminescence intensity with decreas-

Table III.7: Absorption maxima (λ_{max}) with corresponding extinction coefficients and emission maxima (λ_{em}) of [Cr((*t*Bu)CNAr$_3$NC(*t*Bu))$_3$] in different deaerated solvents at 20°C. Measurements were performed with complex concentrations of 10^{-5}M in case of absorption spectroscopy and 10^{-4}M in case of steady-state emission spectroscopy.

solvent	λ_{abs} [nm]	$\varepsilon \times 10^3$ [M^{-1}cm^{-1}]	λ_{em} [nm]	quantum yield ϕ [‰]
THF	233 ($\pi - \pi^*$)	101	630	0.004
	400 (MLCT)	16.3		
	450 (MLCT)	18.3		
	485 (MLCT)	18.5		
toluene	400 (MLCT)	12.8	625	0.01
	450 (MLCT)	15.2		
	485 (MLCT)	15.9		
hexane	233 ($\pi - \pi^*$)	92.4	620	0.003
	400 (MLCT)	12.7		
	450 (MLCT)	16.0		
	485 (MLCT)	18.1		

ing solvent polarity since non-radiative decay pathways decrease due to the increase of the energy gap between ground state and excited state. This appears to not be the case for [Cr((*t*Bu)CNAr$_3$NC(*t*Bu))$_3$].

Mann et. al. suggested the lowest excited state of [Cr(CNPh)$_6$] should have a pronounced singlet character due to its extremely short lifetime, even at low temperature. Since the here-presented complex showed emission at room temperature it is most likely that the excited state is longer lived than the hexakis(aryl isocyanide) complex. Indeed, it was possible to achieve a transient absorption spectrum at room temperature by probing a 10^{-4} M solution in deaerated toluene at 532 nm with laser shots of approximately 10 ns duration. This indicates an excited state lifetime in the range of nanoseconds. In Figure III.28 the obtained spectrum of [Cr((*t*Bu)CNAr$_3$NC(*t*Bu))$_3$] (top) is shown in comparison to the spectrum of [Mo((*t*Bu)CNAr$_3$NC(*t*Bu))$_3$] under similar conditions.

The signal to noise ratio of the upper spectrum is impaired by the relatively short lifetime of the studied compound compared to the length of the laser pulse, but still the MLCT bleach between 400-550 nm is clearly visible. It nicely resembles the form of the ^{1}MLCT absorption observed in UV/Vis spectroscopy. The small positive band around 350 nm is probably caused by the reduced ligand, since the same band is present in the molybdenum compound. In the upper spectrum it is much less intense than in the lower one, which is owed to the high optical density in this spectral region due to the high complex concentration used in this experiment.

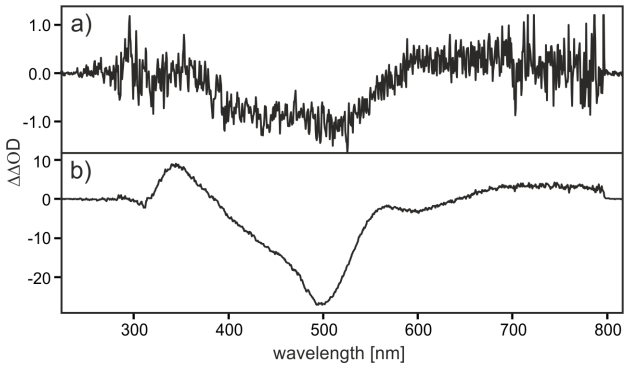

Figure III.28: Transient absorption spectra of solutions of a) 10^{-4} M $[Cr((tBu)CNAr_3NC(tBu))_3]$ in deaerated toluene, and b) 10^{-5} M $[Mo((tBu)CNAr_3NC(tBu))_3]$ in toluene. The spectra were obtained by time integration over 200 ns directly after excitation with a laser pulse of 10 ns duration at 532 nm.

The fact that it was possible to obtain a transient absorption spectrum of $[Cr((tBu)CNAr_3NC(tBu))_3]$ with a nanosecond laser setup indicates an unexpectedly long lifetime. To determine the excited state lifetimes (τ_0) of the Cr(0) compex in different solvents, luminescence decay curves were recorded after excitation at 532 nm with a laser pulse of approximately 30 ps duration (Figure III.29).

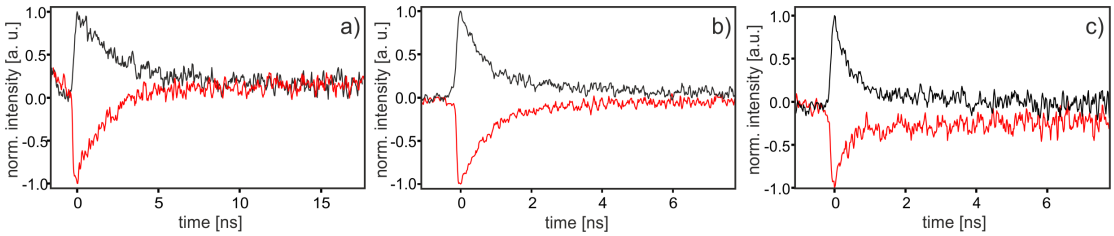

Figure III.29: Luminescence decay (black) and bleach recovery curves (red) recorded after excitation of a 10^{-4} M solution of $[Cr((tBu)CNAr_3NC(tBu))_3]$ in dry and deaerated a) THF, b) toluene, c) hexane at 532 nm with a laser pulse of approximately 30 ps duration.

The decay curves obtained for toluene and hexane showed a bi-exponential behaviour as already observed for the corresponding molybdenum complex, whereas the decay in THF is mono-exponential. In all three solvents the bleach recovery curves were in good agreement with the luminescence decay curves. The resulting lifetimes and their ratios for the bi-exponential cases are summarized in Table III.8.
The listed lifetimes are the only, and therefore the longest, reported for homoleptic Cr(0) complexes at room temperature. Considering that the isoelectronic complex $[Fe(bpy)_3]^{2+}$ is non-emissive due to energetically low lying d-d transitions, the here reported lifetimes can be considered as extraordinarily long. The low emission energy (620-630 nm) in combination

Table III.8: Excited state lifetimes of $[Cr((tBu)CNAr_3NC(tBu))_3]$ in different deaerated solvents at 20 °C. Measurements were performed with complex concentrations of 10^{-4}M.

solvent	emission		absorption		
	τ_1 [ps]	τ_2 [ps]	τ_1 [ps]	τ_2 [ps]	λ_{max}
THF	2628 (100%)	-	1805 (100%)	-	630
toluene	563 (78%)	3738 (22%)	723 (87%)	4931 (13%)	625
hexane	371 (80%)	2922 (20%)	267 (81%)	4529 (19%)	620

with the long lifetimes are indicative for a ^{3}MLCT emissive state.
As already observed for the quantum yield, the solvent dependency of the lifetimes does not follow the typical trend. The expected increase of the lifetime in apolar solvents compared to polar ones, due to the decrease of accessible non-radiative deactivation pathways is not observed. The longest lifetime is found in toluene while hexane and THF show somewhat shorter lifetimes. The cause to this remains unclear up to now.
If the emitting state is indeed a ^{3}MLCT state, the emission maximum is expected to shift with altering polarity of the solvent. Figure III.30 shows the normalized emission spectra in different solvents and the emission maxima are listed in Table III.8.

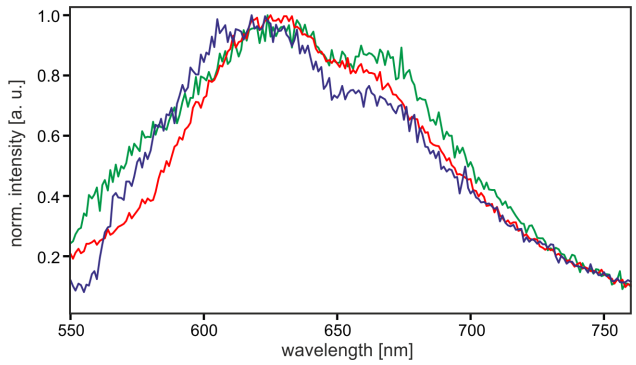

Figure III.30: Normalized steady-state emission spectra of 10^{-4} M $[Cr((tBu)CNAr_3NC(tBu))_3]$ in dry and deaerated THF (green), toluene (red) and hexane (blue) at 20°C. Excitation occurred at 450 nm.

The expected behaviour is not as significant as in the molybdenum compound, since the luminescence is rather broad and appears to consist of two overlapping features, but a small shift in the maximum is observed when comparing the traces of the least polar solvent (hexane, blue trace) to the one of the most polar (THF, green trace). This shift, although not very distinct, is an indicator for the MLCT character of the excited state, which is supported by the electronic similarity to the molybdenum complex in which the emission originates without

doubt from a ^{3}MLCT state.

In order to estimate the energy of the luminescent state, steady-state emission spectra of [Cr((*t*Bu)CNAr$_3$NC(*t*Bu))$_3$] were recorded in organic glasses at 77 K (Fig. III.31). The luminescence bands were expected to be more intense, sharper and blue shifted in comparison with the spectra obtained at room temperature. The sharper form results from the minimization of accessible vibrational modes.

The resulting luminescence spectra were as expected sharper and more intense. They also showed a significant rigidochromic effect, when changing from hexane to THF.

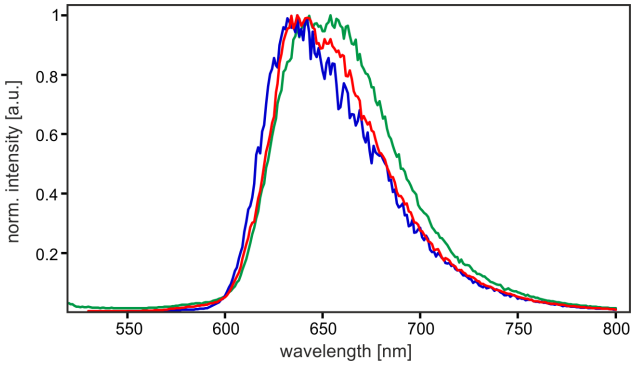

Figure III.31: Comparison of the steady-state emission spectra of [Cr((*t*Bu)CNAr$_3$NC(*t*Bu))$_3$] in deaerated a) 2-methyl-THF (green trace), b) toluene (red trace), c) 2-methylpentane (blue trace) at 77 K. Excitation occurred at λ_{ex}: 450 nm.

The emission maximum shows a very distinct red shift at low temperature in comparison to the ones determined at room temperature (Fig. III.32).

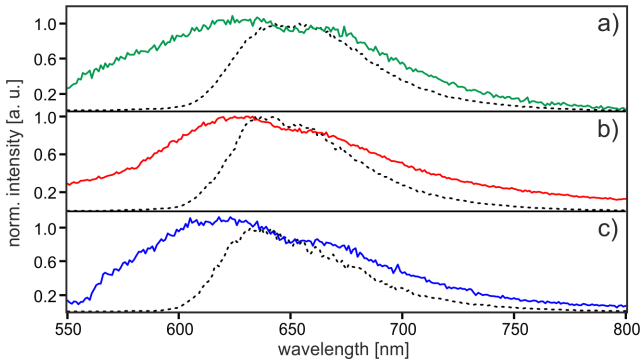

Figure III.32: Comparison of the steady-state emission spectra of [Cr((*t*Bu)CNAr$_3$NC(*t*Bu))$_3$] in a) THF (solid green trace) at 293 K and 2-methyl-THF at 77 K (dashed line), b) toluene (solid red trace) at 293 K and 77 K (dashed line), c) hexane (solid blue trace) at 293 K and 2-methylpentane at 77 K (dashed line). Measurements were performed with complex concentrations of 10^{-4}M. Excitation occurred at 450 nm.

A red shift in the emission maximum with decreasing temperature could indicate for the

presence of a second emitting state (Tab. III.9). In general, multiple emissions are a very rare feature to observe, especially in d^6 metal complexes. One of the few examples reported concern diimine-tetracarbonyl complexes of chromium(0), molybdenum(0) and tungsten(0). For these chromium complexes emission in fluid solution at room temperature was observed. MANUTA et. al. argued that the multiple emission originates from two energetically close MLCT excited states which are in thermal equilibrium with one another and the conversion between the two states is slow enough for the radiative decay to compete with.[95,96] Later, it was shown that the emission at lower energies has significant ^{3}LF character.[97–99]

Table III.9: Emission maxima of [Cr((*t*Bu)CNAr$_3$NC(*t*Bu))$_3$] in different deaerated solvents at 293 K and 77 K. Measurements were performed with complex concentrations of 10^{-4}M.

solvent at r.t. /solvent at 77 K	λ_{max} [nm] at 293 K	λ_{max} [nm] at 77 K	ΔE [cm^{-1}]
THF/2-methyl-THF	630	645	369
toluene/toluene	625	637	301
hexane/2-methylpentane	620	632	306

It is possible that the situation for the [Cr((*t*Bu)CNAr$_3$NC(*t*Bu))$_3$] complex is similar to the one described for the diimine-tetracarbonyl complexes since carbonyls and isocyanides are rather similar to one another. The major difference between those systems is the localisation of the MLCT state. In the heteroleptic complexes it is clearly localized on the diimine ligand, whereas in the here-presented system the complex is homoleptic and therefore several MLCT excited states which are probably localized on different ligands are possible. Actually, this might give rise to the rather little energy difference in the two emission bands. Considering that the presence of two energetically close excited MLCT states in hexakis(arylisocyanide) chromium(0) complexes has been reported[57], the presence of two emitting states seems reasonable. It is possible that due to steric restrains that are present in the system (s. Chapter 3.3.3), the MLCT states are energetically close but geometrically different. The geometrical differences in combination with the rigid coordination geometry might lead to a slow interconversion between the different excited states and thus enable the radiative decay to compete.

If geometrical restricted conversions are the cause to this unusual behaviour, it would explain why a similar effect is not observed in the molybdenum compound, since the smaller chromium atom induces a more rigid coordination environment. Although it shows the same anodic shift of the ground state oxidation potential which is attributed to inter ligand sterical repulsions caused by the smaller ionic radius of Mo^+ compared to Mo^0, its emission maximum is blue shifted at 77 K, as one would expect, and shows no indication for two emitting states. This observation is reasonable considering the smaller size of the chromium atom compared to

molybdenum. The difference in size leads to a more packed structure combined with such a bulky ligand and this might lead to separated excited states.
Another possible explanation results from the very different spin-orbit coupling constants of molybdenum and chromium. While the molybdenum has a spin-orbit coupling constant of 678 cm^{-1}, which is already considerably smaller than the one of copper (857 cm^{-1}), the one of chromium is only 248 cm^{-1}, comparable to the one of phosphorous (230 cm^{-1}).[12] This could lead to rather inefficient intersystem crossing processes and emission from the singlet state might be able to compete with it. If the energy gap between singlet and triplet state is sufficiently small a thermal population of the singlet state from the triplet would be possible, leading to a prolonged singlet state lifetime. This would resemble the process of thermally activated delayed fluorescence (TADF) which is known from copper(I) complexes. However, this should theoretically lead to much longer lifetimes than those observed at room temperature, since slow intersystem crossing process also result in very long lifetimes of triplet excited state and consequently long singlet excited state lifetimes. Additionally, a complex which harvests both singlet and triplet excited states should have exceptionally high quantum yields, but this might be masked by very efficient non-radiative relaxation processes.
The lifetimes in organic glasses at low temperature are expected to increase significantly compared to the ones in liquid solution at room temperature due to the inaccessibility of non-radiative decay pathways. The emission decay curves were recorded after excitation with a laser pulse of approximately 10 ns duration at 532 nm (Fig. III.33).

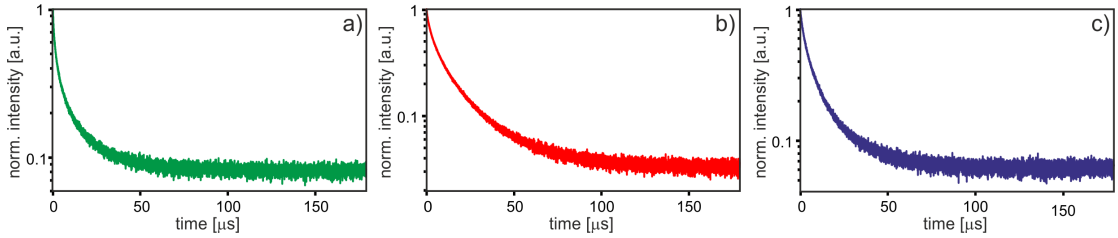

Figure III.33: Emission decay curves of [Cr((*t*Bu)CNAr$_3$NC(*t*Bu))$_3$] in different organic matrices a) 2-methyl-THF b) toluene c) 2-methylpentane at 77 K. Excitation occured at 532 nm with laser shots of approx. 10 ns duration. The emission was detected at the corresponding emission maximum (s. Table III.9).

All three decay curves are bi-exponential, which is likely to be caused by the presence of different sterical confomers that are no longer able to convert into one another. This was also observed in the two molybdenum complexes prepared in this thesis and has been discussed in the supporting information on page S13 of the publication included in Chapter 3.2.
The lifetimes extracted from the decay curves in Figure III.33 are listed in Table III.10.
Each decay kinetic consists of two lifetimes τ_0^1 and τ_0^2, similar to [Mo(CNAr$_3$NC)$_3$] both of them are in the μs range. τ_0^1 found to range from 1.3 to 2.6 μs depending on the glass matrix while τ_0^2 varies from 11.2 to 16.9 μs. The ratio of τ_0^1 to τ_0^2 is around 1:1 for toluene and

Table III.10: Lifetimes of $[Cr((tBu)CNAr_3NC(tBu))_3]$ in different organic glasses at 77 K. Excitation occurred at λ_{ex}: 532 nm and detection at the respective emission maxima listed in Table III.9.

organic matrix	τ_0^1 [μs]	τ_0^2 [μs]
2-methyl-THF	1.2 (66%)	11.2 (34%)
toluene	2.6 (52%)	16.9 (48%)
2-methylpentane	2.5 (58%)	13.3 (42%)

2-methylpentane, but changes a little in favour of τ_0^1 in case of 2-methyl-THF to 2:1.
The time range of both lifetimes points to a spin forbidden transition from the emitting excited state to the ground state. Thus the assignment of the emissive state as a triplet seems to be reasonable.

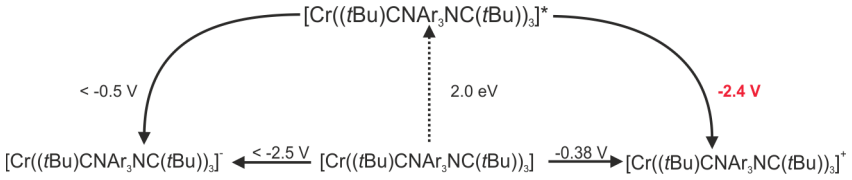

Figure III.34: LATIMER diagram of $[Cr((tBu)CNAr_3NC(tBu))_3]$. Potentials are referenced versus $Fc^{+/0}$.

The excited state energy of the energetical lowest emitting excited state was estimated from the low temperature steady-state emission spectra to be 2.0 eV. Using equation III.2 (Chapter 3.2.4), it is possible to calculate the excited state oxidation potential to be approximately -2.4 V vs. $Fc^{+/0}$. The relevant data are summarized in the LATIMER diagram in Figure III.34.

3.3.5 Photo-Degradation of $[Cr((tBu)CNAr_3NC(tBu))_3]$

As already discussed in Chapter 2.3.1, hexakis(aryl isocyanide) Cr(0) complexes are not emissive in solution due to vibronic coupling of their MLCT states with ligand field states (LF), leading to rapid ligand dissociation.[57,58] Several studies reported the coordination of a solvent molecule in the vacant coordination site.[6,100–102]
However, the here-presented complex exhibits ^{3}MLCT emission in solution. Thus, it has to be concluded that the coupling of the MLCT states with the LF state is rather weak. Nonetheless, the question of photostability of the complex under the employed conditions during the experiments arose. For $[Cr(CNAr)_6]$ a wavelength dependency of the photodissociation was observed with increasing quantum yield ϕ_{Diss} towards higher excitation energy.[57] The lowest excitation wavelength used during the measurements was 450 nm. The photostability of the

Cr(0) complex was assessed by irradiation of the complex (10^{-5} M in dry, deaerated THF and hexane) with a LED lamp (1 W) at 455 nm. UV/Vis absorption spectra were recorded as a function of time (Fig. III.35).

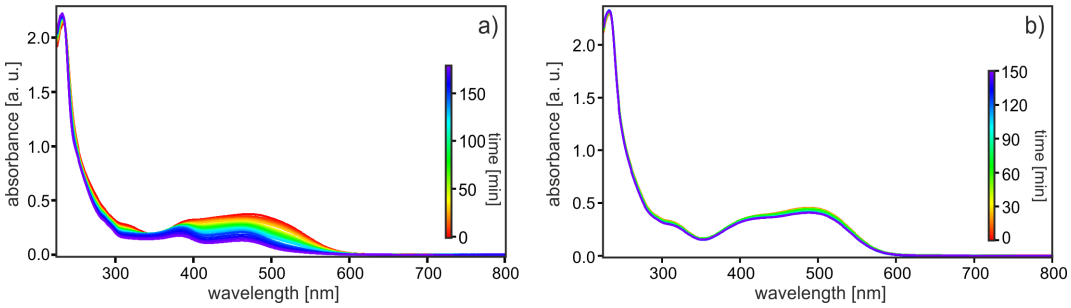

Figure III.35: Uv/Vis absorption spectra of [Cr((*t*Bu)CNAr$_3$NC(*t*Bu))$_3$] in a) deaerated THF b) deaerated hexane after different time intervals of irradiation at 455 nm.

The remaining concentration of [Cr((*t*Bu)CNAr$_3$NC(*t*Bu))$_3$] was determined using the absorbance at 450 nm and the corresponding extinction coefficient determined in Chapter 3.3.4. The MLCT absorption band at 450 nm is expected to be characteristic for the Cr(0) complex and to be well separated from the absorption bands of formed photoproducts. The complex concentration plotted versus irradiation time in THF and hexane are shown in Figure III.36. The depletion curve obtained in THF solution (Fig. III.36 a, green markers) shows a bi-exponential behaviour, with two separate half lifes τ_1 and τ_2 of 7.4 and 70.0 minutes. This, as well as the absence of isosbestic points in the Uv/Vis spectra indicate the presence of at least two non-related decomposition pathways. Additionally, the characteristic absorption of a [Cr(CNAr)$_5$(THF)] species, which is expected to absorb around 580 nm, is not observed.[102] This leads to the conclusion that even though relatively slow photobleaching of the complex is observed, it is most likely not related to the known photodissociation pathways which are initiated by a rapid ligand dissociation step on the sub-picosecond time scale. The bleaching might be caused by reactions with impurities present in the solvent.

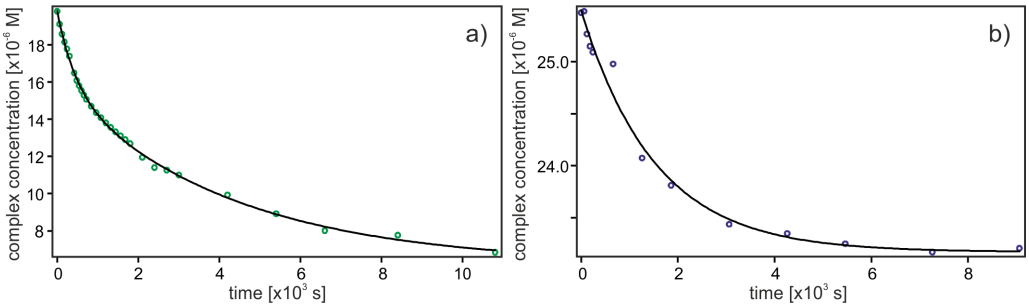

Figure III.36: Depletion curves of $[Cr((t\text{Bu})CNAr_3NC(t\text{Bu}))_3]$ in deaerated a) THF and b) hexane under irradiation at 455 nm. The complex concentration was determined from the absorbance determined at 450 nm.

Figure III.36b shows the depletion of $[Cr((t\text{Bu})CNAr_3NC(t\text{Bu}))_3]$ in deaerated hexane (blue markers) during irradiation at 455 nm. The resulting decay curve is mono-exponential and a half life of 25.5 minutes is obtained. This half life is in between the two half lives observed in THF. This might indicate the presence of only one depletion pathway. It is beyond the focus of this thesis to give a more detailed analysis of this behaviour.
This experiment illustrated the relative robustness of the new $[Cr((t\text{Bu})CNAr_3NC(t\text{Bu}))_3]$ complex over long irradiation periods, providing the certainty that the obtained data represent indeed the properties of the initial complex and not of some kind of subsequently formed decomposition product.
The severely increased photo stability of the complex compared to the hexakis(aryl isocyanide) complexes is rather remarkable and is probably caused by a prevention of efficient population of anti-bonding LF states by the excited MLCT states. Since the exchange of the mono-dentate ligand to a bi-dentate one is assumed to have rather little influence on the position of the LF states, the observed effect is either due to a shift of the MLCT states to lower energy or the prohibition of the structural change responsible for the lowering of ligand field states in energy. The energy of the MLCT excited states might be reduced due to the introduction of the more extended π-system, even within the distorted coordination geometry. The second possible change is a rise in energy of the vibrational modes of the ligand scaffold, which would lead to less efficient coupling between these states and the MLCT states.
Overall, avoiding the population of anti-bonding LF states prevents rapid photodissociation and leads to efficient ^{3}MLCT emission in solution at room temperature.
Even if one of the coordinating isocyanides would dissociate, it would be hold in close proximity of the empty coordination site since the former chelating ligand is still coordinated to the metal center. This might increase the chance of fast re-coordination and the reformation of the initial complex.

3.3.6 Summary

The new complex $[Cr((tBu)CNAr_3NC(tBu))_3]$ was prepared and found to be luminescent in solution at room temperature. The complex possibly emits from multiple thermally equilibrated excited states, which is a known phenomenon in related diimine-tetracarbonyl chromium complexes. This behaviour is in stark contrast to the rapid photodissociation reported for analogous hexakis(aryl isocyanide) complexes. This different behaviour is probably caused by efficient prevention of populating anti-bonding ligand field states, and gives rise to the long excited-state lifetimes compared to other first-row d^6 transition metal complexes.
The rather demanding steric structure of the ligand leads to a very rigid coordination sphere for the metal center, which gives rise to an anodic shift of the ground state oxidation potential, as well as a significant slow down of photo-degradation processes.
This remarkable robustness against photo-bleaching in combination with relatively long excited state lifetimes illustrates the application potential of this kind of earth-abundant photosensitizers, in light harvesting applications (e.g. solar cells).

3.4 Luminescent Homoleptic Nickel(0) Complexes with Chelating Isocyanide Ligands

As shown in Chapter 3.3, it is possible to use chelating bis(isocyanide)triaryl ligands to access first-row transition metal based luminophores. This result gave rise to the question, if it is possible to prepare luminescent complexes which are zero-valent, isoelectronic analogues to the widely investigated Cu(I) complexes.[103,104]
There are very few studies on luminescent Ni(0) complex in the literature and, although some heteroleptic, non-tetrahedral complexes with lifetimes in the microsecond range at room temperature were reported, very little is known about their photophysical properties.[105]
A systematic study concerning the photophysics of heteroleptic Ni(0) complexes bearing carbonyl ligands was published by KUNKELY et al..[99,106,107] They found, that in the investigated complexes $[Ni(CO)_2(PPh_3)_2]$ and $[Ni(CO)_2$(1,3-di-t-butylimidazol-2-ylidene$)_2]$ the emission observed at room temperature is likely to originate from an excited ^{3}MLCT state.
To the best of my knowledge, tetrahedral, homoleptic Ni(0) complexes were only reported to be luminescent in the solid state.[108,109]
Homoleptic isocyanide nickel(0) complexes have been reported[110–117], as well as one example bearing chelating isocyanide ligands[63,64], but their photophysical properties have been ignored.
From this we set out to investigate the luminescence behaviour of homoleptic bis(aryl bis(isocyanide)) nickel(0) complexes.

3.4.1 Synthesis of (Ph)CNAr$_3$NC(Ph) and (Ph)CNArSArNC(Ph) and their nickel(0) complexes

Since, in general, it is a troublesome task to access luminescent d^{10} metal complexes, a careful ligand design is crucial to this objective.
One of the major challenges is to prevent geometrical distortion of the complex upon excitation with light, because this gives rise to rapid excited state relaxation. For this purpose, ligands with a very rigid coordination pocket and sterical demanding substituents in the *ortho* position to the coordination site are commonly used.[14]
In order to achieve an interlocked coordination geometry of the isocyanide ligands in a tetrahedral complex the *tert*-butyl groups of **(*t*Bu)CNAr$_3$NC(*t*Bu)** in *ortho* positions were replaced by phenyl rings, which should be sufficient to hamper the geometrical distortion of the excited state. This resulting ligand **(Ph)CNAr$_3$NC(Ph)** was accessible via a five step synthesis (Fig. III.37).

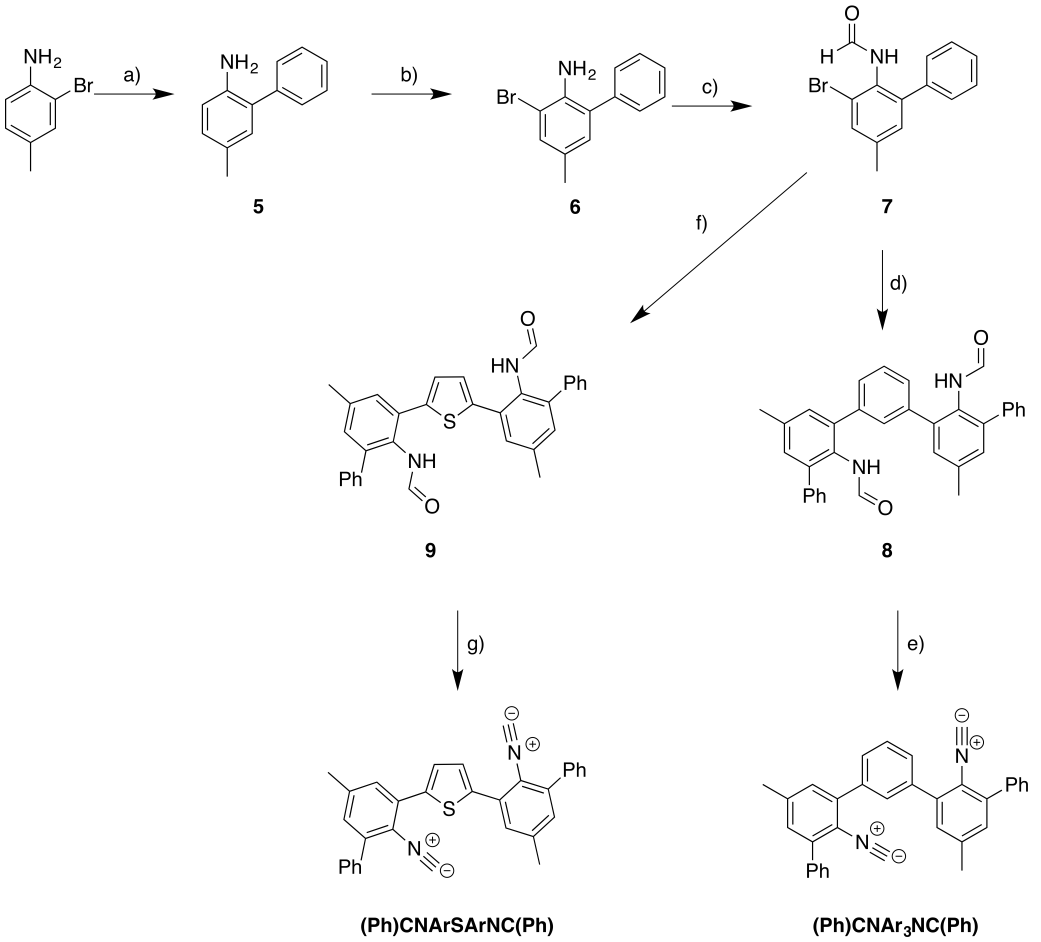

Figure III.37: Synthesis of the phenyl substituted ligands bearing a phenyl (**(Ph)CNAr$_3$NC(Ph)**) and a thiophene backbone (**(Ph)CNArSArNC(Ph)**). a) Phenylboronic acid, K_2CO_3 and $[Pd(PPh_3)_2Cl_2]$ in DME at 80°C overnight, b) aq. HBr, hydrogen peroxide in MeOH at r.t. overnight, c) acetic acid anhydride, formic acid 30 min. at r.t., d) K_2CO_3 and $[Pd(dppf)Cl_2]$ in dioxane/H_2O at 110°C overnight, e) D*i*PA, $POCl_3$ at r.t. overnight, f) $[Pd(dppf)Cl_2]$ in xylene at 140° for 2 d, g) D*i*PA, $POCl_3$ at r.t. overnight.

In a first Suzuki-Miyura coupling reaction of 2-bromo-4-methyl-aniline with phenylboronic acid, 4-methyl-2-phenylaniline **5** was prepared in 93% yield. Bromination of this compound with HBr and hydrogen peroxide in methanol gave 2-bromo-4-methyl-6-phenylaniline **6** in 91% yield.

Although it was possible to perform the coupling reaction to a di(amine)-penta(aryl) system, analogous to the synthesis of **(*t*Bu)CNAr$_3$NC(*t*Bu)** (Chap. 3.2.2), the formation of the bis(formamide) turned out to be rather inefficient. Therefore, an approach similar to the synthesis of the first ligand **CNAr$_3$NC** was used.

The formamide **7** was obtained after stirring in freshly prepared acetic formic anhydride for

30 minutes at room temperature. The product was filtered off and used in the next step without further purification (87%).
A second SUZUKI-MIYURA coupling reaction of formamide **7** and 1,3-bis(4,4,5,5-tetramethyl-1,3,2-dioxaborolan-yl)benzene gave the desired penta(aryl) compound **8** in 91%. This compound was then transformed to the desired ligand **(Ph)CNAr$_3$NC(Ph)** using D*i*PA and $POCl_3$ in 80% yield. The final ligand was obtained in an overall yield of 53% over five steps.

The aryl backbone of the ligand was initially designed to facilitate coordination in an octahedral geometry in which the angle between the two coordination sites of one ligand is 90°. In the case of a tetrahedral coordination sphere, the angle is supposed to be 109.5°. A second ligand with a thiophene backbone instead of a phenyl backbone was developed in contemplation of the changed geometrical demands of the coordination sphere.
The new ligand **(Ph)CNArSArNC(Ph)** was easily accessible by one minor change in the synthetic route.
N-Formyl-2-bromo-4-methyl-6-phenylaniline **7** was already prepared for the synthesis of **(Ph)-CNAr$_3$NC(Ph)**, and the desired thiophene backbone was introduced via a STILLE coupling reaction with commercially available 2,5-bis(tributylstannyl)thiophene, giving **9** in 98%. 1,3-Bis(N-formyl-4-methyl-6-phenylanilin-2-yl)thiophene **9** was then reacted with $POCl_3$ in presence of D*i*PA to yield the second ligand **(Ph)CNArSArNC(Ph)** in 64%.

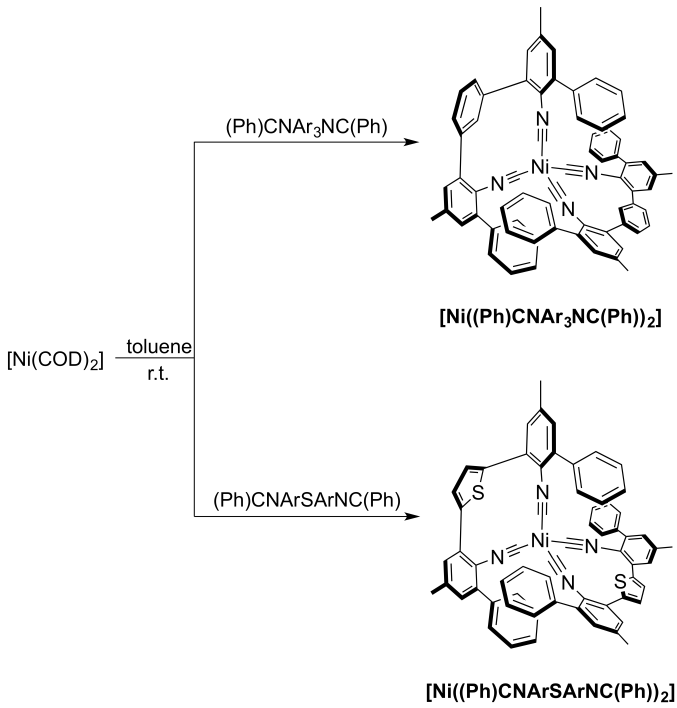

Figure III.38: Synthetic strategy yielding the desired nickel(0) complexes $[Ni((Ph)CNAr_3NC(Ph))_2]$ and $[Ni((Ph)ArSAr(Ph))_2]$.

The Ni(0) complexes were obtained by adding a solution of the appropriate ligand to a solution of $[Ni(COD)_2]$ in toluene (Fig. III.38).
The desired complex $[Ni((Ph)CNAr_3NC(Ph))_2]$ was obtained as an orange air stable solid in 98% yield, and the $[Ni((Ph)ArSAr(Ph))_2]$ complex was isolated as a red air stable solid in 97% yield.

3.4.2 IR-spectroscopy

Figure III.39 shows the FTIR-spectra of the free ligands (top) and corresponding complexes (bottom). The spectra of the ligands (Ph)ArSAr(Ph) (a) and the $(Ph)CNAr_3NC(Ph)$ (c) are rather similar to one another and each exhibits a sharp band at 2119 cm^{-1} which is assigned to the C≡N vibration.

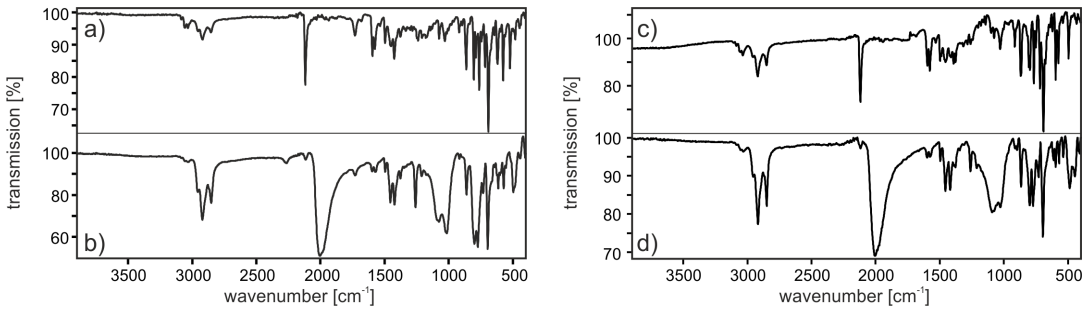

Figure III.39: Solid state FTIR-spectra of the free ligands (a) (Ph)CNArSArNC(Ph) and (c) $(Ph)CNAr_3NC(Ph)$, as well as their corresponding nickel(0) complexes (b) $[Ni((Ph)CNArSArNC(Ph))_2]$ and (d) $[Ni((Ph)CNAr_3NC(Ph))_2]$.

For both complexes, this band is shifted to lower wavenumbers (2004 cm^{-1}) indicating the presence of π-backbonding. Cotton et. al. investigated the donor-acceptor properties of isocyanide ligands in homoleptic Ni(0) complexes and assigned two bands to the C≡N vibration. They ascribed this to a bending of the isocyanide moiety, due to significant π-backbonding, leading to a lower symmetry than ideal T_d.[110]
The here-presented complexes do not show the commonly observed two strong bands[110,112,114], but one broad major vibrational band compared to the free ligand. This is in good agreement with the reported behaviour of chelating arylisocyanide ligands[63]. The spectrum of $[Ni((Ph)CNArSArNC(Ph))_2]$ (Fig. III.39b)) exhibits three small additional bands, which probably originate from C≡N vibrations. A total of four C≡N vibrational bands would correspond to a C_{2v} symmetry, but the major contribution remains the single band at 2004 cm^{-1}. These differences indicates a certain variation in the coordination geometry of the complexes.

3.4.3 Electrochemistry

In order to determine the ground state oxidation potentials of the complexes [Ni((Ph)CNArSArNC(Ph))$_2$] and [Ni((Ph)CNAr$_3$NC(Ph))$_2$], cyclic voltammetry experiments were performed. The experiments were conducted with approx. 1 mM solutions of the respective complex and 0.1 M TBAPF$_6$ as supporting electrolyte in THF. The potentials were referenced versus the Fc$^{+/0}$ couple.

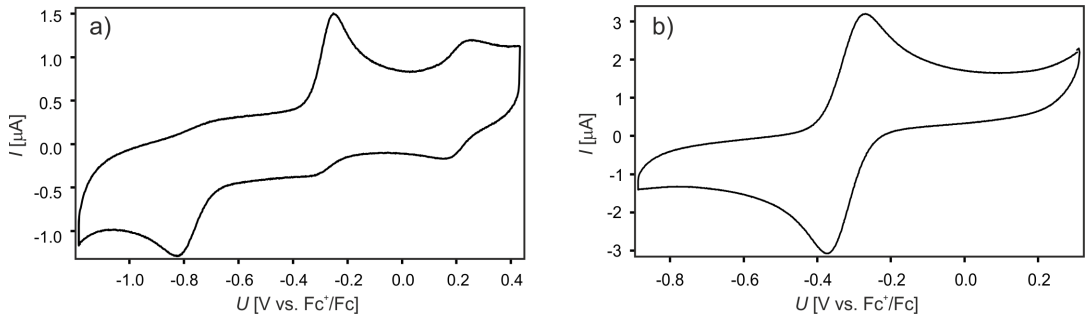

Figure III.40: Cyclic voltammograms of a) [Ni((Ph)CNArSArNC(Ph))$_2$] and b) [Ni((Ph)CNAr$_3$NC(Ph))$_2$] in THF with 0.1M TBAPF$_6$ at 20°C. A glassy carbon working electrode, and two silver wires as counter and quasi reference electrode were used. The scan rate was 0.1 V s^{-1}. The potential was referenced versus the Fc$^{+/0}$ couple.

Although the complexes only differ in the ligand backbone, they behave surprisingly different in the electrochemical experiments (Fig. III.40). [Ni((Ph)CNArSArNC(Ph))$_2$] exhibits a relatively complicated voltammogram (Fig. III.40 a)). [Ni((Ph)CNAr$_3$NC(Ph))$_2$] exhibits one reversible oxidation wave at -0.32 V (Fig. III.40 b)), which is assigned to the Ni$^{+/0}$ couple. A similar wave is observed at -0.3 V in the voltammogram of [Ni((Ph)CNArSArNC(Ph))$_2$], but is mostly irreversible. Only a small shoulder for the cathodic peak is observed. The corresponding main reduction process occurs at -0.76 V. Such an enormous splitting between the oxidation and reduction wave usually indicates reactions taking place on the time scale of cyclic voltammetric experiments. In this case, the process appears to be reversible since the voltammogram remained consistent over several cycles. One possible reaction to occur is the uptake of additional ligands , such as solvent molecules. Isoelectronic five and six coordinated Cu(II) complexes have been described in the literature[118,119]. A reversible second oxidation wave is observed at 0.21 V which is attributed to the Ni$^{2+/+}$ redox couple.
This process was not observed for [Ni((Ph)CNAr$_3$NC(Ph))$_2$]. In this case, scanning to higher potentials showed two weak irreversible oxidation waves, which diminish over several cycles. This might indicate the decomposition of the complex upon further oxidation, since a reduction of the atomic radius leads to a more strained coordination geometry. This effect is probably more pronounced in the ligand with an aryl backbone compared to the one with a thiophene backbone, as it induces a smaller bite angle.

Table III.11: Redox potentials of different tetrahedral Ni(0) complexes vs. $Fc^{+/0}$ at 20°C.

Compound	E^0 (M^+/M^0) [V]	E^0 (M^{2+}/M^+) [V]
$[Ni((Ph)CNAr_3NC(Ph))_2]^{a,b}$	-0.32	-
$[Ni((Ph)CNArSArNC(Ph))_2]^{a,b}$	-0.30^{pa}	0.21
	-0.76^{pc}	
$[Ni(PPh_3)_4]$ [b]	-0.97	-
$[Ni(PEt_3)_4]$ [b]	-1.3	-0.2

Potentials referenced vs. Fc^+/Fc. [a] *this work*. [b] in THF from ref. [120], converted to $Fc^{+/0}$ [75].

Table III.11 summarizes the observed redox potentials. To the best of my knowledge, no reports of redox potentials for isocyanide nickel(0) complexes exist, hence potentials of homoleptic phosphine nickel(0) complexes are given as reference values. The oxidation potentials of both complexes are significantly shifted to higher potentials compared to the phosphine systems, which mirrors the stabilisation of the low-valent metal center by the π-backbonding capacity of the ligand.

3.4.4 Photophysical Properties

Most of the homoleptic isocyanide nickel(0) complexes are reported to be of a white to yellow color.[63,112] Only the tetrakis(2-nitrophenyl isocyanide)nickel(0) was reported by Hahn et. al. to be purple. The absence of significant absorption in the visible spectral range probably lead to the neglect of the photophysical properties of these compounds in prior studies.

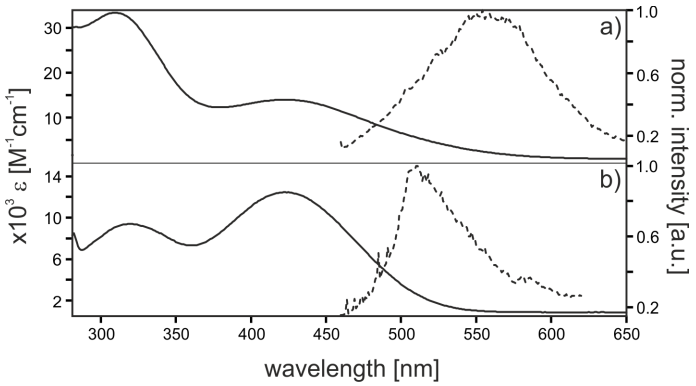

Figure III.41: Absorption (solid traces) and steady-state emission (dashed traces) spectra of a) $[Ni((Ph)CNArSArNC(Ph))_2]$ and (b) $[Ni((Ph)CNAr_3NC(Ph))_2]$ in toluene. Absorption spectra were obtained from 10^{-5} M solutions. Steady-state emission spectra were recorded at 77 K after excitation at 430 nm.

The complexes $[Ni((Ph)CNArSArNC(Ph))_2]$ and $[Ni((Ph)CNAr_3NC(Ph))_2]$, prepared in the

course of this study, are dark red and bright orange, respectively. Therefore, they might be suitable candidates to gain some insight into their potential MLCT excited state behaviour.
The absorption spectra of both compounds are rather similar to each other. Each of them show two broad transition bands. The ones at higher energies are likely ligand-based since they are also present in the spectra of the related chromium(0) complex (see 3.3), as well as the Cu(I) compounds (see Appendix 1.1.5). Although they appear at similar wavelength, they differ strongly in intensity. In $[Ni((Ph)CNArSArNC(Ph))_2]$, the extinction coefficient of this band is found to be 33.5×10^3 $M^{-1}cm^{-1}$, whereas in $[Ni((Ph)CNAr_3NC(Ph))_2]$ it is 9.38×10^3 $M^{-1}cm^{-1}$. This could be caused either by overlaying of different bands or by a different character of these bands, with the one in $[Ni((Ph)CNAr_3NC(Ph))_2]$ being less allowed. This might be caused by the more planar structure of the thiophene-derived ligand, which has a more extended π-system, leading to the transition being more allowed.
The lower energy absorption bands are both found at a maximum of 423 nm and are similar in their extinction coefficient (Tab. III.12). These bands are assigned to ^{1}MLCT transitions, since they are rather intense and too low in energy to be intraligand transitions (IL), as can be seen from the absorption spectra of other metal complexes bearing these ligands (Appendix 1.1.5).

Table III.12: Absorption maxima and the corresponding extinction coefficients for $[Ni((Ph)CNArSArNC(Ph))_2]$ and $[Ni((Ph)CNAr_3NC(Ph))_2]$ in toluene at 20°C. The emission maxima were determined from steady-state emission spectra in the indicated matrix at 77 K. The excitation wavelength was 430 nm.

Complex	λ_{abs} [nm]	$\varepsilon\times10^3$ [$M^{-1}cm^{-1}$]	λ_{em} [nm]	
			MeTHF	toluene
$[Ni((Ph)CNArSArNC(Ph))_2]$	310 (IL) 423 (MLCT)	33.5 12.5	497	554
$[Ni((Ph)CNAr_3NC(Ph))_2]$	319 (IL) 423 (MLCT)	9.38 14.0	506	511

Both complexes emit upon excitation into the ^{1}MLCT band. However, the emission was rather weak and only observed in organic matrices at 77 K.
The steady-state emission spectrum of $[Ni((Ph)CNAr_3NC(Ph))_2]$ shows a relatively sharp band with a maximum at 511 nm. The band shifts only slightly when moving from a toluene matrix to a 2-methyl-tetrahydrofuran matrix (Fig. III.42). Interestingly, only a small STOKES shift is observed. Usually the distortion of excited state towards a planar geometry results in a large STOKES shift of the MLCT emission. The absence of this effect might be interpreted as a indication of a relatively small distortion of the excited state.

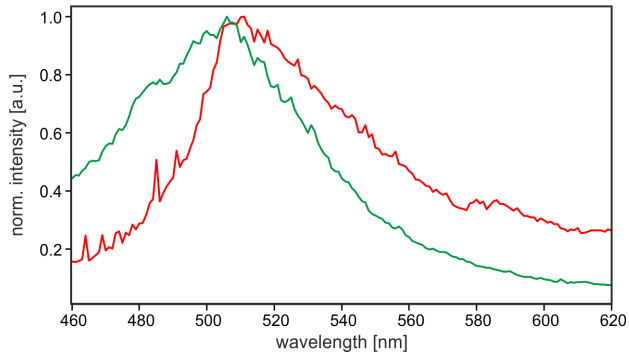

Figure III.42: Steady-state emission spectra of $[Ni((Ph)CNAr_3NC(Ph))_2]$ in matrices of 2-MeTHF (green trace) and toluene (red trace) at 77 K. The samples were excited at 430 nm.

In case of $[Ni((Ph)CNArSArNC(Ph))_2]$, the emission is relatively unstructured and broad, as expected for a MLCT emission. The emission maximum in a toluene matrix is observed at 554 nm and shifts significantly to higher energy (497 nm) in 2-methyl-tetrahydrofuran (Fig. III.43). This is in stark contrast to the expected red-shift upon increasing solvent polarity. The origin of this very different behaviour in terms of matrix effects in the two complexes is not yet understood.

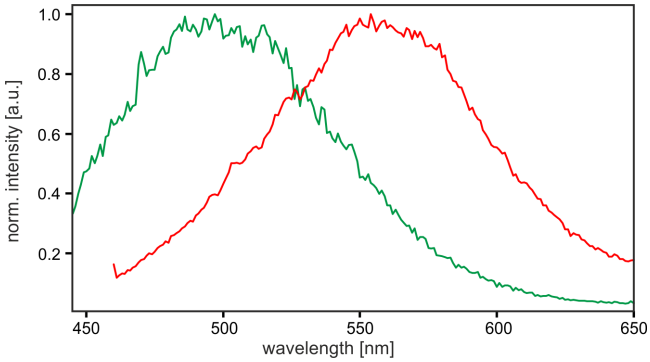

Figure III.43: Steady-state emission spectra of $[Ni((Ph)CNArSArNC(Ph))_2]$ in matrices of 2-MeTHF (green trace) and toluene (red trace) at 77 K. The samples were excited at 430 nm.

In order to gain information about the nature of the emitting state, the lifetimes were determined. Luminescent decay curves were recorded at the corresponding emission maximum (Tab. III.12) in organic matrices at 77 K after excitation at 532 nm with laser pulses of approximately 10 ns duration (Fig. III.44).

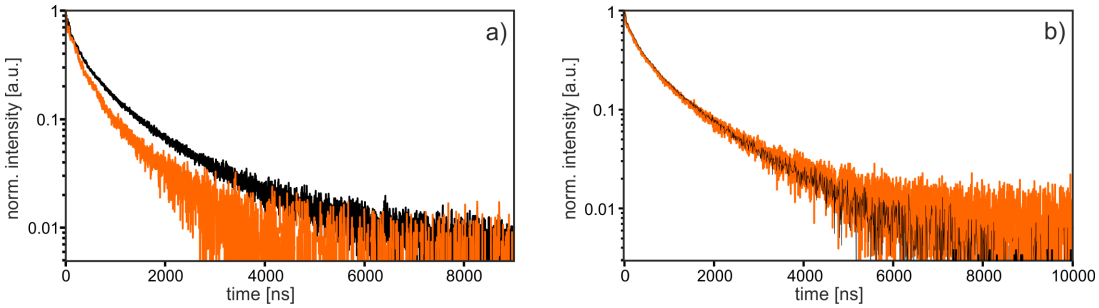

Figure III.44: Luminescent decay curves of [Ni((Ph)CNArSArNC(Ph))$_2$] (black traces) and [Ni((Ph)CNAr$_3$NC(Ph))$_2$] (orange traces) in a) 2-MeTHF and b) toluene at 77 K. The curves were recorded at the corresponding emission maximum (Tab. III.12) after excitation at 532 nm with laser pulses of approximately 10 ns duration.

The decay curves of the emission in 2-methyl-tetrahydrofuran (Fig. III.44 a)) are bi-exponential for both complexes. This is probably due to sterical conformers, which can not interconvert in frozen solutions. The interconversion movements might also be responsible for the absence of emission in solution at room temperature.
The lifetimes of the excited state are identical within the experimental accuracy of 10% in both complexes. The different steepness of the decay curves (Fig. III.44) result from different contribution of the single lifetimes to the decay curve.
In toluene, the decay curves show a tri-exponential decay behaviour with one relatively large lifetime beyond 0.5 milliseconds. This long lifetime has, in both cases, only a very small contribution of $< 1\%$ to the decay curves. The other two lifetimes do not alter upon the changed matrix. The resulting lifetimes and their contribution to the fitting function of the decay curves are summarized in Table III.13.

Table III.13: Excited state lifetimes extracted from bi- and tri-exponential fits of luminescence decay curves of [Ni((Ph)CNArSArNC(Ph))$_2$] and [Ni((Ph)CNAr$_3$NC(Ph))$_2$] in 2-MeTHF and toluene at 77 K. The decay curves were recorded after excitation at 532 nm with laser pulses of approx. 10 ns duration.

life time [μs]	[Ni((Ph)CNArSArNC(Ph))$_2$]		[Ni((Ph)CNAr$_3$NC(Ph))$_2$]	
	MeTHF	toluene	MeTHF	toluene
τ_1	0.19 (60%)	0.23 (57%)	0.20(66%)	0.20 (53%)
τ_2	1.2 (40%)	1.2 (43%)	0.91 (34%)	1.1 (47%)
τ_3	-	91 ($< 1\%$)	-	66 ($< 1\%$)

Surprisingly, the observed shift of the emission maximum upon altering the matrix in case of [Ni((Ph)CNArSArNC(Ph))$_2$] does not result in a corresponding matrix effect for the lifetimes. Also, the observed differences in the emission behaviour between the complex with an aryl

backbone and the one with the thiophene backbone do not lead to different excited state lifetimes.
The relatively long lifetimes indicate that the emitting excited state has triplet character. This is a reasonable assumption, since Ni(0) has a spin-orbit coupling constant similar to copper(I), with its complexes exhibiting ^{3}MLCT emission. The excited state is confirmed to be a MLCT state, since the ^{1}MLCT absorption bands are observed for both complexes and MLCT emission was reported for several nickel(0) complexes.[106,107,109,121] The absence of emission in fluid solution at room temperature is most likely due to efficient non-radiative deactivation processes. This is a known challenge in designing luminescent d^{10} metal complexes. The long and relatively linear isocyanide unit might allow for rapid distortion movements.

3.4.5 Summary

In the course of this project two chelating isocyanide ligands were synthesized in good overall yields (44% and 53%). Both ligands offer sterical demanding phenyl substituents in the *ortho* position to the isocyanide moiety. One of the ligands has a thiophene backbone in order to optimize the bite angle of the coordination site for tetrahedral geometry.
The Ni(0) complexes were isolated in high yields and proved to be air stable in the solid state. They showed different behaviour in electrochemical experiments, probably due to their different capability to adapt a planar coordination geometry upon oxidation of the metal centre. The complex bearing the ligand with an aryl backbone showed one reversible oxidation wave at -0.32 Vvs. $Fc^{+/0}$ which was assigned to the $Ni^{+/0}$ redox couple. The complex with a thiophene backbone showed a more complicated behaviour which is probably caused by reversible reactions taking place upon oxidation on the time scale of the experiment.
Both complexes show strong ^{1}MLCT absorption bands in the visible part of the spectrum. Although no emission was observed in fluid solution at room temperature, the complexes were found to be emissive in organic matrices at 77 K. The emission band for the complex with an aryl backbone is rather sharp and does not show a significant matrix effect, while the complex with a thiophene backbone show a broader emission which shifts towards higher energies in more polar matrices.
The bi- and tri-exponential decay behaviour of the luminescence was rationalized with the presence of different conformers in the solid matrices. The extracted excite-state lifetimes are in the range of microseconds, and it was concluded that the emitting state is likely to have significant ^{3}MLCT character. To the best of my knowledge, this is the second example of homoleptic isocyanide nickel(0) complexes with intense absorption bands in the visible region[114], and the first to be investigated in terms of their electrochemical and luminescence properties.

IV Summary and Conclusion

Limited fossil fuel resources make it necessary to exploit other, sustainable energy sources. In theory, the sun supplies a more than sufficient amount of energy in form of light irradiation.[2] In order to utilize light in chemical reactions, photocatalysts are used. The photocatalyst absorbs light and transforms it into chemical energy via the formation of charge separated states. The employment of light as an energy source allows for demanding reactions to take place under very mild conditions. This makes photocatalysis an appealing method in the synthesis of sensitive organic molecules. Most of the employed catalysts are metal complexes, and many of them derive from precious d^6 metals and are limited in their reduction power.

This thesis comprises two general topics. First, the development of strong photoreductants by lowering the ground state oxidation potential of the photocatalyst. Second, the design of first-row transition metal based luminophores in respect of potential application as photosensitizers in, for example, OLEDs or DSSCs.

In the context of developing strong photoreductants, two separate studies were conducted.

In the first project, a homoleptic ruthenium(II) complex, as well as its iron(II) and osmium(II) homologues bearing electron-rich tetramethoxy-2,2′-bipyridine ligands, were prepared (*Eur. J. Inorg. Chem.* **2015**, *28*, 4666; see also Chapter 3.1). The ruthenium(II) complex was found to be a fairly strong photoreductant and stable in presence of strong acids, such as methanesulfonic acid. Its robustness towards acids is a key advantage over other strong, ruthenium(II) tris(bipyridine) derived reductants (e.g. $[Ru((4,4'\text{-}(Me_2N)bpy)_3]^{2+}$), since it can be employed in proton-coupled electron transfer reaction (PCET) in order to enable demanding reductions to take place. This was illustrated with the photoinduced reduction of acetophenone in a proton-coupled electron transfer reaction upon light excitation.

The second project focused on a new approach to strong photoreductants, since the introduction of electron-rich ligands cannot provide the substantial shifts in the excited state oxidation potentials necessary to access the range of reduction power needed to reduce challenging organic molecules in absence of activating moieties or reagents. The new strategy relies on the use of earth-abundant, low-valent metal centers which exhibit very low ground state oxidation potentials. This lead to the development of several rigid, chelating bis(isocyanide)aryl ligands to ensure their photostability and sufficiently long MLCT excited state lifetimes (Fig. IV.1). Two homoleptic molybdenum(0) complexes were prepared using the ligands **A** shown in Figure IV.1 (*Angew. Chem. Int. Ed.* **2016**, *55*, 11247; see also Chapter 3.2).

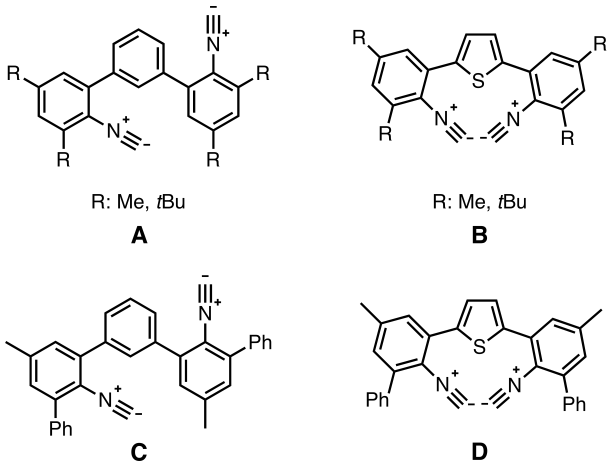

Figure IV.1: Chelating isocyanide ligands synthesized in this thesis.

The molybdenum(0) complex bearing the methyl substituted ligand showed a reversible oxidation wave at -0.4 V vs $Fc^{+/0}$ for the $Mo^{+/0}$ ground state oxidation. Intense ^{1}MLCT transitions occur between 350 nm and 550 nm. The lifetime of the ^{3}MLCT excited state range from 65 ns in deaerated THF to 273 ns in deaerated hexane. The excited state oxidation potential was estimated to be -2.6 V vs $Fc^{+/0}$ and the complex was used in a photocatalytic rearrangement reaction of a substituted acyl-cyclopropane to a dihydrofuran derivative. This rearrangement reaction is triggered by an electron injection into the acyl-cyclopropane unit. The reduction potential of this moiety is so negative that the strong photoreductant $[Ir(ppy)_3]$ is not able to catalyse the reaction. The molybdenum(0) complex yielded 84% of the desired product with a close to maximum TON.

The catalyst was also used in a photocatalytic version of a base-promoted homolytic aromatic substitution (BHAS) reaction. In this context, it was observed that the catalyst is able to abstract halogen anions. This leads to the formation of additional catalytically active species and subsequent catalyst decomposition (Chapter 3.2.1).

In order to overcome this limitation, a second homoleptic molybdenum(0) catalyst bearing the *tert*-butyl substituted chelate ligand was prepared. The complex showed similar absorption and emission properties as the first one, but exhibited much longer excited state lifetimes - from 860 ns in deaerated THF to 1.4 μs in deaerated hexane, and reached quantum yields of up to 20%. Since the ground state oxidation potential (-0.28 V vs $Fc^{+/0}$) showed a small anodic shift compared to the parent complex, the excited state oxidation potential was estimated to be -2.5 V vs $Fc^{+/0}$. Using this catalyst and a substrate with sterical demanding substituents, it was possible to obtain the desired ring closure product in 29% yield with a TON of 6.2 ($TON_{theor.max.}$: 20).

The second molybdenum(0) catalyst showed significantly improved photophysical properties with only a minor increase in excited state oxidation potential. Its sterical demanding substituents prevent the efficient coordination of halogen anions and increases the overall

stability of the complex. Figure IV.2 gives a qualitative overview of reduction power of the herein presented molybdenum(0) catalysts in context of well-established, strongly reducing photocatalysts compared to reduction potentials of several classes of substrate molecules.

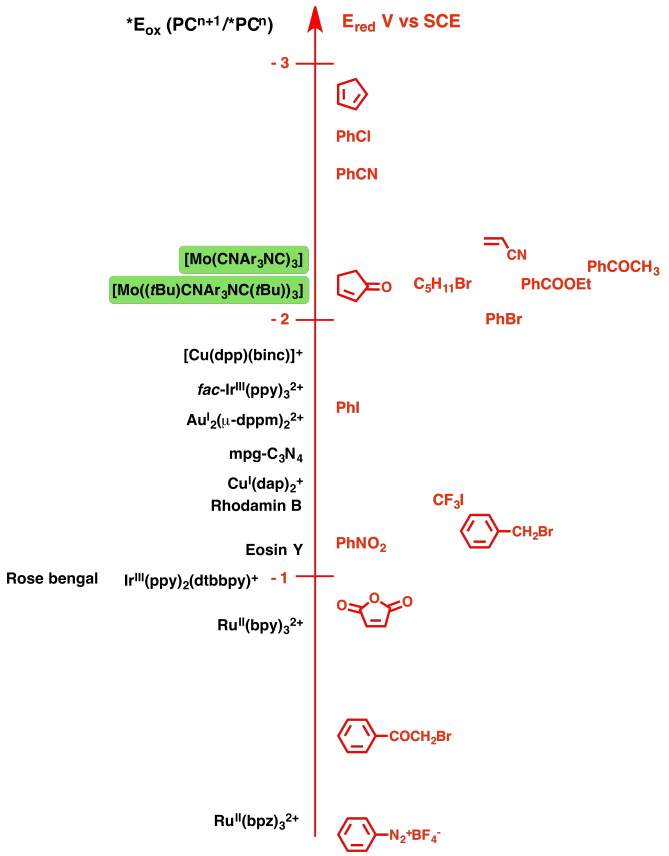

Figure IV.2: Excited state oxidation potential of the prepared molybdenum(0) complexes in relation to other, well-established photocatalysts and in context of the reduction potentials of important organic moieties. Reproduced and modified from ref. [50].

It is evident that the use of rigid, chelating isocyanide ligands with an aromatic backbone give access to robust, strongly reducing molybdenum(0) photocatalysts. Exchanging the commonly used precious metals in photocatalysts for a low-valent, earth-abundant metal center leads to inexpensive compounds that catalyse demanding reduction reactions under visible light irradiation at room temperature.

In the future, the introduction of electron donating or withdrawing substituents in the *para* position to the coordination site would allow for tuning of the complexes properties to ones needs. In order to illustrate their broad application scope and to further establish these compounds as a new class of photocatalysts, they should be subjected to more detailed photocatalytic investigations and more complex catalytic cycles. Additionally, the design of heteroleptic complexes is appealing, since the $[MoCl_4(THF)_2]$ precursor complex already offers

the predisposition for such modifications. This would lead to much more versatile applications, for example as a photosensitizer in a molecular dyad or triad. In order to efficiently design more complicated systems containing these complexes, a deeper understanding of their photophysics is desirable. For this purpose resonance raman studies, TRIR experiments as well as DFT calculations are recommended.
The third topic addressed in this thesis is the development of luminophores based on earth-abundant first-row transition metals. These luminophores might find application as photosensitizers in devices such as OLEDs and DSSCs. In this context, homoleptic complexes of Cr(0), Ni(0) and Cu(I) with chelating isocyanide ligands were investigated.

In analogy to the molybdenum(0) complexes, a chromium(0) complex with the *tert*-butyl substituted ligand **A** (Fig. IV.1) was investigated (see Chapter 3.3). The complex showed three reversible oxidation waves which were attributed to the metal centred oxidations ($Cr^0 \rightarrow Cr^+ \rightarrow Cr^{2+} \rightarrow Cr^{3+}$). The complexes showed ^{1}MLCT absorption bands similar to the molybdenum(0) homologues. Usually, first-row d^6 metal complexes tend to be non-emissive, since rapid, non-radiative relaxation occurs via energetically low lying LF states.[56,88] Nevertheless, the chromium(0) complex is emissive in solution at room temperature. Its excited state is surprisingly long lived, with lifetimes in the nanosecond regime. The transient absorption spectrum resembles the ones obtained from the corresponding molybdenum complex. At 77 K, the emission lifetime is in the range of microseconds and the emission maximum shifts to lower energies. This was interpreted as an indication of emission occurring from a thermally activated state at room temperature. Although the spin multiplicity of the two emissive states remains uncertain, they are expected to be MLCT states. To the best of my knowledge, this is the first homoleptic chromium(0) complex which shows MLCT emission in solution at room temperature.
A deeper understanding of the fundamental photophysical processes is vital to increase the excited state lifetime of this complex. The studied complex is already considerably photostable, but its excited state lifetime is short compared to its molybdenum analogues. Although this is no severe disadvantage for the potential application as surface bound photosensitizer, bimolecular electron transfer reactions are inefficient under these circumstances. Nevertheless, a detailed understanding of the accessible excited states and their behaviour in combination with careful ligand design might allow for the development of chromium(0) complexes with excited state lifetimes that are sufficiently long to perform photoinduced electron transfer catalysis. Additionally, the introduction of anchor groups to the ligand backbone will open the way for this kind of complexes to be tested in DSSCs.

In a fourth project concerning the development of first-row transition metal luminophores, the chelating isocyanide ligands **C** and **D** (Fig. IV.1) were utilized to access luminescent, homoleptic nickel(0) complexes and to study the influence of the backbone on the properties

of these compounds (Chapter 3.4).
Most of the reported homoleptic nickel(0) isocyanide complex are of a white to yellow color. In contrast, both of the here-presented complexes show intense ^{1}MLCT absorption bands with maxima at 423 nm. They are not luminescent in solution at room temperature, but show ^{3}MLCT emission in organic matrices at 77 K with bi-exponential decay behaviour. The two lifetimes (approx. 200 ns and 1.1 μs) probably originate from frozen sterical conformers. Although the excited state lifetimes do not differ between the two complexes, they show very different electrochemical behaviour. The complex bearing the ligand with an aryl ring as a backbone shows a reversible oxidation wave at -0.32 V vs $Fc^{+/0}$, which was assigned to the $Ni^{+/0}$ couple. The complex with a thiophene backbone shows an irreversible oxidation process at -0.30 V vs $Fc^{+/0}$ for the $Ni^{+/0}$ couple, and a reversible oxidation at 0.21 V vs $Fc^{+/0}$ attributed to the $Ni^{2+/+}$ redox couple.
The shape and position of the emission band is strongly influenced by the backbone of the ligand. The complex with an aryl ring backbone has a rather sharp emission band which shifts only slightly to longer wavelength in more polar matrices, whereas the complex with a thiophene backbone shows a rather broad emission which exhibits a significant blue shift in more polar matrices. This highly unusual matrix effect is not understood up to now.
To the best of my knowledge, the here-presented complexes are the first homoleptic nickel(0) complexes to be investigated in terms of their electrochemical and photophysical properties and the second to show significant absorption in the visible spectral range.[114]
The nickel(0) complexes are non-emissive in solution, which might be due to a rather flexible molecular structure. This could be verified by IR experiments in solution, including transient IR spectroscopy. Additionally, their solid state absorption and emission properties might be of interest. In order to gain a fundamental understanding of these compounds, a much broader study employing different ligands would be necessary.
In an additional study, six homoleptic copper(I) complexes were synthesized in order to examine their potential use as blue emitters (e.g. in OLEDs) as well as to identify important structural relationships for the future design of such complexes (Chap.1.1). For this study, all ligands (**A**-**D**) shown in Figure IV.1 were employed.
Although it was possible to obtain homoleptic copper(I) complexes bearing chelating isocyanide ligands that are stable blue emitters, their chemical and photophysical behaviour depends on a subtle interplay between the bite angle induced by the ligand backbone and the geometrical shape and size of the *ortho* substituents. These diverse interactions give rise to some rare and unexpected behaviours such as excitation dependent emission. The presented data might indicate different opposed structural effects, which make a qualitative prediction of backbone or substituent effects difficult.

The copper(I) complexes proved to be blue emitters with very versatile electrochemical and photophysical properties. The excited state lifetimes, as well as the quantum yields in solution

and the solid state, could give an indication of the nature of the emissive state. At this state of knowledge, it is nearly impossible to predict the photophysical or electrochemical behaviour of these complexes. In particular, their structure in solution needs to be better elucidated to achieve a qualitative understanding of the different structural influences.

In the context of this thesis, it was possible to access new, first-row transition metal luminophores and first investigations of their photophysical properties were presented.
Most important, it was also possible to substitute precious metals in photocatalysts with the earth-abundant molybdenum(0). Using this strategy it was possible to extent the accessible potential range for reductive photocatalytic reactions by approximately 0.4 V to more negative potentials.

V Experimental Part

5.1 Equipment and Methods

^{1}H-/^{13}C-NMR spectroscopy was performed with a Bruker Avance III instrument operating at 400/101 MHz frequency and a Bruker Avance III NMR instrument operating at 600/150.9 MHz frequency. Mass spectra were acquired on Bruker esquire 3000 plus and Bruker maxis 4G QTOF EDI spectrometers. MALDI-mass spectra were acquired on a Bruker microflex instrument. Ms. Sylvie Mittelheisser (Department of Chemistry at University of Basel) conducted elemental analyses on a Vario Micro Cube instrument.

For cyclic voltammetry, a Versastat3-200 potentiostat from Princeton Applied Research was used. A glassy carbon disk electrode served as a working electrode, the counter electrode and quasi-reference electrode were two silver wires. Internal potential calibration was achieved by addition of small amounts of ferrocene. The solvent was dry deaerated THF or deaerated dichloromethane containing 0.1 $TBAPF_6$ (tetra(*n*-butyl)ammonium hexafluorophosphate) as an electrolyte. Potential sweep rates were 0.1 V/s if not otherwise noted.

Optical absorption spectroscopy was performed using a Cary 5000 instrument from Varian. Steady-state luminescence spectra were measured on a Fluorolog-322 from Horiba Jobin-Yvon. FTIR spectroscopy was performed with a Bruker Alpha Platinum-ATR instrument. An LP920-KS instrument from Edinburgh Instruments was employed for transient absorption spectroscopy. The frequency-doubled output of a Quantel Brilliant b laser served as an excitation source. The laser pulse duration was approx. 10 ns and the pulse frequency was 10 Hz. The typical pulse energy used for transient absorption studies was 10 mJ. Detection of transient absorption spectra occurred on an iCCD camera from Andor. Single-wavelength kinetics were recorded using a photomultiplier tube. Transient absorption measurements with picosecond time resolution were performed with the TRASS instrument from Hamamatsu, equipped with a C7701-01 streak camera. Excitation occurred with a picosecond mode-locked Nd:YVO4/ YAG laser (PL2251B-20-SH/TH/FH) with PRETRIG option from Ekspla.

Photoredox catalysis experiments were performed in sealed NMR tubes using an M455L2 LED from Thorlabs (1020 mW) for photoirradiation.
General procedure for photocatalysis: The substrate, one equivalent of 2,2,6,6-tetramethylpiperidine (TMP) and a small amount of the catalyst (5-14 mol%) were dissolved in dry

benzene-d_6 in an NMR tube. The solution was frozen in a liquid nitrogen bath, and the NMR tube was sealed under vacuum using a hand-held gas burner. A commercial M455L2 LED from Thorlabs (1020 mW) was used for the photoirradiation experiment, and the photoreaction was performed at room temperature with an excitation wavelength of 455 nm. ^{1}H-NMR spectra were recorded before irradiation (t = 0 h) and after different time intervals of photoirradiation.

5.2 Polydentate Isocyanide Ligands

5.2.1 *tert*-Butyl Substituted Ligands

3,5-Di(*tert*-butyl)-2-nitro-bromobenzene (1)

Following a procedure by W. Rudel[122] 3,5-di(*tert*-butyl)bromobenzene (3.00 g, 11.1 mmol, 1.00 eq.) was dissolved in a mixture of glacial acetic acid (33 mL) and sulfuric acid (98%, 16.5 mL). Fuming nitric acid (3.00 mL) was added and the reaction mixture heated to 80°C for 1.5 h.
After cooling to room temperature the mixture was poured on ice and the aqueous phase extracted three times with dichloromethane. The combined organic phases were dried over Na_2SO_4 and the solvent evaporated.
The resulting residue was subjected to column chromatography (SiO_2, pentane) yielding the desired product as a colorless oil which slowly crystallizes (2.71 g, 8.60 mmol, 77%).

^{1}H-NMR (400 MHz, $CDCl_3$): δ = 7.50 (d, J=1.9 Hz, 1H), 7.49 (d, J= 2.0 Hz, 1H), 1.38 (s, 9H), 1.32 (s, 9H) ppm.

^{13}C-NMR (101 MHz, $CDCl_3$): δ = 154.0, 142.2, 128.8, 124.7, 114.5, 36.6, 35.3, 31.2, 31.0 ppm.

Elemental analysis: found: C, 53.81; H, 6.56; N, 4.69; calc. for $C_{14}H_{20}BrNO_2$: C, 53.51; H, 6.42; N, 4.69.

1,3-Bis(2,4-di(*tert*-butyl)-nitrobenz-6-yl)benzene (2)

1,3-Bis(4,4,5,5-tetramethyl-2,5-dioxaborolan-yl)benzene[72] (0.648 g, 1.90 mmol, 1.00 eq.), 3,5-di(*tert*-butyl)-2-nitro-bromobenzene (**1**) (1.36 g, 4.31 mmol, 2.20 eq.) and potassium carbonate (1.45 g, 10.4 mmol, 5.33 eq.) were suspended in a mixture of dioxane (10 mL) and water (5 mL). The mixture was purged with nitrogen for 20 min. Afterwards [Pd(dppf)Cl_2]· CH_2Cl_2 (80.0 mg, 0.098 mmol, 5 mol%) was added and purging with nitrogen was continued for another

10 min. The mixture was heated to reflux at 110 °C overnight. The phases were separated and the aqueous phase was extracted with dichloromethane (3 x 50 mL). The combined organic phases were dried over Na_2SO_4. The solvent was removed *in vacuo* and the crude product subjected to column chromatography (SiO_2, pentane/DCM, 10:1 → DCM). The product **2** was isolated as a yellow, honey-like oil, which slowly solidified to form an off-white solid (0.881 g, 1.6 mmol, 85 %).

^{1}H-NMR (400 MHz, CD_2Cl_2): δ = 7.60 (d, J=2.1 Hz, 2H), 7.42 (ddd, J= 8.6, 6.6, 0.6 Hz, 1H), 7.37-7.32 (m, 2H), 7.28-7.26 (m, 3H), 1.42 (s, 18H), 1.36 (s, 18H) ppm.

^{13}C-NMR (101 MHz, CD_2Cl_2): δ = 153.2, 148.1, 140.3, 138.4, 134.6, 129.4, 128.8, 128.7, 126.8, 125.3, 36.6, 35.6, 31.5, 31.2 ppm.

MS(ESI$^+$): m/z (%) = 567.22 (100, [M+Na]$^+$), calc. 567.32.

Elemental analysis: found: C, 74.42; H, 8.39; N, 5.27; calc. for $C_{34}H_{44}N_2O_4$ (+0.3 H_2O): C, 74.23; H, 8.17; N, 5.09.

1,3-Bis(2,4-di(*tert*-butyl)-anilin-6-yl)benzene (3)

Procedure A

1,3-Bis(2,4-di(*tert*-buty)l-nitrobenz-6-yl)benzene (**2**) (199 mg, 0.366 mmol, 1.00 eq.) and Pd/C (10% Pd, 2 mg, 0.024 mmol, 0.06 eq.) were stirred in a mixture of DMF (10 mL) and MeOH (5 mL) under a hydrogen atmosphere (11 bar) for 5 days at 50°C. The solution was filtered over celite and the solvent was evaporated. The crude product was subjected to column chromatography (preloading onto SiO_2, gradient: pentane/DCM, 1:1 → DCM) to yield 1,3-bis(2,4-di(*tert*butyl)-anilin-6-yl)benzene (126 mg, 0.260 mmol, 71%) as a colourless solid.

Procedure B

Step 1: Following a general protocol of Gowda et al.[123], hydrazine monohydrate (0.90 mL, 0.930 g, 18.6 mmol, 25.0 eq.) was added to 1,3-bis(2,4-di(*tert*-butyl)-nitrobenz-6-yl)benzene (**2**) (401 mg, 0.734 mmol, 1.00 eq.) and zinc powder (194 mg, 2.94 mmol, 4.00 eq.) in dry MeOH (4 mL). The mixture was heated to reflux overnight. The yellow suspension was diluted with DCM, filtered over celite and washed with brine. The organic phase was dried over Na_2SO_4 and the solvent was evaporated to give the pure intermediate product 1-(2,4-di(*tert*-butyl)-anilin-6-yl)-3-(2,4-di(*tert*butyl)-nitrobenz-6-yl)-benzene (358 mg, 0.696 mmol, 95%) as

a bright yellow solid.

^{1}H-NMR (400 MHz, CD_2Cl_2): δ = 7.60 (d, J= 2.1 Hz, 1H), 7.56-7.25 (m, 6H), 7.03 (d, J= 2.3 Hz, 1H), 3.93 (s, 2H), 1.46 (s, 9H), 1.42 (s, 9H), 1.36 (s, 9H), 1.29 (s, 9H) ppm.

Step 2: Under an inert gas atmosphere 1-(2,4-di(*tert*-butyl)-anilin-6-yl)-3-(2,4-di(*tert*-butyl)-nitrobenz-6-yl)-benzene (358 mg, 0.696 mmol, 1.00 eq.) and Zn powder (196 mg, 3.00 mmol, 4.30 eq.) were suspended in dry MeOH (3 mL). Hydrazine monohydrate (0.90 mL, 0.930 g, 18.6 mmol, 27.0 eq.) was added and the suspension heated to reflux overnight. The mixture was diluted with DCM, filtered over celite and washed with brine. The organic phase was dried over Na_2SO_4 and the solvent was evaporated to give 1,3-bis(2,4-di(*tert*-butyl)-anilin-6-yl)benzene (**3**) (312 mg, 0.648 mmol, 93%) as a light yellow solid.
Isolated yield over two steps: 88%.

^{1}H-NMR (400 MHz, CD_2Cl_2): δ = 7.57-7.47 (m, 2H), 7.47-7.39 (m, 2H), 7.30 (d, J= 2.4, 2H), 7.03 (d, J= 2.3 Hz, 2H), 3.92 (s, 4H), 1.46 (s, 18H), 1.29 (s, 18H) ppm.

^{13}C-NMR (101 MHz, CD_2Cl_2): δ = 142.1, 140.7, 139.9, 133.8, 131.5, 129.7, 129.3, 128.8, 126.0, 123.7, 35.3, 34.7, 32.0, 30.2 ppm.

1,3-Bis(*N*-formyl-4,6-di(*tert*-butyl)-anilin-2-yl)benzene (4)

Formic acid (5 mL, 133 mmol) was added dropwise to acetic anhydride (10 mL, 106 mmol) within 10 min at 0 °C. The mixture was allowed to warm to room temperature and stirred at 50 °C for 2 h. After reaching room temperature the mixture was cooled to 0 °C and 1,3-bis(2,4-di(*tert*-butyl)-anilin-6-yl)benzene (**3**) (0.437 g, 0.90 mmol, 1.00 eq.) was added. The mixture was stirred at 100°C overnight. Ice cooled water (30 mL) was added and the precipitate filtered and washed with water (300 mL). After drying under vacuum, **4** was obtained as a white solid (446 mg, 0.820 mmol, 91 %).

The product is isolated as a mixture of isomers leading to additional signals.
^{1}H-NMR (400 MHz, CD_2Cl_2): δ = 7.96 (d, J = 1.7, 0.4H), 7.88 (d, J= 1.7 Hz, 0.4H), 7.71-7.58 (m, 1.4H), 7.58-7.51 (m, 2.2H), 7.51-7.37 (m, 1H), 7.36 (dd, J= 4.6, 2.3 Hz, 1.2H), 7.33-7.18 (m, 3.6H), 7.16-7.12 (m, 0.8H), 7.16-7.12 (m, 1H), 1.47-1.39 (m, 18H), 1.38-1.33 (m, 18H) ppm.

Due to the presence of several isomers and the low solubility of the compound, no ^{13}C-NMR spectra of satisfying quality were obtained.

IR $\tilde{\nu}$ [cm^{-1}]: 3266 (br, w), 2959 (m), 2905 (w), 2868 (w), 1676 (s), 1594 (w), 1476 (m), 1408 (w), 1392 (m), 1362 (m), 1274 (m), 1247 (m), 1209 (m), 1168 (m), 1111 (w), 1082 (w), 880 (m), 822 (w), 801 (m), 731 (m), 711 (m), 653 (w), 612 (w), 590 (w), 536 (w), 484 (w).

MS(ESI^+): *m/z* (%) = 541.30 (100, $[M+H]^+$), calc. 541.38.

Elemental analysis: found: C, 77.52; H, 8.82; N, 5.08; calc. for $C_{36}H_{48}N_2O_2$ (+0.9 H_2O): C, 77.63; H, 9.01; N, 5.03.

1,3-Bis(6-di(*tert*-butyl)-1-isocyanidebenzene-2-yl)benzene ((*t*Bu)CNAr$_3$NC(*t*Bu))

1,3-Bis(*N*-formyl-4,6-di(*tert*-butyl)anilin-2-yl)benzene (**4**) (200 mg, 0.370 mmol, 1.00 eq.) was dissolved in dry dichloromethane (10 mL) under nitrogen. Di(*iso*-propyl)amine (0.34 mL, 2.60 mmol, 7.00 eq.) was added and the mixture cooled to 0°C. $POCl_3$ (0.2 mL, 1.90 mmol, 5 eq.) was added dropwise. The solution turned dark yellow and was allowed to warm to room temperature. After stirring for 3 h, a solution of Na_2CO_3 in water (1.5 M, 15 mL) was added and the biphasic system vigorously stirred overnight. Saturated $NaHCO_3$ solution (12.6 mL) was added and the aqueous phase was extracted with dichloromethane (2 x 50 mL). The combined organic phases were dried over Na_2SO_4 and the solvent removed *in vacuo*. The product was purified via column chromatography (SiO_2, DCM) and isolated as a yellow oil, which slowly solidified to form an light yellow solid (177 mg, 0.350 mmol, 95 %).

^{1}H-NMR (400 MHz, CD_2Cl_2): δ = 7.62-7.53 (m, 4H), 7.49 (d, *J*= 2.1, 2H), 7.38 (d, *J*= 2.1, 2H), 1.56 (s, 18H), 1.34 (s, 18H) ppm.

^{13}C-NMR (101 MHz, CD_2Cl_2): δ = 172.9, 152.7, 146.2, 141.3, 139.7, 131.0, 129.4, 128.7, 127.2, 126.4, 123.8, 36.1, 35.7, 31.5, 29.7 ppm.

IR $\tilde{\nu}$ [cm^{-1}]: 2960 (s), 2908 (m), 2871 (m), 2112 (s, $\tilde{\nu}$ C≡N), 1736 (w), 1701 (w), 1683 (m), 1593 (m), 1476 (m), 1432 (m), 1410 (m), 1394 (m), 1364 (s), 1327 (w), 1279 (m), 1243 (m), 1200 (m), 1168 (m), 1083 (w), 933 (w), 897 (w), 883 (s), 882 (w), 801 (m), 758 (w), 732 (m), 711 (s), 656 (w), 627 (w), 553 (w).

HR-MS(ESI^+): *m/z* (%) = 527.3391 (100, $[M+Na]^+$), calc. 527.3397.

Elemental analysis: found: C, 83.24; H, 8.77; N, 5.28; calc. for $C_{36}H_{44}N_2$ (+0.05 H_2O, +0.2 CH_2Cl_2): C, 83.17; H, 8.72; N, 5.37.

1,3-Bis(4,6-di(*tert*-butyl)-nitrophen-2-yl)thiophene (12)

3,5-Di(*tert*-butyl)-2-nitro-bromobenzene (**1**) (1.22 g, 3.89 mmol, 2.50 eq.) was dissolved in xylene (20 mL, mixture of isomers), and purged with nitrogen. 2,5-Bis(tributylstannyl)thiophene (1.00 g, 1.55 mmol, 0.86 mL, 1.00 eq.) and [Pd(dppf)Cl_2] (63 mg, 0.07 mmol, 5 mol-%) were added to the reaction mixture. The mixture was stirred at 140°C overnight. The solvent was removed and the residue submitted to column chromatography (SiO_2, preloading onto SiO_2, gradient: pentane → pentane/dichloromethane, 1:1). The product eluted last and was isolated as a bright yellow solid (834 mg, 1.51 mmol, 98%).

^{1}H-NMR (400 MHz, CD_2Cl_2): δ = 7.62 (d, J= 1.9 Hz, 2H), 7.41 (d, J= 1.9 Hz, 2H), 6.98 (s, 2H), 1.43 (s, 18H), 1.37 (s, 18H) ppm.

^{13}C-NMR (101 MHz, CD_2Cl_2): δ = 153.3, 147.8, 140.7, 139.7, 127.8, 127.5, 127.2, 126.2, 36.7, 35.6, 31.4, 31.2 ppm.

Elemental analysis: found: C, 66.17; H, 7.70; N, 4.63; calc. for $C_{32}H_{42}N_2O_4S$ (+0.8 H_2O, +0.25 CH_2Cl_2): C, 66.06; H, 7.58; N, 4.78.

1-(2,4-di(*tert*-butyl)-anilin-6-yl)-3-(2,4-di(*tert*-butyl)-nitrobenz-6-yl)-thiophene

Hydrazine monohydrate (1.86 g, 37.2 mmol, 1.80 mL, 25.0 eq.) was added to 1,3-bis(4,6-di(*tert*-butyl)-nitrophen-2-yl)thiophene (**12**) (800 mg, 1.45 mmol, 1.00 eq.) and zinc powder (388 mg, 5.88 mmol, 4.0 eq.) in dry MeOH (5 mL). The mixture was heated to reflux overnight. The yellow-greenish suspension was diluted with dichloromethane, filtered over celite and washed with brine. The organic phase was dried over Na_2SO_4 and the solvent was evaporated to give the pure intermediate 1-(2,4-di(*tert*-butyl)-anilin-6-yl)-3-(2,4-di(*tert*-butyl)-nitrobenz-6-yl)-thiophene as a bright green solid (755 mg, 1.45 mmol, quant.).

^{1}H-NMR (400 MHz, CD_2Cl_2): δ = 7.62 (t, J= 1.9 Hz, 1H), 7.41 (d, J= 2.1 Hz, 1H), 7.33 (t, J= 1.9 Hz, 1H), 7.19 (d, J= 2.1 Hz, 1H), 7.17 (d, J= 1.3 Hz, 1H), 6.98 (d, J= 1.3 Hz, 1H), 4.25 (s, 2H), 1.48 (s, 9H), 1.43 (s, 9H), 1.37 (s, 9H), 1.32 (s, 9H) ppm.

1,3-Bis(4,6-di(*tert*-butyl)-anilin-2-yl)thiophene (13)

Hydrazine monohydrate (1.86 g, 37.2 mmol, 1.80 mL, 25.0 eq.) was added to 1-(2,4-di(*tert*-butyl)-anilin-6-yl)-3-(2,4-di(*tert*-butyl)-nitrobenz-6-yl)-thiophene (755 mg, 1.45 mmol, 1.00 eq.)

and zinc powder (388 mg, 5.88 mmol, 4.00 eq.) in dry MeOH (5 mL). The mixture was heated to reflux overnight. The yellow suspension was diluted with dichloromethane, filtered over celite and washed with brine. The light green organic phase was dried over Na_2SO_4 and the solvent was evaporated to give 1,3-Bis(4,6-di(*tert*butyl)-anilin-2-yl)thiophene as a green-yellow solid (708 mg, 1.44 mmol, 99%). The product was directly used in the next reaction step without further purification.

^{1}H-NMR (400 MHz, CD_2Cl_2): δ = 7.32 (d, J= 2.3 Hz, 2H), 7.18 (d, J= 2.3 Hz, 2H), 7.16 (s, 2H), 4.24 (s, 4H), 1.48 (s, 18H), 1.31 (s, 18H) ppm.

^{13}C-NMR (101 MHz, CD_2Cl_2): δ = 142.7, 140.8, 140.5, 133.9, 127.3, 126.6, 124.5, 121.2, 35.3, 34.6, 31.9, 30.1 ppm.

1,3-Bis(*N*-formyl-4,6-di(*tert*-butyl)-anilin-2-yl)thiophene (14)

Formic acid (7.80 mL, 207 mmol) was added dropwise to acetic anhydride (15.6 mL, 165 mmol) within 10 min at 0°C. The mixture was allowed to warm to room temperature and stirred at 50°C for 2 h. After reaching room temperature, the mixture was cooled to 0°C and 1,3-bis(2,4-di*tert*-butyl-anilin-6-yl)thiophene (**13**) (708 mg, 1.44 mmol, 1.00 eq.) was added. The mixture was stirred at 100°C overnight. Ice cooled water (45 mL) was added and the precipitate filtered and washed with water (300 mL). After drying under vacuum, the product was obtained as a white solid (612 mg, 1.12 mmol, 80 %).

The product is isolated as a mixture of isomers.
^{1}H-NMR (400 MHz, CD_2Cl_2): δ = 7.53 (m, 10H), 1.40 (m, 36H) ppm.

Due to the presence of several isomers and low solubility of the compound, no ^{13}C-NMR spectra of satisfying quality were obtained.

MS(ESI$^+$): m/z (%) = 569.17 (100, $[M+Na]^+$), calc. 569.32.

IR $\tilde{\nu}$ [cm^{-1}]: 3165 (w), 3077 (w), 2959 (m), 2907 (w), 2869 (w), 1677 (s), 1594 (w), 1570 (w), 1532 (w), 1475 (m), 1432 (w), 1405 (w), 1363 (m), 1289 (m), 1246 (w), 1200 (w), 1169 (w), 879 (w), 841 (w), 802 (w), 755 (w), 724 (w), 654 (w), 639 (w), 594 (w), 494 (w).

1,3-Bis(4,6-di(*tert*-butyl)-1-isocyanidebenzene-2-yl)thiophene ((*t*Bu)CNArSArNC(*t*Bu))

1,3-Bis(*N*-formyl-4,6-di(*tert*-butyl)-anilin-2-yl)thiophene (**14**) (612 mg, 1.12 mmol, 1.00 eq.) was dissolved in dry dichloromethane (35 mL) under nitrogen. Di(*iso*-propyl)amine (1.06 mL, 7.84 mmol, 7.00 eq.) was added and the mixture cooled to 0 °C. $POCl_3$ (0.42 mL, 3.9 mmol, 3.5 eq.) was added dropwise. The solution turned dark yellow and was allowed to warm to room temperature. After stirring for 3 h a solution of Na_2CO_3 in water (1.5 M, 26.4 mL) was added and the biphasic system vigorously stirred overnight. Saturated $NaHCO_3$ solution (23.2 mL) was added and the aqueous phase was extracted with dichloromethane (3 x 50 mL). The combined organic phases were dried over Na_2SO_4 and the solvent removed *in vacuo*. The product was purified via column chromatography (SiO_2, gradient pentane/DCM, 20:1 → pentane/DCM, 1:1) and isolated as a yellow oil, which slowly solidified to form a light yellow solid (260 mg, 0.510 mmol, 45 %).
^{1}H-NMR (400 MHz, CD_2Cl_2): δ = 7.49 (d, J= 2.1 Hz, 2H), 7.45 (d, J= 2.1 Hz, 2H), 7.42 (s, 2H), 1.56 (s, 18H), 1.35 (s, 18H) ppm.

^{13}C-NMR (101 MHz, CD_2Cl_2): δ = 174.5, 152.7, 146.9, 141.1, 133.6, 128.8, 126.5, 124.4, 36.1, 35.6, 31.4, 29.6 ppm.

HR-MS(ESI$^+$): m/z (%) = 533.2958 (100, $[M+Na]^+$), calc. 533.2961.

IR $\tilde{\nu}$ [cm^{-1}]: 2961 (s), 2909 (m), 2872 (m), 2111 (s, $\tilde{\nu}$ C≡N), 1593 (m), 1572 (w), 1477 (m), 1465 (m), 1432 (m), 1408 (m), 1396 (m), 1364 (s), 1311 (w), 1278 (m), 1246 (m), 1199 (m), 1173 (w), 1115 (w), 1052 (w), 1027 (w), 1004 (w), 930 (w), 910 (w), 882 (s), 837 (w), 809 (s), 795 (m), 757 (m), 656 (m).

Elemental analysis: found: C, 79.45; H, 8.33; N, 5.60; calc. for $C_{34}H_{42}N_2S$ (+0.15 H_2O): C, 79.53; H, 8.30; N, 5.46.

5.2.2 Phenyl Substituted Ligands

4-Methyl-2-phenylaniline (5)

For the synthesis of 4-methyl-2-phenylaniline a protocol of Tobisu et al. was used.[124] 2-Bromo-4-methylaniline (3.33 mL, 5.00 g, 26.8 mmol, 1 eq.) and phenylboronic acid (3.92 g, 32.1 mmol, 1.20 eq.) were dissolved in a mixture of 2 M aqueous K_2CO_3 (60.8 mL) and DME (53.7 mL) under nitrogen atmosphere. The solution was purged with nitrogen for 30 min. After that time, $[Pd(PPh_3)_2Cl_2]$ (0.377 mg, 0.530 mmol, 2 mol%) was added and the mixture was heated to 80 °C overnight. After cooling to room temperature ethyl acetate was added

and the phases were separated. The organic phase was washed with water and, after drying over Na_2SO_4, concentrated under reduced pressure. The resulting residue was subjected to column chromatography (SiO_2, pentane/EtOAc, 30:1) to afford compound **5** as a colorless liquid (4.81 g, 26.3 mmol, 98%).

^{1}H-NMR (400 MHz, $CDCl_3$): δ = 7.45 (m, 4H), 7.37-7.30 (m, 1H), 6.98 (d, J= 9.5, 2H), 6.71 (d, J= 7.9, 1H), 3.71 (s, 2H), 2.28 (s, 3H) ppm.

^{13}C-NMR (101 MHz, $CDCl_3$): δ = 140.9, 139.8, 131.1, 129.2, 129.1, 128.9, 128.1, 128.0, 127.2, 116.0, 20.6 ppm.

MS(ESI$^+$): m/z (%) = 183.99 (100, $[M+H]^+$), calc. 184.11.

2-Bromo-4-methyl-6-phenylaniline (6)

For the synthesis of 4-methyl-2-phenylaniline a protocol of Xia et al. was used.[125] 4-Methyl-2-phenylaniline (**5**) (4.81 g, 26.3 mmol, 1.00 eq.) in methanol (56.6 mL) was cooled to 0°C and aqueous HBr (48 wt.-%, 3.56 mL, 31.5 mmol, 1.20 eq.) was added. The mixture was allowed to warm to room temperature and a solution of hydrogen peroxide (30 wt.-% in water, 3.30 mL, 28.9 mmol, 1.10 eq.) in methanol (21 mL) was added dropwise. The mixture was stirred overnight at room temperature. The solvent was removed under reduced pressure and the crude product was dissolved in ethyl acetate. The organic phase was washed with water and brine and dried over Na_2SO_4. The solvent was removed *in vacuo* and the product isolated by column chromatography (SiO_2, pentane/EtOAc, 5:1) as orange crystals (5.41 g, 20.8 mmol, 79 %).

^{1}H-NMR (400 MHz, $CDCl_3$): δ = 7.50-7.41 (m, 4H), 7.42-7.32 (m, 1H), 7.27 (dq, J= 1.5, 0.8 Hz, 1H), 6.89 (dq, J= 1.5, 0.8 Hz, 1H), 4.04 (s, 2H), 2.27 (s, 3H) ppm.

^{13}C-NMR (101 MHz, $CDCl_3$): δ = 139.4, 139.0, 132.1, 130.4, 129.1, 129.0, 128.8, 128.5, 127.7, 109.9, 20.2 ppm.

MS(ESI$^+$): m/z (%) = 261.87 (100, $[M+H]^+$), calc. 262.02.

Elemental analysis: found: C, 59.70; H, 4.88; N, 5.57; calc. for $C_{13}H_{12}BrN$: C, 59.56; H, 4.61; N, 5.34.

N-Formyl-2-bromo-4-methyl-6-phenylaniline (7)

Acetic anhydride (15.2 mL) was cooled to 0°C and formic acid (7.6 mL) was added dropwise within 10 min. The reaction mixture was stirred at 50°C for 2 hours. 2-Bromo-4-methyl-6-phenylaniline (**6**) (1.00 g, 3.80 mmol, 1.00 eq.) was added to the ice cooled reaction mixture and stirring was continued for another 30 min.
Ice cooled water (50 mL) was added and the precipitate was filtered off. The residue was washed with water (250 mL) and subsequently dried at 50°C *in vacuo* overnight. The product was isolated as a light pink solid (954 mg, 3.3 mmol, 87 %).

The product is isolated as a mixture of isomers leading to additional signals.
^{1}H-NMR (400 MHz, CD_2Cl_2): δ = 8.09 (d, J= 1.4 Hz, 0.5H), 7.85 (d, J= 11.3 Hz, 0.5H), 7.5 (dd, J= 1.9, 0.9 Hz, 1H), 7.48-7.29 (m, 5H), 7.15 (dd, J= 10.8, 1.1 Hz, 1H), 7.06-6.81 (m, 1H), 2.38 (s, 3H) ppm.

^{13}C-NMR (101 MHz, CD_2Cl_2): δ = 164.5, 160.1, 142.7, 140.2, 139.7, 139.6, 139.2, 139.0, 133.4, 133.1, 131.9, 131.3, 130.2, 129.8, 129.6, 129.4, 129.1, 128.8, 128.4, 128.2, 123.5, 121.2, 21.1, 21.0 ppm.

Elemental analysis: found: C, 57.95; H, 4.17; N, 4.83; calc. for $C_{14}H_{12}BrNO$: C, 58.07; H, 4.36; N, 5.07.

1,3-Bis(4-methyl-6-phenylanilin-2-yl)benzene

2-Bromo-4-methyl-6-phenylaniline (**6**) (1.16 g, 4.40 mmol, 2.20 eq.), 1,3-bis(4,4,5,5-tetramethyl-2,5-dioxaborolan-yl)benzene[72] (0.663 g, 2.00 mmol, 1.00 eq.) and potassium carbonate (1.48 g, 10.7 mmol, 5.33 eq.) were suspended in a mixture of dioxane (9.7 mL) and water (4.8 mL). The mixture was purged with nitrogen for 15 min. $[Pd(dppf)Cl_2]\cdot CH_2Cl_2$ (82 mg, 0.10 mmol, 5 mol%) was added and the reaction mixture heated to 100°C overnight.
After cooling to room temperature, water was added to the reaction and the aqueous phase extracted with dichloromethane twice. The combined organic phases were dried over Na_2SO_4 and the solvent removed *in vacuo*. The crude product was submitted to column chromatography (SiO_2, pentane/EtOAc, 15:1). The product was isolated as a white solid (458 mg, 1.22 mmol, 61 %).

^{1}H-NMR (400 MHz, CD_2Cl_2): δ = 7.65 (td, J= 1.9, 0.7 Hz, 1H), 7.58-7.41 (m, 11H), 7.40-7.32 (m, 2H), 6.99 (ddd, J= 20, 1.9, 0.7 Hz, 4H), 3.76 (*br* s, 4H), 2.32 (t, J= 0.7 Hz, 6H) ppm.

^{13}C-NMR (101 MHz, CD_2Cl_2): δ = 141.2, 140.6, 138.9, 130.94, 130.87, 130.7, 129.8, 129.7, 129.3, 128.7, 128.5, 128.3, 127.8, 127.7, 20.7 ppm.

IR $\tilde{\nu}$ [cm^{-1}]: 3455 (br, w), 3364 (br, w), 3020 (w), 2914 (w), 2857 (w), 1613 (w), 1593 (m), 1492 (w), 1461 (m), 1434 (m), 1395 (w), 1303 (w), 1241 (w), 1201 (w), 1174 (w), 1072 (w), 1055 (w), 1026 (w), 998 (w), 867 (m), 809 (w), 790 (w), 770 (m), 746 (m), 701 (s), 675 (w), 630 (w), 566 (w), 535 (w), 491 (w), 473 (w).

1,3-Bis(*N*-formyl-4-methyl-6-phenylanilin-2-yl)benzene (8)

N-Formyl-2-bromo-4-methyl-6-phenylaniline (**7**) (930 mg, 3.30 mmol, 2.20 eq.), 1,3-bis(4,4,5,5-tetramethyl-2,5-dioxaborolan-yl)benzene[72] (495 mg, 1.50 mmol, 1.00 eq.) and potassium carbonate (1.10 g, 7.90 mmol, 5.33 eq.) were suspended in a mixture of dioxane (7.3 mL) and water (3.6 mL). The mixture was purged with nitrogen for 45 min. $[Pd(dppf)Cl_2]\cdot CH_2Cl_2$ (61 mg, 0.07 mmol, 5 mol%) was added and the reaction mixture heated to 110°C overnight. After cooling to room temperature water was added to the reaction mixture and the aqueous phase extracted with dichloromethane twice. The combined organic phases were dried over Na_2SO_4 and the solvent removed *in vacuo*. The crude product was submitted to column chromatography (SiO_2, pentane/EtOAc, 20:1) and the product was isolated as an off-white solid (670 mg, 1.35 mmol, 90 %).

The product is isolated as a mixture of isomers.
^{1}H-NMR (400 MHz, CD_2Cl_2): δ = 7.79 (d, J= 1.5 Hz, 0.5H), 7.75-7.69 (m, 1H), 7.67 (d, J= 11.6 Hz, 0.5H), 7.62 (s, 0.5H), 7.60-7.48 (m, 1H), 7.48-7.30 (m, 13H), 7.30-7.18 (m, 4H), 7.12 (d, J= 5.5 Hz, 1H), 6.92 (d, J= 11.6 Hz, 0.5H), 2.46-2.40 (m, 6H) ppm.

^{13}C-NMR (101 MHz, CD_2Cl_2): δ = 166.5, 165.6, 161.2, 160.6, 141.4, 141.3, 140.7, 140.1, 139.4, 139.3, 138.8, 138.5, 138.4, 138.0, 137.9, 137.6, 131.9, 131.8, 131.5, 131.3, 131.2, 131.0, 130.9, 130.7, 130.2, 130.0, 129.5, 129.4, 129.29, 129.27, 129.2, 129.0, 128.74, 128.70, 128.66, 128.2, 128.1, 128.0, 127.9, 14.6 ppm.

IR $\tilde{\nu}$ [cm^{-1}]: 2919 (w), 2853 (w), 1734 (w), 1666 (s), 1596 (w), 1576 (w), 1495 (m), 1385 (m), 1239 (m), 1042 (w), 866 (m), 794 (w), 766 (m), 722 (w), 699 (s), 620 (w), 593 (m), 567 (m), 534 (w), 493 (w), 460 (w).

Elemental analysis: found: C, 79.50; H, 6.16; N, 5.39; calc. for $C_{34}H_{28}N_2O_2$ (+0.35 H_2O, +0.4 $C_4H_8O_2$): C, 79.45; H, 5.98; N, 5.21.

1,3-Bis(4-methyl-6-phenyl-1-isocyanidebenzene-2-yl)benzene ((Ph)CNAr$_3$NC(Ph))

1,3-Bis(*N*-formyl-4-methyl-6-phenylanilin-2-yl)benzene (**8**) (670 mg, 1.35 mmol, 1.00 eq.) was dissolved in dry dichloromethane (42 mL) and di(*iso*-propyl)amine (1.28 mL, 9.40 mmol, 7.00 eq.) was added. The mixture was cooled to 0°C and $POCl_3$ (0.50 mL, 4.70 mmol, 3.50 eq.) was added dropwise. The reaction was stirred at room temperature for 3 h.
Aqueous sodium carbonate solution (31.8 mL, 1.5 M) was added and vigorous stirring continued overnight.
Saturated aqueous sodium bicarbonate solution (27.9 mL) was added and the phases separated. The aqueous phase was extracted with dichloromethane and the combined organic phases were dried over Na_2SO_4 . The solvent was evaporated, the crude product dissolved in pentane and subjected to flash column chromatography (SiO_2, dichloromethane). The product was isolated as a light yellow solid (500 mg, 1.13 mmol, 80%).

^{1}H-NMR (400 MHz, CD_2Cl_2): δ = 7.72 (dt, J= 1.8, 0.9 Hz, 1H), 7.67-7.63 (m, 3H), 7.60-7.41 (m, 10H), 7.34 (dt, J= 1.8, 0.9 Hz, 2H), 7.26 (dd, J=1.8, 0.9 Hz, 2H), 2.46 (s, 6H) ppm.

^{13}C-NMR (101 MHz, CD_2Cl_2): δ = 169.7, 140.4, 140.3, 139.7, 138.6, 138.4, 131.0, 130.9, 130.6, 129.7, 129.5, 129.1, 129.0, 128.8, 120.9, 21.6 ppm.

IR $\tilde{\nu}$ [cm^{-1}]: 3035 (w), 2919 (m), 2850 (w), 2119 (m, $\tilde{\nu}$ C≡N), 1596 (m), 1577 (m), 1530 (w), 1497 (w), 1488 (w), 1454 (w), 1412 (w), 1391 (w), 1376 (m), 1315 (m), 1282 (w), 1260 (w), 1099 (w), 1075 (w), 1029 (w), 914 (w), 867 (m), 805 (m), 795 (m), 766 (m), 750 (w), 717 (m), 691 (s), 675 (m), 656 (w), 620 (w), 596 (m), 574 (m), 495 (m).

Elemental analysis: found: C, 87.11; H, 5.87; N, 5.73; calc. for $C_{34}H_{24}N_2$ (+0.4 H_2O, +0.3 C_5H_{12}): C, 87.12; H, 5.85; N, 5.72.

HR-MS(ESI$^+$): m/z (%) = 483.1834 (100, [M+Na]$^+$), calc. 483.1832.

1,3-Bis(*N*-formyl-4-methyl-6-phenylanilin-2-yl)thiophene (9)

N-Formyl-2-bromo-4-methyl-6-phenylaniline (**7**) (548 mg, 1.88 mmol, 2.50 eq.) was dispersed in xylene (10 mL, mixture of isomers) and the mixture was purged with nitrogen for 15 min. 2,5-Bis(tributylstannyl)thiophene (97 wt-%, 500 mg, 0.755 mmol, 1.00 eq., 0.43 mL) and

[Pd(dppf)Cl_2] (31 mg, 0.04 mmol, 5 mol%) were added under nitrogen. The mixture was heated to 140°C for 48 hours. The solvent was evaporated and the residue subjected to column chromatography (SiO_2, gradient: DCM $\longrightarrow$ DCM/MeOH, 9:1). The product (**9**) was isolated a brownish solid (375 mg, 0.754 mmol, 98 %), which was found to be of sufficient purity for the next step.

^{1}H-NMR (400 MHz, CD_2Cl_2): δ = 7.88-7.79 (m, 1H), 7.76-7.66 (m, 1.5H), 7.59-7.45 (m, 0.5H), 7.49-7.26 (m, 12H), 7.26-7.05 (m, 5H), 2.48-2.31 (m, 6H) ppm.

^{13}C-NMR (101 MHz, CD_2Cl_2): δ = 165.3, 165.1, 161.9, 161.8, 142.0, 141.5, 141.3, 140.8, 140.11, 140.07, 139.7, 139.6, 139.3, 138.7, 138.0, 137.9, 133.4, 133.3, 132.2, 132.1, 131.8, 131.6, 131.5, 131.3, 131.1, 131.0, 130.70, 130.65, 130.0, 129.32, 129.27, 128.5, 128.3, 128.1, 127.93, 127.89, 127.8, 127.6, 127.3, 21.3, 21.2, 14.6, 13.9 ppm.

IR $\tilde{\nu}$ [cm^{-1}]: 3223 (w), 3052 (w), 2914 (w), 2853 (w), 1651 (s), 1594 (m), 1575 (m), 1495 (m), 1434 (m), 1379 (m), 1225 (m), 1181 (w), 1142 (w), 1074 (w), 1026 (w), 863 (m), 806 (w), 782 (w), 765 (m), 720 (w), 697 (s), 640 (w), 627 (m), 614 (m), 594 (w), 567 (m), 461 (w).

MS(ESI$^+$): *m/z* (%) = 525.06 (100, [M+Na]$^+$), calc. 525.16.

1,3-Bis(4-methyl-6-phenyl-1-isocyanidebenzene-2-yl)thiophene ((Ph)CNArSArNC(Ph))

1,3-Bis(*N*-formyl-4-methyl-6-phenylanilin-2-yl)thiophene (**9**) (375 mg, 0.754 mmol, 1.00 eq.) was dissolved in dry dichloromethane and di(*iso*-propyl)amine (0.60 mL, 5.30 mmol, 7.00 eq.) was added. The reaction mixture was cooled to 0°C and $POCl_3$ (0.25 mL, 2.6 mmol, 3.5 eq.) was added dropwise. The reaction was stirred at room temperature for 3 hours. Subsequently aqueous sodium carbonate solution (15.9 mL, 1.5 M) was added and stirring continued overnight.
Saturated aqueous sodium bicarbonate solution (14 mL) was added and the phases separated. The aqueous phase was extracted with dichloromethane and the combined organic phases dried over Na_2SO_4. The solvent was removed *in vacuo*, the residue dissolved in pentane and subjected to column chromatography (SiO_2, dichloromethane). The product was isolated as an off-white solid (224 mg, 0.480 mmol, 64 %).

The product is isolated as a mixture of isomers leading to additional signals.
^{1}H-NMR (400 MHz, CD_2Cl_2): δ = 7.58 (s, 2H), 7.56 - 7.44 (m, 12H), 7.23 (dd, *J*= 1.9, 0.9 Hz, 2H), 2.45 (s, 6H) ppm.

^{13}C-NMR (101 MHz, CD_2Cl_2): δ = 171.7, 141.1, 140.5, 140.4, 138.3, 131.8, 131.4, 130.4, 129.6, 129.1, 129.0, 128.9, 120.2, 21.6 ppm.

IR $\tilde{\nu}$ [cm^{-1}]: 3057 (w), 3033 (w), 2919 (w), 2853 (w), 2118 (s, $\tilde{\nu}$ C≡N), 1730 (w), 1681 (w), 1594 (m), 1575 (w), 1535 (w), 1496 (w), 1449 (w), 1424 (m), 1377 (w), 1333 (w), 1299 (w), 1282 (w), 1238 (w), 1238 (w), 1208 (w), 1177 (w), 1142 (w), 1129 (w), 1129 (w), 1074 (w), 1029 (w), 1014 (w), 1001 (w), 918 (w), 894 (w), 862 (m), 804 (m), 788 (m), 778 (w), 761 (m), 744 (w), 716 (m), 690 (s), 644 (w), 618 (m), 594 (w), 575 (m), 521 (m), 481 (w), 447 (w).

HR-MS(ESI$^+$): m/z (%) = 489.1396 (100, [M+Na]$^+$), calc. 489.1401.

Elemental analysis: found: C, 80.81; H, 5.49; N, 560; calc. for $C_{32}H_{22}N_2S$ (+0.5 H_2O, +0.3 C_5H_{12}): C, 80.92; H, 5.39; N, 5.63.

5.2.3 Synthesis of Methyl Substituted Ligands

The synthetic route used to prepare the building block 2-bromo-4,6-dimethylaniline, as well as the ligand **CNAr$_3$NC** is described in my paper published in *Angew. Chem. Int. Ed.* **2016**, *55*, 11247.

N-Formyl-2-bromo-4,6-di(methyl)aniline (10)

Formic acid (20 mL, 530 mmol) was added dropwise to acetic anhydride (40 mL, 422 mmol) within 10 min at 0 °C. The mixture was allowed to warm to room temperature and was stirred at 50 °C for 2 h. After reaching room temperature the mixture was cooled to 0 °C and 2-bromo-4,6-dimethylaniline (4.71 g, 23.3 mmol, 1.00 eq·) was added. The mixture was stirred at room temperature for 30 min. Ice cooled water (300 mL) was added and the precipitate filtered and washed with water (1 L). After drying under vacuum, product **10** was obtained as a light brown solid (3.59 g, 16.7 mmol, 72 %).

^{1}H-NMR (400 MHz, $CDCl_3$): δ = 8.38 (d, J= 1.5 Hz, 0.57H), 8.14 (d, J= 11.6 Hz, 0.43H), 7.30 (d, J= 18.3 Hz, 1H), 7.13-6.96 (m, 2H), 2.32 (d, J= 6.7 Hz, 2.6H), 2.27 (d, J= 7.9 Hz, 3.4H) ppm.

^{13}C-NMR (101 MHz, $CDCl_3$): δ = 164.8, 159.3, 139.3, 139.2, 137.7, 136.5, 131.6, 131.2, 131.0, 129.9, 122.3, 121.5, 20.8, 20.8, 19.5, 19.4 ppm.

IR $\tilde{\nu}$ [cm^{-1}]: 3328 (w, br), 3015 (w), 2977 (w), 2914 (w), 1651 (s), 1600 (m), 1561 (w), 1503 (s), 1436 (m), 1375 (s), 1273 (m), 1220 (m), 1156 (m), 1115 (m), 1028 (m), 989 (w), 888 (w), 839 (s), 821 (m), 723 (w), 688 (m), 644 (m, br), 585 (m), 552 (m), 521 (m), 457 (m).

Elemental analysis: found: C, 48.41; H, 4.57; N, 6.16; calc. for $C_9H_{10}NOBr$ (+0.2 $CH_3(CO)CH_3$): C, 48.10; H, 4.71; N, 5.84.

1,3-Bis(*N*-formyl-4,6-dimethylanilin-2-yl)thiophene (11)

2,5-Bis(tributylstannyl)thiophene (97 wt.%, 0.26 g, 0.38 mmol, 1.0 eq., 0.22 mL) was added to a suspension of *N*-formyl-2-bromo-4,6-dimethylaniline (**10**) (0.21 g, 0.94 mmol, 2.5 eq.) in dry xylene (5 mL, mixture of isomers) under inert gas. The suspension was purged with nitrogen for 20 min. [$Pd(PPh_3)_4$] was added to the reaction mixture followed by heating to 140 °C overnight. The solvent was removed *in vacuo* and the residue submitted to column chromatography (SiO_2, DCM/MeOH, 9:1). The product was obtained as an off-white solid (107 mg, 0.280 mmol, 73%).

The product was isolated as a mixture of isomers leading to additional signals.
^{1}H-NMR (400 MHz, CD_2Cl_2): δ = 8.09 (m, 1.5H), 7.30 (m, 8.5H), 2.13 (m, 12H) ppm.

^{13}C-NMR (101 MHz, CD_2Cl_2): δ = 169.0, 140.0, 138.7, 138.5, 136.2, 130.7, 130.2, 129.2, 128.9, 122.8, 100.5, 21.5, 19.6 ppm.

MS(ESI^+): *m/z* (%) = 779.80 (100, $[2M+Na]^+$); calc. 779.27.

1,3-Bis(4,6-dimethyl-1-isocyanidebenzene-2-yl)thiophene (CNArSArNC)

1,3-bis(*N*-formyl-4,6-dimethylaniline-2-yl)thiophene (**11**) (97 mg, 0.26 mmol, 1.0 eq.) was dissolved in dry dichloromethane (7 mL) under nitrogen. Dry di(*iso*-propyl)amine (0.24 mL, 1.8 mmol, 7.0 eq.) was added and the mixture cooled to 0 °C. $POCl_3$ (0.70 mL, 7.5 mmol, 2.8 eq.) was added dropwise. The solution turned brown and was allowed to warm to room temperature. After stirring for 3 h, a solution of Na_2CO_3 in water (1.5 M, 5.9 mL) was added and the biphasic system was stirred vigorously overnight. Saturated aqueous $NaHCO_3$ solution (5.2 mL) was added and the aqueous phase was extracted with dichloromethane (3 x 20 mL). The combined organic phases were dried over Na_2SO_4 and the solvent removed *in vacuo*. The product was purified via column chromatography (SiO_2, DCM) and isolated as a

light yellow solid (56 mg, 0.16 mmol, 63 %).

^{1}H-NMR (400 MHz, CD_2Cl_2): δ = 7.54 (s, 2H), 7.28 (s, 2H), 7.11 (s, 2H), 2.45 (s, 6H), 2.37 (s, 6H) ppm.

^{13}C-NMR (101 MHz, CD_2Cl_2): δ = 171.3, 140.3, 140.1, 137.0, 131.1, 130.8, 128.7, 128.6, 121.9, 21.5, 19.8 ppm.

HR-MS(ESI$^+$): m/z (%) = 365.1083 (100, $[M+Na]^+$); calc. 365.1088.

IR $\tilde{\nu}$ [cm^{-1}]: 2916 (w), 2851 (w), 2111 (s, $\tilde{\nu}$ C≡N), 1598 (m), 1576 (w), 1457 (m, br), 1409 (w), 1376 (m), 1316 (w), 1280 (m), 1256 (m), 1200 (m), 1175 (w), 1153 (w), 1123 (w), 1090 (w), 1033 (m), 994 (w), 858 (m), 823 (s), 809 (m), 787 (m), 731 (w), 721 (w), 660 (w), 612 (m), 585 (m), 554 (m), 526 (w), 484 (w).

5.3 Homoleptic Metal Complexes Bearing Chelating Isocyanide Ligands

5.3.1 Zero-Valent Metal Complexes

$[MoCl_4(THF)_2]$

Mo_2Cl_{10} was suspended in dry acetonitrile and stirred at room temperature. The initially black suspension turned dark green. After 30 min the suspension was filtered over a transfer cannula into a fresh flask and dry THF was added dropwise. After stirring for 2 h at room temperature, an orange solid formed which was isolated via filtration under inert atmosphere. The solid was washed with THF and dried *in vacuo* giving $[MoCl_4(THF)_2]$ as an orange solid, which decomposes in air over the course of hours.[126]

$[WCl_4(THF)_2]$

Prior to use cyclopentene was washed with aqueous NaOH (1 M), followed by washing with water and drying over Na_2SO_4. The pre-dried cyclopentene was distilled from powdered NaOH under an argon atmosphere.
Commercially available tungsten hexachloride (3.72 g, 9.4 mmol, 1.0 eq.) was suspended in dry dichloromethane under an atmosphere of dried argon. To the dark suspension cyclopentene (6.32 g, 92.8 mmol, 8.5 mL, 9.8 eq.) was added, and a greenish/dark blue precipitate

was formed. After leaving the reaction mixture at room temperature for 5 to 10 min, the precipitate exothermically re-dissolved causing the mixture to reflux.
After cooling to room temperature the mixture was filtered under inert atmosphere to give a dark brownish solution, which was cooled to 0 °C. To the cooled solution THF (7.88 mL) was added dropwise causing the color to change from dark brown to red brown.
During warming up to room temperature, the color of the solution changed to green and a precipitate formed. After stirring for 1 h at room temperature, the reaction mixture was filtered under inert atmosphere and the precipitate was washed with dry dichloromethane (5×5 mL) to yield $[WCl_4(THF)_2]$ as an insoluble orange to light brown solid, which slowly decomposes in air to form a dark blue solid.

[Mo(CNAr$_3$NC)$_3$]

Sodium amalgam was prepared *in situ* by adding small pieces of sodium (33 mg, 1.4 mmol, 23 eq.) to mercury (4.4 g, 22 mmol, 0.30 mL). A solution of 1,3-bis(4,6-dimethyl-1-isocyanide-benzene-2-yl)benzene (66.6 mg, 0.198 mmol, 3.30 eq.) in dry THF (2 mL) was added, followed by a suspension of $[MoCl_4(THF)_2]$ ((30 mg, 0.060 mmol, 1 eq.) in dry THF (2 mL). After an additional portion of THF (2 mL) was added, the solution was stirred vigorously at room temperature for 48 h. Already after 2 h of stirring the mixture turned dark red.
The dark red solution was transferred in a second Schlenk flask via syringe, followed by filtration under inert gas. The red filtrate was concentrated *in vacuo* and stored in a fridge at −20 °C to give X-ray quality crystals. The solution was transferred to another flask and diluted with dry pentane giving an other fraction of the compound. This fraction had to be washed with pentane several times in order to remove grease.
The red compound is fairly stable in air as a dry solid, but decomposes rather rapidly in aerated solution. Coordinating as well as chlorinated solvents seem to accelerate the decomposition of the compound.

^{1}H-NMR (600 MHz, THF-d$_8$): δ = 8.08 (t, J=1.8 Hz, 3H), 7.49 (t, J=7.7 Hz, 3H), 7.30 (dd, J=7.7 Hz, 1.8 Hz, 6H), 6.94 (s, 6H), 6.89 (d, J= 1.8 Hz, 6H), 2.26 (s, 18H), 2.18 (s (br), 18H) ppm.

^{13}C-NMR (150.9 MHz, THF-d$_8$): δ = 185.0, 140.0, 138.3, 135.0, 134.7, 130.6, 130.5, 130.0, 129.6, 128.5, 126.3, 21.3, 19.6 ppm.

IR $\tilde{\nu}$ [cm^{-1}]: 2962 (w), 1939 (m, $\tilde{\nu}$ C≡N), 1598 (w), 1455 (w), 1258 (s), 1079 (s), 1010 (s), 858 (m), 789 (s), 701 (m), 599 (w), 534 (m), 461 (m), 434 (w).

MALDI-TOF (m/z) = 1106 ($[M]^+$); calc.: 1106.3934.

HR-MS(ESI$^+$): m/z = 1139.3905 ($[M+O_2+H]^+$); calc.: 1139.3910.

[Mo((*t*Bu)CNAr$_3$NC(*t*Bu))$_3$]

Sodium amalgam was prepared *in situ* by adding small pieces of sodium (33 mg, 1.4 mmol, 23 eq·) to mercury (4.4 g, 22 mmol, 0.30 mL). A solution of (*t*Bu)CNAr$_3$NC(*t*Bu) (86.6 mg, 0.172 mmol, 3.30 eq.) in dry THF (2 mL) was added, followed by a suspension of $[MoCl_4(THF)_2]$ (26 mg, 0.052 mmol, 1.00 eq.) in dry THF (2 mL). After an additional portion of THF (2 mL) was added, the solution was stirred vigorously at room temperature overnight. Already after 1 h of stirring the mixture turned dark red.
The dark red solution was transferred to another Schlenk flask via syringe, followed by filtration under inert gas. The red filtrate was concentrated *in vacuo* to yield the desired complex in 68% yield.
In solution several structural isomers of the complex are present which appear to inter convert on the time scale of NMR experiments. This leads to the complicated splitting patterns and broad signal structures observed in ^{1}H as well as ^{13}C spectra.

^{1}H-NMR (600 MHz, THF-d$_8$): δ = 8.05 (m, 2.5H), 7.33 (21.5H), 1.33 (m, 108H) ppm.

^{13}C-NMR (150.9 MHz, THF-d$_8$): δ = 186.3 (br), 175.4.0, 153.1, 147.8 (br), 146.5, 145.3 (br), 144.2, 142.1, 141.3, 140.3, 140.2, 140.04, 139.98, 139.3, 139.1, 136.5, 131.5, 131.3, 131.2, 131.0, 130.98, 130.8, 130.6, 129.9, 129.85, 129.7, 129.68, 129.67, 129.64, 129.3, 129.2, 128.2, 128.1, 127.9, 127.1, 127.07, 125.2, 124.9, 124.0, 123.2, 37.8, 34.3, 31.4, 27.7, 27.0, 25.4, 25.1, 23.3 ppm.

IR $\tilde{\nu}$ [cm^{-1}]: 2953 (m), 2923 (m), 2866 (w), 1951 (s, $\tilde{\nu}$ C≡N), 1593 (w), 1457 (m), 1425 (m), 1389 (m), 1361 (m), 1248 (w), 1203 (w), 880 (m), 841 (w), 797 (w), 719 (w), 696 (m), 537 (m), 506 (w), 447 (w).

HR-MS(ESI$^+$): m/z = 1610.9550 ($[M]^+$); calc.: 1610.9565.

Isotope pattern: 1604.9527 (31.3%) : 1605.9535 (39.1%) : 1606.9552 (40.6%) : 1607.9544 (62.5%) : 1608.9541 (84.4%) : 1609.9561 (87.5%) : 1610.9550 (100%) : 1611.9570 (79.7%) : 1612.9576 (62.5%) : 1613.9585 (46.9%) : 1614.9591 (25%) : 1615.9636 (15.6%).

MALDI-TOF (m/z) = 1610 ($[M]^+$); calc.: 1610.9565.

[Cr((*t*Bu)CNAr$_3$NC(*t*Bu))$_3$]

First [$CrCl_3(THF)_3$] was generated *in situ* following a procedure described by PLUMMER.[63] Anhydrous $CrCl_3$ (6 mg, 0.04 mmol, 1.0 eq.) was stirred in dry THF (1 mL) in presence of activated zinc powder (1.3 mg). After approximately 1 h, a homogeneous greenish solution was formed.
Sodium amalgam was prepared *in situ* by adding small pieces of sodium (12 mg) to mercury (1.6 g, 0.12 mL). A solution of (*t*Bu)CNAr$_3$NC(*t*Bu) (60 mg, 0.12 mmol, 3.1 eq.) in dry THF (2 mL) was added, followed by the freshly prepared solution of [$CrCl_3(THF)_3$]. After an additional portion of THF (2 mL) was added, the solution was stirred vigorously at room temperature overnight. Immediately after the addition of the chromium precursor the mixture turned dark red.
The dark red solution was transferred to another Schlenk flask via syringe, followed by filtration under inert gas. The red filtrate was concentrated *in vacuo* to yield the desired complex in 78% yield.
In solution several structural isomers of the complex are present which appear to inter convert on the time scale of NMR experiments. This leads to the complicated splitting patterns and broad signal structures observed in ^{1}H as well as ^{13}C spectra.

^{1}H-NMR (600 MHz, THF-d$_8$): δ = 8.38 (s, 0.35H), 8.11 (d, J=11.2 Hz, 0.45H), 7.86 (d, J=1.5 Hz, 0.35H), 7.70 (m, 1.45H), 7.55 (m, 9.4H), 7.43 (m, 12H), 1.35 (m, 60H), 1.29 (m, 48H) ppm.

^{13}C-NMR (150.9 MHz, THF-d$_8$): δ = 191.0, 175.4, 165.3, 161.1, 153.1, 152.9, 151.0, 146.5, 144.3, 143.7, 143.5, 143.1, 142.0, 140.8, 140.7, 140.0, 139.0, 131.4, 131.3, 130.3, 129.9, 129.4, 129.2, 128.8, 128.6, 127.7, 127.09, 127.06, 126.71, 126.66, 126.6, 124.12, 124.09, 124.0, 122.1, 36.44, 36.43, 36.42, 36.1, 33.1, 31.62, 31.61, 30.81, 30.78, 29.86, 29.84, 23.7 ppm.

IR $\tilde{\nu}$ [cm^{-1}]: 2955 (m), 2923 (m), 2868 (w), 1954 (s, $\tilde{\nu}$ C≡N), 1682 (w), 1568 (w), 1455 (m), 1425 (m), 1389 (m), 1361 (m), 1299 (w), 1274 (m), 1247 (w), 1201 (w), 1076 (w), 881 (w), 798 (w), 699 (m), 587 (m), 447 (w).

HR-MS(ESI$^+$): m/z = 1565.9933 ([M]$^+$); calc.: 1565.9943.

Isotope pattern: 1562.9964 (4.8%) : 1563.9987 (5.5%) : 1564.9905 (78.5%) : 1565.9933 (100%) : 1566.9960 (68.2%) : 1567.9989 (31.9%) : 1569.0008 (11.2%) : 1570.0033 (3.3%).

MALDI-TOF (m/z) = 1566 ($[M]^+$); calc.: 1565.9943.

[Ni((Ph)CNAr$_3$NC(Ph))$_2$]

This synthesis follows a procedure published by HAHN et al.[114]
[Ni(COD)$_2$] (19 mg, 0.07 mmol, 1.0 eq.) was transferred into a Schlenk tube under inert gas. A solution of the ligand (Ph)CNAr$_3$NC(Ph) (64 mg, 0.13 mmol, 2.0 eq.) in dry, deaerated toluene (2 mL) was added. The mixture immediately turned bright orange. After stirring at room temperature for 1 hour, the solvent was removed and an air-stable, orange solid was obtained in quantitative yield.
In solution, several structural isomers of the complex are present which appear to inter convert on the time scale of NMR experiments. This leads to the complicated splitting patterns and broad signal structures observed in ^{1}H as well as ^{13}C spectra.

^{1}H-NMR (600 MHz, THF-d$_8$): δ = 7.42 (m, 36H), 2.45 (m, 12H) ppm.

^{13}C-NMR (101 MHz, THF-d$_8$): δ = 175.4, 140.7, 139.9, 139.5, 138.0, 136.9, 131.8, 131.0, 130.2, 130.0, 129.8, 129.6, 129.0, 128.4, 124.7, 30.8 ppm.

IR $\tilde{\nu}$ [cm^{-1}]: 2954 (m), 2917 (s), 2849 (m), 2007 (s, $\tilde{\nu}$ C≡N), 1598 (w), 1575 (w), 1496 (m), 1455 (m), 1419 (m), 1377 (w), 1260 (w), 1211 (w), 1091 (s, br), 1024 (m), 865 (m), 798 (m), 773 (m), 729 (w), 696 (s), 612 (w), 595 (w), 569 (w), 536 (w), 486 (m), 445 (m).

MALDI-TOF (m/z) = 978 ($[M]^+$); calc.: 978.32.

[Ni((Ph)CNArSArNC(Ph))$_2$]

This synthesis follows a procedure published by HAHN et al.[114]
[Nickel(COD)$_2$] (13 mg, 0.05 mmol, 1.0 eq.) was transferred into a Schlenk tube under inert gas. A solution of the ligand (Ph)CNArSArNC(Ph) (44 mg, 0.09 mmol, 2.0 eq.) in dry, deaerated toluene (2 mL) was added. The mixture immediately turned dark red. After stirring at room temperature for 1 hour, the solvent was removed and an air-stable, dark red solid was obtained in quantitative yield.
In solution, several structural isomers of the complex are present which appear to inter convert on the time scale of NMR experiments. This leads to the complicated splitting patterns and broad signal structures observed in ^{1}H as well as ^{13}C spectra.

^{1}H-NMR (600 MHz, THF-d_8): δ = 7.27 (m, 32H), 2.44 (m, 12H) ppm.

^{13}C-NMR (150.9 MHz, THF-d_8): δ = 178.5, 142.0, 139.4, 138.6, 138.04, 137.3, 133.7, 131.6, 130.4, 130.1, 129.8, 129.6, 129.1, 128.5, 126.6, 126.2, 125.7, 30.8 ppm.

IR $\tilde{\nu}$ [cm^{-1}]: 2955 (m), 2920 (s), 2851 (m), 2004 (s, br, $\tilde{\nu}$ C≡N), 1730 (w), 1596 (w), 1570 (w), 1495 (w), 1455 (m), 1423 (m), 1376 (m), 1259 (m), 1211 (w), 1076 (s, br), 1015 (s, br), 861 (m), 800 (s), 773 (s), 732 (m), 696 (s), 613 (m), 601 (w), 571 (m), 496 (m).

MALDI-TOF (m/z) = 990 ([M]$^{+}$); calc.: 990.24.

HR-MS(ESI^{+}): m/z (%) = 990.2363 (100, [M]$^{+}$); calc.: 990.2355.

Isotope pattern: 990.2363 (100%) : 991.2388 (86.7%) : 992.2352 (75.6%) : 993.2365 (46.7%) : 994.2336 (24.4%).

5.3.2 Charged Complexes

Copper(I) Complexes

[Cu(CNAr$_3$NC)$_2$](PF$_6$)

Under an atmosphere of inert gas [Cu(MeCN)$_4$](PF$_6$) (50 mg, 0.13 mmol, 1.0 eq.) and CNAr$_3$-NC (90 mg, 0.27 mmol, 2.0 eq.) were dissolved in dry dichloromethane (30 mL) and heated to reflux overnight. After cooling to room temperature the solvent was removed *in vacuo* to obtain pure [Cu(CNAr$_3$NC)$_2$](PF$_6$) as an off-white solid.

^{1}H-NMR (400 MHz, CD_2Cl_2): δ = 7.67 (t, J=7.7 Hz, 2H), 7.57 (t, J=1.7 Hz, 2H), 7.46 (dd, J=7.7 Hz, 1.8 Hz, 4H), 7.19 (d, J=2.2 Hz, 4H), 7.08 (d, J=2.2 Hz, 4H), 2.47 (s, 12H), 2.40 (s, 12H) ppm.

^{13}C-NMR (101 MHz, CD_2Cl_2): δ = 141.8, 140.3, 138.2, 136.3, 131.3, 130.4, 130.3, 130.3, 130.1, 129.5, 121.3, 21.7, 19.2 ppm.

HR-MS(ESI^{+}): m/z (%) = 735.2542 (100, [M]$^{+}$); calc.: 735.2549.

Isotope pattern: 735.2542 (100%) : 736.2574 (53.4%) : 737.25.41 (53.4%) : 738.2561 (24.1%) : 739.2586 (6.8%).

IR $\tilde{\nu}$ [cm^{-1}]: 2151 (m, $\tilde{\nu}$ C≡N), 1596 (w), 1461 (w), 834 (s), 802 (m), 736 (w), 704 (m), 555 (m), 305 (s).

Elemental analysis: found: C, 64.93; H, 5.29; N, 6.41; calc. for $C_{48}H_{40}CuF_6N_4P$(+0.5 $C_4H_{10}O$, +0.15 H_2O): C, 65.20; H, 4.96; N, 6.08.

[Cu(CNArSArNC)$_2$](PF$_6$)

Under an atmosphere of inert gas [Cu(MeCN)$_4$](PF$_6$) (26 mg, 0.07 mmol, 1.0 eq.) and CNArSArNC (48 mg, 0.14 mmol, 2.0 eq.) were dissolved in dry dichloromethane (10 mL) and heated to reflux overnight. After cooling to room temperature the solvent was removed *in vacuo* to obtain pure [Cu(CNArSArNC)$_2$](PF$_6$) as an yellow solid.

^{1}H-NMR (400 MHz, $CDCl_3$): δ = 7.33 (s, 4H), 7.20 (s, 4H), 7.15 (s, 4H), 2.47 (s, 12H), 2.42 (s, 12H) ppm.

[Cu((*t*Bu)CNAr$_3$NC(*t*Bu))$_2$](PF$_6$)

Under an atmosphere of inert gas [Cu(MeCN)$_4$](PF$_6$) (13 mg, 0.04 mmol, 1.0 eq.) and (*t*Bu)-CNAr$_3$NC(*t*Bu) (35 mg, 0.07 mmol, 2.0 eq.) were dissolved in dry dichloromethane (5 mL) and heated to reflux overnight. After cooling to room temperature the solvent was removed *in vacuo* to obtain pure [Cu((*t*Bu)CNAr$_3$NC(*t*Bu))$_2$](PF$_6$) (99%) as an off-white solid.

^{1}H-NMR (400 MHz, CD_2Cl_2): δ = 7.80-7.02 (m, 16H), 1.67-1.43 (m, 36H), 1.42-1-18 (m, 36H) ppm.

^{13}C-NMR (101 MHz, CD_2Cl_2): δ = 185.0, 146.5, 143.1, 139.4, 130.2, 129.8, 129.2, 126.8, 124.3, 120.3, 118.8, 36.1, 35.9, 31.4, 30.0 ppm.

HR-MS(ESI$^+$): *m/z* (%) = 1071.6295 (100, [M]$^+$); calc.: 1071.6305.

Isotope pattern: 1071.6295 (100%) : 1072.6328 (81.4%) : 1073.6308 (74.7%) : 1074.6322 (46.3%) : 1075.6345 (17.7%) : 1076.6380 (4.9 %).

IR $\tilde{\nu}$ [cm^{-1}]: 2960 (w), 2872 (w), 2157 (s, $\tilde{\nu}$ C≡N), 1677 (w), 1591 (w), 1466 (w), 1396

(w), 1365 (w), 1280 (w), 1249 (w), 1201 (w), 1171 (w), 884 (w), 837 (s), 755 (w), 731 (w), 713 (w), 556 (m).

Elemental analysis: found: C, 67.26; H, 7.27; N, 4.60; calc. for $C_{72}H_{88}CuF_6N_4P$ (+2 H_2O, +0.4 CH_2Cl_2): C, 67.51; H, 7.26; N, 4.35.

[Cu((*t*Bu)CNArSArNC(*t*Bu))$_2$](PF$_6$)

Under an atmosphere of inert gas [Cu(MeCN)$_4$](PF$_6$) (18 mg, 0.05 mmol, 1.0 eq.) and (*t*Bu)-CNArSArNC(*t*Bu) (50.0 mg, 0.10 mmol, 2.0 eq.) were dissolved in dry dichloromethane (5 mL) and heated to reflux overnight. After cooling to room temperature the solvent was removed *in vacuo* to obtain pure [Cu(*t*BuCNAr$_3$NC*t*Bu)$_2$](PF$_6$) (55.7 mg, 0.045 mmol, 93%) as an off-white solid.

^{1}H-NMR (400 MHz, CD_2Cl_2): δ = 7.57 (d, J= 2.1 Hz, 4H), 7.53 (d, J= 2.1 Hz, 4H), 7.13 (s, 4H), 1.48 (s, 36H), 1.37 (s, 36H) ppm.

^{13}C-NMR (101 MHz, CD_2Cl_2): δ = 154.6, 146.8, 141.0, 135.6, 128.5, 126.8, 125.3, 122.2, 36.1, 35.9, 31.4, 29.9 ppm.

HR-MS(ESI$^+$): m/z (%) = 1083.5423 (100, [M]$^+$), calc.: 1083.5428.

Isotope pattern: 1083.5423 (100 %), 1084.5451 (78.0 %), 1085.5427 (79.6 %), 1086.5440 (49.4 %), 1087.5441 (21.9 %), 1088.5434 (8.0%), 1089.5449 (2.4 %).

IR $\tilde{\nu}$ [cm^{-1}]: 2959 (m), 2872 (w), 2149 (m, $\tilde{\nu}$ C≡N), 1591 (w), 1477 (w), 1430 (w), 1407 (m), 1365 (w), 1280 (w), 1241 (w), 1201 (w), 884 (w), 836 (s), 761 (w), 657 (w), 556 (m).

Elemental analysis: found: C, 66.27; H, 7.11; N, 4.64; calc. for $C_{68}H_{84}CuF_6N_4PS_2$ (+0.3 H_2O): C, 66.11; H, 6.90; N, 4.53.

[Cu((Ph)CNAr$_3$NC(Ph))$_2$](PF$_6$)

Under an atmosphere of inert gas [Cu(MeCN)$_4$](PF$_6$) (20 mg, 0.05 mmol, 1.0 eq.) and (Ph)CN-Ar$_3$NC(Ph) (50 mg, 0.10 mmol, 2.0 eq.) were dissolved in dry dichloromethane (5 mL) and heated to reflux overnight. After cooling to room temperature the solvent was removed *in*

vacuo to obtain pure $[Cu((Ph)CNAr_3NC(Ph))_2](PF_6)$ as a pale-orange solid (60 mg, 0.05 mmol, 99%).

^{1}H-NMR (400 MHz, CD_2Cl_2): δ = 7.61 (t, J= 7.7 Hz, 2H), 7.53 (t, J= 7.7 Hz, 2H), 7.51-7.28 (m, 28H), 7.23 (s, 4H), 2.48 (s, 12H) ppm.

^{13}C-NMR (101 MHz, CD_2Cl_2): δ = 142.2, 141.3, 139.9, 138.1, 137.3, 131.7, 131.3, 130.3, 130.2, 129.45, 129.41, 129.1, 119.5, 21.8 ppm.

HR-MS(ESI$^+$): m/z (%) = 983.3160 (100, $[M]^+$), calc.: 983.3175.

Isotope pattern: 983.3160 (100%), 984.3191 (72.3%), 985.3169 (69.3%), 987.3207 (14.5%), 988.3246 (3.7%).

IR $\tilde{\nu}$ [cm^{-1}]: 3034 (w), 2923 (w), 2854 (w), 2157 (m, $\tilde{\nu}$ C≡N), 1592 (w), 1575 (w),1486 (w), 1455 (w), 1422 (w), 1345 (w), 1282 (w), 1259 (w), 1178 (w), 1158 (w), 1078 (w), 1028 (w), 874 (w), 833 (s), 806 (m), 771 (m), 732 (m), 699 (s), 661 (w), 613 (w), 600 (w), 572 (w), 555 (m), 496 (w), 474 (w), 444 (w).

Elemental analysis: found: C, 68.89; H, 4.93; N, 4.85; calc. for $C_{68}H_{48}CuF_6N_4P$ (+3 H_2O): C, 69.0; H, 4.60; N, 4.73.

$[Cu((Ph)CNArSArNC(Ph))_2](PF_6)$

Under an atmosphere of inert gas $[Cu(MeCN)_4](PF_6)$ (20 mg, 0.05 mmol, 1.0 eq·) and (Ph)CN-ArSArNC(Ph) (50 mg, 0.10 mmol, 2.0 eq·) were dissolved in dry dichloromethane (5 mL) and heated to reflux overnight. After cooling to room temperature the solvent was removed *in vacuo* to obtain pure $[Cu((Ph)CNArSArNC(Ph))_2](PF_6)$ as a yellow solid (61 mg, 0.05 mmol, 99%).

^{1}H-NMR (400 MHz, CD_2Cl_2): δ = 7.50 (d, J= 1.9 Hz, 4H), 7.47-7.35 (m, 20H), 7.31 (d, J= 1.9 Hz, 4H), 7.18 (s, 4H), 2.51 (s, 12H) ppm.

^{13}C-NMR (101 MHz, CD_2Cl_2): δ = 142.6, 140.1, 139.9, 137.1, 134.1, 132.1, 130.9, 129.34, 129.32, 129.2, 128.9, 120.4, 21.8 ppm.

HR-MS(ESI$^+$): m/z (%) = 995.2295 (100, $[M]^+$); calc.: 995.2298.

Isotope pattern: 995.2295 (100%), 996.2325 (70.6%), 997.2295 (73.2%), 998.2311 (41.5%), 999.2312 (17.9%), 1000.2313 (6.2 %).

IR $\tilde{\nu}$ [cm^{-1}]: 3050 (w), 2923 (w), 2953 (w), 2153 (m, $\tilde{\nu}$ C≡N), 1728 (w), 1592 v, 1576 (w), 1534 (w), 1497 (w), 1451 (w), 1422 (w), 1381 (w), 1284 (w), 1250 (w), 1212 (w), 1178 (w), 1128 (w), 1075 (w), 1026 (w), 833 (s), 769 (m), 728 (m), 698 (m), 625 (w), 573 (w), 555 (m), 516 (w), 475 (w).

Elemental analysis: found: C, 65.68; H, 4.79; N, 4.67; calc. for $C_{64}H_{44}CuF_6N_4PS_2$ (+1.7 H_2O, +0.5 MeCN): C, 65.31; H, 4.40; N, 5.06.

Other Metal Complexes

[Re(CNAr$_3$NC)(CO)$_3$Cl]

$CNAr_3NC$ (200 mg, 0.594 mmol, 1.00 eq.) and $[Re(CO)_5Cl]$ (219 mg, 0.594 mmol, 1.00 eq.) were suspended in dry toluene (30 mL) under inert atmosphere. The reaction mixture was heated to reflux overnight. After approximately 15 min of heating, a precipitate formed which in the later course of the reaction dissolved again.
After cooling to room temperature diethyl ether was added until a precipitate formed. The suspension was filtered and the filtrate left to evaporate to yield $[Re(CNAr_3NC)(CO)_3Cl]$ as a yellow crystalline solid.

^{1}H-NMR (400 MHz, $CDCl_3$): δ = 7.75 (br s, 1H), 7.62 (t, J=7.7 Hz, 1H), 7.40 (d, J=7.6 Hz, 2H), 7.13 (d, J=1.4 Hz, 2H), 7.04 (d, J=1.8 Hz, 2H), 2.52 (s, 6H), 2.39 (s, 6H) ppm.

^{13}C-NMR (101 MHz, $CDCl_3$): δ = 140.3, 139.8, 137.6, 136.3, 130.6, 130.2, 129.3, 122.0, 21.5, 18.9 ppm.

HR-MS(ESI^+): m/z (%) = 661.1621 (100, $[M - Cl - CO + 2\ MeCN]^+$); calc.: 661.1608.

Isotope pattern: 660.1618 (16.5%) : 661.1621 (100%) : 662.1649 (29.0%) : 663.1673 (4.9%) : 738.2561 (24.1%) : 739.2586 (6.8%).

IR $\tilde{\nu}$ [cm^{-1}]: 2186 (m, $\tilde{\nu}$ C≡N), 2153 (m, $\tilde{\nu}$ C≡N), 2026 (s, $\tilde{\nu}$ C≡O), 1970 (s, $\tilde{\nu}$ C≡O), 1913 (s, $\tilde{\nu}$ C≡O), 1709 (m), 1460 (m), 861 (m), 800 (m), 702 (m), 608 (m), 598 (m), 574 (m), 553 (m), 528 (m), 417 (m).

Elemental analysis: found: C, 50.03; H, 3.50; N, 4.32; calc. for $C_{27}H_{20}N_2O_3Cl$ Re (+0.25 $CH_3(CO)CH_3$, +0.45 H_2O): C, 50.14; H, 3.40; N, 4.21.

[Pd(CNAr$_3$NC)Cl$_2$]

$CNAr_3NC$ (55.8 mg, 0.166 mmol, 1.00 eq.) and $K_2[PdCl_4]$ (78.3 mg, 0.240 mmol, 1.44 eq.) were suspended in dry acetonitrile (5 mL) under inert atmosphere. The reaction mixture was heated to reflux overnight. First the mixture turned orange and after 1 h of reflux the color changed to green accompanied by the formation of a precipitate. After refluxing the reaction mixture overnight and cooling to room temperature, the light yellow precipitate was filtered off and washed with acetonitrile. The now white precipitate was washed through the filter with dichloromethane. Evaporation of the solvent gave pure $[Pd(CNAr_3NC)Cl_2]$ (73.3 mg, 0.142 mmol, 86 %) as a white solid.

^{1}H-NMR (400 MHz, CD_2Cl_2): δ = 7.69 (ddd, J=8.1, 7.4, 0.6 Hz, 1H), 7.55 (td, J=1.8, 0.6 Hz, 1H), 7.46 (dd, J=7.7, 1.8 Hz, 2H), 7.23-7.20 (m, 2H), 7.15-7.10 (m, 2H), 2.54 (s, 6H), 2.42 (s, 6H) ppm.

^{13}C-NMR (101 MHz, CD_2Cl_2): δ = 143.1, 140.5, 137.7, 137.6, 131.6, 130.9, 130.6, 130.1, 129.0, 21.9, 19.0 ppm.

IR $\tilde{\nu}$ [cm^{-1}]: 2915 (w), 2226 (s, $\tilde{\nu}$ C≡N), 2210 (s, $\tilde{\nu}$ C≡N), 1633 (w), 1597 (m), 1572 (w), 1462 (m), 1375 (m), 1037 (w), 861 (s), 796 (m), 704 (s), 363 (s), 350 (s), 336 (s)

Elemental analysis: found: C, 52.48; H, 4.48; N, 5.37; calc. for $C_{24}H_{20}Cl_2N_2$ Pd (+0.15 CH_2Cl_2, +1.3 H_2O): C, 52.75; H, 4.20; N, 5.09.

[Pt(CNAr$_3$NC)Cl$_2$]

$CNAr_3NC$ (55.8 mg, 0.166 mmol, 1.00 eq.) and $K_2[PtCl_4]$ (99.5 mg, 0.240 mmol, 1.44 eq.) were suspended in dry acetonitrile (5 mL) under inert atmosphere. The reaction mixture was heated to reflux overnight. Within the first five minutes a yellow precipitate was formed which turned beige overnight. The precipitate was filtered off and washed with acetonitrile until the solvent remained colorless. The white solid was washed through the filter with dichloromethane to give pure $[Pt(CNAr_3NC)Cl_2]$ (53.8 mg, 0.089 mmol, 54 %) after evaporation of the solvent.

^{1}H-NMR (400 MHz, CD_2Cl_2): δ = 7.68 (ddd, J=8.0, 7.3, 0.6 Hz, 1H), 7.56 (td, J=1.8, 0.6 Hz, 1H), 7.45 (dd, J=7.7, 1.8 Hz, 2H), 7.21 (t, J=0.8 Hz, 2H), 7.14-7.11 (m, 2H), 2.53 (s, 6H), 2.41 (s, 6H) ppm.

^{13}C-NMR (101 MHz, CD_2Cl_2): δ = 142.5, 140.4, 137.8, 137.1, 131.5, 130.9, 130.6, 130.1, 128.8, 21.9, 18.9 ppm.

IR $\tilde{\nu}$ [cm^{-1}]: 3480 (w), 2915 (w), 2852 (w), 2232 (s, $\tilde{\nu}$ C≡N), 2202 (s, $\tilde{\nu}$ C≡N), 1631 (w), 1598 (m), 1460 (w), 1375 (w), 1375 (m), 1037 (w), 861 (s), 796 (m), 704 (s), 363 (s), 350 (s), 336 (s)

Elemental analysis: found: C, 49.32; H, 4.12; N, 4.64; calc. for $C_{24}H_{20}Cl_2N_2Pt$ (+0.60 C_4H_8O): C, 49.11; H, 3.87; N, 4.34.

5.4 Substrates for Photocatalytic Experiments

1-(Benzyloxy)-2-iodobenzene (Phenyl-1)

2-Iodophenol (5.00 g, 22.7 mmol, 1.00 eq.) was dissolved in acetone (113 mL) and potassium carbonate (28.3 g, 204 mmol, 9.00 eq.) followed by benzyl bromide (19.43 g, 114 mmol, 5.00 eq.) were added. The mixture was stirred at 65°C for 20 hours. After cooling to room temperature the reaction mixture was filtered and the solvent evaporated. The crude product was subjected to column chromatography (SiO_2, pentane) and the desired product was isolated as a colorless oil (4.73 g, 15.3 mmol, 67%).

^{1}H-NMR (400 MHz, CD_2Cl_2): δ = 7.81 (dt, J=7.9, 1.3 Hz, 1H), 7.51 (dtd, J=7.5, 1.4, 0.7 Hz, 2H), 7.41 (ddt, J=7.1, 6.0, 1.1 Hz, 2H), 7.32 (m, 2H), 6.91 (dd, J=8.3, 1.4 Hz, 1H), 6.74 (tt, J=7.6, 1.0 Hz,1H), 5.51 (s, 2H) ppm.

^{13}C-NMR (101 MHz, CD_2Cl_2): δ = 157.8, 140.1, 137.2, 130.1, 129.1, 128.5, 127.8, 123.3, 113.2, 87.0, 71.4 ppm.

1-((4-(tert-butyl)benzyl)oxy)-2-iodobenzene (*t*BuPhenyl-1)

2-Iodophenol (0.39 g, 1.7 mmol, 1.0 eq.) was dissolved in acetone (8.5 mL) and potassium carbonate (2.07 g, 14.9 mmol, 8.80 eq.) followed by 4-(*tert*-butyl)benzyl bromide (97wt-%, 2.0 g, 8.5 mmol, 1.6 mL, 5.0 eq.) were added. The mixture was stirred at 65°C for 20 hours. After

cooling to room temperature the reaction mixture was filtered and the solvent evaporated. The crude product was subjected to column chromatography (SiO_2, gradient: pentane → pentane/DCM, 10:1) and the desired product was isolated as a white solid (588 mg, 1.64 mmol, 95%).

^{1}H-NMR (400 MHz, CD_2Cl_2): δ = 7.80 (dd, J=7.8, 1.6 Hz, 1H), 7.44 (s, 4H), 7.31 (ddd, J=8.2, 7.4, 1.6 Hz, 1H), 6.92 (dd, J=8.3, 1.4 Hz, 1H), 6.74 (td, J=7.6, 1.4 Hz, 1H), 5.11 (s, 2H), 1.34 (s, 9H) ppm.

^{13}C-NMR (101 MHz, CD_2Cl_2): δ = 157.9, 151.7, 140.0, 134.1, 130.1, 127.7, 126.0, 123.2, 113.2, 87.0, 71.3, 35.0, 31.6 ppm.

2-((2-iodophenoxy)methyl)thiophene (Thio-1)

2-Iodophenol (94 mg, 0.43 mmol, 1.0 eq.) was dissolved in acetone (2.1 mL) and potassium carbonate (531 mg, 3.85 mmol, 9.00 eq.) followed by 3-(bromomethyl)thiophene (250 mg, 2.1 mmol, 0.16 mL, 5 eq.) were added. The mixture was stirred at 65°C for 20 hours. After cooling to room temperature the reaction mixture was filtered and the solvent evaporated. The crude product was subjected to column chromatography (SiO_2, gradient: pentane → DCM) and the desired product was isolated as a colorless oil (109 mg, 0.343 mmol, 80%).

^{1}H-NMR (400 MHz, CD_2Cl_2): δ = 7.80 (dd, J=7.8, 1.6 Hz, 1H), 7.43 (m, 1H), 7.38 (dd, J=5.0, 3.0 Hz, 1H), 7.32 (ddd, J=8.2, 7.4, 1.6 Hz, 1H), 7.22 (dd, J=5.0, 1.3 Hz, 1H), 6.91 (dd, J=8.2, 1.4 Hz, 1H), 6.75 (ddd, J=7.8, 7.4, 1.4 Hz, 1H), 5.14 (s, 2H) ppm.

^{13}C-NMR (101 MHz, CD_2Cl_2): δ = 157.8, 140.1, 138.2, 130.1, 127.4, 126.8, 123.4, 113.2, 87.1, 67.5 ppm.

A Additional Studies

This part summarizes research data which were obtained in the last two months of this thesis and require further investigations to be fully understood.

1.1 Blue Emitting Homoleptic Copper(I) Complex with Chelating Aryl Isocyanide Ligands

In recent years, copper(I) complexes were established as promising candidates in a variety of applications, such as LECs[104,127], OLEDs[4], chromophores in photoinduced electron transfer processes[128–130], and photocatalysis[131–133]. Although copper is earth-abundant, its complexes emerged rather recently as lead structures in photochemical applications. Common to d^{10} metal complexes, their rise was hampered by short excited state lifetimes, low quantum yields and a tendency to lability.[134–136] Over the last decade the understanding of their general photophysical behaviour increased dramatically, and robust complexes with long excited state lifetimes and high luminescence quantum yields were designed.[13–16,137–139] In this context, different ligand system were used in homoleptic as well as heteroleptic complexes, the most prominent being bis-diimine (e.g. bpy, phen) and bis-phosphine (e.g. POP) ligands.[103,140–142]

Monodentate as well as bidentate isocyanides have been less frequently employed in homoleptic complexes than in heteroleptic complexes.[63,64,66,67,131,132,143–149] Although heteroleptic complexes have been explored in terms of their photophysics, as well as application potential in different photo-related fields[131,132,147,148], to the best of my knowledge, only structural studies exist concerning homoleptic Cu(I) isocyanide complexes. One challenge remaining in regards of application, is the design of copper-based blue emitters for usage in OLED devices.[150–152] Heteroleptic complexes are usually preferred over homoleptic ones in terms of photophysical properties. Nevertheless, they tend to be red emitting since their excited state is centered on the ligand with the lowest-energetic π^* orbital, which in many cases is an bis-diimine ligand.

Employing chelating isocyanide ligands in homoleptic complexes should lead to a large HOMO-LUMO splitting, hence resulting in a substantial blue shift of the emission. The chelating ligand in combination with bulky substituents in the α-position to the coordination site should lead to an interlocked structure and thus prevent rapid non-radiative decay via distortion of the excited state.

This project aims at exploring photophysical properties of homoleptic copper(I) complexes

bearing chelating, conjugated isocyanide ligands with regard to their potential application as blue emitters. Additionally, influence of the nature of the backbone and the substituents in the α-position to the coordination site on the photophysical properties shall be identified.

1.1.1 Synthesis of Ligands with a Thiophene Backbone

In order to conduct a systematic study on the influence of the *ortho*-substituents and the chemical nature of the backbone, two additional derivatives of the ligands from previous studies were synthesized. Compared to their parent compounds, both new ligands posses a thiophene backbone instead of the aryl backbone, which increases the bite angle of the coordination site.

The first ligand **CNArSArNC** has methyl groups as *ortho* substituents and is accessible in three steps starting from formamide **10** which was already synthesized in course of the preparation of $\mathbf{CNAr_3NC}$[72] (Fig. A.1).

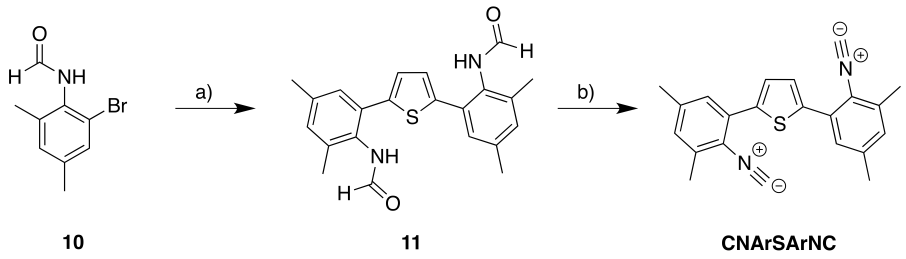

Figure A.1: Synthesis of the methyl substituted ligand **CNArSArNC** bearing a thiophene backbone. a) 2,5-Bis(tris(tetra(butyl))stannyl)thiophene, xylene, 5 mol% [Pd(dppf)Cl_2], 140°C; b) D*i*PA, $POCl_3$, dichloromethane, r.t.

The formamide was coupled to the thiophene backbone in a Stille coupling reaction, yielding the bis(arylformamide)thiophene **11** in 73% yield. The formamide functionalities were transformed to the isocyanides using $POCl_3$ and D*i*PA. The reaction gave the desired ligand **CNArSArNC** in 63% yield. The yield over both steps was 46%.
The second ligand has *tert*-butyl groups as *ortho* substituents. A different synthetic strategy was used in this case, since the related 2-bromo-4,6-di(*iso*-propyl)-*N*-formyl aniline was found to under go neither Stille nor Suzuki-Miyaura coupling under the tested conditions (Fig. A.2). The Stille coupling was performed with the 2-bromo-4,6-di(*tert*-butyl) nitrobenzene **1**, yielding the bis(nitrobenzene) thiophene **12** in excellent yield (98%).

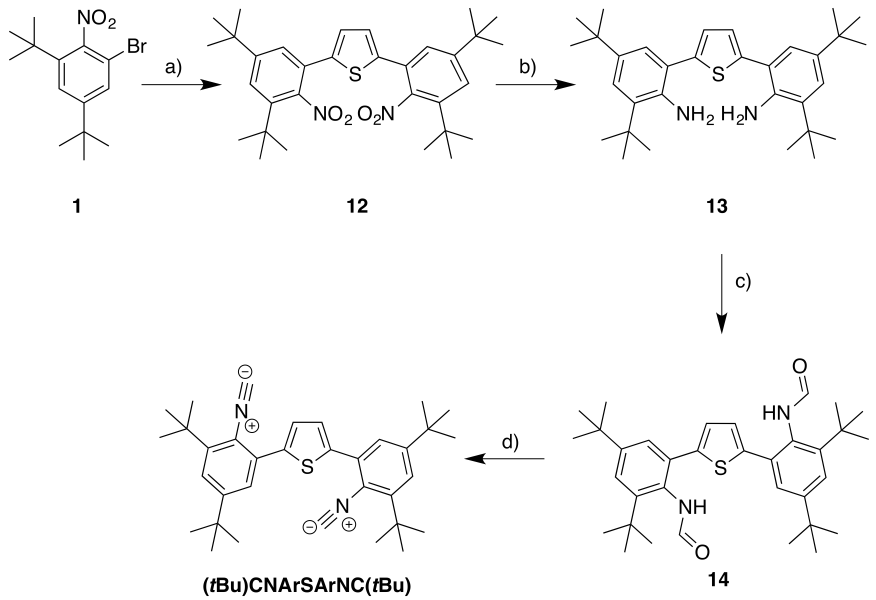

Figure A.2: Synthesis of the thiophene derived, *tert*-butyl substituted ligand **(*t*Bu)CNArSArNC(*t*Bu)**. a) 2,5-Bis((tris(butyl))stannyl) thiophene, xylene, 5 mol% [Pd(dppf)Cl_2], 140°C; b) Zn/hydrazine, MeOH, reflux, overnight, c) acetic acid anhydride, formic acid, reflux, overnight; d) D*i*PA, $POCl_3$, dichloromethane, r.t.

This was followed by a reduction over two steps using zinc powder and hydrazine, giving the diamine **13** in 99% yield over two steps. The diformamide was formed by refluxing the diamine **14** in freshly prepared acetic formic anhydride overnight. The product was isolated by filtration and obtained in 91% yield.
Stirring with D*i*PA and $POCl_3$ at room temperature gave the desired ligand **(*t*Bu)CNArSArNC(*t*Bu)** in moderate yield (45%). The ligand was synthesized via four-step synthesis in an overall yield of 40%.

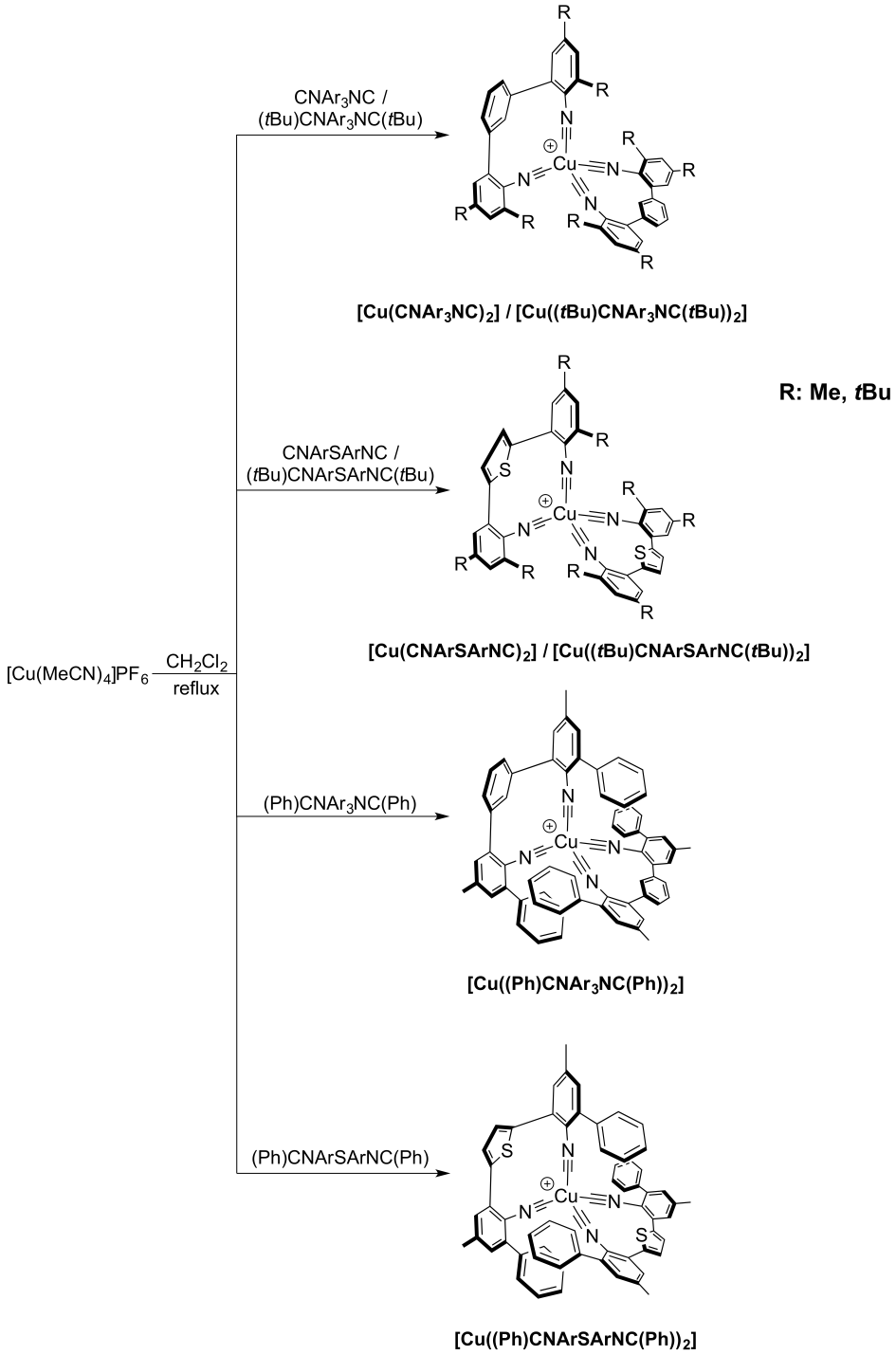

Figure A.3: Synthesis of the six investigated copper(I) complexes.

Six homoleptic copper(I) complexes were synthesized using $[Cu(MeCN)_4]PF_6$ as a precursor complex (Fig. A.3). The respective ligand was refluxed with $[Cu(MeCN)_4]PF_6$ in dry dichloromethane and the pure complex was isolated after removal of the solvent. All complexes showed blue to green emission under irradiation with UV light.

1.1.2 Crystal Structure

It was possible to obtain single crystals of $[Cu(CNAr_3NC)_2]PF_6$ by diffusion of diethyl ether into a saturated solution of the complex in dichloromethane. The obtained X-ray structure is shown in Figure A.4. The complex crystallized in the triclininc space group P-1.

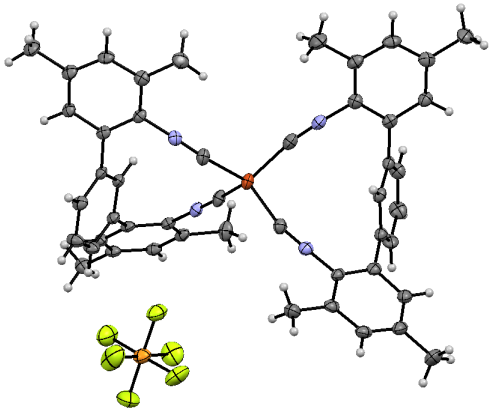

Figure A.4: X-ray structure of $[Cu(CNAr_3NC)_2]PF_6$ obtained by diffusion of diethylether into a saturated dichloromethane solution of $[Cu(CNAr_3NC)_2]PF_6$. Thermal ellipsoids are drawn at the 50% probability level.

The complex is found to be pseudo-tetrahedral with a distinct distortion from the optimal T_d symmetry. The found bite angles of the ligands are 97.7(1)° and 98.5(1)° respectively. The intraligand angles range from 107.0(1)° to 126.00(9)°. The M-C-NR bond is slightly bent from the ideal 180° (162.6(2)°-168.1(2)°). One of the two isocyanide moieties of each ligand is more bent (174.8(2)°, 175.4(2)°) than the other (178.6(2)°, 179.2(2)°). The torsion angle between the backbone phenyl ring and the phenyls bearing the isocyanides is between 52.4(3)° and 60.9(3)°.
The M-CNR bond length vary slightly from 1.945(2) to 1.958(3) Å.

1.1.3 IR-Spectroscopy

The solid state FTIR-spectra of the free ligands (I-V a)) and their corresponding copper(I) complexes (I-V b)) are shown in Figure A.5. They are ordered by increasing bulk of the substituent (from top to bottom) and the nature of the backbone (aryl on the left, thiophene on the right).
The vibrational band of the C≡N moieties is very similar for all ligands with alkyl substituents in *ortho* position (approx. 2111 cm^{-1}) and independent of the backbone. The band shifts slightly to higher wavenumbers for ligands bearing phenyl rings as *ortho* substituents.
The isocyanide vibrational bands of the complexes vary slightly (2149 - 2157 cm^{-1}) but show

no explicit trend.
The shift of the isocyanide band to higher wavenumbers compared to the free ligand is in good agreement with reduced π-backbonding in the presence of positively charged metal centres leading to a bigger contribution of the σ-acceptor capability of the metal, and therefore to a stabilisation of the isocyanide bond.

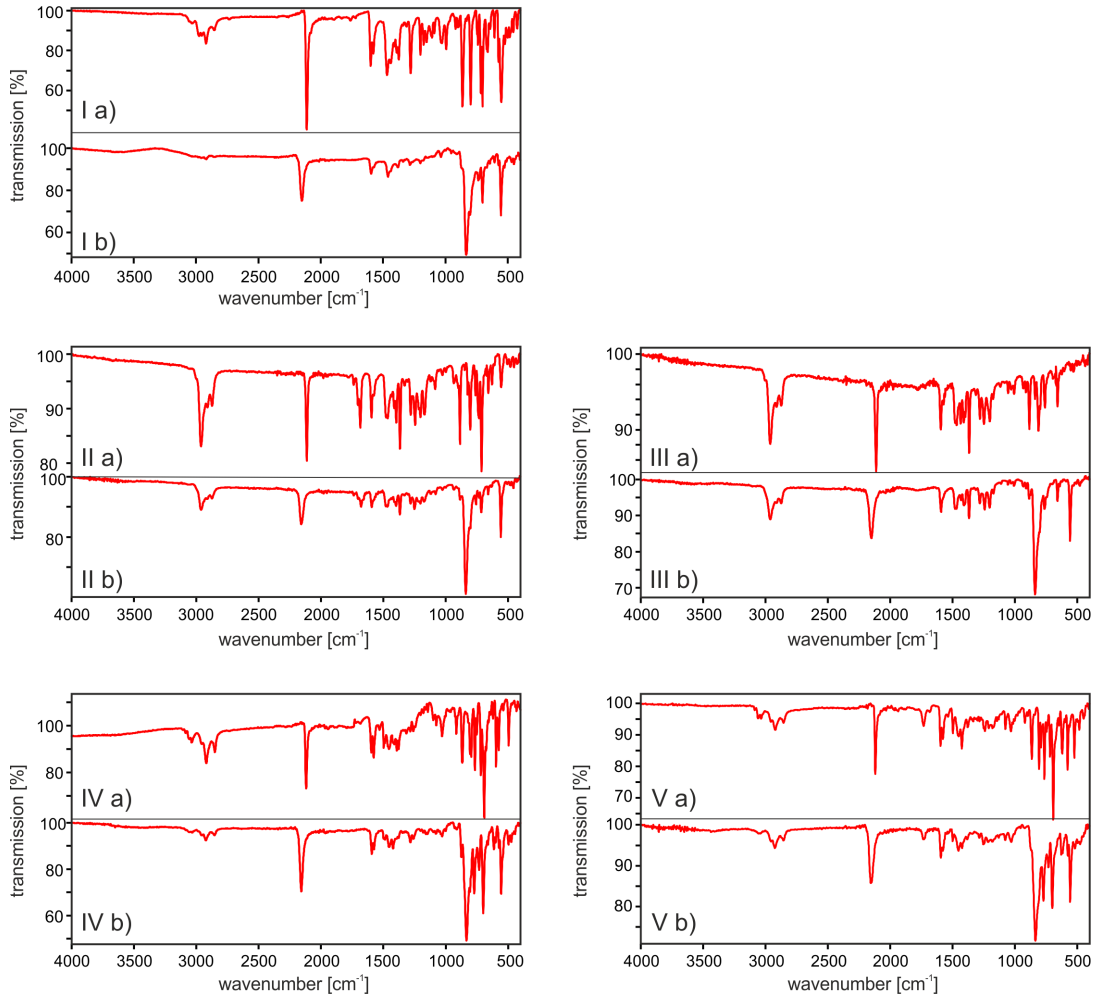

Figure A.5: Solid state FTIR-Spectra of a) the free ligands and b) their corresponding copper(I) complexes. I) (a) $CNAr_3NC$, (b)$[Cu(CNAr_3NC)_2]PF_6$;
II) (a) (tBu)$CNAr_3NC$(tBu), (b) $[Cu((tBu)CNAr_3NC(tBu))_2]PF_6$;
III) (a) (tBu)CNArSArNC(tBu), (b) $[Cu((tBu)CNArSArNC(tBu))_2]PF_6$;
IV) (a) (Ph)$CNAr_3NC$(Ph), (b) $[Cu((Ph)CNAr_3NC(Ph))_2]PF_6$;
V) (a) (Ph)CNArSArNC(Ph), (b) $[Cu((Ph)CNArSArNC(Ph))_2]PF_6$.

1.1.4 Electrochemistry

The electrochemical properties of the copper complexes were investigated using cyclic voltammetry. The measurements were conducted with 0.1M $TBAPF_6$ in dichloromethane using a glassy carbon working electrode and two silver wires as counter electrode and quasi reference

electrode. The potentials were referenced versus the $Fc^{+/0}$ redox couple as internal standard. Figure A.6 shows the obtained cyclic voltammograms. On first sight the voltammograms show very little resemblance to each other and no fully reversible processes are found. Nevertheless, there are three general oxidation processes observed at potentials above 0 V vs $Fc^{+/0}$. The first one is observed slightly below 0.5 V (green box, **A**), a second one around 0.8 V (blue box, **B**) and the third around 1.4 V (both red boxes, **C**). The waves of the reduction cycles vary strongly in their position and intensity.

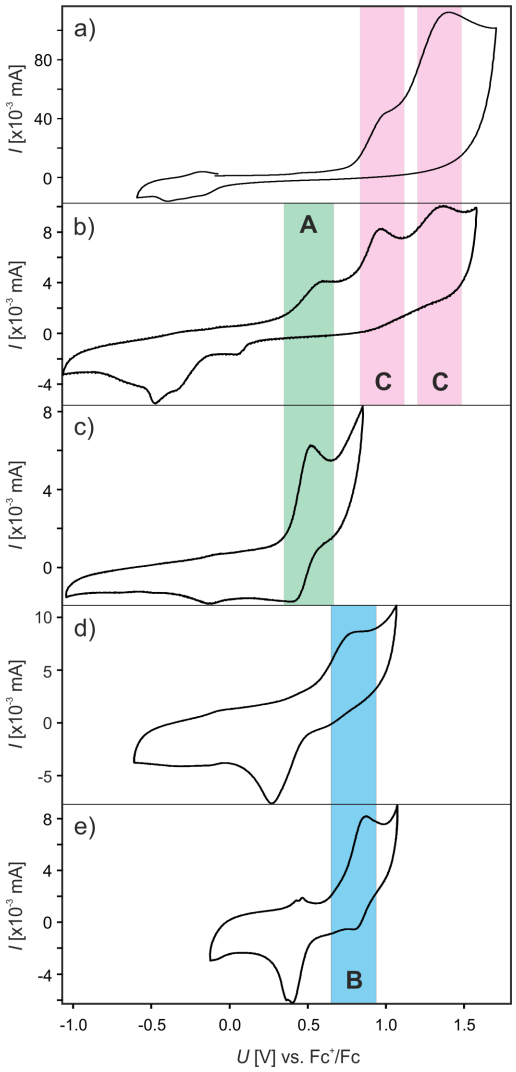

Figure A.6: Cyclic voltammograms of a) $[Cu((tBu)CNArSArNC(tBu))_2]PF_6$, b) $[Cu((Ph)CNAr_3NC(Ph))_2]PF_6$, c) $[Cu(CNAr_3NC)_2]PF_6$, d) $[Cu((tBu)CNAr_3NC(tBu))_2]PF_6$, e) $[Cu((Ph)CNArSArNC(Ph))_2]PF_6$. The measurements were performed using approx. 0.1 mM solutions of the copper(I) complexes with 0.1 M $TBAPF_6$ as supporting electrolyte in DCM at 20°C. A glassy carbon working electrode, and two silver wires as counter and quasi reference electrode were used. The scan rate was 0.1 Vs^{-1}. The potential was referenced versus $Fc^{+/0}$.

$[Cu((tBu)CNAr_3NC(tBu))_2]PF_6$ exhibits the simplest redox chemistry (Fig. A.6 d). It is irreversibly oxidized at 0.66 V and a reduction process is observed at 0.39 V resembling to some extent the behaviour of $[Ni((Ph)CNArSArNC(Ph))_2]$ (see Chapter 3.4.3). As already discussed in the case of the nickel(0) complex, the large splitting between the oxidation and reduction processes might indicate that, upon oxidation of the compound, a reversible reaction is taking place on the time scale of the experiment. The nature of this reaction remains unknown, but it is possible that the uptake of a fifth or even sixth ligand is involved.[118,119]
The voltammogram of $[Cu(CNAr_3NC)_2]PF_6$ (Fig. A.6 c)) shows a similar pattern, although at lower potentials. The oxidative process takes place at 0.45 V and a less easily detectable reduction process is observed in the reductive cycle at 0.49 V. A second wave is found in the reductive cycle at -0.06 V. The splitting between this wave and the one in the oxidative cycle is in the same order of magnitude as the one in the voltammogram of $[Cu((tBu)CNAr_3NC(tBu))_2]PF_6$ and may have the same origin.
The cyclic voltammogram of the related $[Cu((tBu)CNArSArNC(tBu))_2]PF_6$ shows two, instead of one, waves in the oxidative cycle (Fig. A.6 a)) - one at 0.66 V and the second at 1.12 V. Both of them are irreversible. The first one is shifted by +0.24 V compared to the one observed in the derivative with an aryl backbone. After the first cycle three additional waves are arising below 0 V - one in the oxidative cycle at -0.25 V and two at -0.10 V and -0.35 V in the reductive cycle.
Figure A.6 e) depicts the cyclic voltammogram of $[Cu((Ph)CNArSArNC(Ph))_2]PF_6$. An oxidation is observed at 0.79 V in the oxidative cycle and in the reductive cycle a weak wave is found at 0.86 V. The main wave in the reductive cycle is located at 0.46 V with a shoulder at 0.36 V. Again, the same structure is observed for a weak wave in the oxidative cycle at 0.46 V and 0.43 V. Again the rather large splitting between the intense waves of the oxidative and reductive cycle might indicate a reaction taking place. The presence of small waves assigned to the corresponding reversible process points to a process with kinetics comparable to the electron transfer kinetics.
The complex $[Cu((Ph)CNAr_3NC(Ph))_2]PF_6$ exhibits by far the richest electrochemistry (Fig. A.6 b)). The oxidative cycle shows three well separated oxidation process at 0.48 V, 0.88 V and 1.24 V. All of them are irreversible. In the reductive cycle three reduction waves are observed at 0.08 V, -0.26 V and -0.44 V.
The observed redox waves for the different complexes are listed in Table A.1.
In general, one would expect to observe one reversible oxidation wave for the $Cu^{2+/+}$ couple. The oxidation wave observed for $[Cu(CNAr_3NC)_2]PF_6$ and $[Cu((Ph)CNArSArNC(Ph))PF_6$ at 0.45 V and 0.48 V, respectively (Fig. A.6, green box **A**), is assigned to the $Cu^{2+/+}$ oxidation in the unperturbed complexes. These potentials are in good agreement with the value of 0.31 V reported for a $[copper(phenanthroline)(bisisocyanide)]^+$ complex by KNORN et al.[131] The slight anodic shift in case of the here-presented complexes is likely due to the enhanced stabilisation of the Cu(I) center by the additional isocyanide ligand.

A second set of potentials observed at 0.66 V and 0.79 V, respectively, is found for the complexes $[Cu((t\text{Bu})CNAr_3NC(t\text{Bu}))_2]PF_6$ and $[Cu((Ph)CNArSArNC(Ph))_2]PF_6$ (Fig. A.6, blue box **B**). This set is also assigned to the $Cu^{2+/+}$ redox couple. The pronounced anodic shift compared to the first set is thought to illustrate a significant increase in repulsive steric interactions upon oxidation of the metal center. These repulsions possibly originate from distortion of the coordination sphere from tetrahedral to planar. The extent of steric repulsion depends on the steric demand of the *ortho*-substituents of the ligand, as well as on the planarity of the ligand scaffold. In a tetrahedral coordination geometry, the scaffold of (Ph)CNArSAr(Ph) is expected to be more planar than the one of $(t\text{Bu})CNAr_3NC(t\text{Bu})$, since the bite angle between the isocyanide moieties of (Ph)CNArSAr(Ph) is larger than of $(t\text{Bu})CNAr_3NC(t\text{Bu})$. Therefore, a change of the geometry towards a more planar complex structure leads to stronger repulsive inter ligand interactions, resulting in a less favoured oxidation process in the case of $[Cu((Ph)CNArSArNC(Ph))]PF_6$. This is illustrated by a shift of 0.13 V to higher potentials.

Table A.1: Redox potentials of different Cu(I) complexes vs. $Fc^{+/0}$ in dichloromethane at 20°C.

Compound	E_{pa} [V]	E_{pc} [V]
$[Cu(CNAr_3NC)_2]PF_6$	0.45	0.49
		-0.06
$[Cu((t\text{Bu})CNAr_3NC(t\text{Bu}))_2]PF_6$	0.66	0.39
$[Cu((t\text{Bu})CNArSArNC(t\text{Bu}))_2]PF_6$	1.12	-0.10
	0.90	
	-0.25	-0.35
$[Cu((Ph)CNAr_3NC(Ph))_2]PF_6$	1.24	0.08
	0.88	-0.26
	0.48	-0.44
$[Cu((Ph)CNArSArNC(Ph))_2]PF_6$	0.79	0.86
	0.46	0.46
	0.43	0.36

Potentials referenced vs. $Fc^{+/0}$ in dichloromethane, *this work*.

The third set consists of two waves (around 0.9 V and 1.1 V) and occurs in the cyclic voltammograms of $[Cu((t\text{Bu})CNArSArNC(t\text{Bu}))_2]PF_6$ and $[Cu((Ph)CNAr_3NC(Ph))_2]PF_6$. In $[Cu((t\text{Bu})CNArSArNC(t\text{Bu}))_2]PF_6$ these waves are the most easily detectable bands, ob-

served at 0.90 V and 1.12 V.
In $[Cu((Ph)CNAr_3NC(Ph))_2]PF_6$ this particular set is found at 0.88 V and 1.24 V, in addition to the unperturbed $Cu^{2+/+}$ oxidation of the original complex. This set of two waves might belong to a dimeric species that are formed from the monomeric complex in solution. The presence of two bands in this case could indicate an electronic interaction between two copper centres. The observation of the original $Cu^{2+/+}$ wave in $[Cu((Ph)CNAr_3NC(Ph))_2]PF_6$ points to a possible equilibrium between the different species in solution, whereas the absence of this wave in $[Cu((t\text{Bu})CNArSArNC(t\text{Bu}))_2]PF_6$ might indicate the suspected dimer being the major species present in solution. This reasoning is similar to the case of the shifted oxidation potential discussed above. Due to an increase in steric repulsion, the $[Cu((t\text{Bu})CNArSArNC(t\text{Bu}))_2]PF_6$ complex dissociates upon oxidation, forming the potential dimer. In contrast to $[Cu((Ph)CNArSArNC(Ph))_2]PF_6$, the complex appears to readily dissociate upon oxidation. The less favoured dissociation of $[Cu((Ph)CNArSArNC(Ph))_2]PF_6$ might be explained by the ability of a phenyl substituent to arrange itself planar to the second, flat ligand scaffold to allow a more planar configuration. The spherical structure of the *tert*-butyl groups does not allow for such an arrangement, thus a planarization of the complex might lead to ligand dissociation followed by rapid dimer formation.

1.1.5 Excited State Properties

Emission Behaviour in Fluid Solution

Figure A.7 shows the absorption spectra (solid traces) of the prepared copper(I) complexes, as well as the normalized steady-state emission spectra (dashed traces) in deaerated dichloromethane at room temperature. The spectra a) - c) belong to complexes bearing ligands with an aryl backbone in the order of increasing bulk of the *ortho* substituents and the spectra d) - f) belong to the complexes with a thiophene backbone in the same order.
All of the complexes show one or two absorption bands between 230 and 400 nm which shift to longer wavelength with increasing size of the *ortho* substituents, as well as upon exchange of an aryl backbone to a thiophene backbone. Since no well separated ^{1}MLCT absorption bands are observed, as it is the case for e.g. bis(diimine) complexes of copper(I), a definite assignment of certain bands to specific electronic transitions is not made.
All complexes are emissive in fluid solution at room temperature, with emission maxima between 418 nm and 442 nm, and show a relatively large STOKES shift in the magnitude of approximately 100 nm. This is a typical observation for d^{10} metal complexes exhibiting emission from an excited MLCT state, since they tend to undergo large geometrical distortions upon excitation.[13]
Except for $[Cu(CNAr_3NC)_2]PF_6$ (Fig. A.7 a)) all complexes show well-defined emission bands. The emission maxima of the complexes with an aryl backbone are lower in energy than the ones of the complexes with a thiophene backbone (Tab. A.2). The shift gets less pro-

nounced with increasing bulk of the substituent, leading to $[Cu((Ph)CNAr_3NC(Ph))_2]PF_6$ and $[Cu((Ph)CNArSArNC(Ph))_2]PF_6$ having the same emission maximum.

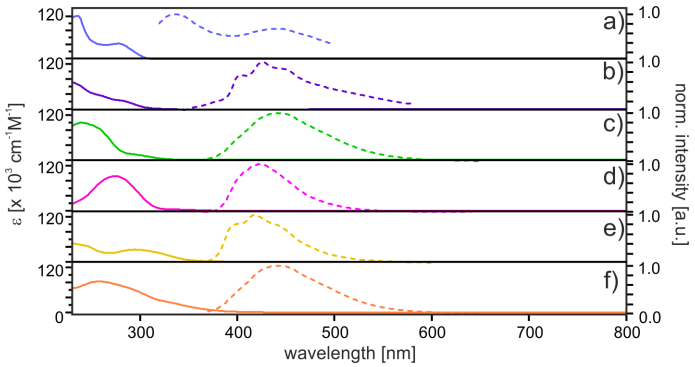

Figure A.7: Absorption (solid traces) and steady-state emission spectra of
a) $[Cu(CNAr_3NC)_2]PF_6$ (blue traces, λ_{ex}:365 nm),
b) $[Cu((t\text{Bu})CNAr_3NC(t\text{Bu}))_2]PF_6$ (purple traces, λ_{ex}:300 nm),
c) $[Cu((Ph)CNAr_3NC(Ph))_2]PF_6$ (green traces, λ_{ex}:350 nm),
d) $[Cu(CNArSArNC)_2]PF_6$ (magenta traces, λ_{ex}:300 nm),
e) $[Cu((t\text{Bu})CNArSArNC(t\text{Bu}))_2]PF_6$ (yellow traces, λ_{ex}:350 nm),
f) $[Cu((Ph)CNArSArNC(Ph))_2]PF_6$ (orange traces, λ_{ex}:350 nm)
in deaerated dichloromethane at 20°C. Solutions of the complexes had concentrations between 1×10^{-5} - 2×10^{-5} M.

The emission behaviour of $[Cu(CNAr_3NC)_2]PF_6$ is rather unique. It shows one or two emission bands after excitation at 280 nm depending if the solution is freshly prepared (two bands) or was left standing under air overnight (one band). The first band is observed at 338 nm and is therefore much higher in energy than the emission bands found for the other complexes, whilst the second band has a maximum at 442 nm, resembling the behaviour of the other complexes. The second band diminishes if the solution is left standing in aerated solvents. The process is also observed if the solution is stored in the dark. The second emission band is slowly regained over the course several freeze-pump-thaw cycles until it exceeds its initial intensity. Up to now, it was not possible to find a satisfying explanation for this phenomenon, although a coordination of O_2 might play a role in this.

Table A.2: Emission maxima of the copper(I) complexes in dichloromethane solution at 20°C.

Compound	λ_{max} [nm]
$[Cu(CNAr_3NC)_2]PF_6$	338, 442
$[Cu(CNArSArNC)_2]PF_6$	423
$[Cu((t\text{Bu})CNAr_3NC(t\text{Bu}))_2]PF_6$	403[a], 426, 452[a]
$[Cu((t\text{Bu})CNArSArNC(t\text{Bu}))_2]PF_6$	397[a], 418, 442[a]
$[Cu((\text{Ph})CNAr_3NC(\text{Ph}))_2]PF_6$	442
$[Cu((\text{Ph})CNArSArNC(\text{Ph}))]PF_6$	442

[a] observed as shoulders.

The emission bands in general are broad and unstructured, except for complexes with *tert*-butyl substituents. The emission bands of each of these two complexes show three well-defined band structures . These bands show a separation of 1345 cm^{-1} for $[Cu((t\text{Bu})CNAr_3NC(t\text{Bu}))_2]$-$PF_6$ and 1282 cm^{-1} for $[Cu((t\text{Bu})CNArSArNC(t\text{Bu}))_2]PF_6$, and are probably due to vibrational modes of the ligands.

Emission Behaviour in Organic Glasses at 77 K

Figure A.8 shows the steady-state emission spectra of four copper(I) complexes bearing ligands with *tert*-butyl (a and c) and phenyl subtsituents (b and d) in dichlormethane at room temperature (black traces) and in *n*-butyronitrile at 77 K. The upper spectra belong to the complexes with ligands including an aryl backbone, and the lower ones to complexes with thiophene derived ligands.

In general, one expects a blue shift of the emission band at low temperature compared to room temperature, caused by the prevention of thermal population of vibrational states and rigidochromic effects for MLCT excited states. This is indeed observed for complexes with thiophene based ligands and both complexes exhibit emission maxima at approx. 405 nm (Fig. A.8 c-d)). In the case of $[Cu((\text{Ph})CNArSArNC(\text{Ph}))_2]PF_6$, two vibrational bands arise at low temperature (1317 cm^{-1} and 1134 cm^{-1}). The band structure visible at room temperature for both complexes bearing *tert*-butyl substituents is not observed at 77 K.

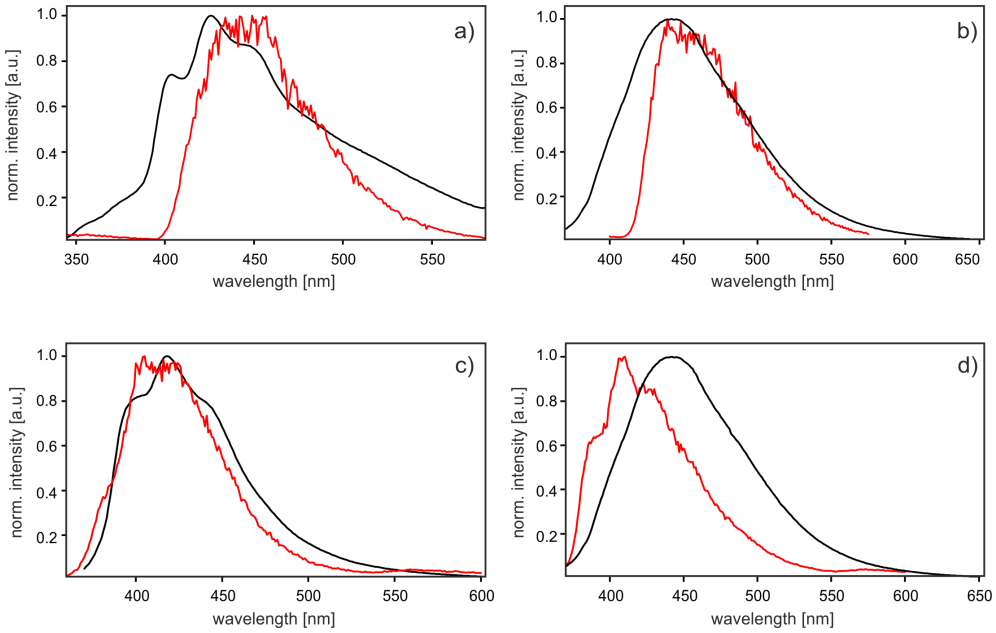

Figure A.8: Steady-state emission spectra in deaerated dichloromethane at 20°C (black traces) and in *n*-butyronitrile at 77 K (red traces) of a) $[Cu((tBu)CNAr_3NC(tBu))_2]PF_6$, b) $[Cu((Ph)CNAr_3NC(Ph))_2]PF_6$, c) $[Cu((tBu)CNArSArNC(tBu))_2]PF_6$ and d) $[Cu((Ph)CNArSArNC(Ph))_2]PF_6$.

The emission bands of the complexes with an aryl backbone in the ligand shift unexpectedly to lower energies at low temperature (Fig. A.8 a-b) and Tab. A.3). This could be due to emission occurring from thermally activated state at room temperature.

Table A.3: Emission maxima of the copper(I) complexes in a *n*-butyronitrile matrix at 77 K.

Compound	λ_{max} [nm]
$[Cu((tBu)CNAr_3NC(tBu))_2]PF_6$	449
$[Cu((tBu)CNArSArNC(tBu))_2]PF_6$	405
$[Cu((Ph)CNAr_3NC(Ph))_2]PF_6$	442
$[Cu((Ph)CNArSArNC(Ph))]PF_6$	386[a], 410, 436[a]

[a] observed as shoulders.

Excitation-Wavelength-Dependent Emission of $[Cu((Ph)CNArSArNC(Ph))_2]PF_6$

The emission of $[Cu((Ph)CNArSArNC(Ph))_2]PF_6$ is excitation-wavelength-dependent in fluid solution at room temperature as well as in an organic matrix at 77 K (Fig. A.9).
This is a rarely observed phenomenon. Even in the few cases reported for molecular, mononuclear transition metal complexes, only two well separated emission bands were observed.[153]

Usually in these studies, the interchange from one emitting state to the second occurs at a well defined wavelength.

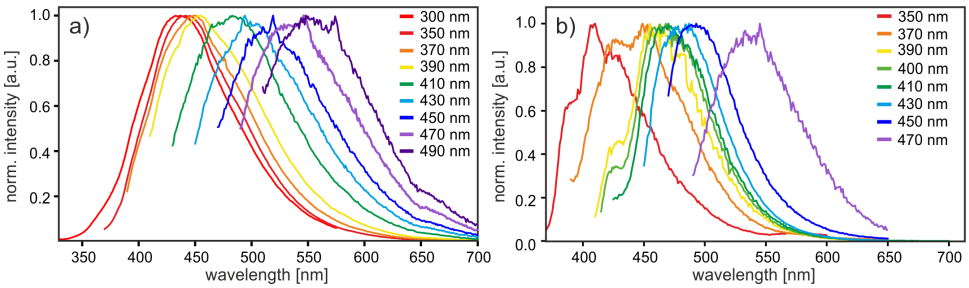

Figure A.9: Steady-state emission spectra of $[Cu((Ph)CNArSArNC(Ph))_2]PF_6$ recorded at different excitation wavelength in a) deaerated dichloromethane at 20°C and b) *n*-butyronitrile at 77 K.

The reports on "continuous" excitation-dependent emission are even rarer.[154,155] This effect is generally ascribed to the presence of different species in solution. Taking the implication of a potential dimeric species from the cyclic voltammetric experiments into account, the presence of different species seems a reasonable explanation, but this remains speculative at present.

In Figure A.9 a) the emission appears to shift approximately linearly with the excitation wavelength until the difference between the emission spectra increases, starting from an excitation wavelength of 410 nm. This wavelength corresponds well with the end of lowest energy absorption band of the complex and might point to a minor species being now the emitter.

The situation is somewhat different in an organic matrix at 77 K (A.8 b)). Large shifts in the emission maxima are observed at low excitation wavelengths (350- 390 nm) as well as a gradual disappearance of the vibrational structure. This is followed by an interval of comparably small shifts of the emission maximum (λ_{ex}: 390-410 nm), followed by a narrow regime of intermediate shifts (λ_{ex}: 430-450 nm). The emission spectrum obtained with the lowest excitation wavelength differs strongly from the others (λ_{ex}: 470 nm). This more complex excitation dependency could be caused by additional conformers which can no longer freely interconvert into one another.

Emission Behaviour in the Solid State

Since some applications rely more on the emission properties of complexes in the solid state than in solution (e.g. OLEDs and LECs), the solid state emission spectra of several complexes were recorded (Fig. A.10 a-e)).

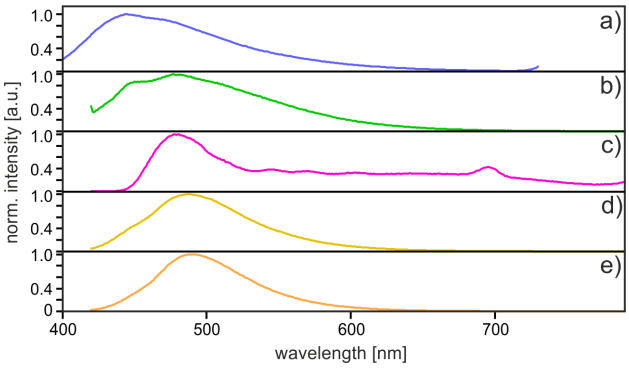

Figure A.10: Powder emission spectra of a) $[Cu(CNAr_3NC)_2]PF_6$, b) $[Cu((tBu)CNAr_3NC(tBu))_2]PF_6$, c)$[Cu((Ph)CNAr_3NC(Ph))_2]PF_6$, d) $[Cu((tBu)CNArSArNC(tBu))_2]PF_6$, e) $[Cu((Ph)CNArSArNC(Ph))_2]PF_6$ at room temperature.

Most of the spectra show a relatively broad, unstructured emission band between 445-490 nm. The emission spectrum of $[Cu((Ph)CNAr_3NC(Ph))_2]PF_6$ shows the expected emission maximum in this range, but instead of approaching the baseline with increasing wavelength, the emission reaches a plateau in intensity of roughly 35% of the maximal intensity observed. This remaining emission decreases over a very broad range of the spectrum and does not reach zero in the recorded range. The origin of this broad emission is not yet understood.

Table A.4: Emission maxima of the copper(I) complexes in the solid state.

Compound	λ_{max} [nm]
$[Cu(CNAr_3NC)_2]PF_6$	445
$[Cu((tBu)CNAr_3NC(tBu))_2]PF_6$	450[a], 477
$[Cu((tBu)CNArSArNC(tBu))_2]PF_6$	488
$[Cu((Ph)CNAr_3NC(Ph))_2]PF_6$	480
$[Cu((Ph)CNArSArNC(Ph))]PF_6$	491

[a] observed as shoulders.

The observed emission maxima are summarized in Tab. A.4. Increasing size of the substituents on the ligand leads to a significant red-shift of the emission band. Exchanging the backbone aryl for a thiophene induces a shift of the emission maximum of 11 nm to the red in both complex pairs. This might be caused by a lowering of the ligand based π^*-orbital due to the more planar structure of the ligand, resulting from a larger bite angle of the isocyanide moiety.

1.1.6 Summary

In total, six new copper(I) bis(arylbisisocyanide) complexes were prepared. For one of the complexes, a crystal structure was obtained and a pseudo-tetrahedral coordination geometry found. All of the complexes showed blue to green emission in solution and in the solid state. The large STOKES shift indicates a significant geometrical distortion of the excited state. This is caused by a formal oxidation of Cu(I) to Cu(II) upon a MLCT transition, leading to a flattenting of the tetrahedral geometry.
The electrochemistry of these complexes mirrors a diverse interplay of steric demand of the substituents, as well as the bite angle of the coordination site. The behaviour of two of the prepared complexes indicate the potential presence of several species in solution. One of these two complexes seems to show excitation-wavelength-dependent emission.
The complexes bearing ligands with a thiophene backbone show the expected blue shift in low temperature emission spectra compared to the ones at room temperature. The emission bands of complexes with aryl-based ligand scaffolds exhibit a red shift upon cooling to 77 K. This suggests the presence of a thermally activated state from which the emission originates at room temperature.
The solid state emission bands shift to the red with increasing substituent size and the exchange of the backbone aryl for a thiophene leads to further decrease of the emission energy. It is possible to prepare stable copper(I) bis(arylbisisocyanide) complexes which are blue emitters. Their electrochemical and photophysical properties strongly depend on the nature of the *ortho* substituents and the bite angle of the coordination site. These diverse interactions lead to a manifold of unexpected effects, including excitation-wavelength-dependent emission, a red shift of emission bands at low temperature, as well as very broad emission band of one of the complexes in the solid state.
Homoleptic copper(I) complexes with chelating isonitrile ligands were found to be a new class of blue emitters that exhibit a series of unusual photophysical behaviours. In order to gain a deeper insight in the origin of these rather unusual phenomena, more detailed studies are necessary. Particularly, the structure of the different complexes in solution is of interest and could be examined by means of IR-spectroscopy. Determination of the lifetimes for the excited states could give some hint toward the nature of the emitting state.

Bibliography

[1] N. Armaroli, V. Balzani, *Chem. Eur. J.* **2016**, *22*, 32–57.

[2] T. Ameri, N. Li, C. J. Brabec, *Energy Environ. Sci.* **2013**, *6*, 2390–2413.

[3] http://www.infomine.com/investment/metal-prices/; visited: 26.07.2016.

[4] B. Bozic-Weber, E. C. Constable, C. E. Housecroft, *Coord. Chem. Rev.* **2013**, *257*, 3089–3106.

[5] K. R. Mann, M. Cimolino, G. L. Geoffroy, G. S. Hammond, A. A. Orio, G. Albertin, *Inorg. Chim. Acta* **1976**, *16*, 97–101.

[6] K. R. Mann, H. B. Gray, G. S. Hammond, *J. Am. Chem. Soc.* **1977**, *99*, 306–307.

[7] W. Sattler, M. E. Ener, J. D. Blakemore, A. A. Rachford, P. J. Labeaume, J. W. Thackeray, J. F. Cameron, J. R. Winkler, H. B. Gray, *J. Am. Chem. Soc.* **2013**, *6*, 10614–10617.

[8] W. Sattler, L. M. Henling, J. R. Winkler, H. B. Gray, *J. Am. Chem. Soc.* **2015**, *137*, 1198–1205.

[9] H. Lesnard, T. Cantat, P. Le Floch, I. Demachy, Y. Jean, *Chem. Eur. J.* **2007**, *13*, 2953–2965.

[10] C. E. Housecroft, A. G. Sharpe, *Inorganic Chemistry*. 4. ed. **2012**, Pearson Education Limited, 649–650.

[11] P. Atkins, J. de Paula, *Physical Chemistry*. 10. ed. **2014**, Oxford University Press, 535–536.

[12] M. Montalti, A. Credi, L. Prodi, M. T. Gandolfi, *Handbook of Photochemistry*. 3. ed. **2006**, CRC Press.

[13] M. Iwamura, S. Takeuchi, T. Tahara, *Acc. Chem. Res.* **2015**, *48*, 782–791.

[14] A. Lavie-Cambot, M. Cantuel, Y. Leydet, G. Jonusauskas, D. M. Bassani, N. D. McClenaghan, *Coord. Chem. Rev.* **2008**, *252*, 2572–2584.

[15] T. Hofbeck, U. Monkowius, H. Yersin, *J. Am. Chem. Soc.* **2015**, *137*, 399–404.

[16] R. Czerwieniec, H. Yersin, *Inorg. Chem.* **2015**, *54*, 4322–4327.

[17] V. Balzani, A. Juris, F. Barigelletti, S. Campagna, P. Belser, A. Von Zelewsky, *Coord. Chem. Rev.* **1988**, *84*, 85–277.

[18] A. Vlček, Jr., *Coord. Chem. Rev.* **1998**, *177*, 219–256.

[19] C. R. Bock, J. A. Connor, A. R. Gutierrez, T. J. Meyer, D. G. Whitten, B. P. Sullivan, J. K. Nagle, *J. Am. Chem. Soc.* **1979**, *101*, 4815–4824.

[20] M. Julliard, M. Chanon, *Chem. Rev.* **1983**, *83*, 425–506.

[21] I. R. Gould, S. Farid, *Acc. Chem. Res.* **1996**, *29*, 522–528.

[22] R. A. Marcus, N. Sutin, *Biochim. Biophys. Acta* **1985**, *811*, 265–322.

[23] N. A. Romero, D. A. Nicewicz, *Chem. Rev.* **2016**, *116*, 10075–10166.

[24] A. Studer, D. P. Curran, *Nat. Chem.* **2014**, *6*, 765–773.

[25] A. Studer, D. P. Curran, *Angew. Chem. Int. Ed.* **2011**, *50*, 5018–5022.

[26] W. Liu, H. Cao, H. Zhang, H. Zhang, K. H. Chung, C. He, H. Wang, F. Y. Kwong, A. Lei, *J. Am. Chem. Soc.* **2010**, *132*, 16737–16740.

[27] C.-L. Sun, H. Li, D.-G. Yu, M. Yu, X. Zhou, X.-Y. Lu, K. Huang, S.-F. Zheng, B.-J. Li, Z.-J. Shi, *Nat. Chem.* **2010**, *2*, 1044–1049.

[28] E. Shirakawa, K. I. Itoh, T. Higashino, T. Hayashi, *J. Am. Chem. Soc.* **2010**, *132*, 15537–15539.

[29] M. Rueping, M. Leiendecker, A. Das, T. Poisson, L. Bui, *Chem. Commun.* **2011**, *47*, 10629–10631.

[30] E. Shirakawa, X. Zhang, T. Hayashi, *Angew. Chem. Int. Ed.* **2011**, *50*, 4671–4674.

[31] E. Doni, S. Zhou, J. A. Murphy, *Molecules* **2015**, *20*, 1755–1774.

[32] C.-L. Sun, Y.-F. Gu, W.-P. Huang, Z.-J. Shi, *Chem. Commun.* **2011**, *47*, 9813–9815.

[33] C. L. Sun, Y. F. Gu, B. Wang, Z. J. Shi, *Chem. Eur. J.* **2011**, *17*, 10844–10847.

[34] G.-P. Yong, W.-L. She, Y.-M. Zhang, Y.-Z. Li, *Chem. Commun.* **2011**, *47*, 11766–11768.

[35] K. S. Masters, S. Bräse, *Angew. Chem. Int. Ed.* **2013**, *52*, 866–869.

[36] J. Cuthbertson, V. J. Gray, J. D. Wilden, *Chem. Commun.* **2014**, *50*, 2575–2578.

[37] M. E. Budén, J. F. Guastavino, R. A. Rossi, *Org. Lett.* **2013**, *15*, 1174–1177.

[38] T. Kawamoto, A. Sato, I. Ryu, *Org. Lett.* **2014**, *16*, 2111–2113.

[39] X. Zheng, L. Yang, W. Du, A. Ding, H. Guo, *Chem. Asian J.* **2014**, *9*, 439–442.

[40] Z. Xu, L. Gao, L. Wang, M. Gong, W. Wang, R. Yuan, *ACS Catal.* **2015**, *5*, 45–50.

[41] Y. Cheng, X. Gu, P. Li, *Org. Lett.* **2013**, *15*, 2664–2667.

[42] L. Zhang, H. Yang, L. Jiao, *J. Am. Chem. Soc.* **2016**, *138*, 7151–7160.

[43] L. Pause, M. Robert, J. M. Savéant, *J. Am. Chem. Soc.* **1999**, *121*, 7158–7159.

[44] S. P. Pitre, C. D. McTiernan, J. C. Scaiano, *Acc. Chem. Res.* **2016**, *49*, 1320–1330.

[45] K. L. Skubi, T. R. Blum, T. P. Yoon, *Chem. Rev.* **2016**, *116*, 10035–10074.

[46] M. H. Shaw, J. Twilton, D. W. C. MacMillan, *J. Org. Chem.* **2016**, *81*, 6898–6926.

[47] S. Dadashi-Silab, S. Doran, Y. Yagci, *Chem. Rev.* **2016**, *116*, 10212–10275.

[48] N. Zhang, S. R. Samanta, B. M. Rosen, V. Percec, *Chem. Rev.* **2014**, *114*, 5848–5958.

[49] M. D. Kärkäs, J. A. Porco, Jr., C. R. J. Stephenson, *Chem. Rev.* **2016**, *116*, 9683–9747.

[50] D. Ravelli, S. Protti, M. Fagnoni, *Chem. Rev.* **2016**, *116*, 9850–9913.

[51] C. K. Prier, D. A. Rankic, D. W. C. MacMillan, *Chem. Rev.* **2013**, *113*, 5322–5363.

[52] I. Ghosh, T. Ghosh, J. I. Bardagi, B. König, *Science* **2014**, *346*, 725–728.

[53] L. Shaw, C. Langford, *Coord. Chem. Rev.* **2002**, *230*, 165–169.

[54] H. Kvapilová, W. Sattler, A. Sattler, I. V. Sazanovich, I. P. Clark, M. Towrie, H. B. Gray, S. Záliš, A. Vlček, *Inorg. Chem.* **2015**, *54*, 8518–8528.

[55] J. E. Monat, J. K. McCusker, *J. Am. Chem. Soc.* **2000**, *122*, 4092–4097.

[56] S. G. Shepard, S. M. Fatur, A. K. Rappé, N. H. Damrauer, *J. Am. Chem. Soc.* **2016**, *138*, 2949–2952.

[57] L. E. Shaw, C. H. Langford, *Inorg. Chem.* **2000**, *39*, 541–546.

[58] E. Maskova, A. Vlček, *Inorg. Chim. Acta* **1996**, *242*, 17–23.

[59] J. F. Hartwig, *Organotransition Metal Chemistry - From Bonding to Catalysis*. Mill Valley, 1. ed. **2010**, University Science Book, Mill Valley.

[60] A. E. Carpenter, C. C. Mokhtarzadeh, D. S. Ripatti, I. Havrylyuk, R. Kamezawa, C. E. Moore, A. L. Rheingold, J. S. Figueroa, *Inorg. Chem.* **2015**, *54*, 2936–2944.

[61] Y. Yamamoto, *Coord. Chem. Rev.* **1980**, *32*, 193–233.

[62] D. T. Plummer, *Synthesis of multidentate nitrile and isonitrile ligands and their transition-metal complexes*, Doctoral dissertation, Iowa State University, **1983**.

[63] D. T. Plummer, R. J. Angelici, *Inorg. Chem.* **1983**, *22*, 4063–4070.

[64] Y. Ito, K. Kobayashi, T. Saegusa, *J. Organomet. Chem.* **1986**, *303*, 301–308.

[65] F. E. Hahn, M. Tamm, *Angew. Chem. Int. Ed.* **1992**, *31*, 1212–1214.

[66] K. Sakata, K. Matsumoto, M. Hashimoto, *Inorg. Chim. Acta* **1994**, *227*, 113–118.

[67] K. Sakata, Y. Yamaguchi, X. Shen, M. Hashimoto, A. Tsuge, *Synth. React. Inorg. Met.-Org. Chem.* **2005**, *35*, 545–551.

[68] M. L. Winzenburg, J. A. Kargol, R. J. Angelici, *J. Organomet. Chem.* **1983**, *249*, 415–428.

[69] A. Naik, *Synthesis and Application of Chiral Novel Bis(isonitrile) Ligands in Catalysis*, Doctoral dissertation, Universität Regensburg, **2010**.

[70] F. Monti, A. Baschieri, E. Matteucci, A. Mazzanti, L. Sambri, A. Barbieri, N. Armaroli, *Faraday Discuss.* **2015**, *185*, 233–248.

[71] F. Hahn, *Angew. Chem. Int. Ed.* **1993**, *33*, 650–665.

[72] L. A. Büldt, X. Guo, A. Prescimone, O. S. Wenger, *Angew. Chem. Int. Ed.* **2016**, *55*, 11247–11250.

[73] D. D. Klendworth, W. W. Welters, R. A. Walton, *Organometallics* **1982**, *1*, 336–343.

[74] D. D. Klendworth, W. W. Welters, R. A. Walton, *J. Organomet. Chem.* **1981**, *213*, C13–C16.

[75] N. G. Connelly, W. E. Geiger, *Chem. Rev.* **1996**, *96*, 877–910.

[76] D. A. Bohling, K. R. Mann, S. Enger, T. Gennett, M. J. Weaver, R. A. Walton, *Inorg. Chim. Acta* **1985**, *97*, L51–L53.

[77] D. A. Bohling, J. F. Evans, K. R. Mann, *Inorg. Chem.* **1982**, *21*, 3546–3551.

[78] K. Suzuki, A. Kobayashi, S. Kaneko, K. Takehira, T. Yoshihara, H. Ishida, Y. Shiina, S. Oishi, S. Tobita, *Phys. Chem. Chem. Phys.* **2009**, *11*, 9850–9860.

[79] C. R. Bock, J. A. Connor, A. R. Gutierrez, T. J. Meyer, D. G. Whitten, B. P. Sullivan, J. K. Nagle, *J. Am. Chem. Soc.* **1979**, *101*, 4815–4814.

[80] J. J. Concepcion, J. W. Jurss, M. K. Brennaman, P. G. Hoertz, A. O. T. Patrocinio, N. Y. Murakami Iha, J. L. Templeton, T. J. Meyer, *Acc. Chem. Res.* **2009**, *42*, 1954–1965.

[81] J. Gong, J. Liang, K. Sumathy, *Renew. Sustain. Energy Rev.* **2012**, *16*, 5848–5860.

[82] A. J. Bard, M. A. Fox, *Acc. Chem. Res.* **1995**, *28*, 141–145.

[83] H. Ozawa, K. Sakai, *Chem. Commun.* **2011**, *47*, 2227–2242.

[84] M. Grätzel, *J. Photochem. Photobiol. C Photochem. Rev.* **2003**, *4*, 145–153.

[85] A. S. Polo, M. K. Itokazu, N. Y. Murakami Iha, *Coord. Chem. Rev.* **2004**, *248*, 1343–1361.

[86] J. R. Winkler, N. Sutin, *Inorg. Chem.* **1987**, *26*, 220–221.

[87] C. Creutz, M. Chou, T. L. Netzel, M. Okumura, N. Sutin, *J. Am. Chem. Soc.* **1980**, *102*, 1309–1319.

[88] T. Duchanois, T. Etienne, C. Cebrián, L. Liu, A. Monari, M. Beley, X. Assfeld, S. Haacke, P. C. Gros, *Eur. J. Inorg. Chem.* **2015**, 2469–2477.

[89] T. C. B. Harlang, Y. Liu, O. Gordivska, L. A. Fredin, C. S. Ponseca, P. Huang, P. Chábera, K. S. Kjaer, H. Mateos, J. Uhlig, R. Lomoth, R. Wallenberg, S. Styring, P. Persson, V. Sundström, K. Wärnmark, *Nat. Chem.* **2015**, *7*, 883–889.

[90] W. S. Mialki, D. E. Wigley, T. E. Wood, R. A. Walton, *Inorg. Chem.* **1982**, *21*, 480–485.

[91] J. P. Bullock, K. R. Mann, *Inorg. Chem.* **1989**, *28*, 4006–4011.

[92] P. M. Treichel, D. W. Firsich, G. P. Essenmacher, *Inorg. Chem.* **1979**, *18*, 2405–2409.

[93] P. M. Treichel, G. J. Essenmacher, *Inorg. Chem.* **1976**, *15*, 146–150.

[94] G. J. Essenmacher, P. M. Treichel, *Inorg. Chem.* **1977**, *16*, 800–806.

[95] D. M. Manuta, A. J. Lees, *Inorg. Chem.* **1983**, *22*, 572–573.

[96] D. M. Manuta, A. J. Lees, *Inorg. Chem.* **1986**, *25*, 1354–1359.

[97] P. C. Servaas, H. K. Van Dijk, T. L. Snoeck, D. J. Stufkens, A. Oskam, *Inorg. Chem.* **1985**, *24*, 4494–4498.

[98] K. A. Rawlins, J. Lees, *Inorg. Chem.* **1989**, *28*, 2154–2160.

[99] D. J. Stufkens, *Coord. Chem. Rev.* **1990**, *104*, 39–112.

[100] K. Iuchi, S. Asada, A. Sugimori, *Chem. Lett.* **1974**, 801–802.

[101] K. Iuchi, S. Asada, T. Kinugasa, K. Kanamori, A. Sugimori, *Bull. Chem. Soc. Jpn.* **1976**, *49*, 577–578.

[102] X. Xie, J. D. Simon, *J. Phys. Chem.* **1989**, *93*, 4401–4404.

[103] A. Barbieri, G. Accorsi, N. Armaroli, *Chem. Commun.* **2008**, 2185–2193.

[104] R. D. Costa, E. Ortí, H. J. Bolink, F. Monti, G. Accorsi, N. Armaroli, *Angew. Chem. Int. Ed.* **2012**, *51*, 8178–8211.

[105] J. V. Caspar, *J. Am. Chem. Soc.* **1985**, *107*, 6718–6719.

[106] H. Kunkely, A. Vogler, *Inorg. Chem. Commun.* **2000**, *3*, 143–144.

[107] H. Kunkely, A. Vogler, *J. Organomet. Chem.* **2003**, *684*, 113–116.

[108] H. tom Dieck, M. Svoboda, T. Greiser, *Z. Naturforsch.* **1981**, *36b*, 823–832.

[109] R. Frem, A. Massabni, A. Massabni, A. Mauro, *Inorg. Chim. Acta* **1997**, *255*, 53–58.

[110] F. A. Cotton, F. Zingales, *J. Am. Chem. Soc.* **1961**, *83*, 351–355.

[111] H. Behrens, K. Meyer, *Z. Naturforsch.* **1966**, *21b*, 489–490.

[112] R. Nast, H. Schulz, H.-D. Moerler, *Chem. Ber.* **1970**, *784*, 777–784.

[113] D. Lentz, M. Anibarro, D. Preugschat, G. Bertrand, *J. Fluor. Chem.* **1998**, *89*, 73–81.

[114] F. E. Hahn, M. Münder, R. Fröhlich, *Z. Naturforsch.* **2004**, *3*, 850–854.

[115] B. J. Fox, M. D. Millard, A. G. DiPasquale, A. L. Rheingold, J. S. Figueroa, *Angew. Chem. Int. Ed.* **2009**, *48*, 3473–3477.

[116] C. L. Perrine, M. Zeller, J. Woolcock, T. M. Styranec, A. D. Hunter, *J. Chem. Crystallogr.* **2010**, *40*, 289–295.

[117] B. M. Emerich, C. E. Moore, B. J. Fox, A. L. Rheingold, J. S. Figueroa, *Organometallics* **2011**, *30*, 2598–2608.

[118] J. K. Burdett, *Inorg. Chem.* **1975**, *14*, 9–12.

[119] E. C. Constable, C. E. Housecroft, J. R. Price, J. A. Zampese, *CrystEngComm* **2010**, *12*, 3163–3171.

[120] T. T. Tsou, J. K. Kochi, *J. Am. Chem. Soc.* **1979**, *101*, 6319–6332.

[121] P. C. Servaas, D. J. Stufkens, A. Oskam, *Inorg. Chem.* **1989**, *28*, 1774–1780.

[122] W. Rudel, *Chem. Ber.* **1963**, *96*, 636–637.

[123] S. Gowda, D. C. Gowda, *Indian J. Chem. - Sect. B Org. Med. Chem.* **2003**, *42*, 180–183.

[124] M. Tobisu, K. Koh, T. Furukawa, N. Chatani, *Angew. Chem. Int. Ed.* **2012**, *51*, 11363–11366.

[125] Z. Xia, J. Huang, Y. He, J. Zhao, J. Lei, Q. Zhu, *Org. Lett.* **2014**, *16*, 2546–2549.

[126] W. Zhang, Y. Lu, J. S. Moore, *Org. Synth.* **2007**, *84*, 163.

[127] R. D. Costa, D. Tordera, E. Ortí, H. J. Bolink, J. Schönle, S. Graber, C. E. Housecroft, E. C. Constable, J. A. Zampese, *J. Mater. Chem.* **2011**, *21*, 16108–16118.

[128] D. R. McMillin, M. T. Buckner, B. T. Ahn, *Inorg. Chem.* **1977**, *16*, 943–945.

[129] B.-T. Ahn, D. R. McMillin, *Inorg. Chem.* **1978**, *17*, 2253–2258.

[130] M. S. Lazorski, R. H. Gest, C. M. Elliott, *J. Am. Chem. Soc.* **2012**, *134*, 17466–17469.

[131] M. Knorn, T. Rawner, R. Czerwieniec, O. Reiser, *ACS Catal.* **2015**, *5*, 5186–5193.

[132] O. Reiser, *Acc. Chem. Res.* **2016**, *49*, 1990–1996.

[133] A. C. Hernandez-Perez, S. K. Collins, *Acc. Chem. Res.* **2016**, *49*, 1557–1565.

[134] D. R. McMillin, K. M. McNett, *Chem. Rev.* **1998**, *98*, 1201–1220.

[135] N. Armaroli, *Chem. Soc. Rev.* **2001**, *30*, 113–124.

[136] R. C. Evans, P. Douglas, C. J. Winscom, *Coord. Chem. Rev.* **2006**, *250*, 2093–2126.

[137] D. G. Cuttell, S. M. Kuang, P. E. Fanwick, D. R. McMillin, R. A. Walton, *J. Am. Chem. Soc.* **2002**, *124*, 6–7.

[138] C. E. McCusker, F. N. Castellano, *Inorg. Chem.* **2013**, *52*, 8114–8120.

[139] M. J. Leitl, V. A. Krylova, P. I. Djurovich, M. E. Thompson, H. Yersin, *J. Am. Chem. Soc.* **2014**, *136*, 16032–16038.

[140] N. Armaroli, G. Accorsi, F. Cardinali, A. Listorti. "Photochemistry and Photophysics of Coordination Compounds" Parts I & II. In *Top. Curr. Chem.*, volume 280, 69–115. **2007**.

[141] S. Keller, E. C. Constable, C. E. Housecroft, M. Neuburger, A. Prescimone, G. Longo, A. Pertegas, M. Sessolo, H. J. Bolink, *Dalton Trans.* **2014**, *43*, 16593–16596.

[142] N. S. Murray, S. Keller, E. C. Constable, C. E. Housecroft, M. Neuburger, A. Prescimone, *Dalton Trans.* **2015**, *44*, 7626–7633.

[143] J. Bailey, M. J. Mays, *J. Organomet. Chem.* **1973**, *47*, 217–224.

[144] A. Bell, M. A. Poulter, *Inorg. Chim. Acta* **1985**, *104*, 171–178.

[145] A. Toth, C. Floriani, A. Chiesi-Villa, C. Guastini, *J. Chem. Soc. Dalt. Trans.* **1988**, 1599–1605.

[146] G. Albertin, D. Baldan, E. Bordignon, *J. Organomet. Chem.* **1989**, *377*, 145–150.

[147] C. S. Smith, K. R. Mann, *J. Am. Chem. Soc.* **2012**, *134*, 8786–8789.

[148] D. B. Bagal, G. Kachkovskyi, M. Knorn, T. Rawner, B. M. Bhanage, O. Reiser, *Angew. Chem. Int. Ed.* **2015**, *4*, 6999–7002.

[149] A. A. Melekhova, A. S. Novikov, K. V. Luzyanin, N. A. Bokach, G. L. Starova, V. V. Gurzhiy, V. Y. Kukushkin, *Inorg. Chim. Acta* **2015**, *434*, 31–36.

[150] R. Czerwieniec, J. Yu, H. Yersin, *Inorg. Chem.* **2011**, *50*, 8293–8301.

[151] M. Osawa, M. Hoshino, M. Hashimoto, I. Kawata, S. Igawa, M. Yashima, *Dalton Trans.* **2015**, *44*, 8369–8378.

[152] M. D. Weber, C. Garino, G. Volpi, E. Casamassa, M. Milanesio, C. Barolo, R. D. Costa, *Dalton Trans.* **2016**, *45*, 8984–8993.

[153] L. Xiao, Y. Xu, M. Yan, D. Galipeau, X. Peng, X. Yan, *J. Phys. Chem. A* **2010**, *114*, 9090–9097.

[154] K. E. Henry, R. G. Balasingham, A. R. Vortherms, J. A. Platts, J. F. Valliant, M. P. Coogan, J. Zubieta, R. P. Doyle, *Chem. Sci.* **2013**, *4*, 2490–2495.

[155] A. B. Scharf, *First-Row Transition Metal Complexes of Dipyrrinato Ligands : Synthesis and Characterization*, Doctoral dissertation, Harvard University, **2013**.